

IMMUNE MODULATION OF THE TUMOUR MICROENVIRONMENT

Helen Kathryn Angell BSc. Hons.

Thesis submitted to the University of Nottingham for
the degree of Doctor of Philosophy

September 2011



ABSTRACT

Regulatory T cells (Tregs) are a distinct lymphocyte lineage, functionally defined as T cells that inhibit an immune response, which is crucial for maintaining peripheral tolerance and the prevention of autoimmunity. Tregs have been implicated in tumour immune evasion, suppressing the anti-tumour immune response, resulting in tumour progression. The aim of this PhD was to recognise how Tregs function and understand how they are able to modulate tumour immunology. In order to research their proposed role in cancer, it was necessary to be able to phenotype, sort and expand functional Tregs. In preliminary research, strategies were designed to phenotype and test the functionality of *ex vivo* Tregs and commercial isolation kits were tested and compared in terms of cost efficiency and effectiveness. The mechanisms of Treg-mediated suppression were investigated, including the necessity for cell-to-cell contact and the involvement of key cytokines. The importance of particular cytokines in Treg-mediated suppression was not clear; but cell contact appears to be required for optimal suppression.

The project then aimed to address whether or not the importance of Tregs highlighted in the literature was reflected in a clinical setting. The significance of immune cell orientation within the tumour microenvironment was researched, investigating the co-localisation between key immune cell subtypes and their correlation with areas of tumour proliferation, apoptosis, hypoxia and vasculature coverage. In order to achieve this successfully, immunohistochemical techniques were optimised and image analysis algorithms were constructed to facilitate rigorous and systematic

quantification of immune cell infiltrates in primary colorectal and metastatic liver cancer patients. Significant increases in the prevalence of Tregs, CD8 cells, macrophages and natural killer (NK) cells were observed within the stroma, compared with the tumour. A metastatic phenotype was alluded to; encompassing elevated Tregs and reduced numbers of CD8 cells.

Further to this, the level of Tregs in the peripheral blood and tumour tissue of liver-metastatic patients were assessed to investigate whether any correlation existed between circulating and tumour-infiltrating Tregs. It was shown that within peripheral blood, patients exhibited a $\text{Treg}^{\text{high}}\text{CD8}^{\text{low}}\text{NK}^{\text{low}}$ phenotype, when compared with healthy volunteers.

Finally, the project aimed to build an *in vitro* human Treg tumour-killing suppression model to examine the ability of Tregs to inhibit NK cell-mediated cytotoxicity. The mechanism for this was investigated, evaluating the importance of the NK group 2 member D (NKG2D) receptor ligand interaction, to mediate cell killing in a transforming growth factor- β dependent manner.

This study adds to the ongoing discussion on the role of immune cells in metastatic development. Accumulating evidence points to a critical role of immune infiltrates in allowing metastatic development, where Tregs support tumour growth by suppressing the host anti-tumour immune response.

ACKNOWLEDGMENTS

In preparing this thesis I have had mentorship from numerous individuals both from within the university and outside of it. It is to these individuals that my heartfelt gratitude and thanks go out to.

First and foremost I would like to gratefully acknowledge the enthusiastic supervision of Professor David Pritchard. It was his great mind that instigated the project, scribbled down whilst waiting at East Midlands airport. I would also like to acknowledge members of the Immune Modulation Group, for their relentless help and insights into immunology. I thank Robert Wilkinson for his constant guidance, inspiring discussions and for opening so many scientific doors for me. I would like to acknowledge members of the Molecular Pathology Group (AstraZeneca) for their unrelenting support, capability and patience.

Finally, I am forever indebted to my parents for their understanding and encouragement when it was most required. It would not have been possible to write this doctoral thesis without the help and support of my friends and family.

Helen Angell

September 2011

Table of Contents

ABSTRACT	I
ACKNOWLEDGMENTS	IV
TABLE OF CONTENTS	1
LIST OF ABBREVIATIONS	5
LIST OF FIGURES	9
LIST OF TABLES	14
CHAPTER 1 - INTRODUCTION	16
1.1. LITERATURE REVIEW	18
1.1.1. The Immune System	18
1.1.2. Innate Immune Response	18
1.1.3. Adaptive Immune Response	19
1.1.4. Natural Killer Cells	23
1.1.5. Regulatory T Cells	28
1.1.6. Regulatory T Cell Markers	34
1.1.7. Tumour Immunology	35
1.1.8. Regulatory T Cells in Cancer	37
1.1.9. Tumour Morphology and Microenvironment	41
1.1.10. Colorectal Cancer	44
1.2. THE AIMS OF THE CURRENT STUDY	49
CHAPTER 2 - WAYS TO WORK WITH TREGS: ISOLATION AND EXPANSION	51
2.1. METHODOLOGY	53
2.1.1. Fluorescence Activated Cell Sorting (FACS) Protocol	53
2.1.2. PBMC Isolation	54
2.1.3. Regulatory T Cell Isolation	55
2.1.4. <i>In vitro</i> Regulatory T Cell Expansion Assay	57
2.2. RESULTS AND DISCUSSION	58
2.2.1. Human Peripheral Blood Phenotyping	58
2.2.2. Regulatory T Cell Isolation from Human Peripheral Blood	72
2.2.2.1 The Dynabeads® Regulatory CD4 ⁺ CD25 ⁺ T Cell Kit, Invitrogen	72
2.2.2.2. The MACS® CD4 ⁺ CD25 ⁺ Regulatory T Cell Kit, Miltenyi Biotec	76
2.2.3. Expansion of Human Isolated Regulatory T Cells	82

2.3. CONCLUSIONS AND FUTURE WORK.....	84
CHAPTER 3 – MECHANISMS OF SUPPRESSION AND TREG FUNCTIONALITY	88
3.1. METHODOLOGY	90
3.1.1. Regulatory T Cell Suppression Assay.....	90
3.1.1.1. Cell Titer 96® Aqueous One Solution Cell Proliferation (MTS) Assay.....	91
3.1.1.2. ³ H-Thymidine Radioactive Assay.....	92
3.1.2. Enzyme Linked Immunosorbant Assay (ELISA)	92
3.1.3. Transwell Assay	93
3.1.4. Method of Statistical Analysis.....	94
3.1.5. Ethics Approval	94
3.2. RESULTS AND DISCUSSION.....	94
3.2.1. Suppression Assay Protocol Optimisation	95
3.2.2. Suppression by Inhibitory Cytokines	102
3.2.3. Cell-Cell Contact Dependent or Independent?.....	108
3.2.4. A Surrogate Cell Line?	112
3.3. CONCLUSIONS AND FUTURE WORK.....	115
CHAPTER 4 – IMMUNE INFILTRATES AND TUMOUR PROGRESSION	117
4.1. METHODOLOGY	119
4.1.1. Cell Pellet Preparation.....	119
4.1.2. Histology Specimen Processing and Embedding.....	120
4.1.3. Section Cutting	122
4.1.4. Haematoxylin and Eosin (H&E).....	122
4.1.5. Immunohistochemistry	123
4.1.6. Image Analysis	125
4.1.7. Ethics Approval	125
4.1.8. Method of Statistical Analysis.....	125
4.2. RESULTS AND DISCUSSION.....	126
4.2.1. Immunohistochemistry Antibody Optimisation	130
4.2.2. Tissue of Interest and Ethics.....	155
4.2.3. Image Analysis	157
4.2.4. Immune Infiltrates in Colorectal Metastatic Liver Samples.....	165
4.2.4.1. Adaptive Immunity	165
4.2.4.1.1. CD8 Positive Cytotoxic T Cells.....	165
4.2.4.1.2. Foxp3 Positive Tregs.....	175
4.2.4.2. Innate Immunity	186
4.2.4.2.1 CD68 Positive Macrophages	186

4.2.4.2.2. CD56 Positive NK Cells	196
4.2.4.3. Tumour Environment	204
4.2.4.3.1. CD31 Positive Vasculature Staining	204
4.2.4.3.2. HIF-1 α Positive Hypoxia Staining	212
4.2.4.3.3. CC-3 Positive Apoptotic Staining	220
4.2.4.3.4 Ki67 Positive Proliferation Staining	230
4.2.4.3.5. α -SMA Stromal Staining	238
4.3. CONCLUSIONS AND FUTURE WORK	243
4.3.1. Immunohistochemistry Optimisation	243
4.3.2. Adaptive Immunity	243
4.3.3. Innate Immunity	250
CHAPTER 5 – A LINK BETWEEN IN SITU AND CIRCULATING TREGS	256
5.1. METHODOLOGY	258
5.1.1. Patient Treg Suppression Assay	258
5.1.2. Whole Blood FACS Analysis	259
5.1.3. <i>In vitro</i> Immunohistochemistry Antibody Staining Assay	259
5.1.4. Image Analysis	261
5.1.5. Tissue Samples and Ethics	262
5.1.6. Method of Statistical Analysis	264
5.2. RESULTS AND DISCUSSION	264
5.2.1. Examining Tregs in CRC Liver Metastatic Patients	264
5.2.2. Additional Immune Cells in CRC Liver Metastatic Patients	272
5.3. CONCLUSION AND FUTURE WORK	284
5.3.1. Examining Tregs in CRC Liver Metastatic Patients	284
5.3.2. Additional Immune Cells in CRC Liver Metastatic Patients	285
CHAPTER 6 – BUILDING AN IN VITRO MODEL AND INTERROGATING THE SYSTEM	288
6.1. METHODOLOGY	291
6.1.1 K562 Cell Killing Assay	291
6.1.2 NKG2D and TGF- β RII FACS Analysis	291
6.1.3 ULBP-2 and MICA FACS Analysis	292
6.1.4 NK Cell Isolation	293
6.1.5 Soluble TGF- β Human FlowCytomix Kit	294
6.1.6. Method of Statistical Analysis	295
6.2. RESULTS AND DISCUSSION	295
6.2.1. K562 Cell Killing Assay with PBMCs	300
6.2.2. FACS Investigation of Model Markers on PBMCs	311

6.2.3. K562 Cell Killing Assay with NK Cells	315
6.2.4. Evaluating TGF- β in CRC Liver Metastatic Patients	335
6.2.5. FACS Investigation of Tumour Markers	337
6.3. CONCLUSIONS AND FUTURE WORK.....	339
6.3.1. Cell Killing Assay.....	339
6.3.2. Investigation of Model Key Players	340
6.3.3. Refined Hypothesis	343
6.3.4. Future Work.....	348
CHAPTER 7 – FINAL CONCLUSIONS	350
7.1. FINAL CONCLUSIONS	352
CHAPTER 8 – APPENDIX.....	357
8.1. ACHIEVEMENTS.....	357
8.1.1. Papers In Preparation	357
8.1.2. Published Abstracts.....	357
8.1.3. Oral Presentations.....	357
8.1.4. Awards	358
8.1.5. Posters	358
8.2. REFERENCES	360

List of Abbreviations

3,3-Diaminobenzidine (DAB)
3-(4,5-dimethylthiazol-2-yl)-5-(3-carboxymethoxyphenyl)-2-(4-sulfophenyl)-2H-tetrazolium (MTS)
4-(2-hydroxyethyl)-1-piperazineethanesulfonic acid (HEPES)
5(6)-Carboxyfluorescein diacetate N-succinidyl ester (CFSE)
 α -Smooth muscle actin (α -SMA)
Analysis of variance (ANOVA)
Aberant crypt foci (ACF)
Antigen-presenting cell (APC)
B lymphocyte (B cell)
Bovine serum albumin (BSA)
Brain (BN)
Calreticulin (CRT)
Cancer-associated fibroblast (CAF)
Cancer testis antigen (CTA)
C-C chemokine ligand (CCL)
C-C chemokine receptor type (CCR)
Cellular adhesion molecule (CAM)
Centre of tumour (CT)
Chronic myelogenous leukaemia (CML)
Cleaved caspase-3 (CC-3)
Cluster designation (CD)
Colony stimulating factor (CSF)
Colorectal cancer (CRC)
Concavalin A (ConA)
Cyclic adenosine monophosphate (cAMP)
Cyclooxygenase (COX)
Cytokine induced killing (CIK)
Cytotoxic T cell (T_c)
Cytotoxic T lymphocyte (CTL)
Cytotoxic T lymphocyte antigen 4 (CTLA4)
Death receptor 5 (DR5)
Dendritic cell (DC)
Disease free survival (DFS)
Enzyme-linked immunosorbent assay (ELISA)

Ethylenediaminetetraacetic acid (EDTA)
Extracellular matrix (ECM)
Foetal bovine serum (FBS)
Foetal calf serum (FCS)
Fluorescein isothiocyanate (FITC)
Fluorescence activated cell sorting (FACS)
Forkhead/winged box helix transcription factor gene (Foxp3)
Forward scatter (FS)
Germinal centre (GC)
Glucocorticoid-induced TNF receptor family related protein (GITR)
Granzyme B (GZB)
Haematoxylin and Eosin (H & E)
Hepatocellular carcinoma (HCC)
Hepatocyte growth factor (HGF)
High-mobility group protein B1 (HMGB1)
Horse raddish peroxidase (HRP)
Human leukocyte antigen (HLA)
Hypoxia-inducible factor-1 alpha (HIF-1 α)
Immunoglobulin G (IgG)
Immunohistochemistry (IHC)
Indoleaminutese 2,3-dioxygenase (IDO)
Induced Treg cell (iTreg)
Interferon- γ (IFN- γ)
Interleukin (IL)
Interleukin-2 receptor (IL-2R)
Intrahepatic cholangiocarcinoma (ICC)
Invasive margin (IM)
Killer cell immunoglobulin-like receptor (KIR)
Larger granular lymphocytes (LGL)
Lymph node (LN)
Mantle (M)
Major histocompatibility complex (MHC)
Mean intensity (MI)
MHC class I chain-related protein (MIC)
Microvessel density (MVD)
Molecular immunology Borstel-1 (MIB-1)
Monoclonal antibody (mAb)

Monocyte chemoattractant protein (MCP)
 Natural cytotoxicity receptor (NCR)
 Natural killer (NK)
 Natural killer cell receptor (NKR)
 Neutralising transforming growth factor- β receptor II (nTGF- β RII)
 Natural killer groups 2 (NKG2)
 Natural killer groups 2 member D (NKG2D)
 Natural killer groups 2 member D ligand (NKG2DL)
 Natural killer T (NKT)
 Natural Treg cell (nTreg)
 Necrotic (N)
 Neural cellular adhesion molecule (NCAM)
 NK cell receptor protein-1 (NK1.1)
 No significance (NO)
 Non-neoplastic tissue (NonNeo)
 Non-neoplastic liver (NNLV)
 Non-small cell lung cancer (NSCLC)
 Nuclear factor kappa B (NF κ B)
 Ovarian cancer (OVC)
 Overall survival (OS)
 Paracortex (P)
 Peripheral blood (PB)
 Peripheral blood lymphocyte (PBL)
 Peripheral blood mononuclear cell (PBMC)
 Phosphate buffered saline (PBS)
 Phosphate buffered saline with tween (PBS-T)
 Phosphodiesterase 3B (PDE3B)
 Phycoerythrin (PE)
 Phycoerythrin Cy5 (Pcy5)
 Phycoerythrin-Texas red conjugate energy coupled dye (ECD)
 Phytohemagglutinin (PHA)
 Placenta (PL)
 Platelet endothelial cell adhesion molecule (PECAM)
 Poly ADP-ribose polymerase (PARP)
 Polymorphonuclear leucocyte (PMN)
 Primary colorectal cancer with no affiliated metastatic disease (MET-)
 Primary colorectal cancer with that developed liver metastatic disease (MET+)

Propidium iodide (PI)
 Prostate mucin antigen (PMA)
 Reactive oxygen intermediates (ROI)
 Reactive oxygen species (ROS)
 Regulatory T cell (Treg)
 Relapse-free survival (RFS)
 Roswell park memorial institute (RPMI)
 Side scatter (SS)
 Small interfering ribonucleic acid (siRNA)
 Soluble transforming growth factor- β (sTGF- β)
 Standard deviation (SD)
 Stroma (S)
 T cell receptor (TCR)
 T lymphocyte (T cell)
 T helper (T_H)
 Tetrameric antibody complex (TAC)
 TNF-related apoptosis-inducing ligand (TRAIL)
 Tonsil (TN)
 Transforming growth factor- β (TGF- β)
 Transforming growth factor- β receptor II (TGF- β RII)
 Tris-buffered saline-tween (TBS-T)
 Tumour (T)
 Tumour-associated antigen (TAA)
 Tumour-associated macrophage (TAM)
 Tumour-infiltrating lymphocyte (TIL)
 Tumour-necrosis factor- α (TNF- α)
 Tumour-node-metastatic (TNM)
 UL16 binding protein (ULBP)
 Vascular emboli, lymphatic invasion and perineural invasion (VELIPI)
 Vascular endothelial growth factor (VEGF)
 Whole blood (WB)

List of Figures

Figure 1.1 Lymphocyte Lineage.....	20
Figure 1.2 The Specific Interaction between Antigen-Presenting Cells and T Cells via Major Histocompatibility Complex (MHC) Molecules.....	22
Figure 1.3 Treg Interaction with Neighbouring T Cells.....	29
Figure 1.4 Diagrammatic Representation of Proposed Treg Suppressive Mechanisms.....	31
Figure 1.5 Tregs in Cancer.....	40
Figure 1.6 The Onset and Development of CRC.....	46
Figure 1.7 TNM Staging of CRC and the Importance of Immune Infiltrates in Disease Progression.....	48
Figure 2.1 FACS Analysis of Monocytes and B cells from Isolated PBMCs.....	59
Figure 2.2 CD8 FACS Analysis of Isolated PBMCs.....	61
Figure 2.3 Foxp3 FACS Analysis of Isolated PBMCs.....	64
Figure 2.4 GITR FACS Analysis of Isolated PBMCs.....	66
Figure 2.5 CD62L FACS Analysis of Isolated PBMCs.....	68
Figure 2.6 CD127 FACS Analysis of Isolated PBMCs.....	70
Figure 2.7 Diagrammatic Representation of Dynabeads® CD4+CD25+ T Cell Isolation Kit, Invitrogen.....	73
Figure 2.8 FACS Analysis of Treg Isolation Using Invitrogen Dynabeads® CD4+CD25+ T Cell Isolation Kit.....	75
Figure 2.9 Diagrammatic Representation of MACS CD4+CD25+ Treg Isolation Kit, Miltenyi Biotec.....	77
Figure 2.10 FACS Analysis of Treg Isolation Using MACS CD4+CD25+ Regulatory T Cell Isolation Kit, Miltenyi Biotec.....	79
Figure 2.11 Differences in Donor Cell Isolation Numbers Using Invitrogen Dynabeads® CD4 ⁺ CD25 ⁺ T Cell Isolation Kit.....	81
Figure 2.12 Expanded Treg Numbers and FACS Analysis Comparing Populations.....	83
Figure 3.1 Treg Suppression of ConA or PHA/PMA Stimulated PBMCs, MTS.....	97
Figure 3.2 Treg Suppression of ConA or PHA/PMA Stimulated Effector Cells, MTS.....	99
Figure 3.3 Treg Suppression of PHA Stimulated Effector Cells, via 3H-Thymidine Incorporation.....	101
Figure 3.4 IL-10 ELISA of Supernatants from Treg Suppression of PHA Stimulated Effector Cells.....	104

Figure 3.5 IFN-gamma ELISA of Supernatants from Treg Suppression of PHA Stimulated Effector Cells.....	107
Figure 3.6 Diagrammatic Representation of the Transwell System.....	109
Figure 3.7 Transwell Suppression Activity of Tregs.....	111
Figure 3.8 Transwell Suppression Activity of Karpas-299 Cell Line with FACS Analysis.....	114
Figure 4.1 Cell Pellet Procedure for Optimisation of IHC Staining.....	132
Figure 4.2 IHC Foxp3 Antibody Protocol Validation on Cell Pellets.....	134
Figure 4.4 IHC CD4 Antibody Protocol Validation across Human Lymph Node and Tonsil Tissue.....	138
Figure 4.5 IHC CD8 Antibody Protocol Validation across Human Lymph Node and Tonsil Tissue.....	140
Figure 4.6 IHC CD56 Antibody Protocol Validation across a Selection of Human Tissue with Matched H&E Staining.....	142
Figure 4.7 IHC Foxp3 Antibody Protocol Validation across Human Lymph Node and Tonsil Tissue.....	144
Figure 4.8 IHC Ki67 Staining across a Selection of Human Tissue with Matched H & E Staining.....	146
Figure 4.9 Key Immune Cell IHC Staining Across Human CRC Primary Tissue.....	148
Figure 4.10 IHC Staining of Key Markers Taken Across Human CRC Primary Tissue.....	154
Figure 4.11 Genie™ Classifier Mark Up.....	158
Figure 4.12 Example Genie™ Analysis Output.....	160
Figure 4.13 Genie™ Analysis of Stroma and Tumour.....	162
Figure 4.14 Genie™ Analysis of Foxp3 Algorithm in Stroma and Tumour.....	164
Figure 4.15 CD8 Cell Infiltrates in Primary CRC vs Metastatic Liver.....	166
Figure 4.16 Comparison of CD8 Cells in MET+ and MET- Primary CRC Tissue.....	168
Figure 4.17 CD8 Cells in Liver Metastatic CRC and Matched Non-Neoplastic Tissue.....	170
Figure 4.18 Example Image of CD8 Immune Cells in Liver Metastatic CRC.....	172
Figure 4.19 Overall Evaluation of CD8 Cells in Tumour and Stroma.....	174
Figure 4.20 Foxp3 Cell Infiltrates in Primary CRC vs Metastatic Liver.....	176
Figure 4.21 Comparison of Foxp3 Cells in MET+ and MET- Primary CRC Tissue.....	178
Figure 4.22 Foxp3 Cells in Liver Metastatic CRC and Matched Non-Neoplastic Tissue.....	181
Figure 4.23 Example Image of CD8 and Foxp3 Cells Co-localisation at the Tumour Edge.....	183
Figure 4.24 Overall Evaluation of Foxp3 Cells in Tumour and Stroma.....	185
Figure 4.25 CD68 Macrophage Infiltrates in Primary CRC vs Metastatic Liver.....	187
Figure 4.26 Comparison of CD68 Cells in MET+ and MET- Primary CRC Tissue.....	189
Figure 4.27 CD68 Cells in Liver Metastatic CRC and Matched Non-Neoplastic Tissue.....	191
Figure 4.28 Example Image of Infiltrating CD68 Cells at the Tumour Edge.....	193

Figure 4.29 Overall Evaluation of CD68 Cells in Tumour and Stroma.....	195
Figure 4.30 CD56 NK Cell Infiltrates in Primary CRC vs Metastatic Liver.....	197
Figure 4.31 Comparison of CD56 Cells in MET+ and MET- Primary CRC Tissue.....	199
Figure 4.32 CD56 Cells in Liver Metastatic CRC and Matched Non-Neoplastic Tissue.....	201
Figure 4.33 Overall Evaluation of CD56 Cells in Tumour and Stroma.....	203
Figure 4.34 CD31 MVD in Primary CRC vs Metastatic Liver.....	205
Figure 4.35 Comparison of CD31 MVD in MET+ and MET- Primary CRC Tissue.....	207
Figure 4.36 CD31 MVD in Liver Metastatic CRC and Matched Non-Neoplastic Tissue.....	209
Figure 4.37 Overall Evaluation of MVD in Tumour and Stroma.....	211
Figure 4.38 HIF-1 α in Primary CRC vs Metastatic Liver.....	213
Figure 4.39 Comparison of HIF-1 α in MET+ and MET- Primary CRC Tissue.....	215
Figure 4.40 HIF-1 α in Liver Metastatic CRC and Matched Non-Neoplastic Tissue.....	217
Figure 4.41 Overall Evaluation of Hypoxia in Tumour and Stroma.....	219
Figure 4.42 CC-3 in Primary CRC vs Metastatic Liver.....	221
Figure 4.43 Comparison of CC-3 in MET+ and MET- Primary CRC Tissue.....	223
Figure 4.44 CC-3 in Liver Metastatic CRC and Matched Non-Neoplastic Tissue.....	225
Figure 4.45 Overall Evaluation of Apoptosis in Tumour and Stroma.....	227
Figure 4.46 Example Images of Hypoxic and Apoptotic Areas of Necrosis.....	229
Figure 4.47 Ki67 in Primary CRC vs Metastatic Liver.....	231
Figure 4.48 Comparison of Proliferation in MET+ and MET- Primary CRC Tissue.....	233
Figure 4.49 Ki67 in Liver Metastatic CRC and Matched Non-Neoplastic Tissue.....	235
Figure 4.50 Overall Evaluation of Proliferation in Tumour and Stroma.....	237
Figure 4.51 Example Images of α -SMA Staining and Genie™ Analysis.....	239
Figure 4.52 Percentage Area of Tumour and Stroma.....	241
Figure 4.53 Concluding Statistical Correlations Observed for CD8 Cells.....	245
Figure 4.54 Concluding Statistical Correlations Observed for Tregs.....	247
Figure 4.55 Statistical Correlation Between CD8/Treg Cell Ratio in the Tumour and Stroma, Linked with Tumour Proliferation.....	249
Figure 4.56 Concluding Statistical Correlations Observed for Macrophages.....	251
Figure 4.57 Diagrammatic Summary of Current Findings and Prognostic Factors within Literature.....	253
 Figure 5.1 Metastatic Liver Patient Treg Suppression of PHA Stimulated Effector Cells, via 3H-Thymidine Incorporation.....	266
Figure 5.2 Optimisation of Whole Blood FACS Analysis Protocol.....	269
Figure 5.3 Whole Blood FACS Analysis of Foxp3 ⁺ Tregs in CRC Metastatic Patients Compared to Healthy Volunteers.....	271

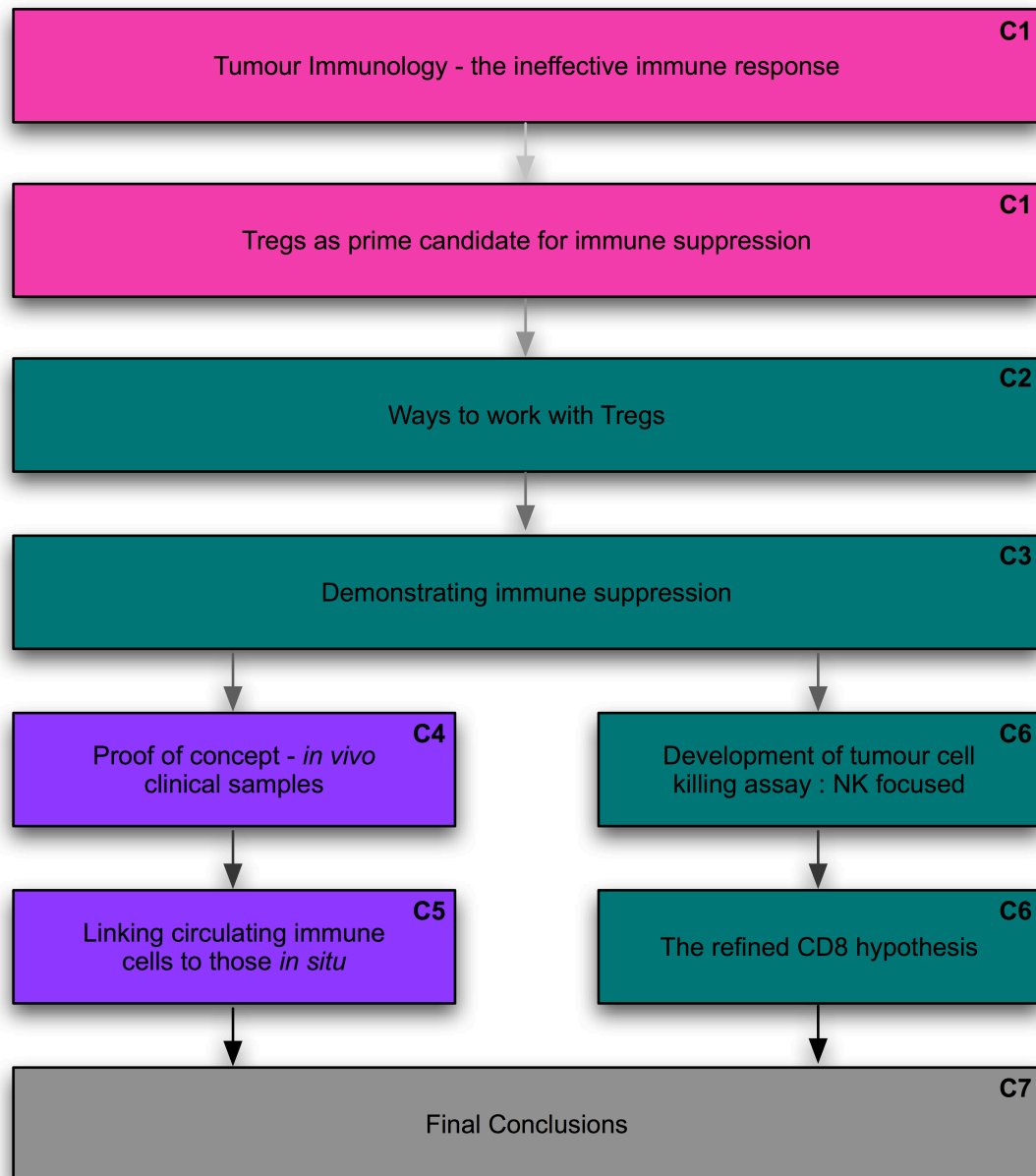
Figure 5.4 Whole Blood FACS Analysis of CD8 ⁺ Cells in CRC Metastatic Patients Compared to Healthy Volunteers.....	273
Figure 5.5 Whole Blood FACS Analysis of CD56 ⁺ CD3 ⁻ NK Cells and CD56 ⁺ CD3 ⁺ NKT Cells in CRC Metastatic Patients Compared to Healthy Volunteers.....	275
Figure 5.6 IHC Study of Tumour and Stromal Tregs in CRC Metastatic Patients, linked to Matched Whole Blood FACS Analysis.....	277
Figure 5.7 The Relationship Between Circulating Tregs and their Prevalence at the Tumour Site.....	279
Figure 5.8 IHC Study of Tumour and Stromal CTLs in CRC Metastatic Patients, linked to Matched Whole Blood FACS Analysis.....	281
Figure 5.9 The Relationship Between Circulating CTLs and their Prevalence at the Tumour Site.....	283
 Figure 6.1 Diagrammatic Representation of Natural Killer Cell and Tumour Interaction.....	296
Figure 6.2 Diagrammatic Representation of Treg Suppression of Natural Killer Cells and Tumour Interaction.....	299
Figure 6.3 FACS Analysis of K562 Cell Killing Assay with PBMCs.....	302
Figure 6.4 Extended K562 Cell Killing Assay with PBMCs.....	304
Figure 6.5 An Extended K562 Cell Killing Assay with PBMCs.....	306
Figure 6.6 Failure of Treg Mediated Suppression of K562 Cell Killing Assay with PBMCs..	308
Figure 6.7 Treg Mediated Suppression of K562 Cell Killing Assay with PBMCs.....	310
Figure 6.8 Investigation of NKG2D Expression.....	312
Figure 6.9 Investigation of TGF- β RII Expression.....	314
Figure 6.10 Diagrammatic Representation of the EasySep [®] Human NK Isolation Procedure.....	316
Figure 6.11 K562 Cell Killing Assay with Isolated NK Cells.....	318
Figure 6.12 FACS Analysis of Isolated NK Cells.....	320
Figure 6.13 Treg Mediated Suppression of K562 Cell Killing Assay with NK Cells Isolated from the same Donor.....	322
Figure 6.14 The Effect of a Neutralising anti-NKG2D Antibody on NK Cell Killing of K562 Cells.....	324
Figure 6.15 FACS Analysis of Isolated NK Cells with Neutralising anti-NKG2D Antibody...	326
Figure 6.16 Treg Mediated Suppression of K562 NK Cell Killing is abrogated by neutralising TGF- β RII Antibody.....	328
Figure 6.17 Treg Production of Soluble TGF- β	330
Figure 6.18 TGF- β 1 Mediated Suppression of K562 NK Cell Killing is abrogated by neutralising TGF- β RII Antibody.....	332

Figure 6.19 FACS Analysis of NKG2D Expression on Isolated NK Cells with increasing amounts of Soluble TGF- β	334
Figure 6.20 Concentration of Soluble TGF- β in Blood of CRC Liver Metastatic Patients Compared to Healthy Volunteers.....	336
Figure 6.21 FACS Analysis Investigating the Expression of MICA and ULBP-2 on a Selection of Tumour Cell Lines.....	338
Figure 6.22 Further Developed Diagrammatic Representation of Treg Suppression of Natural Killer Cells and Tumour Interaction.....	342
Figure 6.23 NKG2D FACS Analysis of Isolated CD8 Cells.....	344
Figure 6.24 FACS Analysis of NKG2D Expression on Isolated CD8 Cells with increasing amounts of Soluble TGF- β	346
 Figure 7.1 Concluding Diagrammatic Representation of Immune Cell Interactions within the Tumour Microenvironment.....	 355

List of Tables

Table 4.1 A Summary of the Tissue Processing Programme Used.....	121
Table 4.2 The Multiple Combinations of Optimisation Assays Carried Out.....	136
Table 4.3 A Summary of Markers.....	150
Table 4.4 A Summary of the Tissue Used.....	156
Table 5.1 A Summary of the Tissue Used.....	263

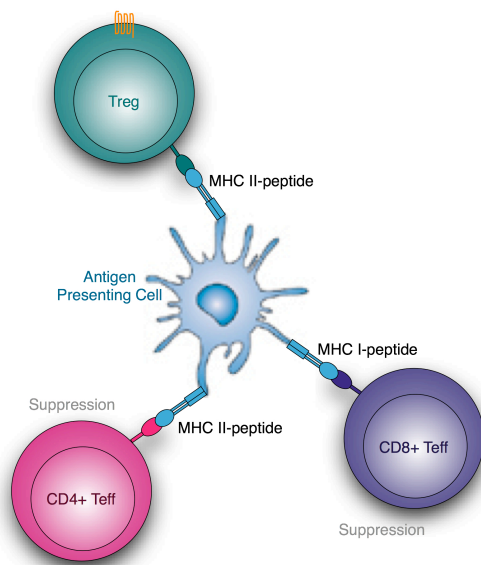
Chronological Framework of Thesis Progression



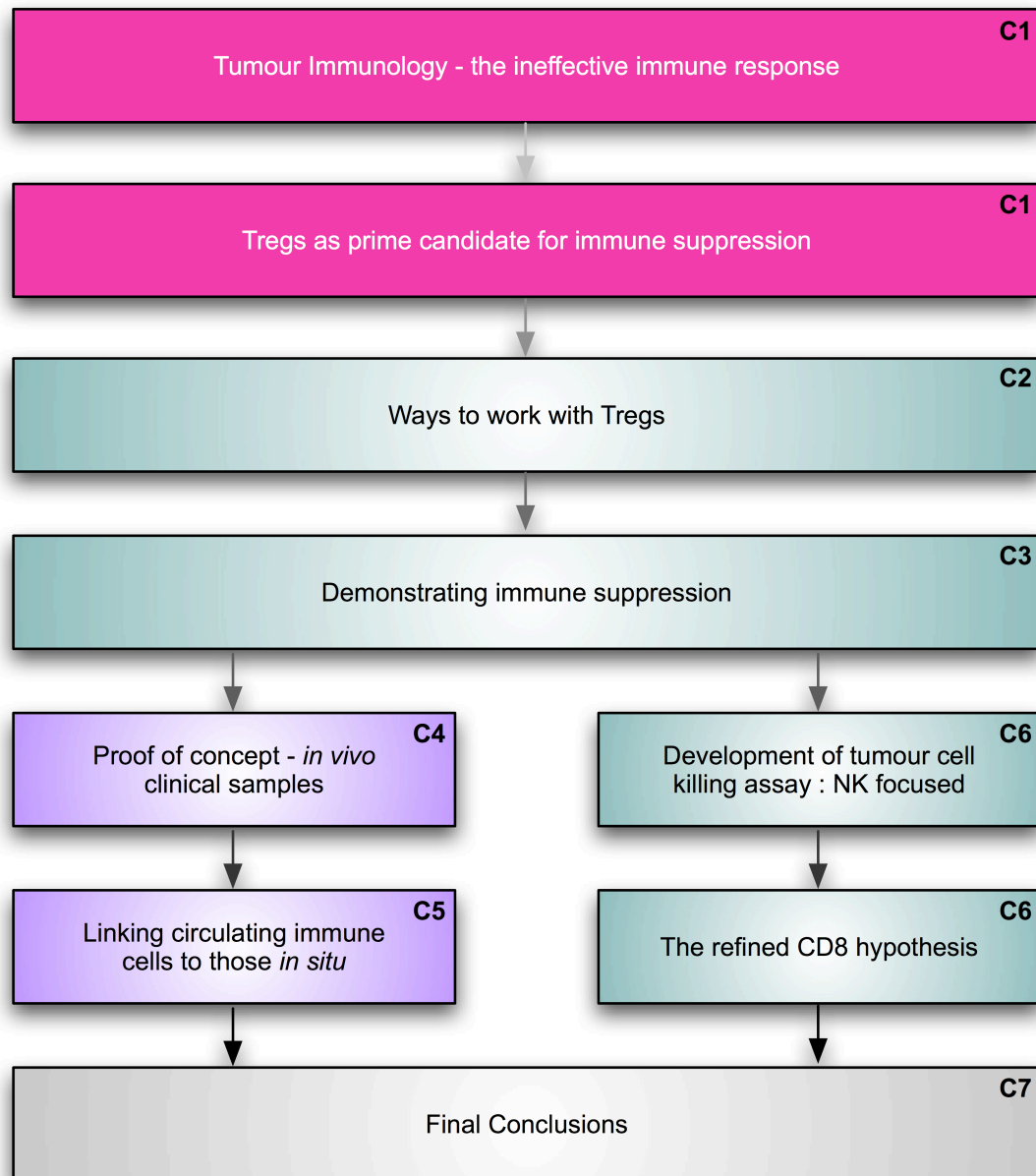
■ Literature ■ *In vitro* ■ *Ex vivo* **C1** Chapter 1

1. CHAPTER ONE

Introduction



Chronological Framework of Thesis Progression



■ Literature ■ *In vitro* ■ *Ex vivo* **C1** Chapter 1

1.1. LITERATURE REVIEW

1.1.1. The Immune System

The immune system evolved to mediate protection from pathogens such as viruses and bacteria, primarily functioning to eliminate infectious agents and to minimise the damage they cause. The site of infection and the characteristics of the pathogen largely determine the immune response, which involves recognition of the pathogen followed by a reaction against it. The immune response is made up of two systems commonly described as innate and adaptive immunity. The innate response involves molecular and cellular components present before the onset of infection and does not alter on repeated exposure. The adaptive response is highly specific to particular pathogens and has an aspect of ‘memory’, improving its function with each successive encounter with the same pathogen (Medzhitov, 2007).

1.1.2. Innate Immune Response

Innate immunity uses primitive non-specific recognition systems to provide what is commonly termed ‘the first line of defence’ from infectious disease. A large proportion of the components involved in the innate immune response are employed prior to infection. They consist of molecular and cellular mechanisms, which confer disease-resistant properties via recognition of common classes of pathogen molecules. An important innate defence mechanism is phagocytosis. Here, phagocytic cells such as macrophages, dendritic cells (DCs), monocytes, and polymorphonuclear neutrophils engulf infectious particles or abnormal cells. Soluble

molecules also play a significant role in innate immunity. Examples include the protein, lysozyme, which is found in mucous secretions and is capable of cleaving bacterial cell walls, and the interferon proteins produced by virus-infected cells, which induce an anti-viral state in neighbouring cells.

1.1.3. Adaptive Immune Response

In contrast to the broad recognition ability of the innate immune response, adaptive immunity has a high degree of specificity, an element of immunologic memory and self non-self recognition (Medzhitov, 2007). An adaptive immune response occurs after the initial exposure and functions in a highly interactive way with the innate immune system. Lymphocytes and the antibodies they produce are central to the adaptive response, coordinating specific recognition of individual pathogens. Lymphocytes can be subdivided into B lymphocytes (B cells) and T lymphocytes (T cells) (Figure 1.1).

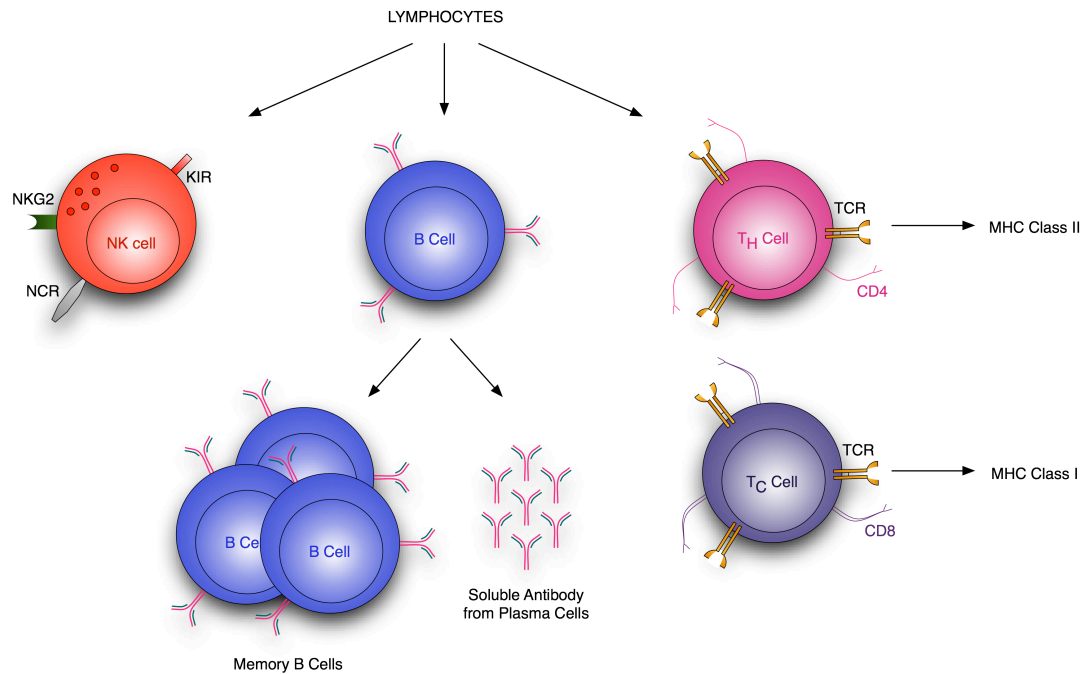


Figure 1.1 Lymphocyte Lineage

Lymphocytes are subdivided into B cells and T cells. Maturation of B cells occurs in the bone marrow, leading to each B cell expressing a solitary antibody molecule. Antigen binding causes division and differentiation of B cells into memory B cells, which express identical antibodies, or effector B cells that secrete the antibody in a soluble form. T cells mature in the thymus and express an exclusive antigen-binding molecule, the T-cell receptor (TCR). T cells are subdivided into T helper (T_H) cells and cytotoxic T (T_C) cells. T_H cells express CD4 and recognise antigen associated with Major Histocompatibility Complex (MHC) Class II, whereas T_C cells express CD8 and recognise antigens bound to MHC Class I. Natural killer (NK) cells are defined as large granular lymphocytes and constitute the third kind of cell from the lymphoid progenitor. They do not have TCRs or surface immunoglobulins but commonly express CD16 and CD56, members of the natural killer group 2 (NKG2) family, natural cytotoxicity receptors (NCRs) and killer cell immunoglobulin-like receptors (KIRs).

B cells mature in the bone marrow and each expresses a unique membrane-bound antibody molecule. The binding of an antigen to a B cell antibody causes rapid division of that cell, which then differentiates into a memory B cell that expresses the same membrane-bound antibody or an effector B cell (plasma cell) that functions to secrete the antibody in a soluble form.

Pluripotent haematological cells in the bone marrow, migrate and mature in the thymus, forming T cells. Mature T cells express an exclusive antigen-binding molecule, the T cell receptor (TCR). T cells can be further subdivided into T helper (T_H) and cytotoxic T (T_C) cells, distinguished by the presence of CD4 (T_H) or CD8 (T_C) membrane glycoproteins (Figure 1.1). T cells recognise antigens that are bound to specific antigen-presenting domains of major histocompatibility complex (MHC) molecules (Figure 1.2). There are two types of MHC molecules, class I MHC and class II MHC, which can bind a broad spectrum of antigenic peptides. T_H cells generally recognise MHC class II bound antigens and T_C cells recognise antigens bound to MHC class I molecules.

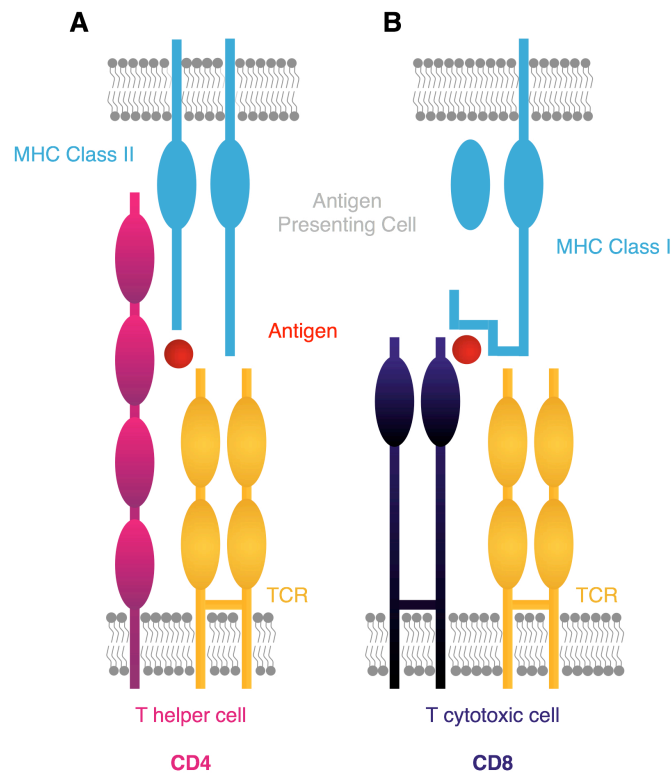


Figure 1.2 The Specific Interaction between Antigen-Presenting Cells and T Cells via Major Histocompatibility Complex (MHC) Molecules.

A) CD4 T helper cells (pink) recognise antigens bound to class II MHC molecules on antigen-presenting cells. B) CD8 T cytotoxic cells (dark blue) recognise only antigens associated with class I MHC molecules. The ovals in the diagrams represent characteristic protein folds. Figure adapted from Kuby et al., 2007.

Antigen-presenting cells (APCs) are phagocytic cells that present fragments of engulfed particles on their surface. T cells can interact with phagocytic cells to aid in the destruction of engulfed particles. The digested particles are firstly cut into oligonucleotides that are 18–22 amino acids long and then loaded onto MHC class II molecules. These are then presented to $CD4^+$ T_H cells, which in turn causes activation of B cells to produce antibodies that exclusively recognise the specific antigen. Antibodies produced as a consequence of antigen presentation are released into circulation and upon binding result in neutralisation of the infectious particle.

1.1.4. Natural Killer Cells

First described in 1975 as a lymphocyte subset capable of cytotoxicity against leukaemia cells (Kiessling et al., 1975), $CD3^-CD56^+$ Natural killer (NK) cells represent 5–15% of circulating lymphocytes. NK cells have distinct morphological features of larger granular lymphocytes (LGL) and can be distinguishable from T and B lymphocytes by cytokine profile, surface phenotype and their ability to mediate cytotoxicity against a broad range of targets including tumour cells (Whiteside and Herberman, 1994). They express characteristic cell-surface receptors, such as NK cell receptor protein-1 (termed NK1.1). Mature, circulating NK cells can be distinguished from other peripheral blood mononuclear cells (PBMCs) by a combination of CD56, CD16 and CD2, and the absence of markers such as CD3 and CD14. NK cells are important players in the innate immune system; they require no priming and so confer early protection against tumour transformation and intracellular pathogens. They are cytotoxic towards tumour cells without prior

immunisation, rapidly secreting large amounts of cytokines including interferon- γ (IFN- γ), tumour necrosis factor- α (TNF- α) and chemokine ligands (CCLs) such as CCL3, CCL4 and CCL5 that influence innate and adaptive immune responses (Ghiringhelli et al., 2006; Zimmer et al., 2008).

The mechanisms and molecular basis of NK cell target recognition and interactions between NK cells and their targets are topics that have gained increasing interest. NK cells trigger apoptosis and target cell death in potentially harmful cells via several steps involving intimate contact and the delivery of a lethal dose of granzyme A through the perforin/granzyme pathway. MHC class I molecules are key regulators of NK cell activity that are expressed ubiquitously on healthy cells and provide NK cells with a means of identifying 'self'. Almost all mature NK cells express inhibitory receptors specific for autologous MHC class I molecules, described as the 'missing-self' hypothesis. Several inhibitory receptors for MHC class I molecules have since been identified, including the killer cell immunoglobulin-like receptor (KIR) family and the lectin-like CD94/NKG2a receptor. A network of cell-surface receptors, including members of the natural killer groups 2 (NKG2) family, KIR family and natural cytotoxicity receptors (NCRs), including NKp46, NKp30 and NKp44, orchestrate target cell recognition. These receptors collaborate with cytokine receptors, Toll-like receptor 9 and possibly adhesion molecules to coordinate the recognition and disposal of dangerous cells, whilst avoiding normal autologous cells. The recognition event precedes NK cell binding, involving various cellular adhesion molecules (CAMs). Depending on the repertoire of activating and inhibitory

receptors engaged by tumour cell ligands, NK cells are triggered and activation leads to the exocytosis of secretory lysosomes and the release of their cytotoxic contents (Whiteside and Herberman, 1994). The major cytotoxic proteins are granzymes and perforin. Perforin facilitates the entry of the granzymes into the target cell cytoplasm, which initiates a cascade of intracellular events involving rapid induction of reactive oxygen species (ROS), caspase activation, loss of mitochondrial membrane potential and DNA fragmentation, all leading to target-cell death (Martinvalet et al., 2005).

NK cells have an indisputable role in cell-mediated cytotoxicity and guarding against malignant cells (Wahl et al., 2006). NK cells also coordinate the transition between innate and adaptive immune responses through interactions with DCs and secretion of cytokines and chemokines. Evidence supports the hypothesis that NK cells are hindered in eliminating tumour cells and that these innate defenders of the host are subject to suppression by regulatory T cells (Tregs) (Wahl et al., 2006).

In humans, the activating receptor NKG2 member D (NKG2D), is a potent stimulatory immunoreceptor broadly expressed on most NK cells, CD8 T cells, and $\gamma\delta$ T cells (Wiemann et al., 2005). Engagement of NKG2D by its ligand (NKG2DL) results in activation of NK-mediated cell killing and cytokine secretion or co-stimulation of cytotoxic T-lymphocytes (CTLs). NKG2D is a receptor for the stress-inducible and tumour-associated MHC class I chain-related proteins A (MICA) and B (MICB); and members of the cytomegalovirus UL16 binding proteins (ULBP) family ULBP1-4 and REA1G. NKG2DLs are up-regulated in tumours, which should

render the tumour cells sensitive to NKG2D-dependent cell killing. MIC molecules are expressed in association with cell stress, infection or malignant transformation. *In vitro*, cell stress-inducible MIC molecules are expressed by many tumour cell lines and up-regulated upon infection with human *Escherichia coli* (Groh et al., 1999). Expression of NKG2DL on NK-resistant tumour lines has been shown to mediate tumour elimination (Cerwenka et al., 2000) and ectopic expression of NKG2D ligands causes rejection of tumour cells by NK and CTL cells in syngeneic mice (Parmiani 2009), illustrating the relevance of NKG2D signalling in immunosurveillance against tumours. However, tumours have developed multiple ways to evade the NKG2D-mediated immune response (Guerra et al., 2008). Literature illustrates that some tumour cells evade NK lysis by releasing soluble MIC molecules to adjust NKG2D-mediated tumour immune surveillance (Groh et al., 1999). Tumour cells shed NKG2DL, resulting in increased levels in the peripheral blood of cancer patients. This causes reduced cell-surface expression of NKG2D on NK cells, CD8⁺ T cells, and $\gamma\delta$ T cells and evasion of tumour immunity. Shedding of MICA molecules from tumour cells by metalloproteases results in reduced NKG2DL surface density and so further adds to evading NK cell recognition (Groh et al., 1999). Observations also show that the NKG2D receptor undergoes ligand-induced endocytosis followed by degradation (Groh et al., 2002). Discrepancies in NKG2DL mRNA and protein expression suggest some regulation at the post-transcriptional level, possibly controlled by cellular microRNAs (Stern-Ginossar and Mandelboim, 2009). Post-transcriptional regulation of NKG2D ligands permits a rapid response to

stress signals, allowing successful expression without the false effect of fluctuations of mRNA levels.

NK cells and CTLs perform complementary roles in immune responses directed against viruses and tumours (Topham and Hewitt, 2009). CTLs are antigen specific and recognise peptides derived from virus and tumour antigens presented by MHC class I molecules. Down-regulation of MHC class I is often observed in tumours and virus-infected cells, allowing escape of CTL killing. NK cells can continue to recognise and kill cells that have reduced surface expression of MHC class I molecules. MHC class I molecules are recognised by NK cell inhibitory receptors where engagement inhibits NK cell activation and a lack of interaction can activate NK cytotoxicity (Topham and Hewitt, 2009).

Depletion of NK and natural killer T (NKT) cells in mice by administration of the anti-NK1.1 monoclonal antibody (mAb) resulted in a two- or three-fold increase in susceptibility to methylcholanthrene-induced tumour formation compared to control non-NK cell depleted mice (Guerra et al., 2008; Smyth et al., 2001). In humans, patients suffering from Chediak-Higashi syndrome, a disorder that results in abnormal NK cell cytotoxic function, have a 200-fold increased risk of developing malignancy (Kobayashi, 1985). In conclusion, human and mouse studies strongly suggest an important role for NK cells in tumour immunosurveillance.

1.1.5. Regulatory T Cells

The immune system discriminates between self and non-self antigens, establishing and maintaining self-tolerance, while still retaining the ability to initiate appropriate immune responses (Bluestone and Abbas, 2003). Regulation of the immune response is a complex process in which Tregs play a central role. Since their discovery in the 1960s, the notion of ‘suppressive T cells’ has long been debated (Gershon et al., 1967; Gershon and Kondo, 1971). Interest in the concept of T cell-mediated suppression resurfaced in the mid 1990s after a sub-population of CD4⁺ T cells that co-expressed the α -chain of interleukin-2 receptor (IL-2R), CD25, was found to be crucial for the control of auto-reactive T cells *in vivo* (Sakaguchi et al., 1995). The suppressive function of CD4⁺CD25⁺ T cells was demonstrated *in vitro* by inhibiting approximately 80 % of CD25⁻ cell proliferation when at a ratio of one CD25⁺ T cell to four CD25⁻ T cells (Read et al., 1998; Takahashi et al., 1998; Thornton and Shevach, 1998).

It is now well established that Tregs are a distinct lymphocyte lineage, functionally defined as T cells that inhibit an immune response by influencing the activity of another cell type (Colombo and Piconese, 2007; Shevach, 2004). Tregs are capable of regulatory properties that affect a variety of immune cells, including CD4⁺CD25⁻ T cells, CD8⁺ T cells, DCs, NK cells, and B cells (Beyer and Schultze, 2006; Piccirillo and Shevach, 2001) (Figure 1.3).

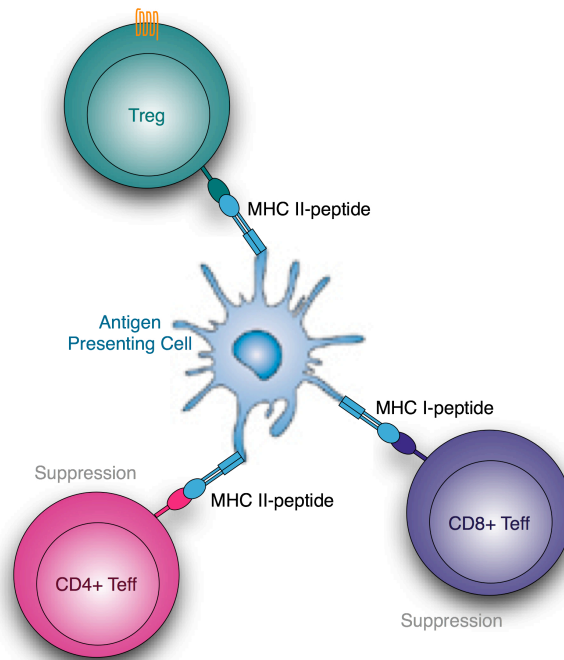


Figure 1.3 Treg Interaction with Neighbouring T Cells

Tregs that recognise a particular antigen may be responsible for suppression of T cells that recognise any other antigen presented by the same antigen-presenting cell. Tregs specific for one antigen can therefore facilitate a tolerance to several antigens.

Tregs are crucial for maintaining peripheral tolerance and the prevention of autoimmunity (Zimmer et al., 2008). However, their mechanism of action still remains an area of active investigation. *In vitro* studies have suggested that Treg-mediated suppression is cell contact dependent, as suppression was not seen when CD25⁺ Tregs and effector T cells were separated by a permeable membrane (Nakamura et al., 2004; Tanchot et al., 2004; Thornton and Shevach, 1998). Several mechanisms of action have been described but the topic still remains controversial and needs further investigation (van Maren et al., 2008; Vignali et al., 2008; Zimmer et al., 2008) (Figure 1.4).

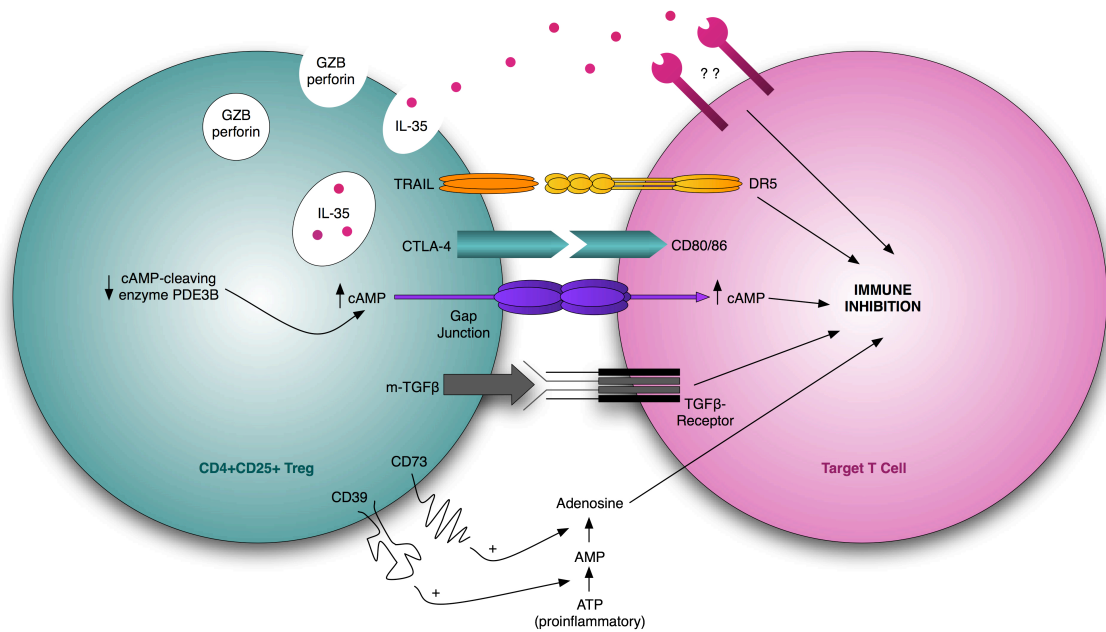


Figure 1.4 Diagrammatic Representation of Proposed Treg Suppressive Mechanisms

A summary of the multiple possible suppressive mechanisms employed by naturally occurring Tregs. Cell contact dependent suppression has been shown to involve cytotoxic T-lymphocyte activation antigen 4 (CTLA-4), membrane bound transforming growth factor β (m-TGF- β) and secretion of granzyme B (GZB) or perforin. The aforementioned suppressive mechanisms cannot explain Treg suppression entirely and so further mechanisms have since been suggested. Expression of the ectonucleotidase CD39 is seen on Tregs and functions to degrade adenosine triphosphate (ATP) into adenosine monophosphates (AMPs) and CD73 catabolises the conversion of AMPs into adenosine. Removal of pro-inflammatory ATP and subsequent production of immunosuppressive adenosine could function as an additional suppressive mechanism of Tregs. Apoptosis is induced via activation of the tumour necrosis factor (TNF)-related apoptosis-inducing ligand (TRAIL)/death receptor 5 (DR5) pathway. Activated Tregs up-regulate TRAIL, and DR5 is increasingly expressed on activated effector cells. The cAMP-cleaving enzyme phosphodiesterase 3B (PDE3B) is reduced in Tregs, resulting in elevated levels of cAMP. Intracellular transport of cAMP to a target cell occurs via gap junctions and leads to immune suppression from inhibition of cell activation, proliferation and cytokine production. Finally, Interleukin-35 (IL-35) is an inhibitory cytokine preferentially expressed in Tregs that may also confer suppression. Figure adapted from van Maren et al., 2008.

CD25⁺ Tregs represent approximately 7–10 % of peripheral CD4⁺ T cells (Rudge et al., 2006). These lymphocytes are specialised in suppressing excessive or inappropriate immune responses, for example, responses to self-antigens in autoimmune disease and environmental substances in allergy. Autoimmune diseases similar to that in humans can be produced in rodent models by depleting the Treg population (Shevach, 2002). However, misplaced Treg responses can impede host protective immunity in infectious disease and cancer (Sakaguchi and Powrie, 2007).

Treg precursors are derived from bone marrow cells and then mature in the thymus. Thymus developed Tregs are generated in a burst of activity during the early stages of foetal and neonatal T cell development (Itoh et al., 1999). In the thymus CD25⁺Foxp3⁺ differentiated Tregs are activated via stimulation of their TCR complex. Stimulation requires recognition of their specific antigen, presented on MHC class II molecules, and signals through the cytokine receptor γ -chain, CD132 (Huang et al., 2005; Maloy and Powrie, 2005).

This stimulation of precursor T cells results in their maturation or deletion depending on the ‘strength’ of their interaction between the TCR and MHC via what is known as the Goldilocks selection process (Yun and Bevan, 2001). This determines a cell’s fate by initiating apoptosis when a signal is too weak due to lack of MHC recognition or too strong due to recognition of self-antigens. The thymus-induced regulatory cells are CD4⁺ and typically express high levels of IL-2R (CD25) as well as the co-stimulatory molecule CTL antigen 4 (CTLA4) and the TNF-superfamily member

GITR (glucocorticoid-induced TNF receptor family related protein) (Bluestone and Abbas, 2003). The forkhead/winged box helix transcription factor gene, Foxp3, has also been shown to be specifically expressed within the Treg population.

CD4⁺CD25⁺Foxp3⁺ Tregs developed in the thymus are frequently termed ‘natural’ Tregs (nTregs) because they carry out a regulatory function during normal surveillance of self-antigens (Bluestone and Abbas, 2003). Tregs that develop in the periphery are often termed ‘adaptive’ or ‘induced’ Tregs (iTregs). iTregs are generated in the periphery from naïve effector CD4⁺CD25⁻ T cells by stimulation via cytokines such as transforming growth factor (TGF)- β , and IL-2, and also by immature DCs (Thorstenson and Khoruts, 2001; Valencia and Lipsky, 2007). TGF- β is an immunosuppressive cytokine expressed on the surface of CD4⁺CD25⁺ T cells. TGF- β specific antibodies are able to prevent suppression *in vitro* and CD25⁺ Tregs are not able to suppress CD8⁺ cells lacking the TGF- β receptor (Chen et al., 2005). However, it is still unclear whether CD25⁺ Tregs directly produce TGF- β themselves or induce bystander cells to do so. The presence of IL-2 is seen to be important in maintaining the function of Tregs (de la Rosa et al., 2004). IL-2 appears to be dispensable for the development of Tregs in the thymus but essential for their maintenance in the periphery. Activation of naïve CD4⁺ T cells drives them to produce IL-2 and also to express the IL-2 receptor (CD25) (Maloy and Powrie, 2005). Some research suggests that IL-2 is produced by activated effector T cells, and not by Tregs, suggesting that effector T cells need to be activated before Tregs can be activated (Rudge et al., 2006).

Although the concept of thymus- and periphery-generated Tregs is generally accepted within the literature, some studies have shown that a small percentage of CD4⁺CD25⁻ cells express Foxp3, and these cells can gain CD25 expression when transferred into a lymphopenic environment (Zelenay et al., 2005).

Natural Tregs are phenotypically in an activated or antigen primed state, which makes them difficult to distinguish from activated effector or memory T cells, as every T cell expresses CD25, CTLA4 and GITR, for example, once activated. High expression of the subtype of receptor for vitamin folic acid, FR4, can distinguish between naïve and activated T cells (Yamaguchi et al., 2007).

1.1.6. Regulatory T Cell Markers

CD25 provides a good marker for Tregs in murine models, as animals can be held under pathogen-free conditions. Humans, however, are constantly exposed to foreign antigens, leading to the possibility of elevated levels of activated CD25⁺ effector T cells.

CTLA-4 and GITR are also among the possible cell-surface markers associated with Treg phenotype and function. CTLA4 interacts with the CD80 and CD86 ligands and has been proposed as a mechanism for mediating contact suppression (Rudge et al., 2006) (Figure 1.4). CD25⁺ Tregs express CTLA4 constitutively on their surface, while effector T cells up-regulate it upon activation (Takahashi et al., 2000). Anti-CTLA4 antibodies abrogate suppression *in vitro* (Takahashi et al., 1998) and

injection of anti-CTLA4 antibody prevents Treg-mediated disease suppression (Liu et al., 2001; Read et al., 2000) and allows tumour rejection (Lee et al., 2004b; Suttmüller et al., 2001).

Tregs are enriched by, but not homogenous, in the expression of these aforementioned markers. In search for more specific Treg markers, it has been proposed that the transcription factor Foxp3 is uniquely expressed by the majority of CD4⁺CD25⁺ Tregs, while it remains virtually undetectable in effector T cells (Fontenot et al., 2003). Research suggests that activation of CD4⁺CD25⁻ T cells does not cause up-regulation of Foxp3, allowing activated and regulatory CD4⁺ cells to be readily distinguished (Rudge et al., 2006). However, the reliability of Foxp3 as a specific Treg marker is still in question due to recent reports on the expression of human Foxp3 in activated T cells without a suppressive phenotype (Beyer and Schultze, 2006). Although human CD4⁺CD25^{high} T cells are most enriched for Foxp3⁺ T cells, some research has shown Foxp3⁺ cells within the CD4⁺CD25^{low} T cell population (Beyer and Schultze, 2006). Morgan *et al* revealed Foxp3 mRNA expression in both CD25⁻ PBMCs and CD8⁺ cells (Morgan et al., 2005). The lack of more specific Treg markers is a major reason why many functionally relevant aspects of Tregs are still unknown (Beyer and Schultze, 2006).

1.1.7. Tumour Immunology

The basic concepts of tumour immunology are a matter of great debate. Cancer cells are indigenous to the body and are therefore in many respects indistinguishable from

the body's normal cells. A key question within tumour immunology has been whether the immune system can recognise cancer cells as a threat and kill them. Over the last decade there has been accumulating evidence suggesting the immune system contributes to tumour defence.

Research has shown that cancer cells display certain distinctive antigens on their surface that may provoke a specific antibody response. Tumour-specific CTLs have been isolated from patients with melanomas and used to identify genes encoding tumour-associated antigens (TAAs). CD8 CTLs recognise MHC class I restricted antigens expressed on the surface of tumour cells. These TAAs have included genes identified as cancer testis antigen (CTA), such as MAGE, BAGE and GAGE, which are expressed in many human tumours but not in normal tissue. Evidence for the ability to recognise antigens selectively expressed on autologous tumour cells but absent from autologous normal cells is an attractive target for therapeutic intervention. This characteristic feature of TAAs makes them promising for cancer-specific immunotherapy, opening up new possibilities for immunotherapy of cancer, including the induction of a tumour-specific CTL response against defined tumour antigens (Mami-Chouaib et al., 2002). Research has identified a large number of tumour antigens from cancer patients; however, loss of TAA expression and secretion of immunosuppressive cytokines are some of the main mechanisms in which tumours evade CTL recognition (Gilboa, 1999).

1.1.8. Regulatory T Cells in Cancer

An increase in the number of Tregs leads to an imbalance in the immune system, which then favours unresponsiveness. This situation is evident in cancer, to the point where tumours are no longer attacked by immune cells (Colombo and Piconese, 2007). Cancer-bearing hosts provide a favourable environment for Treg expansion as a large panel of cancers overexpress TGF- β , which correlate with advanced stages of malignancy and decreased survival (Yamaguchi et al., 2007). The involvement of Tregs in cancer has been described in three separate stages: elimination, representing the host-protective actions of immunity; equilibrium, which potentially maintains cancer in a dormant state; and escape, where tumours emerge and grow in an unrestrained manner. The involvement of the immune system in detecting, eliminating and promoting tumour growth has loosely been termed ‘cancer immunoediting’ (Bui et al., 2006; Dunn et al., 2002; Schreiber et al., 2011).

Many studies have illustrated an increase in the prevalence of Tregs in cancer patients. Elevated levels of Tregs are seen in the peripheral blood (PB) of breast and pancreas cancer patients, where IL-10 and TGF- β secreting Tregs have been found in tumour-infiltrating lymphocytes (TILs) and regional lymph nodes infiltrated by tumour (Liyanage et al., 2002). Research has also shown significant increases in the proportions of CD4⁺CD25⁺ T cells in PB, tumours, and ascites of patients with non-small cell lung cancer (NSCLC) and late-stage ovarian cancer (OVC) (Woo et al., 2001). The frequency of CD4⁺CD25⁺Foxp3⁺ Tregs in peripheral blood lymphocytes (PBLs) has also been reported as being elevated in gastric and oesophageal cancer

patients (Mizukami et al., 2008a). However, in contrast, no significant increase in PBL Treg frequency was observed in patients with gastric cancer compared to normal healthy donors (Mizukami et al., 2008b).

Current evidence indicates that failure of endogenous tumour surveillance mechanisms can result in tumour progression via escaping immune recognition and the anti-tumour immune response (Bui et al., 2006). Patients with elevated Treg levels show reduced survival rates, and the accumulation of Tregs is related to disease progression (Mizukami et al., 2008b; Wolf et al., 2005). Evidence suggests that depleting Tregs leads to rejection of transplanted tumours in murine models (Shimizu et al., 1999).

Having studied the accumulation of Tregs within cancer, it is also important to understand the trafficking behaviour of Tregs and their localisation to and within the tumour microenvironment. Tumour-related factors mediate Treg trafficking to the microenvironment of a tumour. The macrophage-derived chemokine, CCL22, has been shown to induce the migration of Tregs through its receptor CCR4 and impair anti-tumour immunity in ovarian cancer (Curiel et al., 2004). Tregs can also migrate in response to CCL17 via the same CCR4 receptor (Ishida and Ueda, 2006). Tregs strongly express CCR4 on their surface. The mechanism for CCL22 and CCL17 up-regulation has not yet been clarified; however, it has been suggested that the tumour microenvironment induces macrophages to secrete these chemokines (Mizukami et al., 2008a). It has also been reported that both CCL17 and CCL22 are produced by DCs (Imai et al., 1999; Vulcano et al., 2001) and a correlation has been observed

between the level of CCL22 and CCL17 and the frequency of Foxp3⁺ Tregs in tumours (Mizukami et al., 2008a). The involvement of Tregs in cancer is summarised in Figure 1.5.

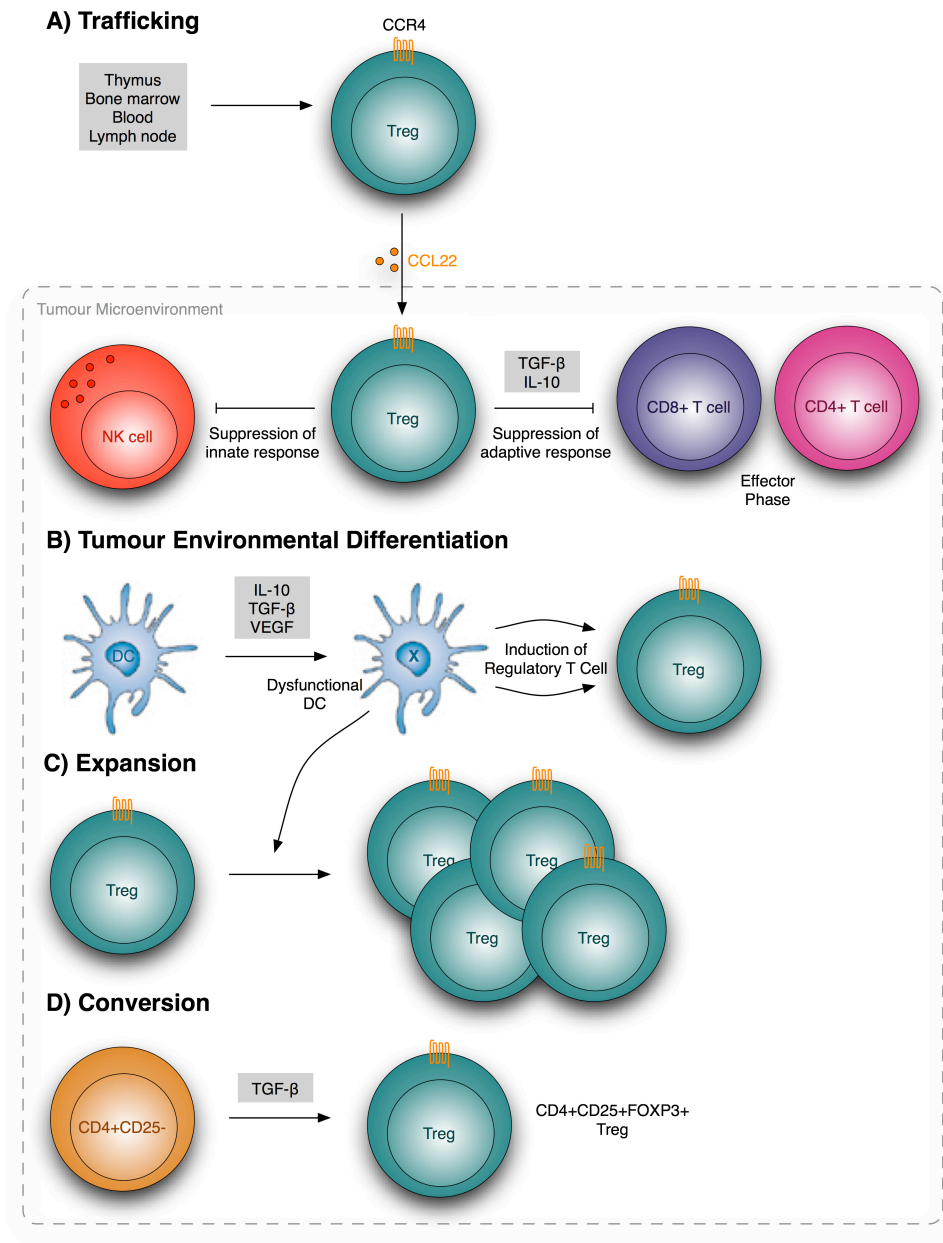


Figure 1.5 Tregs in Cancer

A) The macrophage-derived chemokine, CCL22, facilitates the migration of Tregs into the tumour microenvironment via the CCR4 receptor. Tregs also migrate in response to CCL17 via the same CCR4 receptor. Once in the tumour microenvironment, Tregs function to suppress both the innate and adaptive arms of the immune system. B) Cytokines, including interleukin-10 (IL-10), transforming growth factor- β (TGF- β) and vascular endothelial growth factor (VEGF) within the tumour microenvironment lead to dysfunctional dendritic cells (DCs), which subsequently induce Tregs. Additional expansion occurs through C) the proliferation of pre-existing Tregs and D) the conversion of naïve precursors into 'de novo' induced Tregs. Figure is a graphical compilation of the information within the literature.

Accumulating evidence points to a critical role for Tregs in blunting the anti-tumour immune responses. It is now widely acknowledged that inhibiting Treg function in cancer patients may contribute to the success of new therapies, specifically immunotherapies (Colombo and Piconese, 2007). Although research into Treg biology is intensifying, many questions remain unanswered.

1.1.9. Tumour Morphology and Microenvironment

Weinberg and Hanahan summarised the importance of the tumour microenvironment in their seminal review 'Hallmarks of Cancer' (Hanahan and Weinberg, 2000). A growing number of studies have subsequently demonstrated the association between angiogenesis, infiltrating immune cells and aggressive tumour progression with the tumour microenvironment (Pietras and Ostman, 2010).

The tumour microenvironment is made up of a number of entities, including many different cell types, such as: pericytes, smooth muscle cells, endothelial cells and their precursors, fibroblasts, cancer-associated fibroblasts (CAFs), myofibroblasts, neutrophils, eosinophils, basophils, mast cells, T and B lymphocytes, NK cells, APCs such as macrophages, and DCs (Coussens and Werb, 2002). The dynamic and reciprocal interactions between neoplastic cells and the aforementioned components of the tumour microenvironment orchestrate events involved in tumour development. It therefore becomes as essential to understand the workings of the tumour microenvironment as it is to understand the transformed cancer cells themselves (Lorusso and Ruegg, 2008).

Recent research has focused on the tumour–‘host’ interface, investigating the tumour microenvironment, with a particular interest in the importance of stromal tissue. Malignant cells directly intermingle with components of the stroma and thus stromal elements play a pivotal role in tumour progression. Tumour-associated stroma is a complex medium, previously likened to a wound-healing reaction (Dvorak, 1986).

Initially the tumour microenvironment releases a number of growth factors in response to tumour hypoxia and areas of necrosis. These growth factors, for example, colony stimulating factor (CSF)-1 and TGF- β , are chemoattractive for monocytes and macrophages, which in turn secrete additional growth factors that change tumour cell properties and behaviour. The tumour microenvironment becomes saturated with factors, including vascular endothelial growth factor (VEGF)-A and -C and cyclooxygenase (COX)-2, that stimulate tumour cell proliferation, survival, motility and angiogenesis (Coussens and Werb, 2002; Lorusso and Ruegg, 2008).

Chemokines in the tumour microenvironment recruit cells, rendering the tumour-associated stroma inundated with various different immune infiltrates, including tumour-associated macrophages (TAMs). Elevated numbers of TAMs have been affiliated to tumour initiation and progression (Lin et al., 2007; Lorusso and Ruegg, 2008). Macrophages can assume either an M1 or M2 phenotype. M1 macrophages are activated in response to IFN- γ or microbe exposure and have a high capacity to present antigens. A M1 phenotype is associated with high IL-12 and IL-23

production and activation of a Type I T cell response. It has been suggested that M1 macrophages are cytotoxic towards tumour cells and release high amounts of toxic intermediates such as reactive oxygen intermediates (ROI) and TNF (Allavena et al., 2008). The M2 phenotype is induced by IL-4, IL-13, IL-10 and immune complexes. M2 macrophages have poor antigen presentation and suppress the Type I T_H response. Macrophages with a M2 phenotype are affiliated with tissue re-modelling and promotion of angiogenesis, key contributors to tumour progression and invasion. The tumour microenvironment plays an important role in determining the M1/M2 fate of TAMs.

CAFs are the most predominant cell within the tumour-infiltrating stroma and are found within many cancers (Pietras and Ostman, 2010). Extensive research has highlighted the importance of CAFs and various subtypes of stromal fibroblasts in tumour initiation, progression and metastasis (Anderberg et al., 2009; Camps et al., 1990). CAFs stimulate tumour cell proliferation via an assortment of growth factors, cytokines and hormones. In addition, the ability of tumours to escape apoptosis has been linked to the survival signals they receive from stromal components, including insulin-like growth factor-1 and -2 (LeBedis et al., 2002). CAFs are also providers of extra-cellular matrix (ECM) such as collagen, thought to be involved in malignant growth and invasion due to its cross-linking properties (Levental et al., 2009). CAFs contribute to the epithelial-to-mesenchymal transition of tumour cells by TGF- β and hepatocyte growth factor (HGF) secretion. This facilitates ECM remodelling and the tumour cells' ability to invade surrounding tissue and gain a more metastatic

phenotype (Bhowmick et al., 2004). CAFs also play an important, and well researched, role in angiogenesis. Research has suggested that CAFs produce higher amounts of pro-angiogenic factors than that of tumour cells (Thijssen et al., 2004).

Host fibroblasts (also referred to as myofibroblasts) are differentiated fibroblasts that express α -smooth muscle actin (α -SMA) and have been linked to tumourigenesis. In a study of 192 colorectal cancer (CRC) patients who had samples assessed for α -SMA, high α -SMA expression was associated with significantly poorer overall survival (OS) and shorter disease free survival (DFS) (Tsujino et al., 2007). In addition, mast cells and neutrophils can also support tumour progression by sustaining inflammation and secreting tumour-promoting cytokines (Lorusso and Ruegg, 2008)

Changes in the proportions of stroma within primary tumours could reflect disease progression (Pietras and Ostman, 2010). Intra-tumour stroma percentage has been reported as a prognostic parameter. CRC patients with a high percentage of tumour-associated stroma have been shown to have poorer prognosis, where OS and DFS were significantly lower in patients with high stromal-tumour content (Tsujino et al., 2007; West et al., 2010).

1.1.10. Colorectal Cancer

Despite significant advances in its treatment CRC is still the third most common cause of cancer death in the United Kingdom. The series of events leading to the

development of CRC was first proposed by the Vogelstein group in 1990 and has since been well characterised (Fearon and Vogelstein, 1990). CRC carcinogenesis arises from the accumulation of genetic ‘hits’ that result in the initiation of neoplastic transformation. The tissue first becomes hyperplastic and then follows a particular pattern resulting in disease progression. Genes in the normal epithelium mutate, which leads to the formation of aberrant crypt foci (ACF) and other dysplastic lesions, resulting in benign adenomas. This state of growth can be subdivided into early, intermediate and late adenomas. Disease progression then results in carcinoma development and eventually metastatic carcinoma (Weitz et al., 2005). In addition to the series of events resulting in CRC development, the model also described two key concepts: gatekeeper genes and caretaker genes (Fearon and Vogelstein, 1990). Gatekeeper genes are tumour suppressing genes that often regulate growth, such as the Ras genes and adenomatous polyposis coli genes. Caretaker genes are involved in the maintenance of genetic stability. The series of events contributing to CRC development are summarised in Figure 1.6.

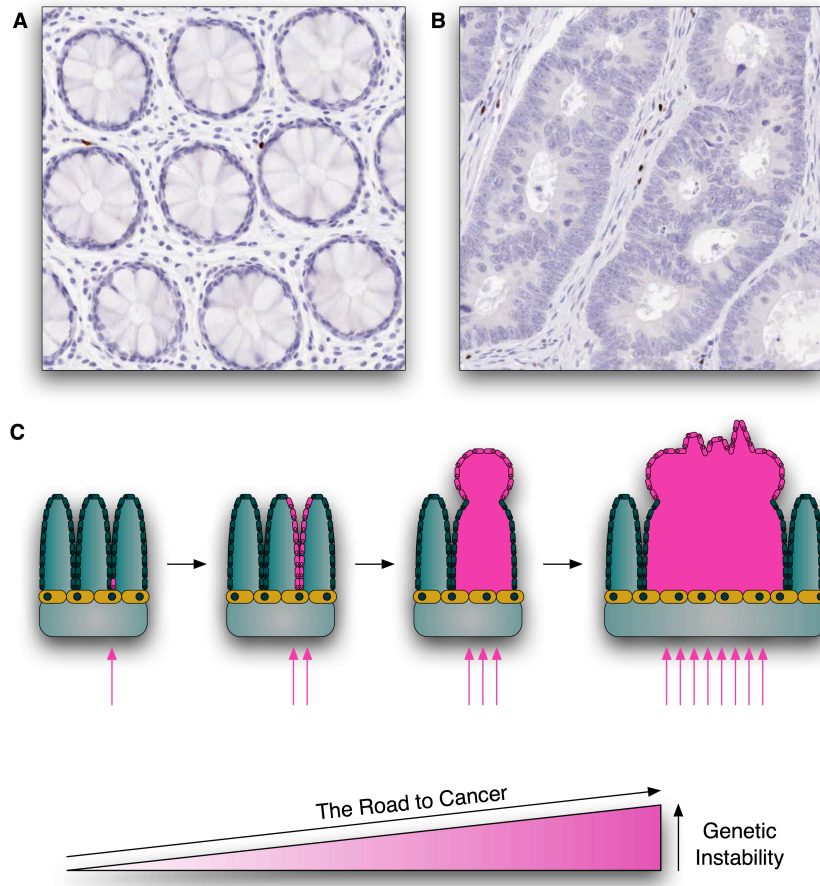


Figure 1.6 The Onset and Development of CRC

Example immunohistochemistry images (at x 20 original magnification) highlight the structural changes within the tissue during the development of CRC from A) non-neoplastic highly organised villi to B) the irregular structures observed in tumour tissue. C) The adenoma carcinoma sequence is often initiated by mutations in gatekeeper genes, which regulate cell growth, such as the adenomatous polyposis coli and RAS gene, in addition to other tumour suppressor genes. Repeated 'hits' (pink arrows) result in the tissue becoming hyperplastic, forming dysplastic crypts. Disease progression facilitates the formation of aberrant crypt foci (ACF) and adenoma development, which later develops into a carcinoma. Figure is a graphical compilation of the information within the literature.

Following tumour resection, anatomic extent of the tumour is pathologically assessed and assigned a tumour-node-metastatic (TNM) stage. TNM stages are used to estimate post-operative outcome, where the system relies on the tumour depth and absence or presence of nodal and distant metastasis to estimate prognosis and plan treatment (Figure 1.7A).

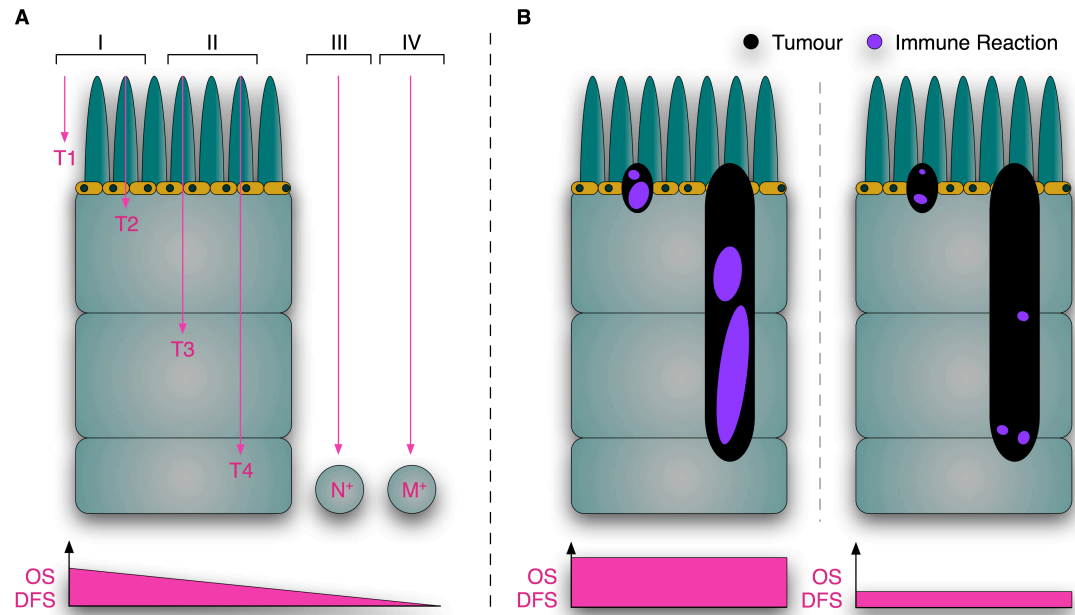


Figure 1.7 TNM Staging of CRC and the Importance of Immune Infiltrates in Disease Progression

A) The tumour-node-metastasis staging classification (I–IV) is based on the extent of the primary tumour (T1–4), and the presence or absence in lymph nodes (N) and distant metastasis (M). The system is far from perfect at predicting clinical outcome, including overall survival (OS) disease-free survival (DFS). B) A strong immune reaction (purple) has been shown to correlate with a favourable prognosis, despite the TNM staging, whereas a weak immune infiltrate is associated with a poor prognosis. Figure adapted from (Pages et al., 2008) and (Galon et al., 2007).

The primary treatment for colon cancer is surgery (TNM I), followed by the addition of chemotherapy for TNM II–III. Adjuvant chemotherapy is recommended for patients with distant metastasis and nodal disease (TNM IV). TNM staging provides a system to classify risk according to disease progression, where localised disease has better prognosis, compared to distant metastasis, which has the worst. However, this system is often imprecise as 20–30 % of TNM I stage patients with localised tumours, experience relapse (Pages et al., 2008). Subsequent research was therefore required to determine a strong prognostic marker, regardless of tumour progression. Galon *et al* have since demonstrated that the prevalence of immune infiltrates and their type, density and location has a prognostic significance superior to those of the TNM stages I–III (Figure 1.7B). It has been suggested that the prevalence of post-surgical immune infiltrates, and not tumour status, is the key indicator for reoccurrence, metastasis and therefore clinical outcome (Galon et al., 2007; Pages et al., 2008).

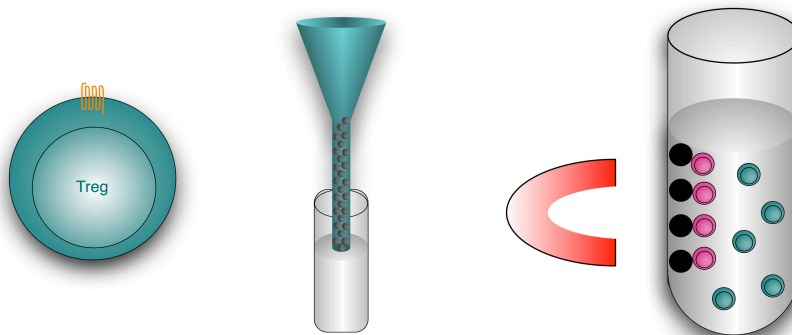
1.2. THE AIMS OF THE CURRENT STUDY

Despite the fact that activated immune cells exist in cancer patients, the immune system often fails to prevent tumour establishment and progression. Increasing evidence supports the essential role of $CD4^+CD25^+Foxp3^+$ Tregs in inducing tolerance to tumours. It is now widely acknowledged that inhibiting Treg function in cancer patients may contribute to the success of new therapies. The aim of this PhD project was to firstly begin to recognise how Tregs function and understand how they are able to suppress such a wide range of cell populations. This involved addressing questions such as: what molecular mechanisms are involved in Treg-mediated

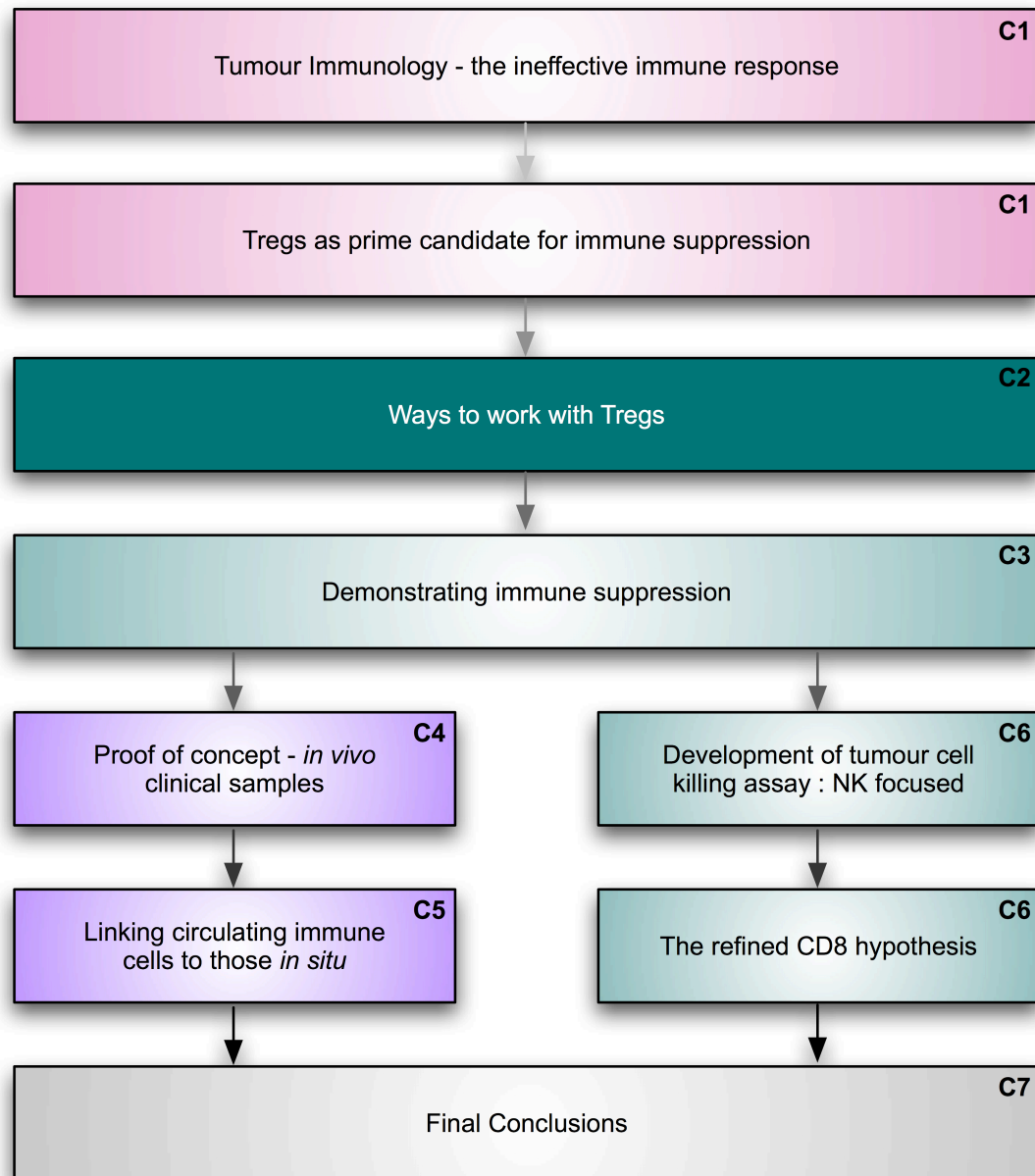
suppression? Is suppression cell contact dependent? Which cytokines, if any, are involved in this suppression? The project then aimed to address whether or not the importance of Tregs highlighted in the literature was reflected in a clinical setting. The study aimed to investigate the significance of immune cell orientation within the tumour microenvironment, understanding the co-localisation between key immune cell subtypes and their correlation with areas of tumour proliferation, apoptosis, hypoxia and vasculature coverage. The comparison of Treg accumulation between cancer patients and healthy volunteers was also scrutinised with the aim of addressing the involvement of Tregs in actively suppressing the anti-tumour immune response, influencing survival rates and disease progression. The aim was to analyse the level of Tregs in the peripheral blood of primary CRC and liver metastatic patients and to investigate whether any correlation existed between this and infiltrating Tregs 'in situ'. The project then aimed to build an *in vitro* human Treg suppression model, initially investigating the interaction between CD4⁺CD25⁺ and CD4⁺CD25⁻ cell populations. Additional levels of complexity were added, incorporating tumour cells and further subdivisions of T-cell populations, including NK cells. The purpose of this model was to gain an insight into the role of Tregs within the tumour microenvironment and suppression of anti-tumour immunity. Initial studies worked with healthy volunteers and then progressed into using liver metastatic patient samples. This *in vitro* model could be employed to screen for Treg targets, initially using small interfering ribonucleic acid (siRNA) and then finally via an antibody directed therapeutic approach. This compilation of assays could provide a platform to validate lead antibodies produced against a selected Treg target.

2. CHAPTER TWO

Ways to Work with Tregs: Isolation and Expansion



Chronological Framework of Thesis Progression



■ Literature ■ *In vitro* ■ *Ex vivo* C1 Chapter 1

CD25⁺ Tregs represent approximately 7–10 % of peripheral CD4⁺ T cells. The first aim of this PhD project was to successfully isolate Tregs for use in subsequent assays. Overcoming problems such as limited cell number and phenotypically distinguishing Tregs from activated effector or memory T cells was a fundamental requirement.

2.1. METHODOLOGY

2.1.1. Fluorescence Activated Cell Sorting (FACS) Protocol

A Beckman Coulter FC 500 flow cytometer allows a sample to be injected into a continuous laminar flow. This formulates a fluid flow system, which draws the sample into a single cell stream that is passed through a perpendicular laser beam. Individual cells cause light to scatter and fluorescent dyes to emit light at various frequencies. Two common measurements taken for each cell are forward scatter (FS) and side scatter (SS). FS gives an approximate size of the cell, whereas SS (detected at 90° to the laser) measures the granularity or complexity of the cell. In a peripheral blood sample, lymphocyte, monocyte and neutrophil populations can be segregated using FS and SS, with debris and dead cells excluded. Fluorescence labelling allows investigation of specific cellular molecules; where fluorescent emissions are collated into corresponding channels.

1×10^6 cells were transferred to fluorescence activated cell sorting (FACS) tubes and washed in 1 ml FACS buffer (2 % foetal calf serum [FCS] in phosphate buffered

saline [PBS]) by centrifugation at $250 \times g$ for 5 minutes. A pre-titrated volume of surface-staining antibody was added and the tubes agitated, followed by a 20-minute incubation step at room temperature, protected from light. Cells were then fixed by adding 1 ml of a commercial fixing buffer (BioLegend) and incubating for 15 minutes at room temperature, protected from light. Cells were centrifuged for 5 minutes at $250 \times g$ and the supernatant removed. If intracellular staining was required, for example for Foxp3, the samples were permeabilised in 1 ml permeabilising buffer (0.1 % w/v saponin in PBS) for 15 minutes at room temperature protected from light. Centrifugation at $250 \times g$ for 5 minutes was carried out and the supernatant removed prior to the addition of a pre-titrated volume of staining antibody in permeabilising buffer for 30 minutes at room temperature, protected from light. Cells were finally washed and re-suspended in 500 μ l FACS buffer and stored at 4 °C until required for analysis.

2.1.2. PBMC Isolation

Histopaque-1077 (Sigma-Aldrich, Cat 1077-1) and isolation buffer (PBS w/o Ca/Mg, 0.1 % bovine serum albumin [BSA], 2 mM ethylenediaminetetraacetic acid [EDTA]) were prepared and brought to room temperature. Blood was taken by venipuncture into a tube containing sodium heparin (250 IU/ml; Heparin Sodium Mucous, CP Pharmaceuticals Ltd, Wrexham UK, BN42073). This was centrifuged at $600 \times g$ for 8 minutes at room temperature, the plasma removed and isolation buffer added to make up to the original volume. 25 ml was then layered over two 20 ml Histopaque-1077 and centrifuged at $800 \times g$ for 20 minutes at room temperature without braking

to form a gradient. PBMCs were recovered from the interface and combined for each donor. This was made up to 35 ml with isolation buffer and layered onto 15 ml of Histopaque-1077 and centrifuged at $160 \times g$ for 20 minutes at room temperature without braking. 20 ml of the supernatant was removed to eliminate platelets and then further centrifuged at $350 \times g$ for 20 minutes at room temperature without braking. PBMCs were recovered from the interface. Cells were washed once in isolation buffer and then centrifuged at $400 \times g$ for 8 minutes at 4°C . Two additional wash steps in isolation buffer were carried out with two $225 \times g$ for 8 minutes at 4°C centrifugation steps. 10 μl was aliquoted and removed for cell counting using a 1:4 dilution with 0.4 % Trypan Blue Solution (Sigma-Aldrich). 1×10^6 cells were removed for FACS analysis.

2.1.3. Regulatory T Cell Isolation

Treg isolation was achieved using a Dynabeads[®] Regulatory CD4⁺CD25⁺ T Cell Kit (Invitrogen, Cat 113.63D) and carried out according to the manufacturer's instructions. In brief, 500 μl isolation buffer, 200 μl foetal bovine serum (FBS) and 200 μl Antibody Mix Human CD4 were added per 5×10^7 of isolated PBMCs and incubated for 20 minutes at 4°C . 10 ml of cold isolation buffer was added to wash cells at $350 \times g$ for 8 minutes. The supernatant was removed and discarded. The cell pellet was re-suspended in 2 ml of cold isolation buffer. 1 ml of re-suspended Depletion MyOne Dynabeads[®] were added, mixed well and incubated for 15 minutes at room temperature with rolling and tilting. The bead-bound cells were re-

suspended by vigorous pipetting, followed by the addition of 3 ml of isolation buffer and placed in the magnet stand for 3 minutes. The supernatant containing the bead-free CD4⁺ T cells was then transferred to a new tube and replaced on the magnet for a further 3 minutes to remove residual Depletion MyOne Dynabeads[®]. 10 µl was removed for cell counting. The cells were centrifuged for 8 minutes at 350 × g and re-suspended in isolation buffer to a concentration of 1.5 × 10⁷ CD4⁺ cells per ml. 1 × 10⁶ cells were removed for FACS analysis.

200 µl of Dynabeads[®] CD25 was added per 1.5 × 10⁷ of CD4⁺ cells. This was mixed well and incubated for 25 minutes at 4 °C with rolling and tilting. This was then placed in the magnet for a minimum of 1 minute before carefully removing the supernatant containing the CD4⁺CD25⁻ (effector) cells. The tube was removed from the magnet and the bead-bound cells were carefully re-suspended in 5 ml isolation buffer by gently shaking the tube. The tube was then returned to the magnet for a minimum of 1 minute and the supernatant removed and discarded. This wash step was then repeated.

Roswell Park Memorial Institute (RPMI)-1640 cell culture media (Sigma, Cat R0883) was prepared (10 % FBS, 2mM L-glutamine, 0.05 mM sodium pyruvate, 0.05 mM non-essential amino acids, 25 mM HEPES Buffer, 0.05 mM 2-mercaptoethanol, 100 IU/ml penicillin, 100 µg/ml streptomycin). Bead-bound cells were re-suspended in 500 µl RPMI (1% FBS). 80 µl of DETACHaBEAD was then added and incubated for 45 minutes at room temperature with tilting and rotation.

This was then transferred to a 15 ml tube. Meanwhile, CD4⁺CD25⁻ cells were counted by trypan blue exclusion and 1×10^6 cells removed for FACS analysis. The tube was then returned to the magnet for a minimum of 1 minute and the supernatant, containing the CD4⁺CD25⁺ cells, carefully removed and transferred to a new tube. The Dynabeads[®] were washed twice in 1 ml RPMI (1 % FBS) to obtain the residual cells the supernatant collected after separation using the magnet. 10 ml of RPMI (1 % FBS) was added to wash the cells, followed by centrifugation for 8 minutes at $350 \times g$. This wash step was then repeated and a 10 μ l aliquot removed for cell counting. The supernatant was discarded and cells re-suspended in culture medium.

2.1.4. *In vitro* Regulatory T Cell Expansion Assay

Isolated Tregs were re-suspended in X Vivo 15 medium (Lonza, BioWhittaker[®] BE04-418F) with 5 % Human AB serum and plated onto round bottom 96-well plates at approximately 1×10^6 cells per ml. 1×10^5 IU/ml of human IL-2 (PeproTech, Cat 200-02) and 10 μ g/ml of purified anti-CD28 super agonist (Ansell, Cat 177-020) were added to positive wells (negative controls contained 5 % AB serum only). Cells were maintained at 37 °C in a humidified atmosphere containing 5 % v/v CO₂ for 28 days, with an additional 5×10^4 IU/ml of IL-2 added every fourth day. Media was changed weekly by centrifuging at $250 \times g$ for 5 minutes and replacing with fresh 5 % AB serum X vivo media containing 1×10^5 IU/ml of human IL-2 and 10 μ g/ml of purified anti-CD28 super agonist. 1×10^6 cells were removed for counting and FACS analysis. Cell surface staining was carried out on fixed cells, looking at

phycoerythrin Cy5 (PeCy5) anti-CD4, Phycoerythrin-Texas red conjugate energy coupled dye (ECD) anti-CD3 and phycoerythrin (PE) anti-CD25, followed by internal staining for Alexa 488 anti-Foxp3 as described in section 2.1.3.

2.2. RESULTS AND DISCUSSION

2.2.1. Human Peripheral Blood Phenotyping

An overall understanding of phenotyping immune cells and analysing different populations via flow cytometric analysis was a fundamental requirement for this study. To facilitate this, healthy volunteers were recruited to donate 50 ml of peripheral blood (PB). PBMCs were isolated over histopaque (section 2.1.2) and 1×10^6 cells were removed for FACS analysis. Polymorphonuclear leucocytes (PMNs) can be distinguished from mononuclear cells by their lobulated nuclei. Fluorescein isothiocyanate (FITC) anti human-CD14 was then used in combination with antibodies against CD4, CD3 and CD25 to distinguish monocytes within the PBMC population (Figure 2.1).

CD14 is a 53–55 kDa glycoprotein expressed on monocytes, interfollicular macrophages and some DCs. The $CD3^-CD25^-CD14^+$ monocytic population is highlighted in blue (Figure 2.1A) and can be easily identified from the lymphocyte population (shown in grey). In addition, specific staining of B cells can be achieved using an anti human-CD19 antibody. CD19 is a 95 kDa transmembrane glycoprotein expressed on B cells during all stages of development, although some follicular DCs can also express CD19. Signalling through CD19 induces tyrosine phosphorylation, calcium flux and proliferation of B cells.

Once the lymphocyte population had been detected, further staining was used to identify the individual immune cell sub-populations, such as CD8. CD8 is a 32–34 kDa cell surface receptor expressed on thymocytes and a subpopulation of mature T cells and NK cells. CD8 binds to MHC class I and, through its association with protein tyrosine kinase p56lck, plays a role in T cell development and activation of mature T cells.

By gating on lymphocytes and then staining with CD4, CD3, CD25 and CD8, various CD8 populations can be distinguished (Figure 2.2). CD8 staining was seen on the $CD4^-$ population and predominantly $CD3^+$, with a smaller fraction of $CD3^-CD8^+$.

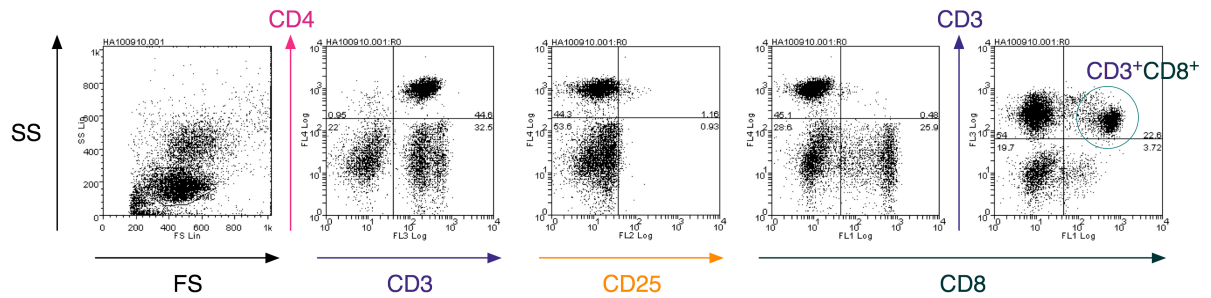


Figure 2.2 CD8 FACS Analysis of Isolated PBMCs

PBMCs were isolated from 50 ml healthy human blood and 1×10^6 cells were removed for FACS analysis. A pre-titrated volume of surface antibodies was added; PeCy5 anti-CD4, ECD anti-CD3, PE anti-CD25 and FITC anti-CD8. Cells were then fixed and data were acquired on a Beckman Coulter FC 500 flow cytometer and analysed using Weasel software.

Tregs are a key immune cell within this study and therefore it was crucial to be able to identify them correctly. Various Treg markers have previously been suggested within the literature. CD25 provides a good marker for Tregs in murine studies, as the animals are often held under pathogen-free conditions and so do not experience any CD25 upregulation. Humans however are constantly exposed to foreign antigens, leading to the possibility of elevated levels of activated CD25⁺ effector T cells. As discussed previously, a large amount of research has been invested into developing human Treg markers (Beyer and Schultze, 2006; Fontenot et al., 2003; Morgan et al., 2005; Rudge et al., 2006).

GITR, L-selectin (CD62L) and CTLA4 are among the possible cell-surface markers suggested to be associated with Treg phenotype and function. CTLA4 interacts with the CD80 and CD86 ligands and has been proposed as a mechanism for mediating contact suppression (Rudge et al., 2006) (Figure 1.4). CD25⁺ Tregs express CTLA4 constitutively on their surface, while effector T cells up-regulate it upon activation (Takahashi et al., 2000). Anti-CTLA4 antibodies abrogate suppression *in vitro* (Takahashi et al., 1998) and injection of anti-CTLA4 antibody prevents Treg mediated disease suppression (Liu et al., 2001; Read et al., 2000) and resulted in tumour rejection (Lee et al., 2004b; Suttmuller et al., 2001).

Tregs are enriched by, but not homogenous in the expression of these aforementioned markers. In search for more specific Treg markers, it has been proposed that the transcription factor Foxp3 is uniquely expressed by the majority of CD4⁺CD25⁺ Tregs, while it remains virtually undetectable in effector T cells (Fontenot et al.,

2003). Research suggests that activation of CD4⁺CD25⁻ T cells does not cause up-regulation of Foxp3, allowing activated and regulatory CD4⁺ cells to be readily distinguished (Rudge et al., 2006). However, the reliability of Foxp3 as a specific Treg marker is still in question due to reports that argue Foxp3 is expressed in human activated T cells without a suppressive phenotype (Beyer and Schultze, 2006). Although human CD4⁺CD25^{high} T cells are mostly enriched for Foxp3⁺, some research has shown Foxp3⁺ cells within the CD4⁺CD25^{low} T cell population (Beyer and Schultze, 2006). Morgan *et al* revealed Foxp3 mRNA expression in both CD25⁻ PBMCs and CD8⁺ cells (Morgan et al., 2005). The lack of more specific Treg markers is a major reason that many functionally relevant aspects of Tregs are still unknown (Beyer and Schultze, 2006). This study uses CD4⁺CD25⁺Foxp3⁺ to identify Tregs (Figure 2.3).

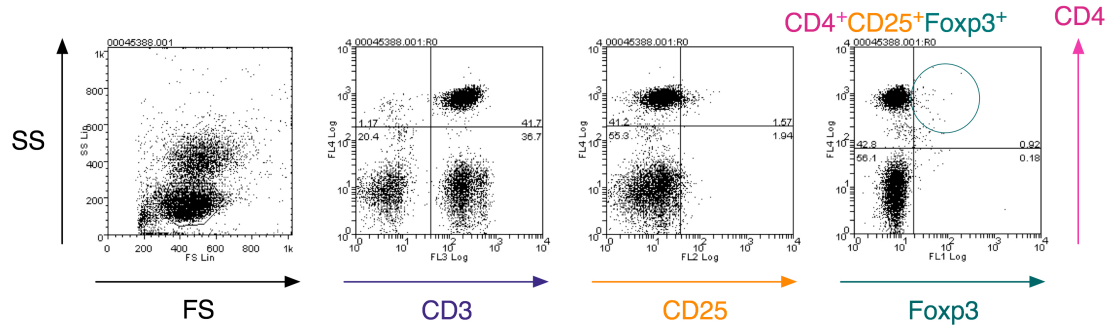


Figure 2.3 Foxp3 FACS Analysis of Isolated PBMCs

PBMCs were isolated from 50 ml healthy human blood and 1×10^6 cells were removed for FACS analysis. A pre-titrated volume of surface antibodies was added; PeCy5 anti-CD4, ECD anti-CD3 and PE anti-CD25. Cells were then fixed and permeabilised followed by intracellular staining using Alexa 488 anti-Foxp3. Data were acquired on a Beckman Coulter FC 500 flow cytometer and analysed using Weasel software.

To further confirm the Treg population used within this study additional characterisation was achieved, including their expression of GITR (Figure 2.4) and CD62L (Figure 2.5), in agreement with previous literature (Rudge et al., 2006)

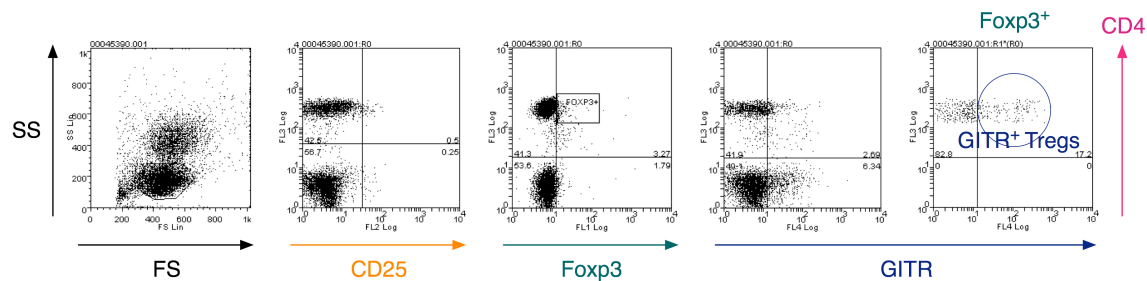


Figure 2.4 GITR FACS Analysis of Isolated PBMCs

PBMCs were isolated from 50 ml healthy human blood and 1×10^6 cells were removed for FACS analysis. A pre-titrated volume of surface antibodies was added: ECD anti-CD4, PE anti-CD25, PeCy5 anti-GITR. Cells were then fixed and permeabilised followed by intracellular staining using Alexa 488 anti-Foxp3. Data were acquired on a Beckman Coulter FC 500 flow cytometer and analysed using Weasel software. Glucocorticoid-induced TNF receptor family related protein (GITR) analysis was carried out on a Foxp3+ gated plot.

Consistent with previous findings, Foxp3 Tregs showed GITR expression. Here we see 17.2 % of Foxp3 gated Tregs expressed GITR (Figure 2.4).

CD62L is expressed on the majority of B cells, naïve T cells and a subset of memory T and NK cells. CD62 binds CD34, GlyCam and MAdCAM-1. CD62L is involved in leukocyte homing, rolling and tethering, but it has also been reported that a neutralising CD62L antibody will inhibit Treg expansion and functionality. Knockdown of Foxp3 has also been shown to reduce the expression of CD62L (Antons et al., 2008). FACS analysis of isolated PBMCs showed an increased CD62L mean intensity (MI) of 29.6 expression on Foxp3⁺ cells compared to a MI of 15.6 on the Foxp3⁻ population (Figure 2.5).

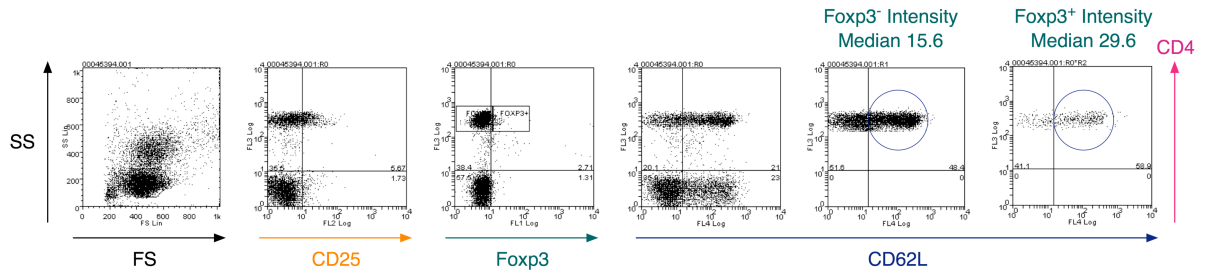


Figure 2.5 CD62L FACS Analysis of Isolated PBMCs

PBMCs were isolated from 50 ml healthy human blood and 1×10^6 cells were removed for FACS analysis. A pre-titrated volume of surface antibodies was added: ECD anti-CD4, PE anti-CD25, PeCy5 anti-CD62L. Cells were then fixed and permeabilised followed by intracellular staining using Alexa 488 anti-Foxp3. Data were acquired on a Beckman Coulter FC 500 flow cytometer and analysed using Weasel software. CD62L analysis was carried out on FOXP3+/- gating and the intensity median is shown.

CD127, also known as the IL-7R α , complexes with CD132 to form the multifunctional IL-7R. CD127 is a type I glycoprotein with a molecular weight of 75–80 kDa and is expressed by immature B cells through the early pre-B stage, by thymocytes during several stages of their development and on most mature T cells, with transient down-regulation upon activation. Binding of IL-7 results in signal transduction, which occurs through several tyrosine kinase pathways, including the Jak/STAT pathway. IL-7 is indispensable for lymphocyte development and the control of homeostatic proliferation of T cells in the periphery. CD127 expression is down-regulated on CD4⁺CD25⁺ Tregs where Foxp3⁺ CD127^{low} are highly enriched for the regulatory T cell phenotype (Gobert et al., 2009). Foxp3⁺ Tregs had a MI of 15.0 for CD127 compared to Foxp3⁻ cells, which showed a CD127 MI of 43.7, in agreement with previous literature (Figure 2.6).

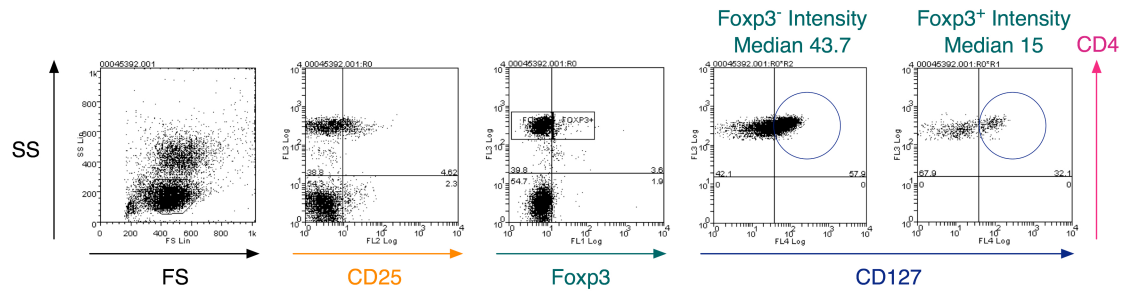


Figure 2.6 CD127 FACS Analysis of Isolated PBMCs

PBMCs were isolated from 50 ml healthy human blood and 1×10^6 cells were removed for FACS analysis. A pre-titrated volume of surface antibodies was added: ECD anti-CD4, PE anti-CD25, PeCy5 anti-CD127. Cells were then fixed and permeabilised followed by intracellular staining using Alexa 488 anti-Foxp3. Data were acquired on a Beckman Coulter FC 500 flow cytometer and analysed using Weasel software. CD127 analysis was carried out on Foxp3⁺/ - gating and the intensity median is shown.

CD4 and CD25 have been the main markers used for Treg isolation, resulting in cells with potent suppressive properties consistent with the literature (Figueroa-Tentori et al., 2008). The identification of Foxp3 has been a key development in facilitating human Treg isolation. Research using mAbs specific for human Foxp3 via intracellular staining has shown that cells expressing the highest levels of intracellular Foxp3 protein also represented the population of CD4 T cells expressing the highest levels of CD25 (Roncador et al., 2005). Unfortunately, research has also demonstrated that many activated (non-regulatory) human T cells can also express Foxp3 (Morgan et al., 2005; Vignali et al., 2008; Wang et al., 2007). Interestingly, it has been shown that Tregs express a high level of folate receptor 4 in comparison to activated effector T cells, a possible method to distinguish the populations (Yamaguchi et al., 2007). It is also important to recognise that Tregs could actually be more of a heterogeneous population, with two distinct subsets classified by expression of MHC class II dimmer human leukocyte antigen (HLA) DR^{+/-} (Baecher-Allan et al., 2006). Therefore, a cocktail of surface markers would perhaps be the preferred option to facilitate the correct isolation and characterisation of Tregs. A growing number of candidates for human Treg-specific cell surface markers have been discussed at length (Vignali et al., 2008; Yi et al., 2006). For this study the following markers were chosen to identify Tregs using FACS analysis: CD3, CD4, CD25, and Foxp3.

2.2.2. Regulatory T Cell Isolation from Human Peripheral Blood

Tregs are relatively infrequent in human blood, ranging from only 1–5 % of T cells. It was therefore integral to this PhD project that efficient protocols for the isolation of PB Tregs were established, in order to allow phenotypical and functional analysis of *ex vivo* Treg populations. The development of a consistent, in-house assay to accomplish reliable Treg isolation was thus a fundamental requirement. There are a variety of commercial Treg isolation kits available. Each kit was tested individually and the isolation data compared, critiquing their Treg recovery and efficiency, both in terms of cost and laboratory time.

2.2.2.1 The Dynabeads[®] Regulatory CD4⁺CD25⁺ T Cell Kit, Invitrogen

The Dynabeads[®] Regulatory CD4⁺CD25⁺ T Cell Kit facilitates Treg isolation from *ex vivo* PBMCs involving a series of steps using magnetic Dynabeads[®] and specific antibodies to sequentially remove various cell populations (Figure 2.7).

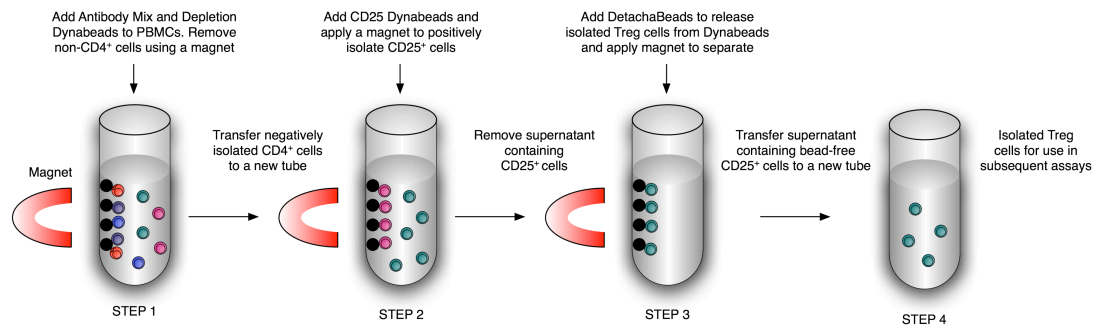


Figure 2.7 Diagrammatic Representation of Dynabeads® CD4+CD25+ T Cell Isolation Kit, Invitrogen

Step 1 involves the use of a magnet to remove non-CD4⁺ cells from peripheral blood mononuclear cells (PBMCs) using an Antibody Mix and Depletion Dynabeads®. CD25 Dynabeads® are then added in Step 2 allowing removal of CD25⁺ effector cells in the supernatant. DETACHaBEADS are then added in Step 3 to separate CD4⁺CD25⁺ Tregs from the magnetic beads to allow use in subsequent assays. Figure adapted from http://invitrogen.com/content/sfs/posters/Treg%20poster_web.pdf.com.

The following cell populations were isolated: CD4⁺ cells, CD4⁺CD25⁻ effector cells and CD4⁺CD25⁺ Tregs. 1×10^6 cells from each isolated population was extracted for FACS analysis (Figure 2.8).

FACS analysis was achieved by firstly gating on the PBMC population based on scatter properties. 37.1 % of the PBMC population was CD3⁺CD4⁺ cells; purity was increased to 88.8 % by sorting for CD4⁺ cells. Within the CD4⁺CD25⁻ effector cell population, only 0.91 % of CD4⁺CD25⁺ cells were observed showing very little contamination of cell populations. The kit then allowed sorting of Tregs (CD4⁺CD25^{high}), where a purity of 71.8 % was achieved, of which 72.1 % were also Foxp3⁺. It has previously been demonstrated in humans that Tregs are best purified if only the 2–3 % of CD4 cells that express the highest levels of CD25 are isolated (Baecher-Allan et al., 2001). Restricting the isolation to CD25^{high} cells increases the homogeneity of the Treg population, as previously indicated by function and by surface expression of CD45RO, CD122, and CD62L^{high} (Baecher-Allan et al., 2001). Data are consistent with published isolations (Bresatz et al., 2007).

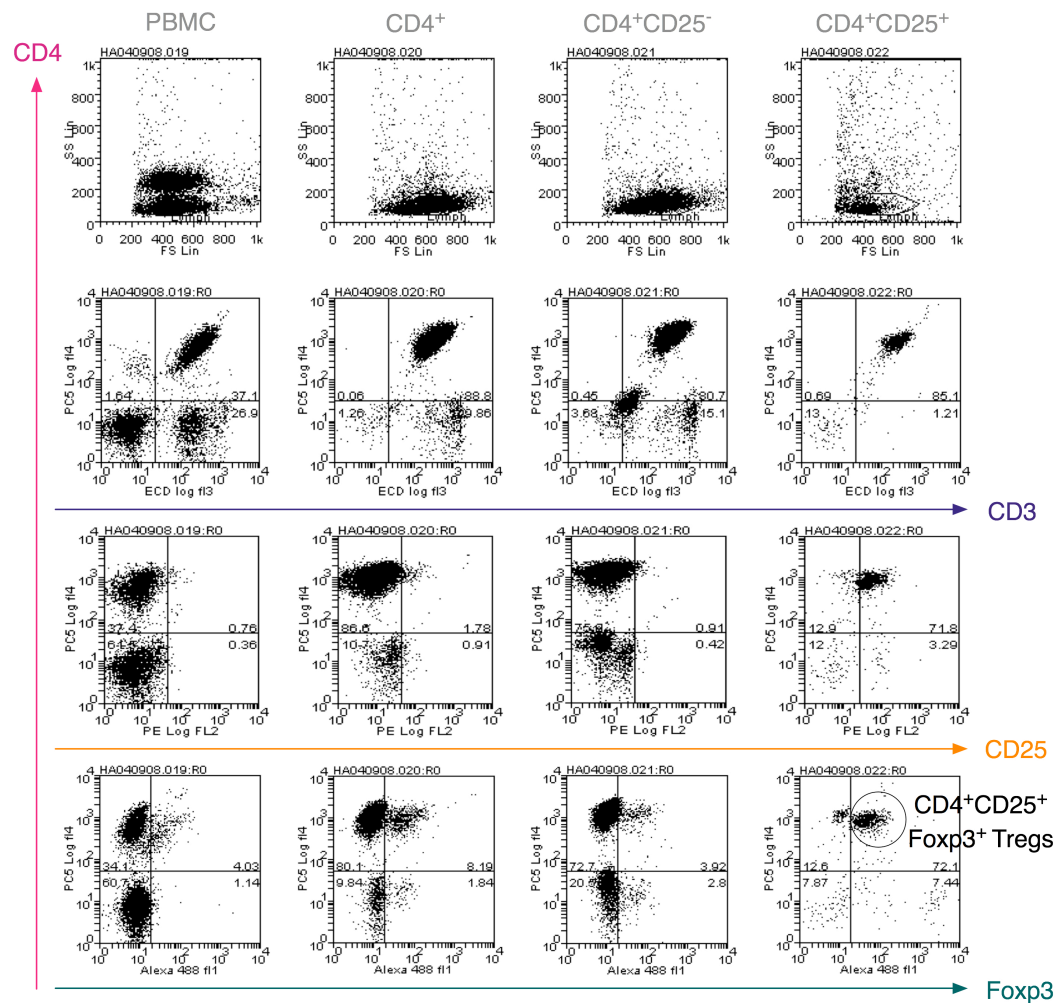


Figure 2.8 FACS Analysis of Treg Isolation Using Invitrogen Dynabeads® CD4⁺CD25⁺ T Cell Isolation Kit

Following the manufacture's protocol, Tregs were isolated from 50 ml healthy human blood using Invitrogen's Dynabeads® CD4⁺CD25⁺ T Cell Isolation Kit, Invitrogen Treg isolation kit. At each cell isolation step 1×10^6 cells were removed for FACS analysis. A pre-titrated volume of the following surface antibodies was added: PeCy5 anti-CD4, ECD anti-CD3 and PE anti-CD25. Cells were then fixed and permeabilised followed by intracellular staining using Alexa 488 anti-Foxp3. Data were acquired on a Beckman Coulter FC 500 flow cytometer and analysed using Weasel software.

2.2.2.2. The MACS[®] CD4⁺CD25⁺ Regulatory T Cell Kit, Miltenyi Biotec

A second isolation kit was then investigated: MACS[®] CD4⁺CD25⁺ Regulatory T Cell Isolation Kit from Miltenyi Biotec. The kit was developed for the isolation of CD4⁺CD25⁺ cells from PBMCs and includes a cocktail of biotinylated antibodies and Anti-Biotin MicroBeads for depletion of non-CD4⁺ T cells and CD25 MicroBeads for subsequent positive selection of the CD4⁺CD25⁺ cells, all carried out on specific columns (Figure 2.9).

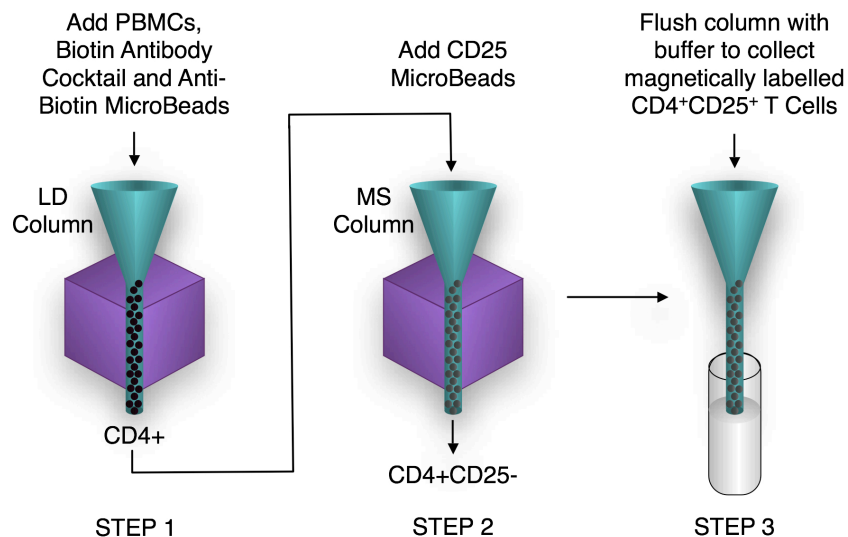


Figure 2.9 Diagrammatic Representation of MACS® CD4⁺CD25⁺ Treg Isolation Kit, Miltenyi Biotec

The kit consists of a cocktail of biotinylated antibodies and anti-biotin MicroBeads for depletion of non-CD4⁺ T cells and CD25 MicroBeads for subsequent positive selection of CD4⁺CD25⁺ cells. Step 1 involves adding peripheral blood mononuclear cells (PBMCs) with Biotin Antibody Cocktail and Anti-Biotin MicroBeads to isolated CD4⁺ cells on an LD Column. These are then added with CD25 MicroBeads in Step 2 and subjected to an MS Column to isolate CD4⁺CD25⁻. The column is then flushed with buffer to elute CD4⁺CD25⁺ cells.

As a comparison to the previous kit, the same cell populations were isolated and 1×10^6 cells were analysed by FACS (Figure 2.10).

Once again the FACS data were gated on the PBMC population and then analysed for CD4 and CD3 expression. 46.1 % of the PBMC population were $CD3^+CD4^+$ and this increased to 97.1 % following the CD4 sort. Only 0.08 % of cells were $CD25^+$ within the $CD4^+CD25^-$ effector cell population. 70.6 % of cells were $CD4^+CD25^+Foxp3^+$; however, the corresponding $CD4^+CD25^+$ population, within the Treg sort, did not correlate, at only 3.24 %.

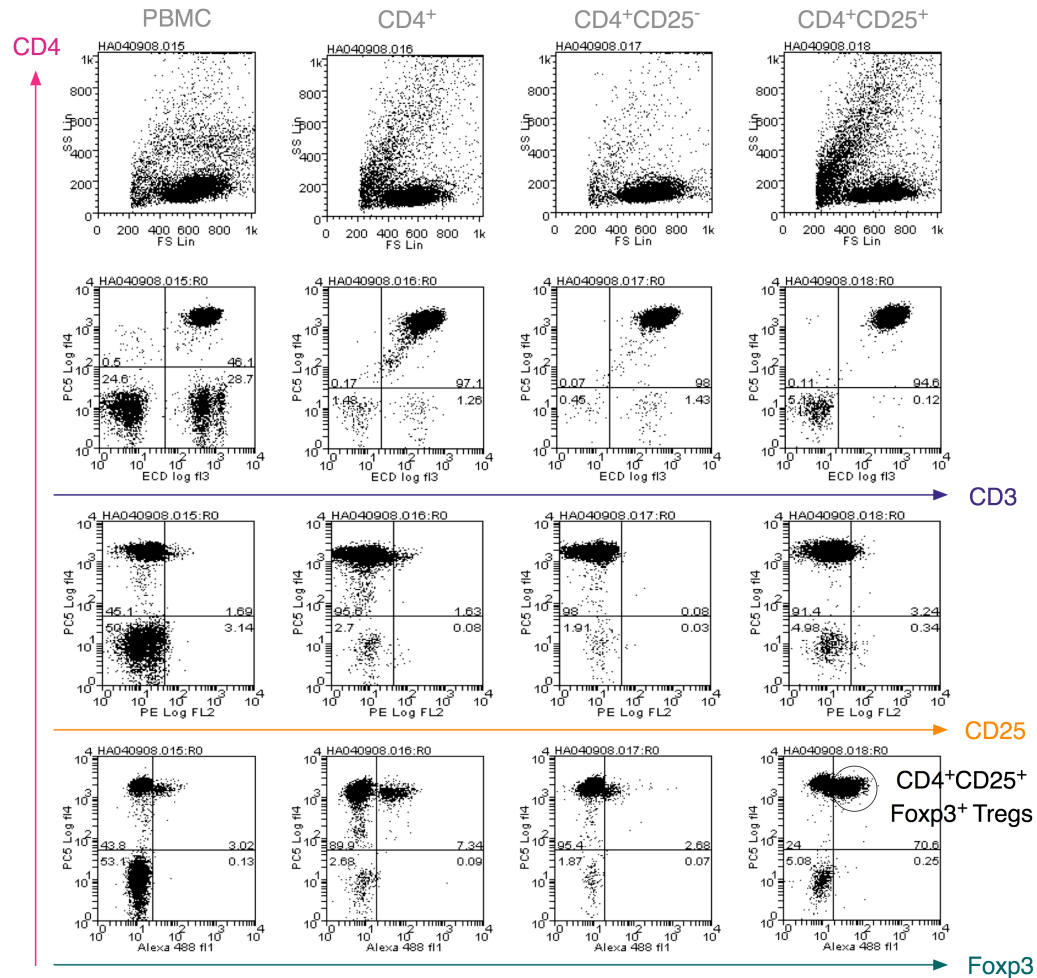


Figure 2.10 FACS Analysis of Treg Isolation Using MACS[®] CD4⁺CD25⁺ Regulatory T Cell Isolation Kit, Miltenyi Biotec

Following the manufacture's protocol, Tregs were isolated from 50 ml healthy human blood using MACS[®] CD4⁺CD25⁺ Regulatory T Cell Isolation Kit. At each cell isolation step 1 x 10⁶ cells were removed for FACS analysis. A pre-titrated volume of the following surface antibodies was added: PeCy5 anti-CD4, ECD anti-CD3 and PE anti-CD25. Cells were then fixed and permeabilised followed by intracellular staining using Alexa 488 anti-Foxp3. Data were acquired on a Beckman Coulter FC 500 flow cytometer and analysed using Weasel software.

It was not possible to do a direct comparison between these two kits, looking at the same patient on the same day, due to the intensity of the work and time restrictions. It is therefore necessary to take into account any discrepancies between samples that may affect the results. However, these data are representative of three individual isolations using both kits.

Conventionally, mouse Tregs have been characterised as $CD4^+CD25^+$ and can be effectively isolated based on staining for expression of these. Trouble arises, however, when isolating human Tregs because activated T cells up-regulate CD25 expression and therefore this affects the purity of the Treg isolation. Consequently, seasonal differences must be taken into account; for example, during influenza or allergy seasons a substantial proportion of human $CD4^+$ T cells may express CD25 (Vignali et al., 2008). Therefore, this must be accounted for when assessing Treg isolations from donors throughout the year.

As $CD25^+$ Tregs only represent approximately 7–10 % of peripheral $CD4^+$ T cells (Rudge et al., 2006), a fundamental difficulty when working with Tregs is the issue of low cell number. Cell numbers from 8 different isolations can be seen in Figure 2.11, highlighting the inter-assay differences and limited Treg numbers.

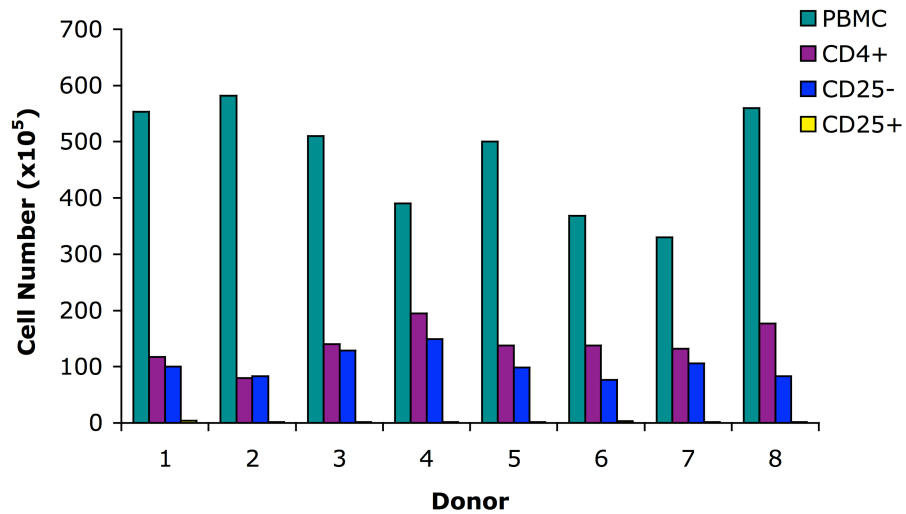


Figure 2.11 Differences in Donor Cell Isolation Numbers Using Invitrogen Dynabeads® CD4⁺CD25⁺ T Cell Isolation Kit

Following the manufacturer's protocol, Tregs were isolated from 50 ml healthy human blood using Invitrogen's Dynabeads® CD4⁺CD25⁺ T Cell Isolation Kit, Invitrogen Treg isolation kit. At each cell isolation step 1×10^6 cells were removed for cell counting.

Additional limitations also apply, including the amount of blood you can take from a volunteer and how frequently you can take blood from the same donor. All these restraints result in limited Treg numbers and so hinder the number and size of assays possible post-isolation.

2.2.3. Expansion of Human Isolated Regulatory T Cells

The constraint of limited Treg numbers from healthy donors has led to the development of Treg expansion protocols (Maloy and Powrie, 2005; Sakaguchi et al., 1995). Maintenance of an undifferentiated cell line of this type would reduce the problem of limited Treg numbers and facilitate cell-based assays to further understand Treg mechanisms. Research has shown that Tregs can be expanded *in vitro* for cell-based therapies, either alone or in combination with DCs (Bresatz et al., 2007).

Tregs are anergic *in vitro* and do not proliferate or produce IL-2 in response to conventional T-cell stimuli (TCR stimulation). This anergy can be broken by the addition of high doses of exogenous IL-2 and anti-CD28 or the use of mature DCs as APCs.

Following the methodology described in 2.1.3, Tregs were isolated and then cultured and expanded over a 3-week period. Treg numbers were calculated at weekly intervals and FACS analysis carried out to assess phenotype (Figure 2.12A).

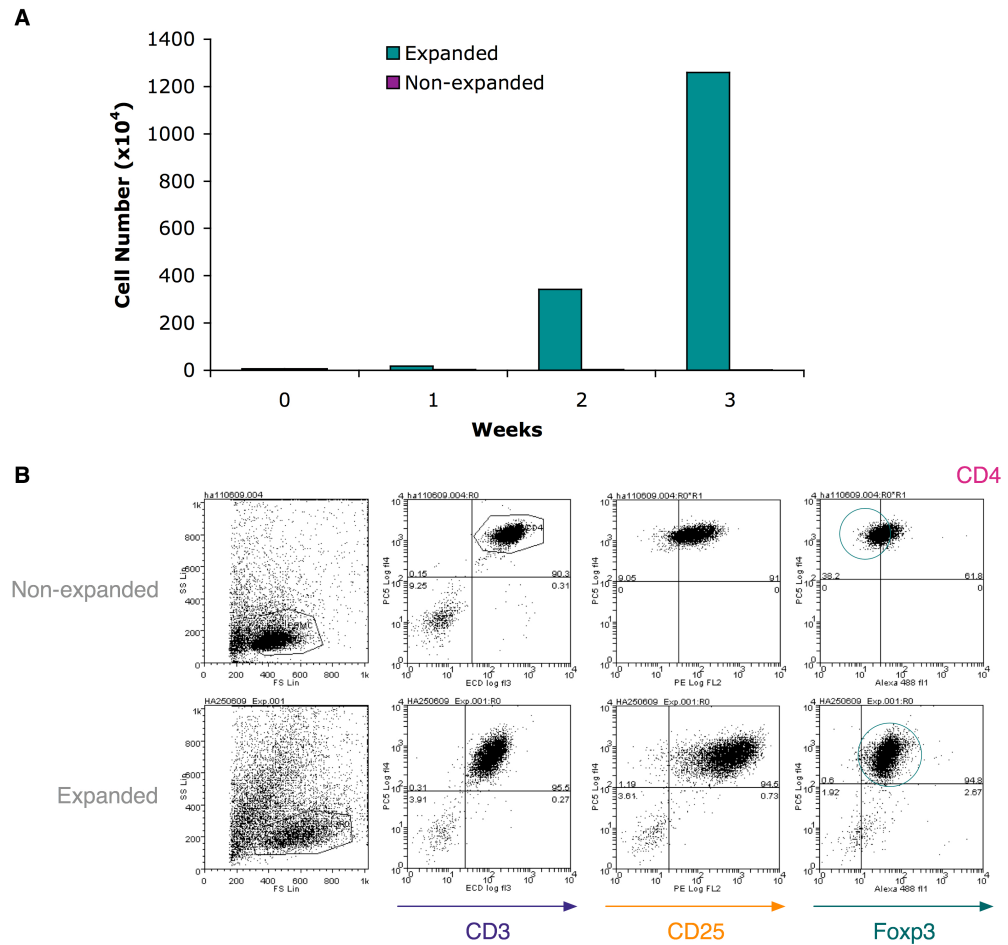


Figure 2.12 Expanded Treg Numbers and FACS Analysis Comparing Populations

A) Tregs were isolated from 50 ml healthy human blood, and re-suspended in X Vivo media (5 % Human AB serum). Cells were split equally into expanded and none expanded populations and plated at approximately 1×10^6 cells per well with 1×10^6 U/ml of human IL-2 and 10 g/ml of purified anti-CD28 super agonist (expanded cells only). Cells were maintained at 37 °C in a humidified atmosphere containing 5 % v/v CO₂ for 28 days, with an additional 5×10^6 IU/ml of IL-2 added every fourth day. Cells were counted and re-seeded with fresh media weekly and 1×10^6 cells removed for FACS. Data are representative of n = 1 experiments. B) Surface staining was carried out on fixed cells, looking at PeCy5 anti-CD4, ECD anti-CD3 and PE anti-CD25, followed by internal staining for Alexa 488 anti-Foxp3. Data were acquired on a Beckman Coulter FC 500 flow cytometer and analysed using Weasel software, comparing initial isolation Tregs to those expanded for 3 weeks.

As seen in Figure 2.12A, Tregs expand in culture from 6.25×10^4 to 1.26×10^7 over 3 weeks. The success of this expansion protocol is reflected in the FACS data (Figure 2.12B), where the Treg phenotype shows little change and purity remains at 94.8 %.

Treg proliferation is not readily observed *in vitro*; therefore questions arise regarding the use of expanded cells to represent a true Treg population.

Research has shown an alternative approach to Treg expansion whereby $CD4^+CD25^+$ T cells are cultured in conditioned medium derived from tumour cells RENCA or TRAMP-C2, which have similar characteristics as those of naturally occurring Tregs such as Foxp3, IL-2 production, high IL-10 and TGF- β .

2.3. CONCLUSIONS AND FUTURE WORK

Although there are conflicting data in the literature with regards to Treg markers, the author is confident that Treg selection based on a $CD4^+CD25^+Foxp3^+$ phenotype was the best choice within the constraints of the current study. Expression of Foxp3 in $CD4^+$ T cells has been shown to correlate with their suppressive ability (Walker et al., 2003). It is the author's opinion that Tregs represent a population of cells that exhibit varying plasticity, perhaps changing their cell-surface expression fingerprint with great fluidity. In an ideal world, a large cohort of markers would be implemented to further distinguish different subtypes of Tregs. Unfortunately, this was beyond the scope of the current study. A decision was required to select the most appropriate markers that would facilitate Treg identification throughout the entire study.

The difficulty in obtaining enough Tregs for experimental work was an underlying problem throughout this study. The number of Tregs was successfully expanded *ex vivo* over a 4-week period. Despite validating the expanded Treg phenotype, the author was apprehensive to solely rely on these cells. By pushing Tregs into a proliferate phenotype, their role in subsequent assays could greatly differ to that of *in vivo* Tregs. For this reason it was decided to use freshly isolated Tregs for all subsequent experiments.

In addition, research has demonstrated the use of Rapamycin to expand both murine and human CD4⁺CD25⁺Foxp3⁺ functional Tregs (Battaglia et al., 2006). Suppression most often involved polyclonal stimulation methods that range from undefined allogeneic responses to mitogenic lectins (phytohemagglutinin [PHA], Concanavalin A [ConA]) or to the use of different mAbs against CD3 in the presence or absence of anti-CD28 co-stimulation. Moreover, stimulation with anti-CD3 or anti-CD28 in different physical forms, such as immobilised versus soluble, or at different concentrations provides different strengths of signal to the target cells, influencing the suppressive ability of the effector cells.

The conversion of CD4⁺CD25⁻ into CD4⁺CD25⁺ cells may provide an additional method to acquire the required numbers of Tregs. Research has shown that CD4⁺CD25⁺ T cells generated as a result of stimulation of CD4⁺CD25⁻ T cells, express Foxp3 and acquire Treg function (Apostolou and von Boehmer, 2004). Anti-CD3 stimulation in the presence of TGF- β *in vitro* has been shown to result in the

stimulation of CD25⁺ Foxp3-expressing suppressor T cells (Apostolou and von Boehmer, 2004). TGF- β plays a critical role in the conversion of CD4⁺CD25⁻ into CD4⁺CD25⁺, demonstrated by using a neutralising TGF- β antibody (Zheng et al., 2004), where mAb TGF- β treatment reduced the conversion of CD4⁺CD25⁻ into Tregs and subsequently Treg mediated suppression of anti-tumour immunity (Zheng et al., 2004). However, similar problems as those faced with expanding Tregs would arise if the conversion, via chronic antigenic stimulation, gave rise to regulatory T cell subsets that appeared to be distinct from natural CD25⁺ suppressor cells.

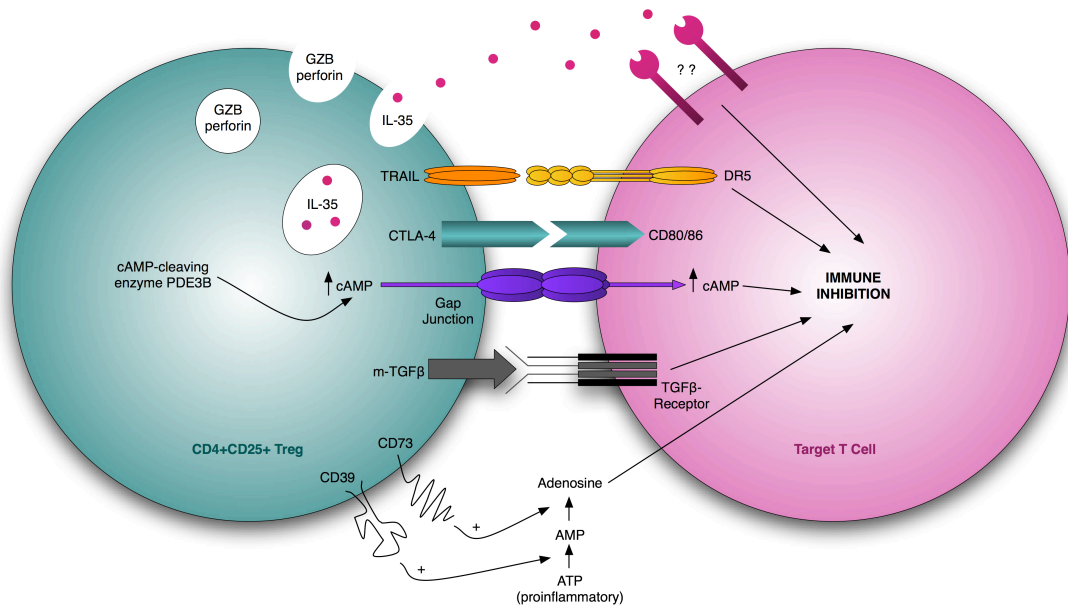
Due to the restraints of obtaining large repeated volumes of healthy PB, future work could include investigation into the use of cord blood. Cord blood is a good source of Tregs because it is available in large quantities, most of which is generally disposed of. The proportion of Tregs in this tissue has been shown to be approximately the same as that observed in adult blood (Bresatz et al., 2007). Further to this, Treg work has been carried out using buffy coat supplied from the National Blood Service, which could be an additional option to overcome any problems with isolation of Tregs from healthy volunteers.

Summary: Identification of Tregs and the ability to distinguish them from other cell types was essential and completed successfully. Regular isolation of Tregs from peripheral blood was a fundamental requirement of this PhD. The development of a consistent, in-house assay to accomplish reliable Treg isolation was therefore a principal requirement. The Dynabeads[®] Regulatory CD4⁺CD25⁺ T Cell Kit provided

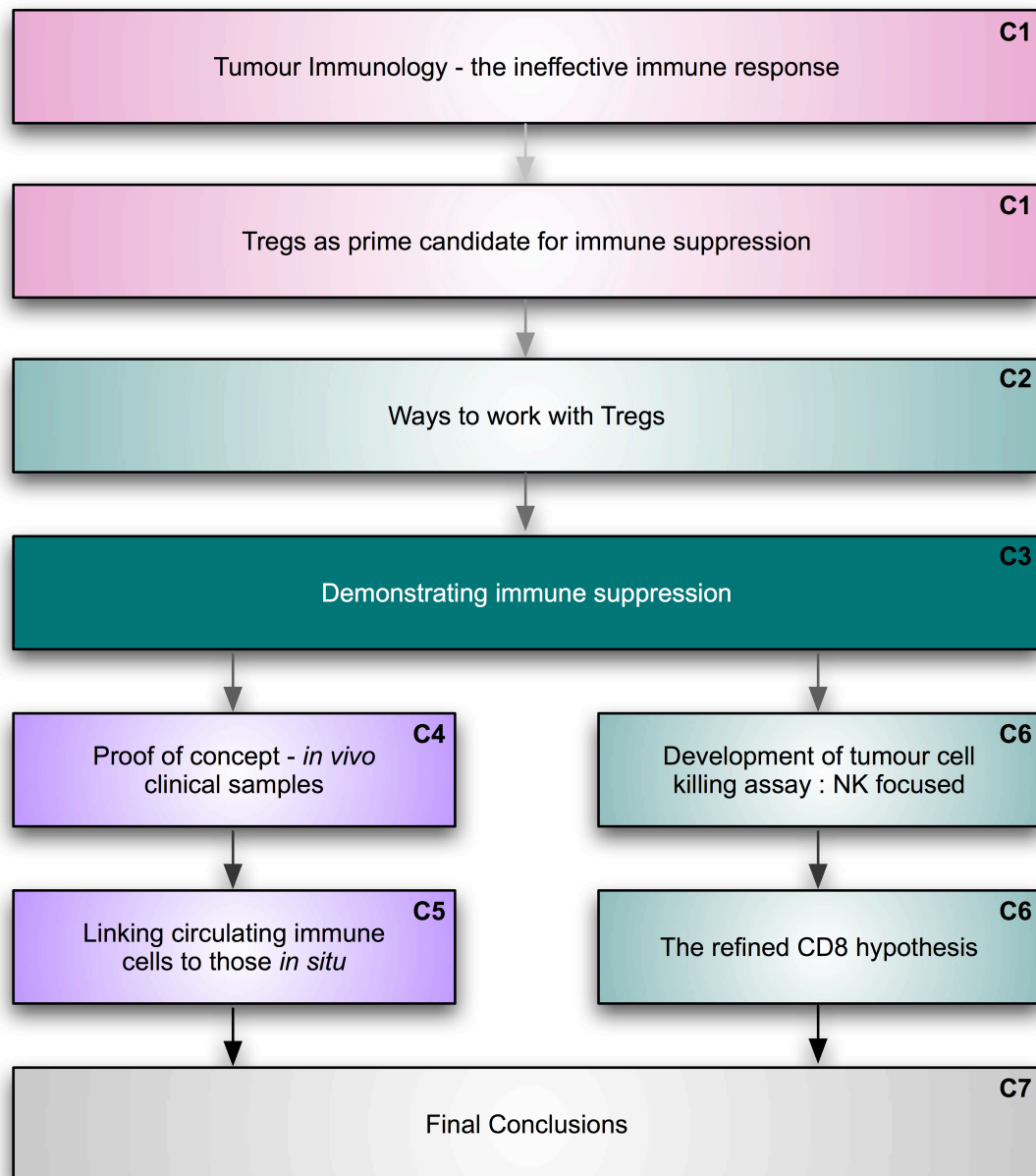
consistently reliable isolation of Tregs to a high level of purity and showed little contamination of other cell types. Successful in vitro expansion of isolated Tregs was achieved using IL-2 and purified anti-CD28 super agonist. Expanded Tregs retained their phenotype, as evaluated by FACS.

3. CHAPTER THREE

Mechanisms of Suppression and Treg Functionality



Chronological Framework of Thesis Progression



■ Literature ■ *In vitro* ■ *Ex vivo* **C1** Chapter 1

A failure of endogenous tumour surveillance can result in tumour progression via active suppression of the anti-tumour immune response. To recognise how Tregs function and understand how they are able to suppress such a wide range of cell populations is vital. This chapter focused on beginning to understand which molecular mechanisms are involved in Treg mediated suppression. Research investigated the importance of cell contact dependency and the involvement of particular cytokines in Treg-mediated effector cell suppression.

3.1. METHODOLOGY

3.1.1. Regulatory T Cell Suppression Assay

The suppressive ability of CD4⁺CD25⁺ Tregs when co-cultured with effector cells is a key requirement to show Treg-mediated suppression activity. Isolated effector cells (section 2.1.1.) were seeded at 5×10^4 cells per well in 100 μ l suppression media (RPMI, 10 % FBS, 0.5 mM Sodium pyruvate, 0.05 mM NeAA, 25 mM HEPES) in a 96-well round bottom Nunc Tissue Culture Plate (Nuclon™ Surface, Cat 163320). Isolated Tregs were then added (50 μ l) at 0:2, 0:1, 1:0 1:5, 1:10, and 1:20 Treg:effector cell ratios. Effector cells were stimulated with 50 μ l of Lectin from *Phaseolus vulgaris* (red kidney bean) PHA (Sigma, L1668-5MG) and Prostate mucin antigen (PMA) or ConA at 10 μ g/ml in a final well volume of 200 μ l. Triplicates of stimulated and non-stimulated wells were carried out for all cell ratios. 0:1 and 0:2 ratios are control wells to illustrate effector cell proliferation, with 0:2 representing the highest number of cells seen in any well to examine any restriction in

proliferation due to elevated cell number and reduced nutrients. Cells were cultured at 37 °C in a humidified atmosphere containing 5 % v/v CO₂ for 96 hours. The suppressive ability of Tregs was then determined via various proliferation assays as described below.

3.1.1.1. Cell Titer 96® Aqueous One Solution Cell Proliferation (MTS) Assay

This assay uses a reagent composed of a tetrazolium compound; 3-(4,5-dimethylthiazol-2-yl)-5-(3-carboxymethoxyphenyl)-2-(4-sulfophenyl)-2H-tetrazolium inner salt (commonly called MTS) and an electron-coupling reagent, phenazine ethosulfate. The reagent consists of 1.9 mg/ml MTS and 300 µM PES in Dulbecco's PBS. Cells chemically reduce MTS into soluble formazan in tissue culture media at 492 nm. MTS measures dehydrogenase enzyme activity found in metabolically active cells and therefore the production of formazan is proportional to cell number and intensity is an indication of cell viability. MTS reagent was added to the cell suspension at a 1:5 dilution and incubated for 3 hours. Cells were quantified using spectrometry at 492 nm against a known standard curve of cell number of the same cell type. Prior to the proliferation assay, 100 µl of the supernatant was carefully removed from each well and stored at – 80 °C until used for enzyme-linked immunosorbent assay (ELISA) analysis.

3.1.1.2. ³H-Thymidine Radioactive Assay

[Methyl-³H]-thymidine (TRA120 aqueous solutions 37 mBq, 1 mCi, B499 185 Gbq/mmol 5 Ci/mmol, Amersham) at 0.5 µCi per well was added for the final 18 hours of a day 5 assay. Plates were harvested on day 5 and, following the addition of scintillation fluid (Microscint™ PerkinElmer, Cat 6013611), were left to dry at 37 °C in a humidified atmosphere containing 5 % v/v CO₂ for 2 hours prior to being read on a Microplate Scintillation & Luminescence Counter (TopCount NXT™, Packard).

3.1.2. Enzyme Linked Immunosorbant Assay (ELISA)

ELISA assays were carried out to investigate the cytokines present in the supernatants of the aforementioned suppression assays. Prior to the addition of [Methyl-³H]-thymidine, 100 µl of the culture media was carefully extracted from each well. This was then stored at – 80 °C until required. ELISA plates were pre-coated with 2 µg/ml purified anti-human IL-10 (BioLegend, Clone JES3-12GB, Cat 501501) or IFN-γ (BioLegend, Clone NIB42, cat 502401) in coating buffer (0.5 M Tris-HCl, pH 8.9) at 50 µl per well and left overnight at 4 °C. Plates were then washed three times in PBS Tween (0.05 % v/v Tween 20) followed by a blocking step in 5 % v/v Marvel for 30 minutes at 37 °C. Three more wash steps were then carried out before plating out a titration of corresponding standard of Recombinant Human IL-10 (Peprotech, Cat 200-10) and IFN-γ (Peprotech, Cat 300-02) at a top concentration of 10 ng/ml and a dilution of × 0.5. 50 µl per well of defrosted supernatant was then added to the plate and incubated for 1 hour 45 minutes at room temperature. Four

wash steps were then carried out preceding the addition 50 µl per well biotin antibodies at 2 µg/ml IFN-γ (BioLegend, Clone 4S.B3, Cat 502504) and 1 µg/ml IL-10 (BioLegend, Clone JES3-12GB, Cat 501502) and incubated for 1 hour and 30 minutes at room temperature. Plates were washed again six times and then 50 µl per well Streptavidin HRP (PharMinutesgen, Cat 554066) was added for 30 minutes at room temperature. A further 10 wash steps were carried out prior to the addition of 50 µl per well HP Solution (1:30 sodium acetate buffer, 1:5 hydrogen peroxide and 1 mg/ml 3,3',5,5'-tetra methylbenzidine dihydrochloride, in H₂O) for 5–30 minutes. The reaction was stopped with 50 µl 2M H₂SO₄ then read on a MRX plate reader (Dynex Technologies) at 450 nm.

3.1.3. Transwell Assay

Isolated effector cells (see parts 2.1.1. of Treg isolation procedure) were seeded at 5×10^4 cells per well in 100 µl media in a 96-well Flat Bottom Costar Tissue Culture Plate (3513). Tregs or Karpas-299 cells were then seeded onto membrane inserts with a pore size of 0.4 µm (Corning® Transwell™ Permeable Supports) at 1:5, 1:10 and 1:20 ratios in 50 µl of media. Effector cells were stimulated with a combination of 10 µg/ml PHA in a final well volume of 200 µl. Triplicates of stimulated and non-stimulated wells were carried out for all cell ratios. Plates were then incubated for 96 hours at 37 °C, 5 % v/v CO₂. The suppressive ability of Tregs or Karpas-299 cells was then determined via methyl-³H-thymidine incorporation as described previously.

3.1.4. Method of Statistical Analysis

Data points were in triplicate and graphically expressed as the mean, where error bars depicted standard deviation (SD). Further analysis was then carried out to quantify any trends in the data, using Prism® 5 software. To analyse the repeat measured data within this chapter, a one way analysis of variance (ANOVA) was firstly implemented to determine any significant differences. A Tukey's multiple comparison post test was then implemented to further distinguish p values between data groups.

3.1.5. Ethics Approval

All samples were acquired with written informed consent and given ethical approval by Nottingham Research Ethics Committee, REC reference BT/04/2005, first granted in 2005.

3.2. RESULTS AND DISCUSSION

Tregs are involved in suppressive control of a broad spectrum of immune responses, encompassing those against autologous tumour cells, allergens, pathogenic microbes, allogeneic organ transplants and the foetus during pregnancy (Miyara and Sakaguchi, 2007). $CD4^+CD25^+$ Tregs are potent immuno-suppressors that are critical in the maintenance of self-tolerance (Bresatz et al., 2007).

The ability of CD4⁺CD25⁺ Tregs to suppress activated T cells has been demonstrated clearly in both murine (Sakaguchi et al., 1995) and human (Levings et al., 2001; Stephens et al., 2001) studies. Identification of Foxp3 established a link between the CD4⁺CD25⁺ Treg suppression of auto-reactive T cells. This correlation between Foxp3 expression and suppressor function has been well established in murine models (Fontenot et al., 2003; Kasprowicz et al., 2003) and to a lesser degree in humans (Kuniyasu et al., 2000; Peng et al., 2004).

3.2.1. Suppression Assay Protocol Optimisation

Human T cell suppressor function may be assayed using isolated human PB Tregs and stimulated T effector cells. Tregs inhibit the proliferation of CD4⁺CD25⁻ effector cells, providing an *in vitro* culture assays model to potentially assess their *in vivo* suppressive ability. A variety of assay methods have previously been utilised and various techniques used to quantify suppression. Protocol optimisation was therefore essential, investigating assay technique, cell populations and effector cell stimulants.

Initially, the Cell Titer 96® Aqueous One Solution Cell Proliferation Assay, utilising MTS, was investigated (as described in section 3.1.1.1). Preliminary experiments studied the suppressive effects of CD4⁺CD25⁺ Tregs on stimulated PBMCs (Figure 3.1).

The MTS experiment required a preliminary cell titration assay in order to extrapolate cell number. The assay investigated 1.5, 2, 3 and 20 hour incubation periods of MTS

reagent, in order to determine optimal conditions for subsequent suppression assays (data not shown). It was decided that 3 hours gave optimal results, providing a compromise between assay time and reliability. Suppression assays were then carried out to investigate the effects of isolated CD4⁺CD25⁺ Tregs co-cultured stimulated PBMCs with ConA (Figure 3.1A) or a combination of PHA and PMA (Figure 3.1B).

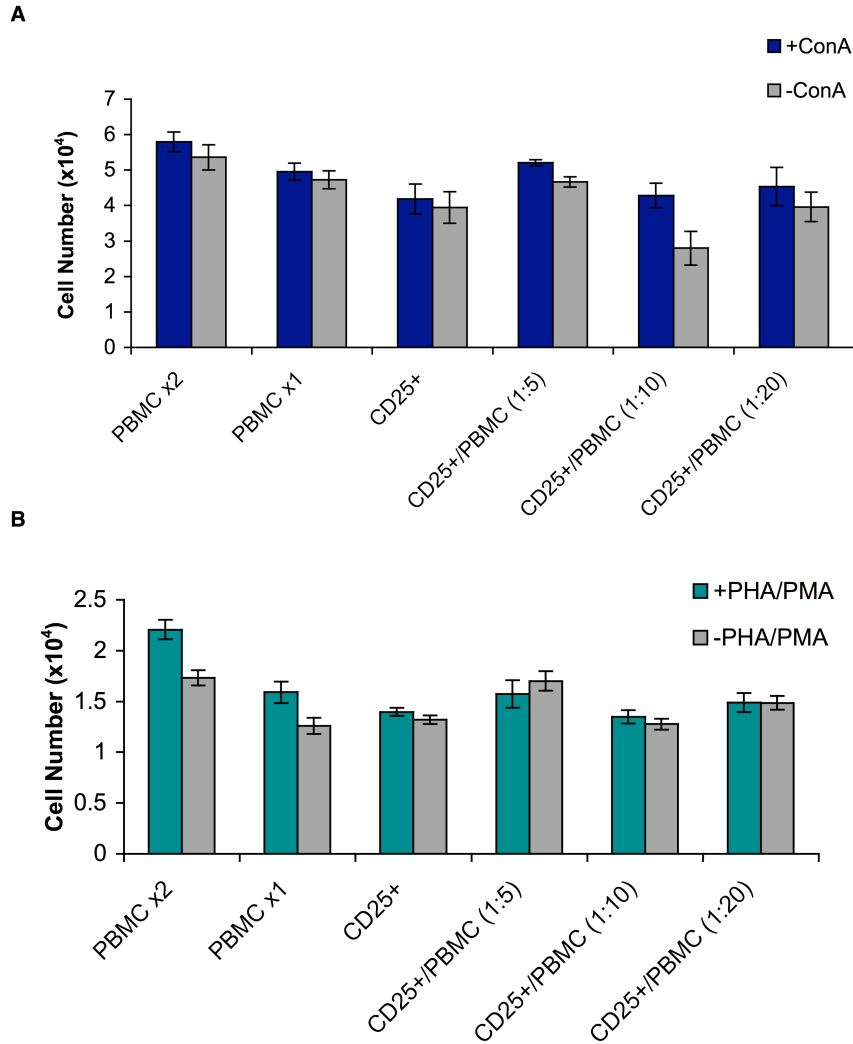


Figure 3.1 Treg Suppression of ConA or PHA/PMA Stimulated PBMCs, MTS

CD4⁺CD25⁺ Tregs and peripheral blood mononuclear cells (PBMCs) were isolated from 50 ml blood from a healthy volunteer, as previously described. PBMCs, stimulated with either A) Concavalin A (ConA) or B) a combination of Phytohemagglutinin (PHA) and Prostate mucin antigen (PMA), were plated at 5×10^4 cells per well. CD4⁺CD25⁺ cells were then added at 0:2, 0:1, 1:0, 1:5, 1:10 and 1:20 Treg:PBMC cell ratios. Cells were cultured at 37 °C in a humidified atmosphere containing 5 % v/v CO₂ for 96 hours. A 1:5 dilution of MTS reagent was added for 3 hours and suppression quantified using a spectrometry at 492 nm against a known standard curve of PBMC cell number. Results were evaluated using Prism 5. Data are a mean of triplicates from a single plate (\pm SD), statistically analysed using a one way ANOVA and Tukey's multiple comparison post-test (ns).

Results indicated a lack of significant Treg suppressive activity against stimulated PBMCs with both ConA and PHA/PMA. The MTS read out was very low and made extrapolation of cell number difficult. It was therefore decided to use isolated CD4⁺CD25⁻ effector cells to increase suppression susceptibility (Figure 3.2).

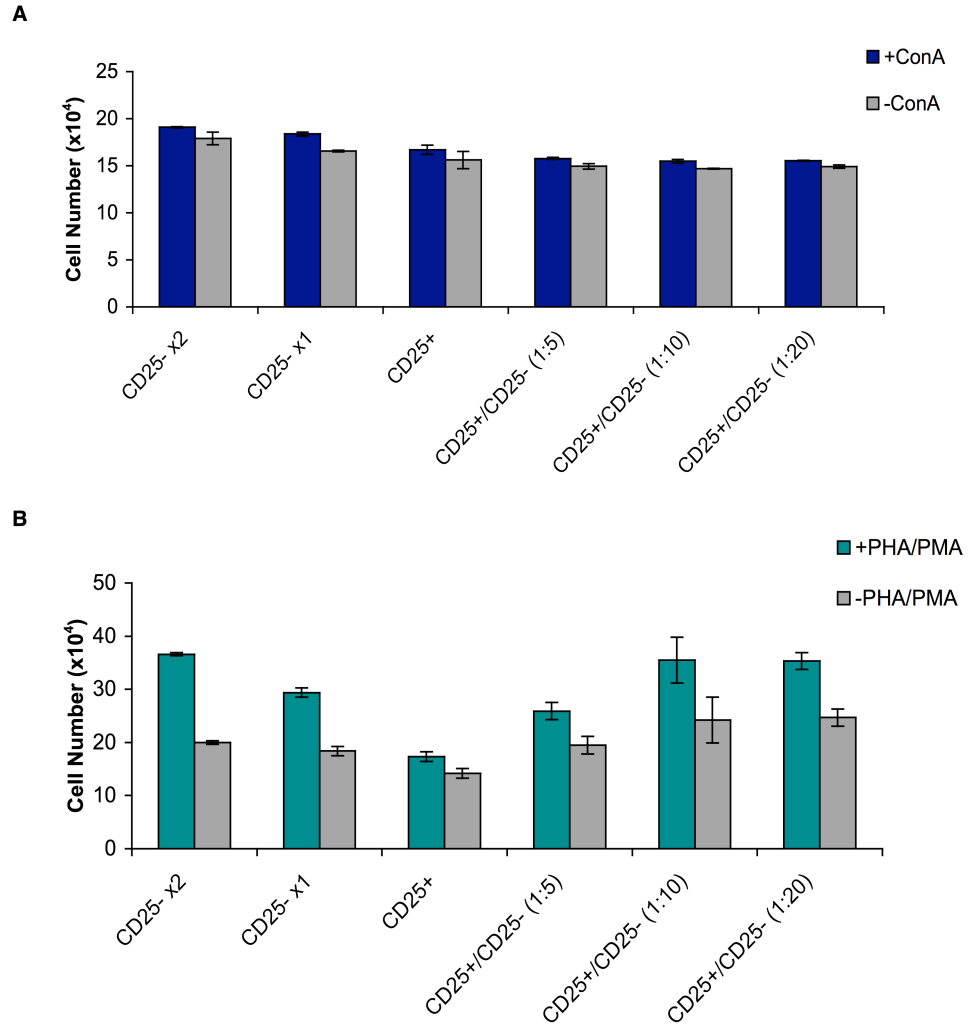


Figure 3.2 Treg Suppression of ConA or PHA/PMA Stimulated Effector Cells, MTS

CD4⁺CD25⁺ Tregs and CD4⁺CD25⁻ effector cells were isolated from 50 ml blood from a healthy volunteer as previously described. CD4⁺CD25⁻ cells, stimulated with either A) Concavalin A (ConA) or B) a combination of Phytohemagglutinin (PHA) and Prostate mucin antigen (PMA), were plated at 5×10^4 cells per well. CD4⁺CD25⁺ cells were then added at 0:2, 0:1, 1:0, 1:5, 1:10 and 1:20 Treg:effector cell ratios. Cells were cultured at 37 °C in a humidified atmosphere containing 5 % v/v CO₂ for 96 hours. A 1:5 dilution of MTS reagent was added for 3 hours and suppression quantified using a spectrometry at 492 nm against a known standard curve of effector cell number. Results were evaluated using Prism 5. Data are a mean of triplicates from a single plate (\pm SD), statistically analysed using a one way ANOVA and Tukey's multiple comparison post-test (ns).

Again results were disappointing, showing no effect when stimulated with ConA and only general trends of suppression against PHA/PMA stimulated effector cells but no significant results. It was thus decided to continue with PHA alone as a stimulant and change the technique used to quantify cell proliferation and suppression. A ^3H -thymidine incorporation assay was therefore used, where co-cultures were pulsed with 0.5 μCi of [Methyl- ^3H]-thymidine for the final 18 hours of the assay. ^3H -thymidine is incorporated into replicating cells, providing a readout of proliferation and therefore allows measurement of suppression (Figure 3.3).

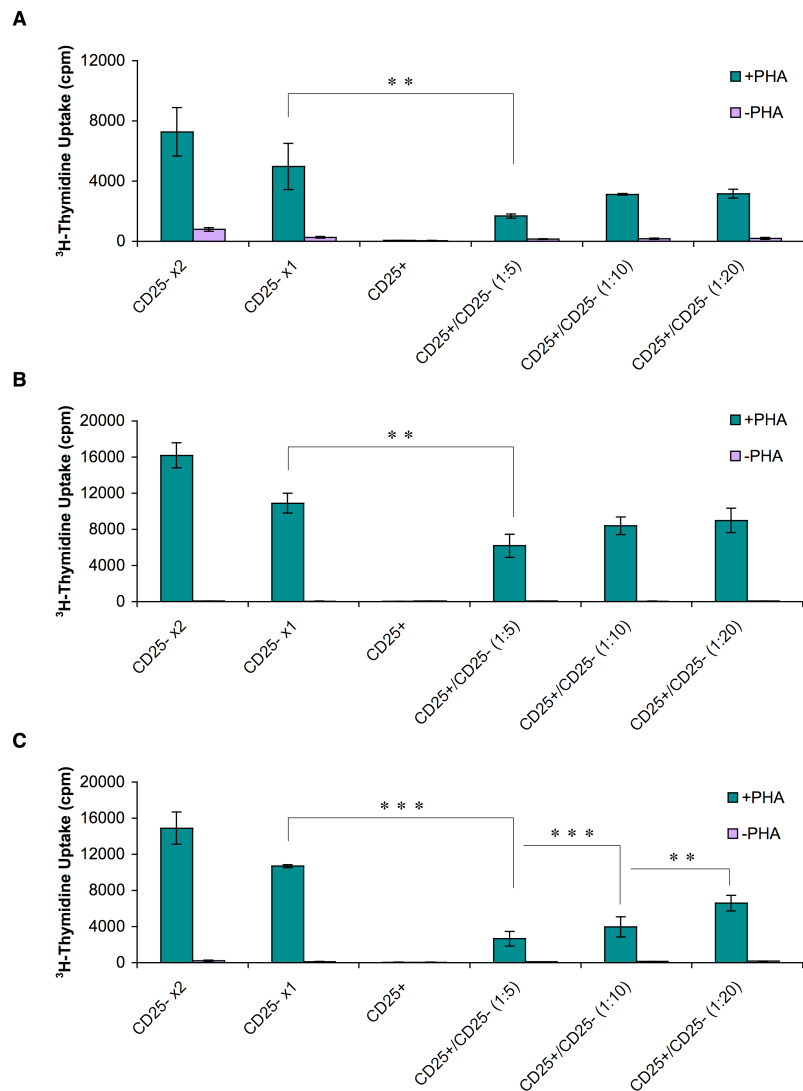


Figure 3.3 Treg Suppression of PHA Stimulated Effector Cells, via 3H-Thymidine Incorporation

CD4⁺CD25⁺ Tregs and CD4⁺CD25⁻ effector cells were isolated from 50 ml blood from a healthy volunteer as previously described. CD4⁺CD25⁻ cells were plated at 5×10^4 cells per well with CD4⁺CD25⁺ cells at 0:2, 0:1, 1:0, 1:5, 1:10 and 1:20 (Treg:effector cell ratios) and stimulated with 10 μ g/ml Phytohemagglutinin (PHA). Cells were cultured at 37 °C in a humidified atmosphere containing 5 % v/v CO₂ for 96 hours. Wells were pulsed with 0.5 μ Ci of [Methyl-3H]-thymidine for the final 18 hours of the assay before harvesting and thymidine incorporation quantified on a Microplate beta Scintillation Counter. Data are a mean of triplicates from a single plate (\pm SD), statistically analysed using a one way ANOVA and Tukey's multiple comparison post test (** $p < 0.01$, *** $p < 0.001$). Data are representative of three different experiments, where A), B) and C) show variation between donors.

When cultured, CD4⁺CD25⁻ cells responded with robust proliferation in the presence of PHA, whereas the CD4⁺CD25⁺ cells did not. Co-culture of the two populations resulted in a significant reduction in the level of proliferation, as measured by [Methyl-³H]-thymidine incorporation. The level of suppression correlated with the ratio of CD4⁺CD25⁻:CD4⁺CD25⁺ cells in the culture, with more CD25⁺ cells resulting in increased levels of suppression of CD25⁻ cell proliferation. Suppression was not due to exhaustion of nutrients within the well as addition of the same amount of CD25⁻ cells instead of CD25⁺ cells did not cause suppression ($\times 2$ CD25⁻ control). These results are robust and representative of three experiments, comparing the same and different cell donors, and findings are in agreement with previous literature (Apostolou and von Boehmer, 2004). The suppressive function of CD4⁺CD25⁺ T cells was demonstrated *in vitro* by inhibiting approximately 80 % of CD25⁻ cell proliferation when at a ratio of one CD25⁺ T cell to four CD25⁻ T cells (Read et al., 1998; Takahashi et al., 1998; Thornton and Shevach, 1998).

3.2.2. Suppression by Inhibitory Cytokines

Various molecular and cellular events have been described to explain the mechanism(s) of Treg mediated suppression. However, none of the proposed mechanisms can explain all aspects of suppressive activity. It is possible that various combinations of several mechanisms are operating, depending on the milieu and the type of immune responses.

To further understand how CD4⁺CD25⁺ Tregs function to inhibit effector T cells, ELISA assays were carried out on the supernatants of suppression cultures. 100 µl of supernatant was carefully extracted from the suppression assay cultures prior to [Methyl-³H]-thymidine incorporation and assayed for relevant cytokines.

Inhibitory cytokines such as IL-10 have been the focus of considerable attention as mediators of Treg-induced suppression. Although the general importance of IL-10 as a suppressive mediator is undisputed, its contribution to the function of naturally occurring Tregs is still a matter of debate. An ELISA was carried out to investigate the amount of IL-10 present in the supernatant of suppression assay wells (Figure 3.4).

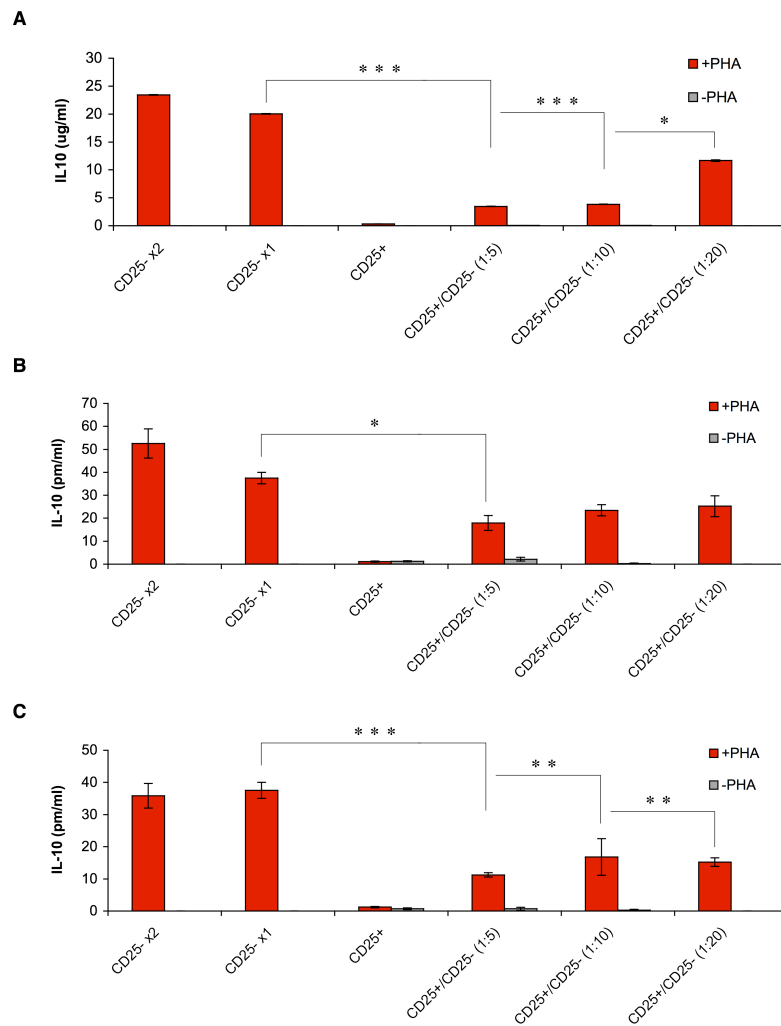


Figure 3.4 IL-10 ELISA of Supernatants from Treg Suppression of PHA Stimulated Effector Cells

100 μ l of supernatant was carefully removed from the wells of the CD4⁺CD25⁺ Treg suppression assay. ELISA plates were pre-coated with purified anti-human IL-10 antibody overnight, followed by a blocking step in 5 % Marvel. 50 μ l per well of supernatants were added, along with a titration of recombinant human IL-10 standard for 120 minutes. Biotin anti-human IL-10 antibody was then added (90 minutes) followed by a Streptavidin HRP incubation step for 30 minutes. Plates were developed using HP Solution for 5–30 minutes and stopped with 2M H₂SO₄ prior to reading on a MRX plate reader at 450 nm. Results were evaluated using Prism 5. Data are a mean of triplicates from a single plate (\pm SD), statistically analysed using a one way ANOVA and Tukey's multiple comparison post-test (* $p < 0.05$, ** $p < 0.01$, *** $p < 0.001$). Data are representative of three different experiments, where A), B) and C) show variation between donors.

An interesting trend was observed, showing elevated levels of IL-10 in CD4⁺CD25⁻ effector cell only wells (CD4⁺CD25⁻ × 1, CD4⁺CD25⁻ × 2) and reduced levels of IL-10 in CD4⁺CD25⁺ Treg wells. Levels of IL-10 increased when Treg numbers were reduced (Figure 3.4). This trend was observed in three experiments and does not support the idea that IL-10 is involved in Treg-mediated suppression. There are discrepancies within the literature with regards to whether or not Tregs secrete IL-10. In contrast to what is normally reported on IL-10 secretion by Tregs, but in agreement with the current study, Baecher-Allan and Hafler (2006) found that effector cells, stimulated with strong TCR activation, primarily produced IL-10. In addition, IL-10 was found to be higher in the supernatant from effector cells compared to that observed from effector-Treg cocultures and was absent from wells containing only Tregs. The authors concluded that Tregs were inhibiting IL-10 production or utilising the IL-10 within the supernatant (Baecher-Allan and Hafler, 2006).

In vitro studies using neutralising antibodies or T cells unable to produce or respond to IL-10 have suggested that IL-10 may not be essential for Treg function, and IL-10 deficient Tregs were still capable of suppression. However, this is in contrast to data from *in vivo* studies, that indicated Treg mediated suppression is IL-10 dependent (Roncarolo et al., 2006).

Collectively, the picture that appears to be emerging is that IL-10 production by Tregs is still debated and contradicting data has been published on the relative

importance of IL-10 as a mechanism of Treg-mediated suppression. It is however agreed that IL-10 is not the only Treg mechanism of suppression and it can be speculated that its role may be dependent on the target organism or disease.

In addition to IL-10, the classical pro-inflammatory cytokine, IFN- γ , was investigated. IFN- γ is secreted by Th1 cells, NK cells, and by CD4 and CD8 CTL effector cells following immune activation. IFN- γ produces a variety of physiological and cellular response via transcription regulation, resulting in immunoregulatory and anti-tumour properties (Schroder et al., 2004).

A significant increase of IFN- γ was observed in the presence of Tregs and subsequent suppression (Figure 3.5). This was unexpected as IFN- γ production is associated with proliferation of stimulated effector cells (Byeon et al., 2009), and it is thought that Tregs inhibit its production (Ghiringhelli et al., 2006).

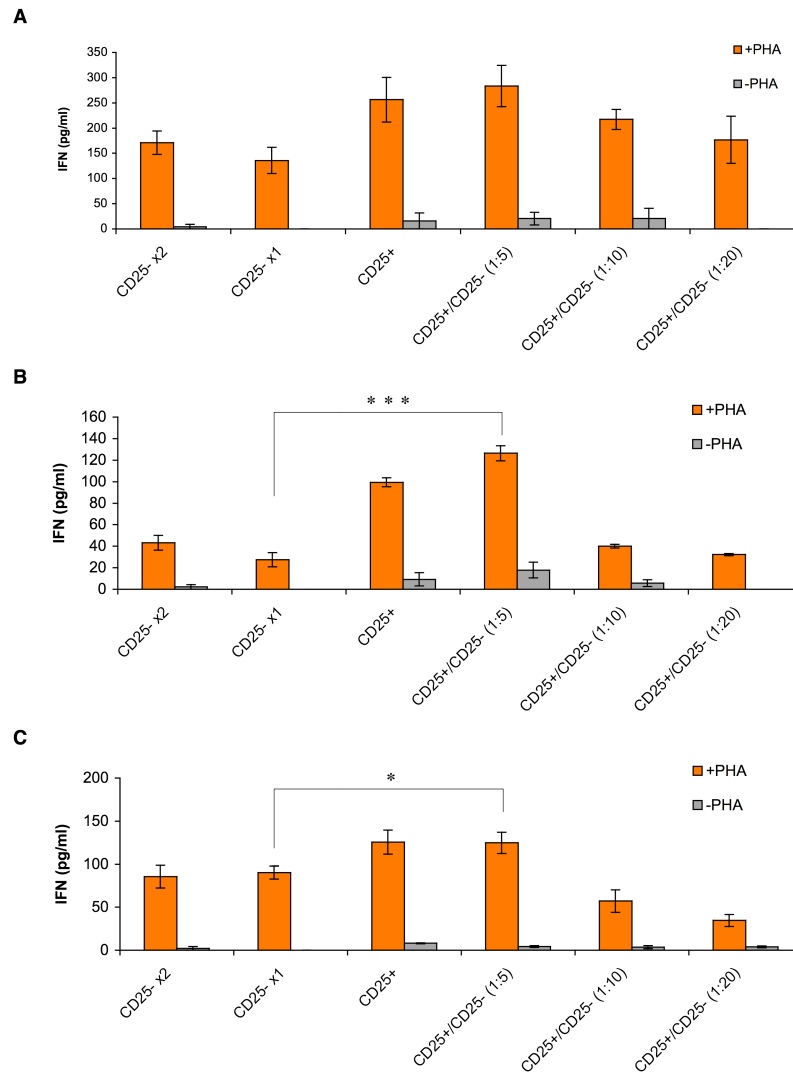


Figure 3.5 IFN-gamma ELISA of Supernatants from Treg Suppression of PHA Stimulated Effector Cells

100 μ l of supernatant was carefully removed from the wells of the CD4⁺CD25⁺ Treg suppression assay. ELISA plates were pre-coated with purified anti-human interferon- γ (IFN- γ) antibody overnight, followed by a blocking step in 5 % Marvel. 50 μ l per well of supernatants were added, along with a titration of recombinant human IFN- γ standard for 120 minutes. Biotin anti-human IFN- γ antibody was then added (90 minutes) followed by a Streptavidin HRP incubation step for 30 minutes. Plates were developed using HP Solution for 5–30 minutes and stopped with 2M H₂SO₄ prior to reading on a MRX plate reader at 450 nm. Data are a mean of triplicates from a single plate (\pm SD), statistically analysed using a one way ANOVA and Tukey's multiple comparison post test (** $p < 0.001$, * $p < 0.05$).

Data are representative of three different experiments, where A), B) and C) show variation between donors.

The author would like to suggest that perhaps the reason behind this unexpected IFN- γ profile is due to the use of PHA as a stimulant. Antigenic TCR engagement results in no subsequent Treg activation; however, mitogenic PHA stimulation could by-pass normal cell signalling activation pathways and result in activation of downstream components, such as nuclear factor kappa B (NF κ B) (Long et al., 2009; Niederman et al., 1992).

Research has highlighted discrepancies in the involvement of various cytokines in Treg suppression. It then begs the question, if cytokines only play a partial role in Treg mediated suppression, are additional cell-to-cell contact-dependent mechanisms playing a more significant role?

3.2.3. Cell-Cell Contact Dependent or Independent?

The unusual cytokine profile and inconsistencies in cytokine involvement described previously led to the investigation of additional suppressive mechanisms, specifically focusing on the concept of cell-contact mediated suppression. In order to investigate whether cell-to-cell contact is a requirement for Treg suppression, a transwell system was designed (Figure 3.6).

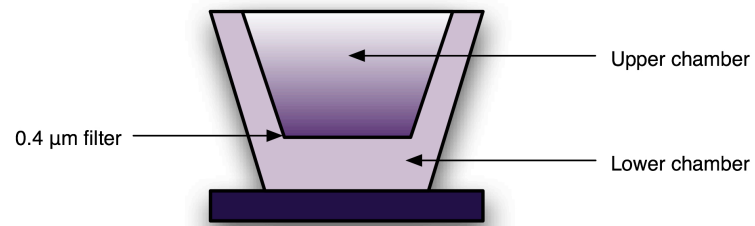


Figure 3.6 Diagrammatic Representation of the Transwell System

Stimulated effector cells were seeded at 3×10^4 cells per well in 1.5 ml of media into the lower chamber. $CD4^+CD25^+$ Tregs were then added onto the $0.4 \mu\text{m}$ membrane insert (Corning Transwell™) in 500 μl media at various Treg:effector cell ratios.

A direct comparison between the two assay systems was investigated using isolated effector cells and Tregs, from the same donor, on the same day. The co-cultured environment of the suppression assay (described previously) was removed in the second assay, eliminating cell-to-cell contact between effector and Tregs via the transwell system. The suppression activity was measured using ^3H -thymidine incorporation and levels of cytokines investigated using ELISAs (Figure 3.7).

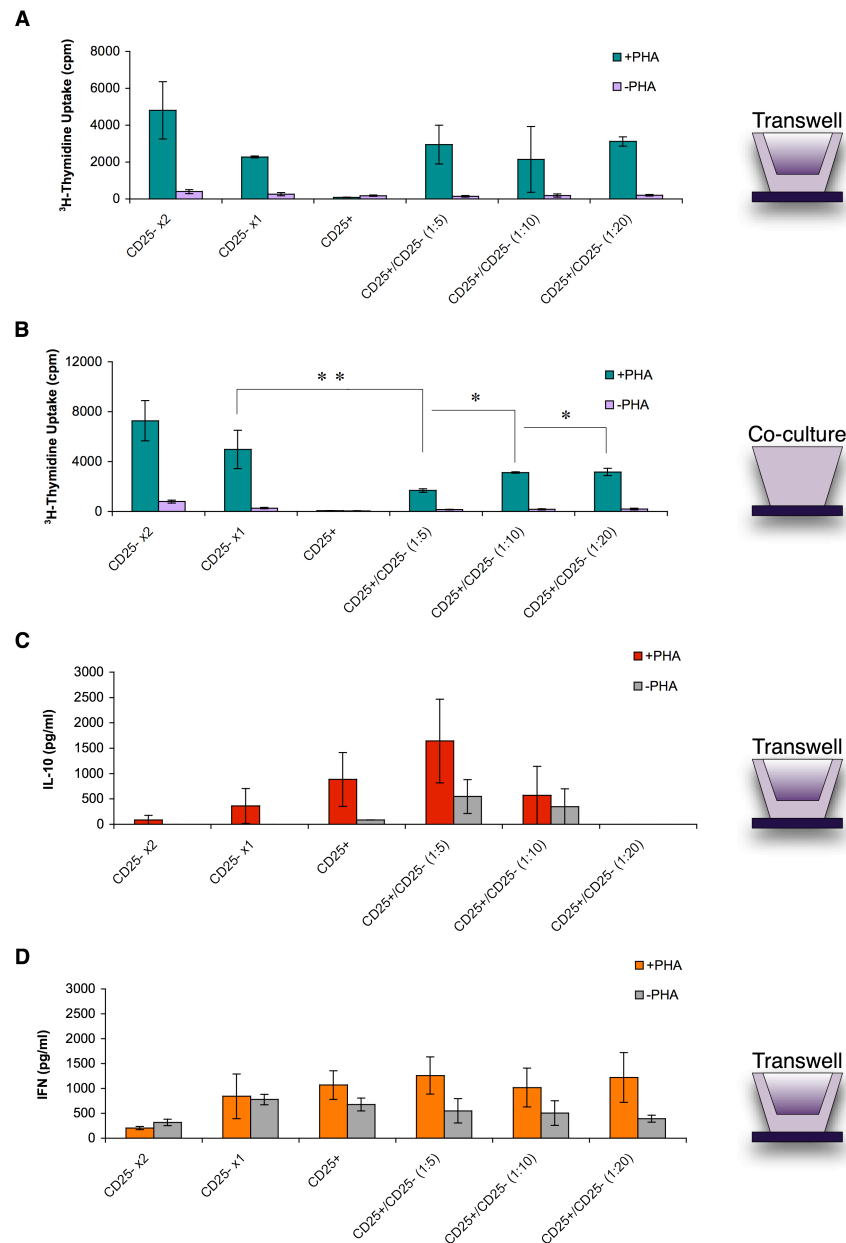


Figure 3.7 Transwell Suppression Activity of Tregs

Isolated effector cells stimulated with 10 µg/ml PHA were seeded at 5×10^4 cells per well in 100 µl of media into the lower chamber of the transwell system. CD4⁺CD25⁺ Tregs were then added onto the 0.4 µm membrane insert (Corning Transwell™) in 50 µl media seeded at 1:5, 1:10 and 1:20 Treg:effector cell ratios. A) Transwell and B) normal suppression was accessed via ³H-Thymidine incorporation. C) The presence of IL-10 and D) IFN-γ was determined using an ELISA on well supernatants. Data are a mean of triplicates from a single plate (± SD) and is representative of n = 3 experiments, statistically analysed using a one way ANOVA and Tukey's multiple comparison post test (* p < 0.05, ** p < 0.01).

Results show a lack of significant Treg-mediated suppression when cultured in a transwell system, compared to the suppression observed when co-cultured with effector cells. The levels of IL-10 and IFN- γ present within the supernatants were very low and showed no general trends. The transwell system removes both cell-to-cell contact and also close cell proximity. These studies have demonstrated that *in vitro* CD4⁺CD25⁺ cells suppress co-cultured effector cells via a mechanism involving cell contact or close proximity. These results are in agreement with previous literature indicating that Treg-mediated suppression is cell contact dependent, as suppression was not seen when CD25⁺ Treg and CD25⁻ effector cells were separated by a permeable membrane (Nakamura et al., 2004; Tanchot et al., 2004; Thornton and Shevach, 1998). Several mechanisms responsible for suppression have been proposed but the topic still remains controversial and requires further work (Zimmer et al., 2008).

3.2.4. A Surrogate Cell Line?

Due to the limited numbers of Tregs and difficulties with isolation, a replacement cell line would be favourable for use in preliminary studies and optimisation. A cell line, designated Karpas-299, was established from blast cells from the peripheral blood of a 25-year-old male with T cell non-Hodgkin lymphoma. Research has suggested that the Karpas-299 are able to suppress PHA/PMA stimulated effector cells and express Treg markers such as CD25, Foxp3, CD62L and TGF- β (Wolke et al., 2006). Therefore, it is possible that this cell line could act as a surrogate Treg for *in vitro* experiments.

The suppressive ability of the Karpas-299 cell line when co-cultured with effector cells is a key requirement to show Treg-like properties. Due to the allogeneic effect a co-culture would cause, the transwell system was implemented. Corning® Transwell™ Permeable Supports enabled the two different cell types to be cultured within the same well without direct cell-to-cell contact.

Unlike Tregs, Karpas-299 cells are not anergic *in vitro* and so proliferate excessively by themselves (Figure 3.8A). In a co-culture situation this would greatly affect the suppression assay readout as no distinction is made between the two cell populations; however, in a transwell system only the lower chamber containing the effector cells undergo ³H-thymidine incorporation for suppression measurement. However, even with elevated Karpas-299 cell numbers, no significant suppression of PHA-stimulated effector cells was observed. FACS analysis of the Karpas-229 cells showed positive staining for CD4 and CD25; however, Foxp3 remained negative (Figure 3.8B).

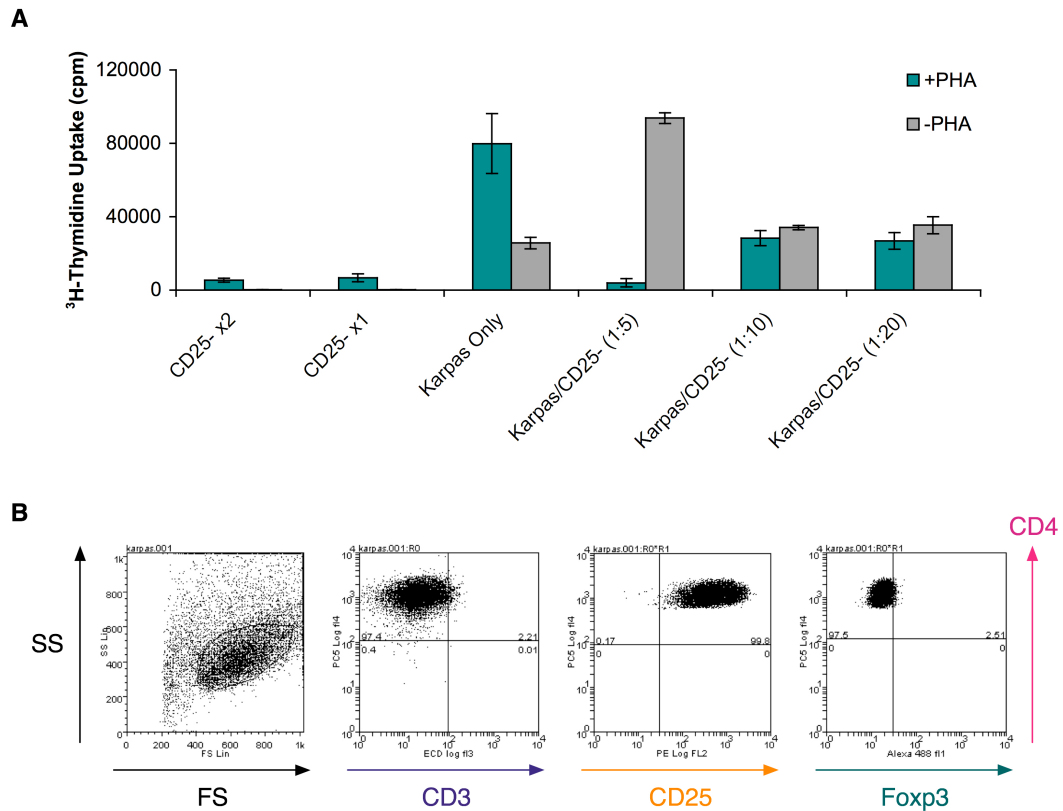


Figure 3.8 Transwell Suppression Activity of Karpas-299 Cell Line with FACS Analysis

A) Isolated effector cells stimulated with 10 $\mu\text{g/ml}$ PHA were seeded at 5×10^4 cells per well in 100 μl of media into the lower chamber of the transwell system. Karpas-299 cells were then added onto the 0.4 μm membrane insert (Corning Transwell™) in 50 μl media seeded at 1:5, 1:10 and 1:20 Karpas:effector cell ratios. Suppression was accessed via ^3H -Thymidine incorporation. Data are a mean of triplicates from a single plate (\pm SD) and is representative of $n = 3$ experiments. B) 1×10^6 Karpas cells were removed for FACS analysis. A pre-titrated volume of the following surface antibodies was added; PeCy5 anti-CD4, ECD anti-CD3 and PE anti-CD25. Cells were then fixed and permeabilised followed by intracellular staining using Alexa 488 anti-Foxp3. Data were acquired on a Beckman Coulter FC 500 flow cytometer and analysed using Weasel software.

In addition, previous transwell suppression work showed that this system was not suitable for measurement of Treg suppression and therefore concerns would arise if using the Karpas-299 cell line as a Treg replacement. Different mechanisms must be involved in order to have a suppressive effect, which leads to the question: would it be a representative surrogate cell line?

3.3. CONCLUSIONS AND FUTURE WORK

Despite some safety concerns and a popular trend to move away from the use of radiation techniques, tritiated thymidine incorporation provided the most sensitive and reproducible assay to determine Treg-mediated suppression of immune cell proliferation. To investigate the suppressive ability of Tregs, a reciprocal immune cell population was required. Utilising a mixed PBMC population for this role was not successful; however, isolation of a CD25⁻ population worked well, when stimulated with PHA.

The current study highlighted discrepancies in the involvement of pro-inflammatory and suppressive cytokines in Treg-mediated suppression. The use of antigenic instead of mitogenic stimulation could provide further understanding in this area and therefore scope for future research. However, when further investigating Treg suppression in a transwell system, results suggest that *in vitro* CD4⁺CD25⁺ Tregs suppress effector cells via a mechanism involving cell contact or close proximity. Research is in agreement with previous literature but the topic still remains

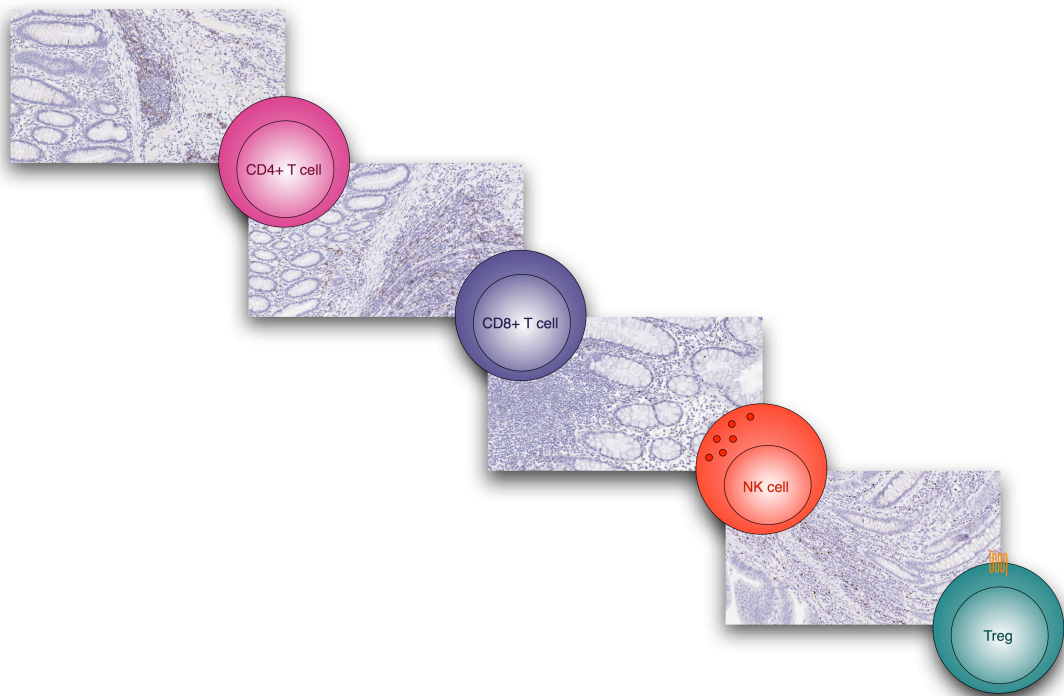
controversial and could require additional investigation (Nakamura et al., 2004; Tanchot et al., 2004; Thornton and Shevach, 1998).

A surrogate cell line to replace difficulties in Treg isolation and limited numbers would be desirable. Unfortunately, the Karpas-299 cell line did not show a significant trend in Treg-like suppression of stimulated effector cells and lacked Foxp3 expression. In addition, the Karpas-299 cell line would need to be utilised in a transwell system; an assay already determined not appropriate in the understanding of Treg-mediated suppression mechanisms.

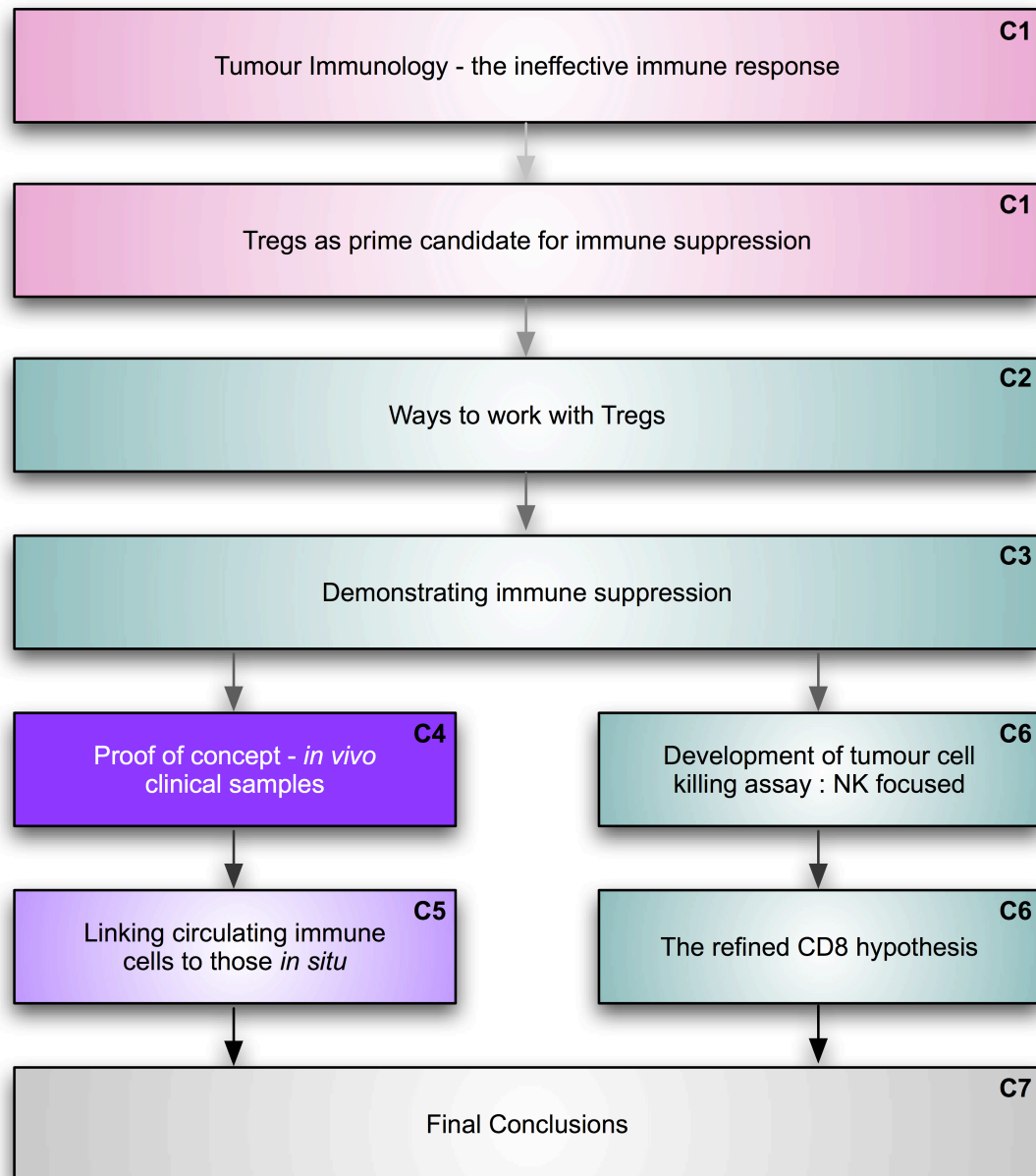
***Summary:** Protocol optimisation demonstrated that 'in vitro' $CD4^+CD25^+$ cells suppression of PHA stimulated effector cells was favourable and [Methyl- 3H]-thymidine incorporation was the most sensitive technique. The current study has shown that the role of cytokines in Treg-mediated suppression is still unclear and requires further investigation. However, classical $CD4^+CD25^+$ Tregs are thought to suppress via a cell contact-mediated mechanism. Despite what previous literature suggests, the Karpas-299 cell line does not suppress $CD4^+CD25^-$ effector cells, a key requirement for a surrogate Treg cell line.*

4. CHAPTER FOUR

Immune Infiltrates and Tumour Progression



Chronological Framework of Thesis Progression



■ Literature ■ *In vitro* ■ *Ex vivo* **C1** Chapter 1

At this stage in the PhD a foundation of knowledge, understanding the importance of Tregs in tumour immunology, was achieved. Tregs were selected as the prime candidate for modulating tumour immunology. The successful isolation and ways to work with Tregs was accomplished. In addition, hypothesised Treg-mediated mechanisms of suppression were tested. It was then necessary to determine whether or not the importance of Tregs highlighted in the literature was reflected in a clinical setting. The tumour microenvironment is thought to provide a favourable milieu for Treg expansion, where elevated numbers of Tregs result in an imbalance within the immune system. Research has advocated that this imbalance favours unresponsiveness and facilitates tumour escape of immune recognition. Questions remain unanswered with regards to the importance of immune cell location at the tumour site. This chapter aimed to investigate the significance of immune cell orientation within distinct tumour and non-neoplastic regions. Additionally, the implication of co-localisation between key immune cell subtypes was scrutinised. Immune cell infiltrates were then correlated with areas of tumour proliferation, apoptosis, hypoxia and vasculature coverage.

4.1. METHODOLOGY

4.1.1. Cell Pellet Preparation

The cells of interest, for example Tregs, were isolated from 50 ml healthy blood as previously described. Cells were then fixed in 4 % formaldehyde for 24 hours and centrifuged at $350 \times g$ for 5 minutes. Cells were then washed in PBS followed by a second wash in 80 % ethanol. Cells were finally centrifuged at $350 \times g$ for 5 minutes

and the cell pellet re-suspended in molten histogel (HG 4000-012, Thermo Scientific). This uniform mixture was transferred to an eppendorf lid and allowed to set. The cell pellet was then loosened with a clean probe and stored in 80 % ethanol until processing.

4.1.2. Histology Specimen Processing and Embedding

Tissue or cell pellets were processed on a Shandon Excelsior Tissue Processor (Thermo Electron Corporation), following the manufacturer's instructions. In brief, specimens were fixed in 4 % formaldehyde for 24 hours and then placed into RA Lamb Embedding Cassettes (Thermo Scientific, 83500). Cassettes were then loaded into the processor and underwent the following program (Table 4.1).

Table 4.1 A Summary of the Tissue Processing Programme Used

Processing Programme					
Reagent	Hold/Use	Time (hrs)	Drain (sec)	Vacuum	Stir
Alcohol 1	30 °C	1.00	30	On	5
Alcohol 2	30 °C	1.00	30	On	5
Alcohol 3	30 °C	1.00	30	On	5
Alcohol 4	30 °C	1.00	30	On	5
Alcohol 5	30 °C	1.30	30	On	5
Alcohol 6	30 °C	1.30	60	On	5
Xylene 1	30 °C	1.00	30	On	5
Xylene 2	30 °C	1.00	30	On	5
Xylene 3	30 °C	1.00	120	On	5
Wax 1	60 °C	0.45	90	On	5
Wax 2	60 °C	1.00	90	On	5
Wax 3	60 °C	1.20	120	On	5

On completion of the processing program, specimens were embedded on a Shandon Histocentre 3 (Thermo Electron Corporation). Low melting point and polymer-free paraffin cell wax (Cell Path Plc., GCA-0302-00A) was used in embedding moulds. When dry, blocks were trimmed of excess wax using a Shandon PARA TRIMMER[®] and left overnight to solidify.

4.1.3. Section Cutting

Prior to cutting, specimen blocks were placed on ice for 30 minutes. Superfrost[®] Plus slides (VWR International, 081610-9, 25 × 75 × 1.0 mm) were printed on a Leica IP5. 4.0 µm thick sections were cut using a Leica RM2255 Microtome with a Shandon MB35 Premier Microtome Blade (35°/80 mm, Thermo Electron Corporation). Sections were then placed in a Leica HI1210 water bath to spread before being transferred onto the corresponding slide and moved to a heat block to dry. Sections were then left overnight at 37 °C to fix to the slide.

4.1.4. Haematoxylin and Eosin (H&E)

Slides were dewaxed and rehydrated using a Leica Autostainer XL. In brief, this involved a series of wash steps firstly in two xylene (Sigma-Aldrich, 33817) baths followed by two 100 % ethanol (UK IDA standard, Sigma-Aldrich, 458600) baths, one 70 % ethanol bath and finally a water bath. Sections were stained with Carazzi's Haematoxylin Gill III (Surgipath, 01540BBE), followed by a wash step in Shandon Bluing Reagent (Thermo Scientific, 6769002). Finally, the slides were introduced to

Eosin (alcoholic solution, Leica Microsystems, 01600BBE) before being dehydrated in ethanol and cleared using xylene on a Leica Autostainer XL. Slides were mounted using Premier Cover Glass slips (24 mm × 50 mm, Surgipath[®]) with Histomount[™] (National Diagnostics, HS-103) on a Leica CV5030 and left to dry prior to viewing on a Leica DM4000B microscope.

4.1.5. Immunohistochemistry

Slides were dewaxed and rehydrated using a Leica Autostainer XL. Following this, where appropriate, antigen retrieval was performed using a pressure vessel in a RHS2 Microwave Rapid Histoprocessor (Milestone). The appropriate target retrieval solution was added, pH6 (Dako, S1699), pH8 EDTA or pH9 (Dako, S2367). Slides were heated to 110 °C for 5 minutes and then cooled under running water for 15 minutes. The Autostainer 720 (Lab Vision) was then used to perform all antibody stains, washes and block steps, where antibodies were made up in tris-buffered saline-tween (0.05 %, TBS-T). On completion of the pre-treatment process, sections were marked with an upper and lower boundary, using a waterproof pen (Dako, S2002) and pre-rinsed in TBS-T. 3 % H₂O₂ was applied for 10-20 minutes at room temperature to block endogenous peroxidase activity. Slides were washed twice in TBS-T. Avidin block (Vector Labs, SP-2001) was applied for 20 minutes followed by a TBS-T wash. Biotin Block (Vector Labs, SP-2001) was applied for 20 minutes followed by an additional TBS-T wash. Slides were incubated for 20 minutes with serum-free protein block (Dako, X0909), which was then blown off the slides (a wash step was not performed at this stage). Sections were incubated with primary antibody

for 60 minutes. The current study used the following antibodies at the corresponding optimised concentrations: mouse anti-human Foxp3 IgG1 (5 µg/ml, Clone 236A/E7, Abcam 20034), mouse anti-human CD8 IgG2b (0.5 µg/ml, Clone 4B11, Leica NCL-CD8-4B11), mouse anti-human CD56 IgG1 (0.5 µg/ml, Clone 1B6, Leica NCL-L-CD56-1B6), mouse anti-human Ki67 IgG1 (0.35 µg/ml, Clone MIB-1, Dako M7240), mouse anti-human CD68 IgG1 (0.2 µg/ml, Clone PG-M1, Dako M0876), rabbit anti-human CD31 (0.27 µg/ml, CHG-CD31-PI, AstraZeneca in house), rabbit anti-human cleaved caspase-3 (5 µg/ml, Clone D175, Cell Signalling Technology 9661), mouse anti-human α -SMA IgG2a (2 µg/ml, Clone 1A4, Sigma A2547) and mouse anti-human HIF-1 α , IgG1 (5 µg/ml, Clone 54, Becton Dickinson 610950). Following the primary antibody incubation, slides were washed twice in TBS-T. Slides were incubated with the optimised detection methods: Vector Elite ABC kit (PK6101) or Mouse/Rabbit Envision HRP-linked polymer (Dako, K4001), for 30 minutes. When using the Envision HRP-linked detection method, previous avidin and biotin blocking steps were not required. Slides were washed twice in TBS-T and then incubated in 3,3-Diaminobenzidine (DAB, D/K3468) solution for 10 minutes. Slides were rinsed twice in distilled water and removed from the autostainer. Sections were counterstained with Carazzi's Haematoxylin Gill III (Surgipath, 01540BBE), dehydrated in ethanol and cleared using xylene, all carried out on the Leica Autostainer XL. Slides were then mounted using Premier Cover Glass slips (24 mm \times 50 mm, Surgipath[®]) with Histomount[™] (National Diagnostics, HS-103) on a Leica CV5030 and left to dry before viewing on a Leica DM4000B microscope.

4.1.6. Image Analysis

Analysis of IHC images was achieved using a ScanScope digital scanner (Aperio Technologies Ltd.) and images were taken at x 20 original magnification. Images were viewed and organised using ImageScope viewer and Spectrum operating system. Each scanned image was annotated for analysis to exclude areas of glass, dark background staining or poor sample quality. Genie™ pattern recognition software was used for the automated quantitative assessment of immune infiltrates within specific regions of tissue. Genie™ classifiers were generated for the separation of areas of tumour, stroma, lymphatic aggregates, non-neoplastic tissue and glass (as described in section 4.2.3).

4.1.7. Ethics Approval

All samples used were sourced from the AstraZeneca Alderley Park Biobank, which is a licenced premises under the Human Tissue Act (2004) (HTA number 12109) and has NRES ethical approval as a tissue bank (07/MRE08/29). All third party providers to the Alderley Park Biobank have passed an approval process at AstraZeneca and all samples were acquired by those providers with written informed consent.

4.1.8. Method of Statistical Analysis

Data were collated into certain groups and graphically expressed as the mean, where error bars depicted SD. Further analysis was then carried out to quantify any trends in the data, using Prism® 5 software and Spotfire® programmes. Paired data

underwent a t-test to determine any significant differences. If the data assumed a normal distribution pattern, a paired or unpaired t-test was carried out. If the data did not assume a normal distribution pattern, a ranked method was selected. For paired rank testing a Wilcoxon test was carried out. For unpaired rank testing a Mann-Whitney analysis was used.

4.2. RESULTS AND DISCUSSION

It is becoming increasingly apparent that tumours contain various cells from the immune system, including inflammatory infiltrates of innate immunity (macrophages, neutrophils, NK cells and DCs) and also infiltrates of the adaptive immune response (B lymphocytes, cytotoxic T cells and Tregs) (Pages et al., 2008). Galon's group were one of the first to characterise tumour-infiltrating immune cells, specifically CD45RO memory T cells, in large cohorts of human CRCs and solidified the association between tumour progression and inflammation (Pages et al., 2005). These tumour infiltrating immune cells live in a milieu of chemokines and cytokines produced by the tumour cells and stromal cells, as well as the immune cells themselves. Interactions between tumour cells and immune infiltrates are complex and result in a balance between tumour promotion and tumour suppression. Increasing evidence supports the idea that immune infiltration into the tumour microenvironment could result in a strong parameter influencing clinical outcome, regardless of the tumour stage (Pages et al., 2008).

The involvement of the immune system in the early stages of metastasis has been studied histologically using tissue microarrays to investigate the *in situ* adaptive response in the centre and margin of 415 CRC tumours. Early stages of the metastatic process, including vascular emboli, lymphatic invasion and perineural invasion, have been collectively termed “VELIPI”. Negative VELIPI were seen to be associated with strong immune infiltrates that gave longer DFS and OS in patients (Pages et al., 2005). The type, density and location of immune cells was also studied in CRC. When CD3, CD8, CD45RO and granzyme B (GZB) were looked at in the centre of the tumour (CT) and at the invasive margin (IM), patients without recurrence of disease had higher immune cell densities (Galon et al., 2006; Pages et al., 2008). Potential implications of these findings have been reviewed (Galon et al., 2007) and their prognostic significance investigated (Pages et al., 2008).

The immune systems association with areas of tumour proliferation (Ki67) and apoptosis (M30) in 435 samples of primary CRC was assessed by immunohistochemical staining (Camus et al., 2009). CD8/CD3 T cell density ratio was investigated in relation to clinical outcome and high proportions of CD8 cytotoxic T cells within the primary tumour was associated with reduced risk of relapse (Camus et al., 2009). A comparison between patients presenting no metastases (MET- stages I–II), patients with invaded lymph nodes (MET+ stage III) and/or distant organ metastases (stage IV) was achieved. Patients were classified according to the mean percentage of CD3⁺CD5⁺ cells among total cells within tumours (CD3⁺CD5⁺Hi or CD3⁺CD5⁺ Lo). Large-scale FACS analysis showed no difference in the distribution of TAMs, NK cells, NKT cells, or B cells between

MET⁻Lo and MET⁺Lo patients. However, MET⁺Hi patients showed significantly lower levels of TAMs, cytotoxic T cells (CD3⁺CD8⁺) and NKT cells density compared with MET⁻Hi patients. No significant difference was seen between T_H cells (CD3⁺CD4⁺) or Tregs (CD4⁺CD25^{hi}). CD8⁺/CD4⁺ and CD8⁺/CD3⁺ cell ratios were significantly higher in MET⁻Hi patients compared with MET⁺ Hi and MET⁺ Lo patients (Camus et al., 2009).

The extent of the immune reaction at the tumour site also correlates with clinical outcome in stages I and II of CRC (Pages et al., 2009). An excellent review, summarising the work over the last decade, has recently been published and highlights the key questions that still remain (Pages et al., 2010). The question of the prognostic role of Tregs in human CRC appears to be complex and ambiguous. Curiel *et al.*, (2004) reported that the increase in Tregs correlated with tumour staging and reduced survival in ovarian carcinoma (Curiel et al., 2004). Subsequent data are in agreement with this in other solid tumours such as NSCLC (Woo et al., 2001), gastric (Mizukami et al., 2008b) and hepatocellular carcinoma (HCC) (Fu et al., 2007). In contrast to this, data has accumulated suggesting that elevated Tregs may not always be associated with poor prognosis. For example Salama *et al.*, (2009) reported an increase in Foxp3 density within the tumour associated with better OS (Salama et al., 2009). Galons group found no association between Foxp3, CTLA-4, GITR, IL-10, TGF- β and the presence of intratumoural or distant metastasis (Pages et al., 2008).

The clinicopathologic significance of Tregs and CD8 cells during hepatocarcinogenesis has also been studied and the prevalence of Tregs was suggested as an unfavourable prognostic marker (Kobayashi et al., 2007). The infiltration of Tregs and CD8 cells between HCC and primary hepatic adenocarcinoma, intrahepatic cholangiocarcinoma (ICC) as well as between primary and metastatic liver tumours was studied. In addition, 59 patients with metastatic liver tumours from primary CRC were evaluated for Treg prevalence. Analysis of the antitumour response (Tregs and CD8 T cells) in primary HCC (n = 235), intrahepatic metastatic foci (n = 27) and liver metastasis from primary CRC (n = 59) was evaluated. The prevalence of Tregs was higher in primary tumours than metastatic. Tregs were elevated in HCC compared to non-tumour tissue or healthy liver samples, where low-Treg groups showed improved OS and DFS compared to high-Treg groups (Kobayashi et al., 2007). Analysis of additional immune infiltrates such as CD3, CD8, CD45RO, GZE, CD57 (cytotoxic T cells and NK cells), CD1a (immature DCs), cytokeratin-8, T-Bet (T_H1 cells) and CD68 (macrophages) has been assessed and associated with survival in CRC (Mlecnik et al., 2010a). Extensive work was achieved using a platform of techniques (gene expression, phenome mapping, immunohistochemistry (IHC) of TMAs and T cell TCR repertoire) to identify immune-related genes associated with patient prognosis and absence of tumour recurrence. The phenotypes and locations of intratumoral immune cells were assessed for correlations with DFS. The evaluation of Tregs, however, was absent from the study.

Ratios of immune cells have also been studied, such as CXCR3/Foxp3 ratio (Ohtani and Yoshie, 2010) and CD8/Foxp3 cell ratio as a predictive marker for survival in CRC (Suzuki et al., 2010).

In CRC, T cells are distributed in different tumoral areas; in the CT within the stroma and tumour glands, at the IM, and in lymphoid structures resembling germinal centres at the tumour periphery. More precise analysis of Tregs within the tumour microenvironment is required, including investigation of their location in the CT and IM of the tumour, the proportions of Tregs versus helper and cytotoxic T cells and their role in metastatic development. Tumour-infiltrating immune cells have been analysed in detail by gene-expression profiling and flow cytometry; however, gaps in the literature are apparent when looking at in situ co-localisation of CD8 cells, NK cells, Tregs and macrophages by IHC.

The current study aimed to determine in a large cohort of CRC patients whether the functional orientation, density, and co-localisation of immune cell populations within distinct tumour territories (CT, IM, stroma) change with areas of tumour proliferation, apoptosis or hypoxia and to evaluate any changes between primary CRC and metastatic liver patients.

4.2.1. Immunohistochemistry Antibody Optimisation

Initially, staining protocol optimisation was a fundamental requirement. To aid in this process, various cell pellet plugs were made to provide positive and negative

controls. Immune cells were isolated from human PB as previously described and then prepared to form a paraffin embedded pellet (Figure 4.1).

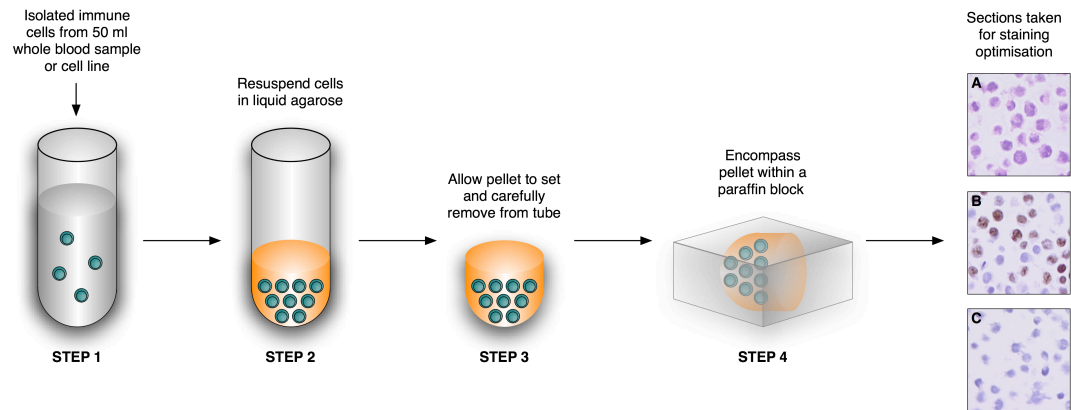


Figure 4.1 Cell Pellet Procedure for Optimisation of IHC Staining

Immune cells were isolated from 50 ml blood from a healthy volunteer, as previously described, or cultured cell lines were harvested. Cells were counted and 1×10^6 removed for FACS analysis. The remaining cells were resuspended in agarose and allowed to set, forming a pellet. This pellet was then embedded into a paraffin block for IHC staining protocol optimisation. Sections were then used for staining optimisation. Example images (at x 20 original magnification) showing K562 cells stained with A) H & E, B) anti-human Ki67 antibody and C) isotype control.

This process was carried out for CD4⁺CD25⁺ Tregs, CD25⁻ cells, CD8⁺ cells, CD56⁺ cells and CD8⁻CD56⁻ cells. In addition, an unrelated cell line, K562, was also used to provide a true negative control.

Example staining images of the CD4⁺CD25⁺ Treg pellet and CD25⁻ Effector control pellet are shown in Figure 4.2, stained for Foxp3 and also the proliferation marker, Ki67. Foxp3 positive staining was seen in the CD4⁺CD25⁺ plug (Figure 4.2J) but was absent from the CD25⁻ effector cell control (Figure 4.2F). In addition, proliferation was observed in the CD25⁻ effector cells (Figure 4.2G) but was absent from the non-proliferating Tregs (Figure 4.2K).

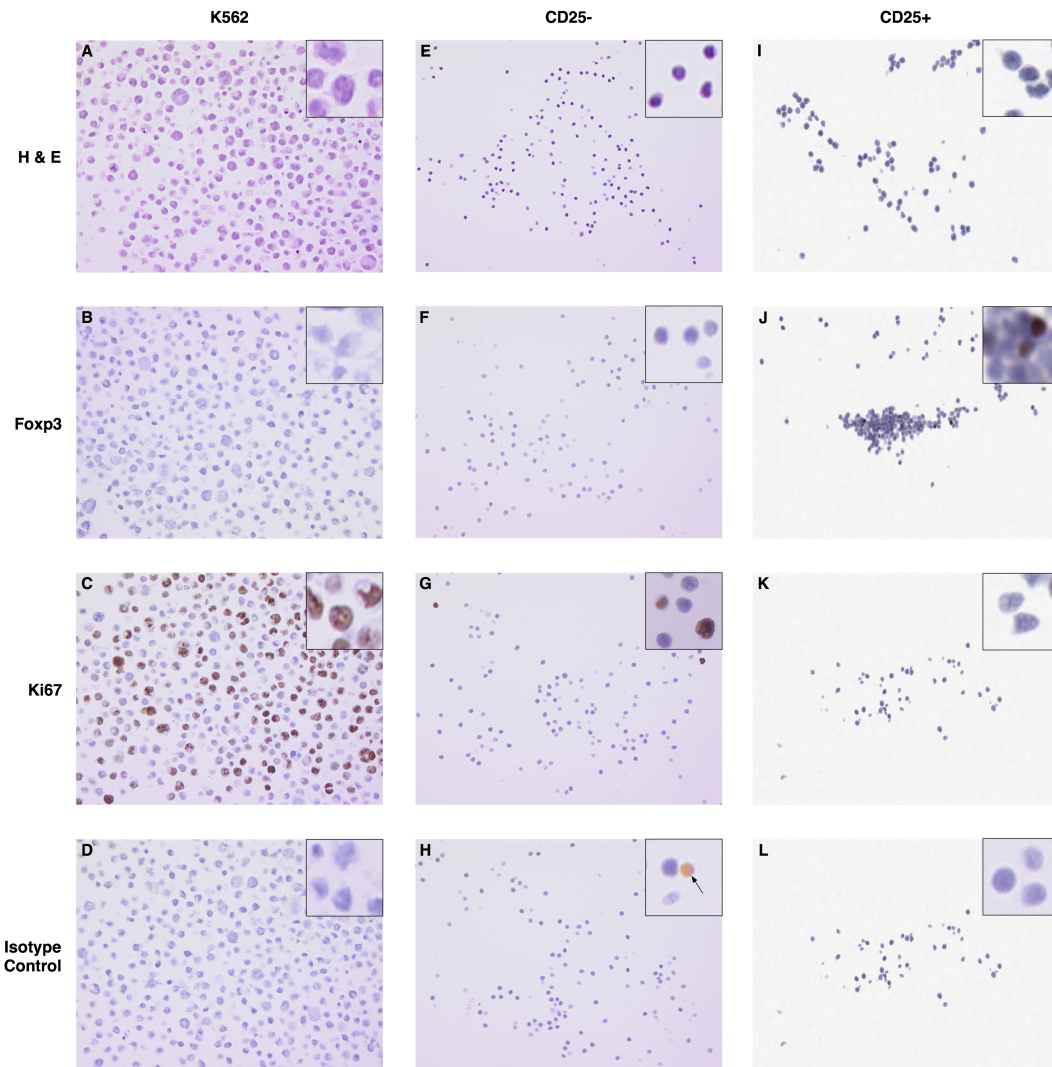


Figure 4.2 IHC Foxp3 Antibody Protocol Validation on Cell Pellets

Sections of K562 (A, B, C, D), CD25⁻ effector (E, F, G, H) and CD25⁺ Treg (I, J, K, L) cell pellets were de-waxed and re-hydrated followed by a pH 6 citrate antigen retrieval step. Sections were blocked in 3 % H₂O₂ followed by a serum-free protein block. Mouse anti-human Foxp3 (5 µg/ml) antibody (B, F, J), mouse anti-human Ki67 (0.35 µg/ml) antibody (C, G, K) or corresponding isotype controls (D, H, L) were incubated for 1 hour. Sections were incubated for 30 minutes in Mouse Envision HRP-linked polymer followed by two TBS-T wash steps. Liquid DAB was then added for 10 minutes before the sections were rinsed with water and counter-stained with Haematoxylin Gill III. Following dehydration in ethanol and clearing in xylene, sections were mounted with cover slips and left to air dry prior to visualisation. (Arrow, example remaining red blood cell from isolation procedure).

Development of these cell pellets enabled confidence in the presence of Tregs and subsequent successful staining protocol optimisation. Unfortunately, the optimal staining conditions differed for cell pellets and sections of tissue. For this reason, it was decided to move into human tissue. Further validation was achieved by running the antibodies of interest across different human tissues known to either be positive or negative for the different immune cells. Altered staining conditions greatly affect the specificity and quality of the staining, which are unique for individual antibodies, and therefore each stage of the protocol required optimisation. Due to the fixation of the tissue and embedding procedure, an antigen retrieval step was frequently required, in which the tissue was heated in a pressurised vessel using an optimal buffer to ‘free’ the target for antibody binding. Blocking steps to prevent non-specific binding were critical to minimise background staining. Endogenous peroxidase within the tissue can result in false positive staining as it reacts with the visualisation methods used. Any endogenous peroxidase activity was therefore quenched by incubating the specimen with an appropriate endogenous peroxidase blocking reagent, such as hydrogen peroxide. Different tissue and cells contain different levels of peroxidase and so optimisation of this step was required. A serum block or serum-free protein block was also necessary and required optimisation to prevent the ‘fc’ portion of the antibody sticking non-specifically to the tissue. The final protocol step that needed optimisation was the detection method used. The two methods tested within this study were Envision (Dako, K4001) and Vector Elite. Alongside optimising these staining steps, antibody concentration was also titrated. A summary of the optimisation carried out for this work is detailed in table 4.2.

Table 4.2 The Multiple Combinations of Optimisation Assays Carried Out

Antibody Concentration		Antigen Retrieval		Peroxidase Block		Serum Step		Detection Method
0.5 µg/ml		None						
1 µg/ml		Buffer		10 min		SF		Envision
5 µg/ml	x	pH 6 Citrate	x	20 min	x	S	x	ABC
10 µg/ml		pH 8 EDTA						
		pH 9						

(S, serum; SF, serum-free; ABC, Vector Elite ABC kit; EDTA, Ethylenediaminetetraacetic acid).

This validation and optimisation work was run across human lymph node and tonsil control tissue. Lymphoid tissue provides a good source of immune cells and so acts as a reliable positive control tissue. Lymphoid tissue contains spherical aggregates of lymphocytes called lymphoid follicles. Follicles responding to antigen have less densely stained germinal centres (GCs) and are described as secondary follicles (Figure 4.4D). The lymphocyte population of the GCs consists predominately of B cells in various stages of maturation, and possibly some macrophages. It is for this reason that lymphoid tissue provides such an excellent control for CD4, CD8 and Foxp3 T cell markers, as these should be absent from the GC, as seen in Figure 4.4, 4.5 and 4.7.

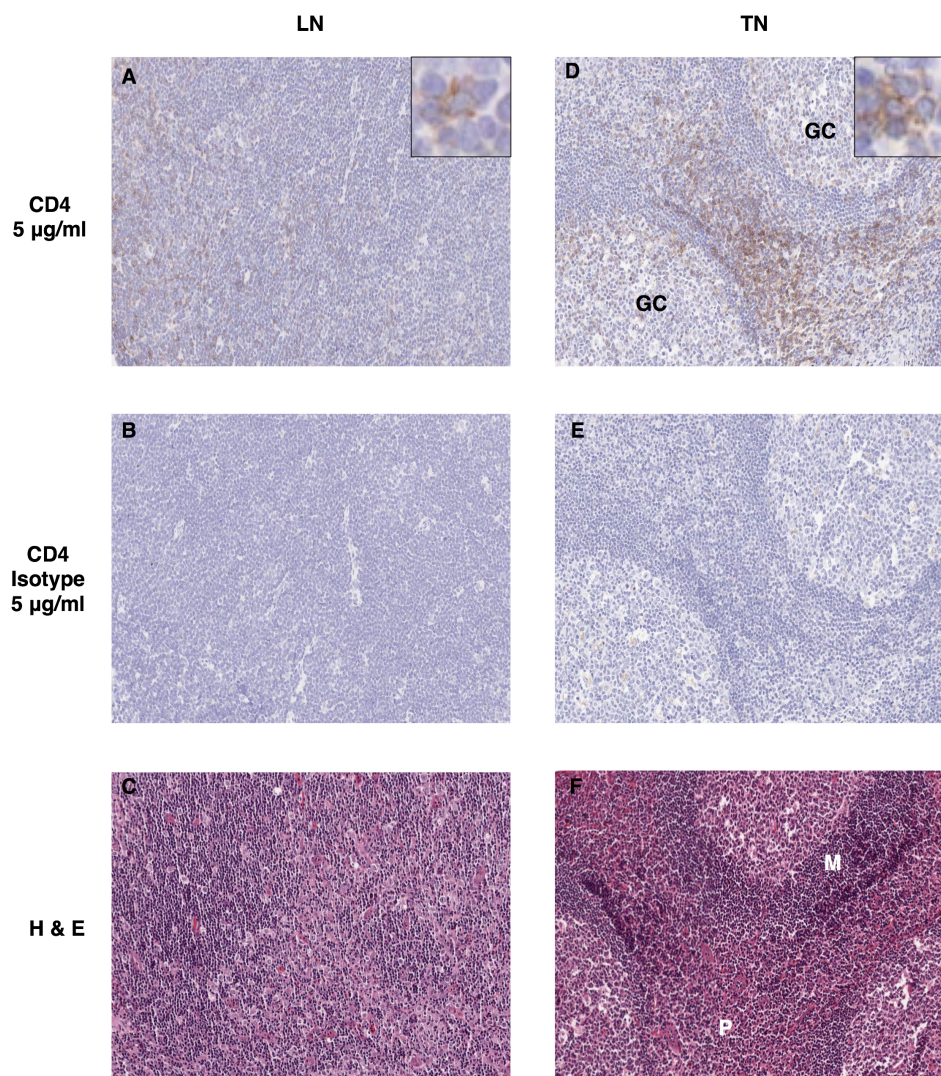


Figure 4.4 IHC CD4 Antibody Protocol Validation across Human Lymph Node and Tonsil Tissue

Human lymph node (LN) and tonsil (TN) tissue was de-waxed and re-hydrated followed by a pH6 citrate antigen retrieval step. Sections were blocked in 3 % H₂O₂ followed by a serum free protein block. Mouse anti-human CD4 IgG1 (5 µg/ml) antibody (A, D) or IgG1 isotype control (B, E) was then incubated for 1 hour. Sections were incubated for 30 minutes in Mouse Envision HRP-linked polymer followed by two TBS-T wash steps. Liquid DAB was then added for 10 minutes before the sections were rinsed with water and counter-stained with Haematoxylin Gill III. Following dehydration in ethanol and clearing in xylene, sections were mounted with cover slips and left to air dry prior to visualisation. Haematoxylin and Eosin (H & E) staining was also carried on each tissue type (C, F) as previously described. CD4 T cells are mainly present in the paracortex (P) and the mantle zone (M) but absent from the germinal centres (GC) containing small naive B cells. Images at x 20 original magnification.

Small naïve B cells and some T cells form in the dark mantle (M) zone; however, the paracortex (P) is predominately composed of T cells (Figure 4.4F). A similar pattern was observed for both CD4 and CD8 cells (Figure 4.5).

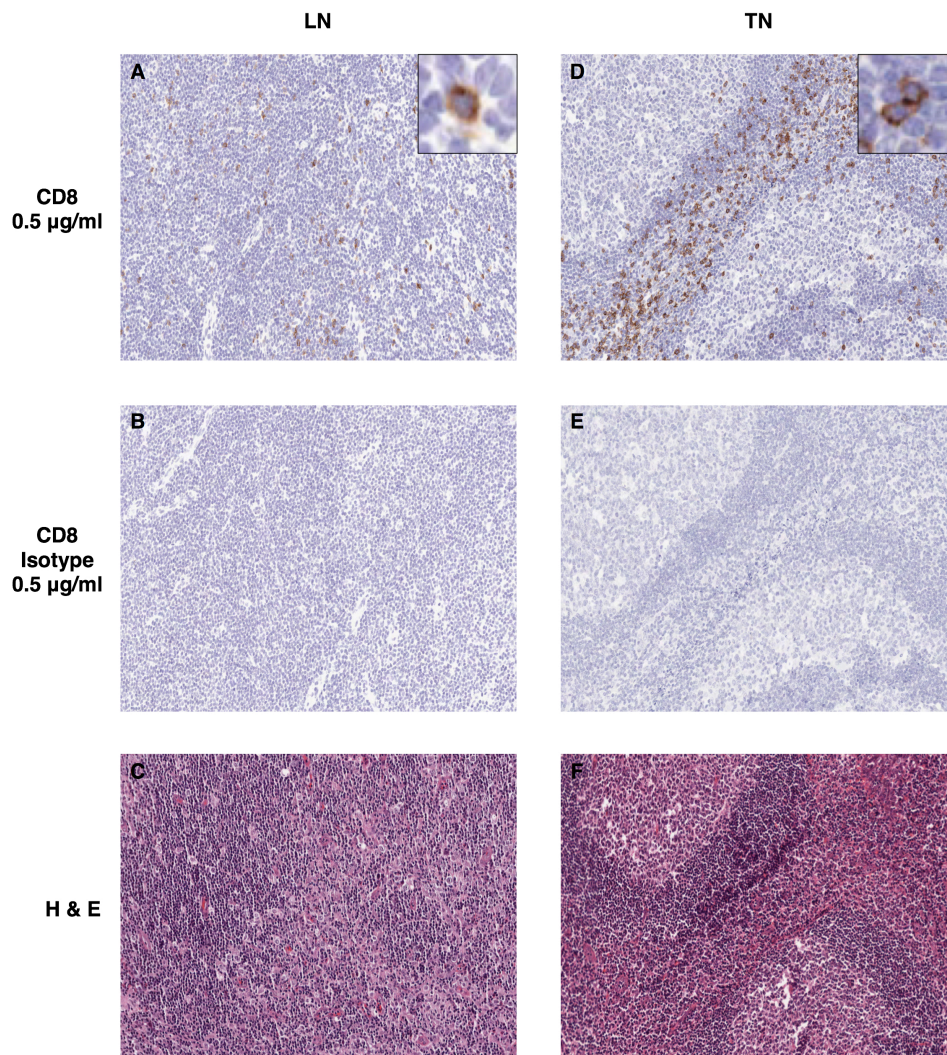


Figure 4.5 IHC CD8 Antibody Protocol Validation across Human Lymph Node and Tonsil Tissue

Human lymph node (LN) and tonsil (TN) tissue was de-waxed and re-hydrated followed by a pH6 citrate antigen retrieval step. Sections were blocked in 3 % H₂O₂ followed by a serum-free protein block. Mouse anti-human CD8 IgG2b (0.5 µg/ml) antibody (A, D) or IgG2b isotype control (B, E) was then incubated for 1 hour. Sections were incubated for 30 minutes in Mouse Envision HRP-linked polymer followed by two TBS-T wash steps. Liquid DAB was then added for 10 minutes before the sections were rinsed with water and counter-stained with Haematoxylin Gill III. Following dehydration in ethanol and clearing in xylene, sections were mounted with cover slips and left to air dry prior to visualisation. Haematoxylin and Eosin (H & E) staining was also carried on each tissue type (C, F), as previously described. Images at x 20 original magnification.

For NK cell staining, CD56-NCAM antibody was selected. CD56 provides good staining for NK cells; however, it is a neural cellular adhesion molecule and so also stains neuronal cells. Due to this potential cross-reactivity, cerebellum (brain) tissue was introduced as an additional positive control, and placenta as a negative control (Figure 4.6).

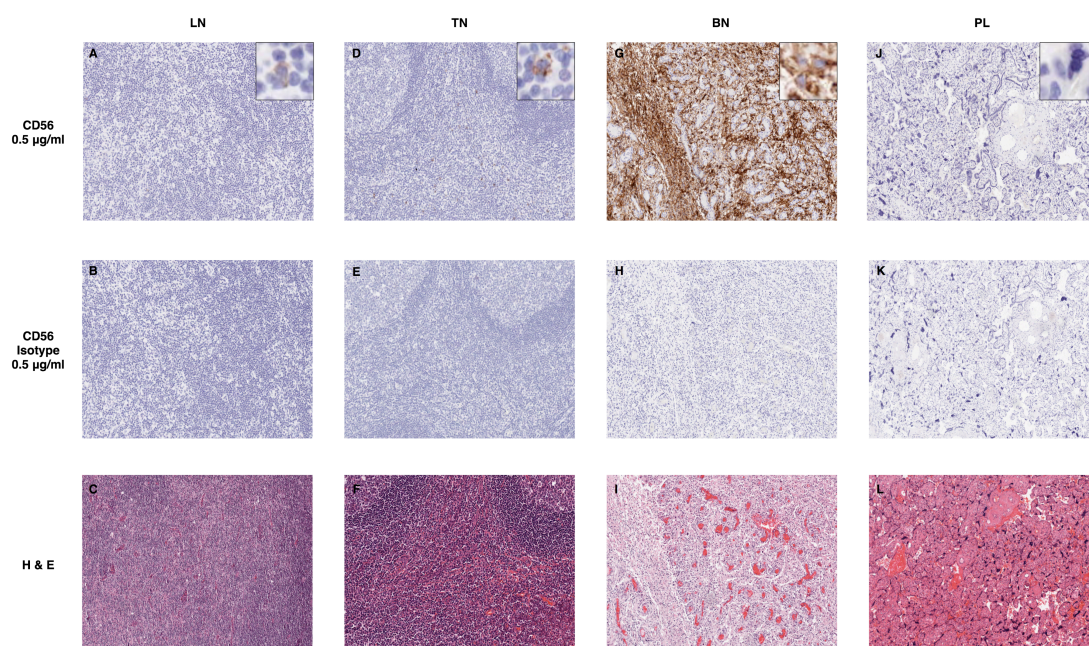


Figure 4.6 IHC CD56 Antibody Protocol Validation across a Selection of Human Tissue with Matched H & E Staining

Lymph node (LN), tonsil (TN), brain (BN) and placenta (PL) sections were de-waxed and re-hydrated followed by a pH6 citrate antigen retrieval step. Sections were blocked in 3 % H₂O₂ followed by a serum-free protein block. Mouse anti-human CD56 IgG1 (0.5 µg/ml) antibody (A, D, G, J) or IgG1 isotype control (B, E, H, K) was then incubated for 1 hour. Sections were incubated for 30 minutes in Mouse Envision HRP-linked polymer followed by two TBS-T wash steps. Liquid DAB was then added for 10 minutes before the sections were rinsed with water and counter-stained with Haematoxylin Gill III. Following dehydration in ethanol and clearing in xylene, sections were mounted with cover slips and left to air dry prior to visualisation. Haematoxylin and Eosin (H & E) staining was also carried on each tissue type (C, F, I, L), as previously described. Images at x 20 original magnification.

Figure 4.6 shows good specific staining of CD56⁺ NK cells within lymph node and tonsil tissue. In agreement with previous literature there is an absence of NK cells from the GCs. Strong positive staining was observed within brain tissue as expected, highlighting the cross-reactivity of the antibody for nerve cells. This was not a problem for the current study, as even small twig-like nerves, present in colorectal tissue, were easily distinguished from NK cells both by eye and also using analytical algorithms.

Foxp3 antibody validation was also carried out across human tonsil and lymph node tissue (Figure 4.7). Following protocol optimisation, good specific staining was achieved at 5 µg/ml. As T cells, they are absent from the germinal centres and found predominately throughout the paracortex area.

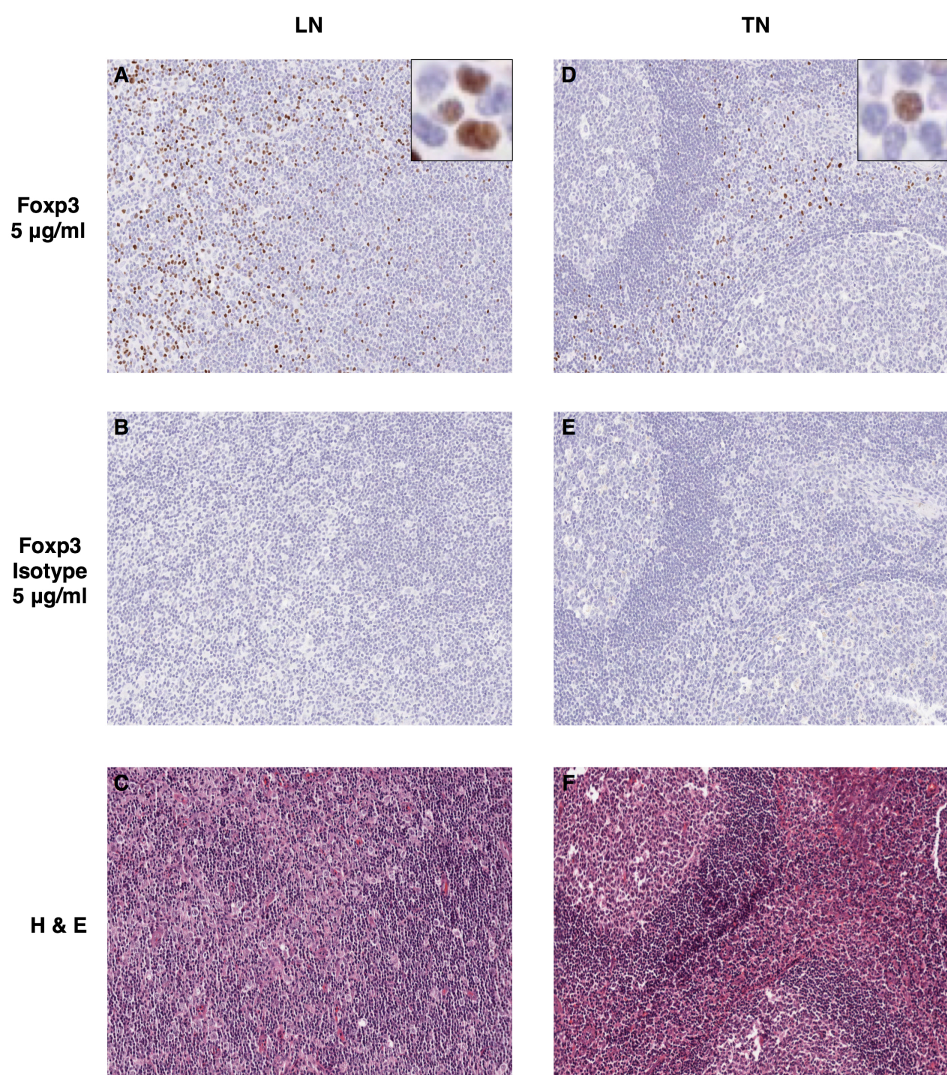


Figure 4.7 IHC Foxp3 Antibody Protocol Validation across Human Lymph Node and Tonsil Tissue

Lymph node (LN) and tonsil (TN) tissue was de-waxed and re-hydrated followed by a pH6 citrate antigen retrieval step. Sections were blocked in 3 % H₂O₂ followed by a serum-free protein block. Mouse anti-human Foxp3 IgG1 (5 µg/ml) antibody (A, D) or IgG1 isotype control (B, E) was then incubated for 1 hour. Sections were incubated for 30 minutes in Mouse Envision HRP-linked polymer followed by two TBS-T wash steps. Liquid DAB was then added for 10 minutes before the sections were rinsed with water and counter-stained with Haematoxylin Gill III. Following dehydration in ethanol and clearing in xylene, sections were mounted with cover slips and left to air dry prior to visualisation. Haematoxylin and Eosin (H & E) staining was also carried on each tissue type (C, F), as previously described. Images at x 20 original magnification.

During this optimisation work, a validated antibody was included as an internal positive control. Here the proliferation marker, Ki67 was used (Figure 4.8).

The lymphatic structures are further highlighted when staining for proliferation. Using Ki67 the highly proliferating B cells were very apparent within the germinal centres (Figure 4.8D).

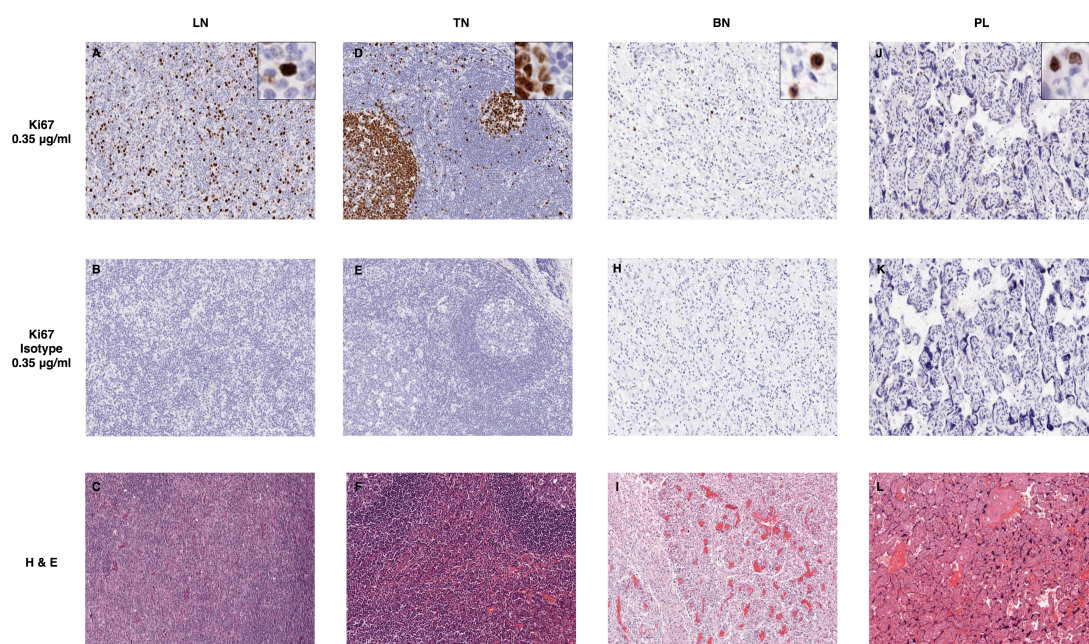


Figure 4.8 IHC Ki67 Staining across a Selection of Human Tissue with Matched H & E Staining

Lymph node (LN), tonsil (TN), brain (BN) and placenta (PL) tissue was de-waxed and re-hydrated followed by a pH6 citrate antigen retrieval step. Sections were blocked in 3 % H₂O₂ followed by a serum-free protein block. Mouse anti-human Ki67 IgG1 (0.35 µg/ml) antibody (A, D, G, J) or IgG1 isotype control (B, E, H, K) was then incubated for 1 hour. Sections were incubated for 30 minutes in Mouse Envision HRP-linked polymer followed by two TBS-T wash steps. Liquid DAB was then added for 10 minutes before the sections were rinsed with water and counter-stained with Haematoxylin Gill III. Following dehydration in ethanol and clearing in xylene, sections were mounted with cover slips and left to air dry prior to visualisation. Haematoxylin and Eosin (H & E) staining was also carried on each tissue type (C, F, I, L), as previously described. Images at x 20 original magnification.

Following full antibody validation and staining optimisation, markers with matched isotype controls were run across a sample of primary CRC tumour tissue (Figure 4.9).

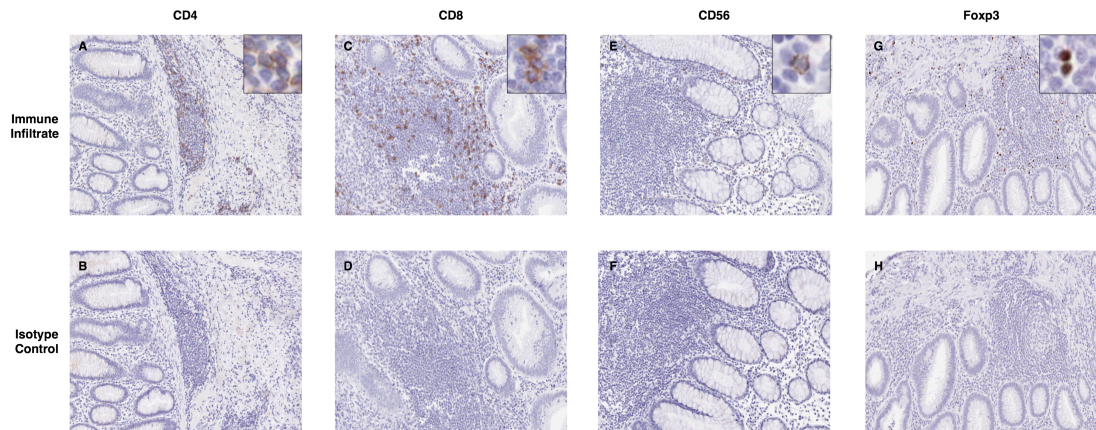


Figure 4.9 Key Immune Cell IHC Staining Across Human CRC Primary Tissue

Tissue was de-waxed and re-hydrated followed by a pH 6 citrate antigen retrieval step. Sections were blocked in 3 % H_2O_2 followed by a serum-free protein block. Mouse anti-human CD4 (A), CD8 (C), CD56 (E) or Foxp3 (G) antibodies or corresponding isotype controls (B, D, F, H) were then incubated for 1 hour. Sections were incubated for 30 minutes in Mouse Envision HRP-linked polymer followed by two TBS-T wash steps. Liquid DAB was then added for 10 minutes before the sections were rinsed with water and counter-stained with Haematoxylin Gill III. Following dehydration in ethanol and clearing in xylene, sections were mounted with cover slips and left to air dry prior to visualisation. Images at x 20 original magnification.

Optimal staining protocols can vary across different tissue. It was therefore necessary to test the methodology across the tissues of interest: colorectal and liver. Liver tissue contains a very high level of endogenous peroxidase. It was therefore necessary to increase the hydrogen peroxidases blocking incubation from 10 to 20 minutes to ensure the quenching reaction was fully complete.

In addition to immune infiltrates, a selection of markers were chosen to be incorporated into the study, with the aim of understanding more about the localisation of immune infiltrates with different aspects of the tumour microenvironment. These markers and a summary of the rationale for choosing them are depicted in Table 4.3.

Table 4.3 A Summary of Markers

Marker	For	Reference
<i><u>Immune Infiltrates:</u></i>		
<i>CD4</i>	T cell	Donskov and von der Masse, 2006; Kobayashi et al., 2007; Ohtani and Yoshie, 2010
<i>CD8</i>	Cytotoxic T cell	Kobayashi et al., 2007; Camus et al., 2009; Pages et al., 2009; Mlecnik et al., 2010
<i>Foxp3</i>	Tregs	Kobayashi et al., 2007; Ohtani and Yoshie, 2010
<i>CD56</i>	NK cell	Trzonkowski et al., 2004; Donskov and avon der Maase, 2006; Bamias et al., 2007; Mlecnik et al., 2010
<i>CD68</i>	Macrophages	Krogh Jensen et al., 2009; Mlecnik et al., 2010
<i><u>Tumour Microenvironment:</u></i>		
<i>CC-3</i>	Cleaved caspase-3 Apoptosis	Camus et al., 2009
<i>Ki67</i>	Proliferation	Camus et al., 2009; Brown and Gatter, 2002
<i>CD31</i>	Vasculature	Smith et al., 2001
<i>HIF-1α</i>	Hypoxia	Dewhirst et al., 2008; Matsumoto et al., 2010
<i>α-SMA</i>	Smooth muscle Stroma	Wang et al., 2006

Linking the type, density and location of immune cell infiltrates with areas of proliferation, apoptosis, hypoxia and vasculature was key to help understand the tumour microenvironment and the impact the immune system had on tumour progression.

Caspase-3 is one of the key executioners of apoptosis, as it is responsible for the proteolytic cleavage of many key proteins such as the nuclear enzyme poly ADP-ribose polymerase (PARP). Activation of caspase-3 requires proteolytic processing of its inactive form into activated cleaved caspase-3 (CC-3) p17 and p12 fragments. CC-3 therefore provided a reliable marker for apoptosis.

Alongside apoptosis, cell proliferation was also assessed using Ki67. Ki67 is a large 395 kDa protein that undergoes phosphorylation and dephosphorylation during mitosis, which is vital for cell proliferation (Brown and Gatter, 2002). Ki67 is routinely used as a marker of proliferation as it is a cell cycle related nuclear protein, expressed by proliferating cells in all phases of the active cell cycle (G1, S, G2 and M phase) but absent in resting (G0) cells. The anti-Ki67 antibody used in this study was the molecular immunology Borstel-1 (MIB-1) clone. Ki67 has a very specific localisation pattern within the nucleus, which changes during the cell cycle. It has an estimated half-life of 60–90 minutes, highly regulated by precise synthesis and degradation systems (Brown and Gatter, 2002).

In addition, the current study measured the levels of hypoxia. Hypoxia in tumours is caused by an imbalance in oxygen supply and demand, where regions of tumour are

beyond the diffusion distance of oxygen (Dewhirst, 2009; Vaupel and Mayer, 2007). Numerous studies have demonstrated the link between hypoxia and tumour treatment resistance. Intratumoral hypoxia causes increased expression and activity of hypoxia-inducible transcription factor-1 α (HIF-1 α) and thus provides a good marker of hypoxic tissue. HIF-1 is a heterodimeric transcription factor that consists of two subunits, HIF-1 α and HIF-1 β , which both belong to the helix-loop-helix proteins of the Per-ARNT-Sim family. HIF-1 regulates the transcription of a broad range of genes that facilitate responses to a hypoxic environment, including regulation of angiogenesis, erythropoiesis, the cell cycle, metabolism and apoptosis. HIF-1 α is widely expressed but normally rapidly degraded in normoxic cells by the ubiquitin/proteasomal pathway. HIF-1 α plays an important role in tumour progression, angiogenesis, metastasis and treatment resistance (Dewhirst et al., 2008).

There appears to be an agreement within the literature of an association between areas of hypoxia and poorly organised vasculature system. It was therefore decided to investigate the prevalence of blood vessels within the tumour, using CD31 as a marker. CD31, also known as platelet endothelial cell adhesion molecule-1 (PECAM-1), is a 130 kDa integral membrane glycoprotein expressed on the surface of endothelial cells.

Blood vessels consist of endothelial cells and pericytes. Pericytes are seen as important regulators of vessel function and angiogenesis. They are enveloped by basement membrane and are closely associated with endothelial cells in the

microvasculature. Pericytes express α -SMA and are thought to have a contractile function. α -SMA will therefore stain the supporting cells of the vascular system and co-localise with CD31. α -SMA is also used as an indicator for stromal elements (Smith et al., 2010). In addition, as a marker for smooth muscle, α -SMA staining is observed in the muscular regions of colorectal tissue.

In addition to the immune infiltrates described previously, the prevalence of infiltrating macrophages was also investigated. Here CD68 was used as a human macrophage cell marker (Mlecnik et al., 2010b).

Again, staining optimisation was required to run these markers across CRC and liver metastatic tissue. Example staining images are illustrated in Figure 4.10, where clean isotype controls demonstrating antibody specificity can be observed.

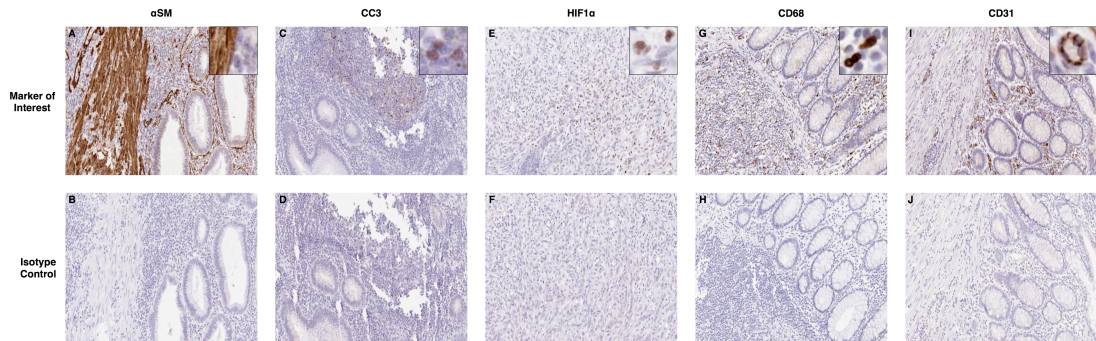


Figure 4.10 IHC Staining of Key Markers Taken Across Human CRC Primary Tissue

Tissue was de-waxed and re-hydrated followed by a pH 6 citrate antigen retrieval step. Sections were blocked in 3 % H₂O₂ followed by a serum-free protein block. Mouse anti-human alpha smooth muscle (α -SMA, A), cleaved caspase-3 (CC-3, C), hypoxia induced factor-1 alpha (HIF-1 α , E), CD68 (G) or CD31 (I) antibodies or corresponding isotype controls (B, D, F, H, J) were then incubated for 1 hour. Sections were incubated for 30 minutes in Mouse Envision HRP-linked polymer followed by two TBS-T wash steps. Liquid DAB was then added for 10 minutes before the sections were rinsed with water and counter-stained with Haematoxylin Gill III. Following dehydration in ethanol and clearing in xylene, sections were mounted with cover slips and left to air dry prior to visualisation. Images at x 20 original magnification.

Specific staining of CC-3 and HIF-1 α can be seen in areas of hypoxia. α -SMA and CD31 co-localise around blood vessels and α -SMA stains the stromal elements successfully. Staining for macrophages using CD68 was successfully optimised, where specific macrophages can be seen in Figure 4.10G. Species-specific isotype controls remained clean for all antibodies used (Figure 4.10B, D, F, H, and J).

4.2.2. Tissue of Interest and Ethics

The aim of this study was to evaluate a large cohort of patients for the orientation, density, and co-localisation of immune cells and to evaluate any differences between primary CRC and metastatic liver patients. Tissue selection was therefore very important to ensure the answers to these questions could be obtained. Three different sample groups were used, summarised in Table 4.4. All samples used were sourced from the AstraZeneca Alderley Park Biobank, which is a licenced premises under the Human Tissue Act (2004) (HTA number 12109) and has NRES ethical approval as a tissue bank (07/MRE08/29). All third party providers to the Alderley Park Biobank have passed an approval process at AstraZeneca and all samples are acquired by those providers with written informed consent.

Table 4.4 A Summary of the Tissue Used

1. Primary CRC with matched metastatic liver samples (n = 14)

Matched primary and secondary samples taken from the same patient were very valuable to this study to investigate the changes in immune infiltrates during the metastatic process. These primary samples were termed positive for metastasis (MET+)

Abbreviation	Tissue	Females	Average Age at Study (years)	Males	Average Age at Study (years)	n = Total	Tissue Source
Primary Tumour	Primary CRC tumour (MET+)	3	67.67	4	67.75	7	Indvmed
Mets Tumour	Matched metastatic liver tumour	3	67.67	4	67.75	7	Indvmed

2. Primary CRC alone (n = 25)

Primary CRC samples that did not go on to develop a metastatic phenotype (MET-) were also important to evaluate the changes in immune infiltrates between MET+ and MET-.

Abbreviation	Tissue	Females	Average Age at Study (years)	Males	Average Age at Study (years)	n = Total	Tissue Source
Tumour (MET-)	Primary CRC tumour, metastatic free at time of study	6	79.33	12	64.92	18	Indvmed
Stroma (MET-)	Primary CRC tumour-associated stroma, metastatic free at time of study	6	79.33	12	64.92	18	Indvmed
Tumour (MET+)	Primary CRC tumour, positive for liver metastasis (overlap with group 1)	3	68.33	4	67.5	7	Indvmed
Stroma (MET+)	Primary CRC tumour-associated stroma, positive for liver metastasis (overlap with group 1)	3	68.33	4	67.5	7	Indvmed

3. Liver metastatic CRC with adjacent non-neoplastic and matched distant normal liver (n = 80)

Metastatic CRC samples with matched distant normal samples were selected to enable a comparison between tumour adjacent non-neoplastic tissue and distant non-neoplastic samples.

Abbreviation	Tissue	Females	Average Age at Study (years)	Males	Average Age at Study (years)	n = Total	Tissue Source
Tumour (Tumour)	Liver metastatic tumour	INA	INA	INA	INA	40	MCRC
Tumour (Stroma)	Liver metastatic tumour-associated stroma	INA	INA	INA	INA	40	MCRC
Tumour (NonNeo)	Liver metastatic tumour-adjacent non-neoplastic	INA	INA	INA	INA	40	MCRC
Normal (Stroma)	Matched distant normal liver stroma	INA	INA	INA	INA	40	MCRC
Normal (NonNeo)	Matched distant normal liver non-neoplastic	INA	INA	INA	INA	40	MCRC

(INA, information not available; MCRC, Manchester Cancer Research Centre).

4.2.3. Image Analysis

Analysis of IHC images is often time consuming and subject to large variability. Digitally acquired images were achieved using a ScanScope digital scanner (Aperio Technologies Ltd.). Images were viewed and organised using ImageScope viewer and Spectrum operating system. Genie™ pattern recognition software (Aperio Technologies Ltd.) was used for the automated quantitative assessment of immune infiltrates within specific regions of tissue. Genie™ classifiers were generated for the separation of areas of tumour, stroma, lymphatic aggregates, non-neoplastic tissue and glass (Figure 4.11).

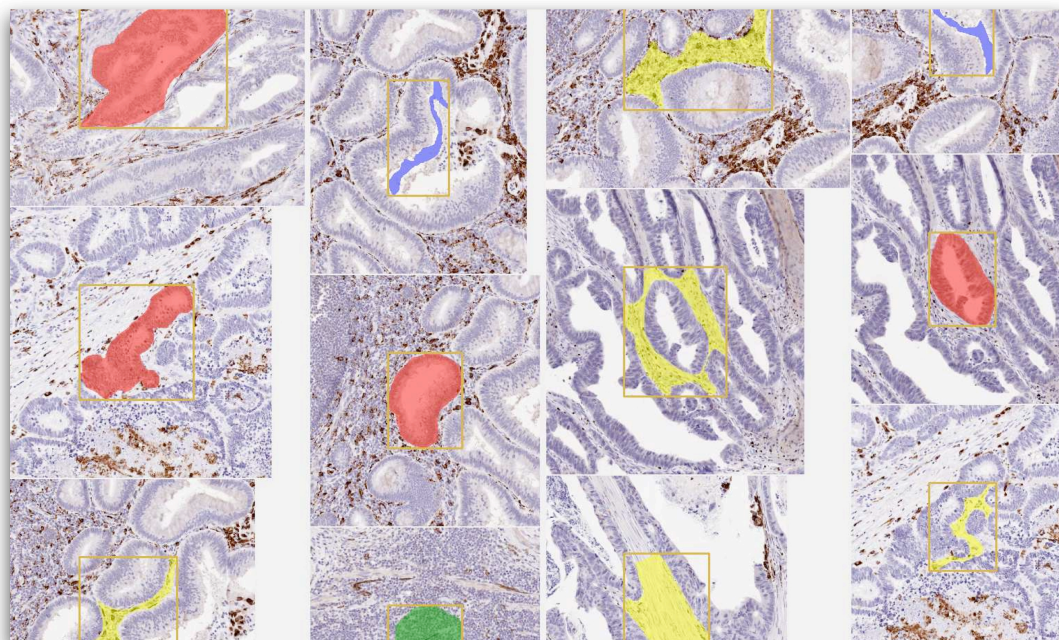


Figure 4.11 Genie™ Classifier Mark Up

Genie™ pattern recognition software (Aperio Technologies Ltd.) was implemented to distinguish different areas of tissue. Genie™ Classifiers were trained to recognise these patterns by manually marking up example areas. Areas identified included tumour (red), stroma (yellow), lymphatic (green) and background glass (blue).

Mark-up images were implemented to train the Genie™ classifiers to recognise the appropriate regions. Genie™ classifiers were then combined with appropriately tuned image analysis algorithms for the quantification of different markers. A nuclear algorithm was modified to quantify the number of immune cells, expressed as a percentage of the total number of cells within the area of interest (percentage positive cells %). The areas of stroma and lymphatic aggregate were combined and are herein termed ‘stroma’, resulting in three analysis outputs (Figure 4.12).

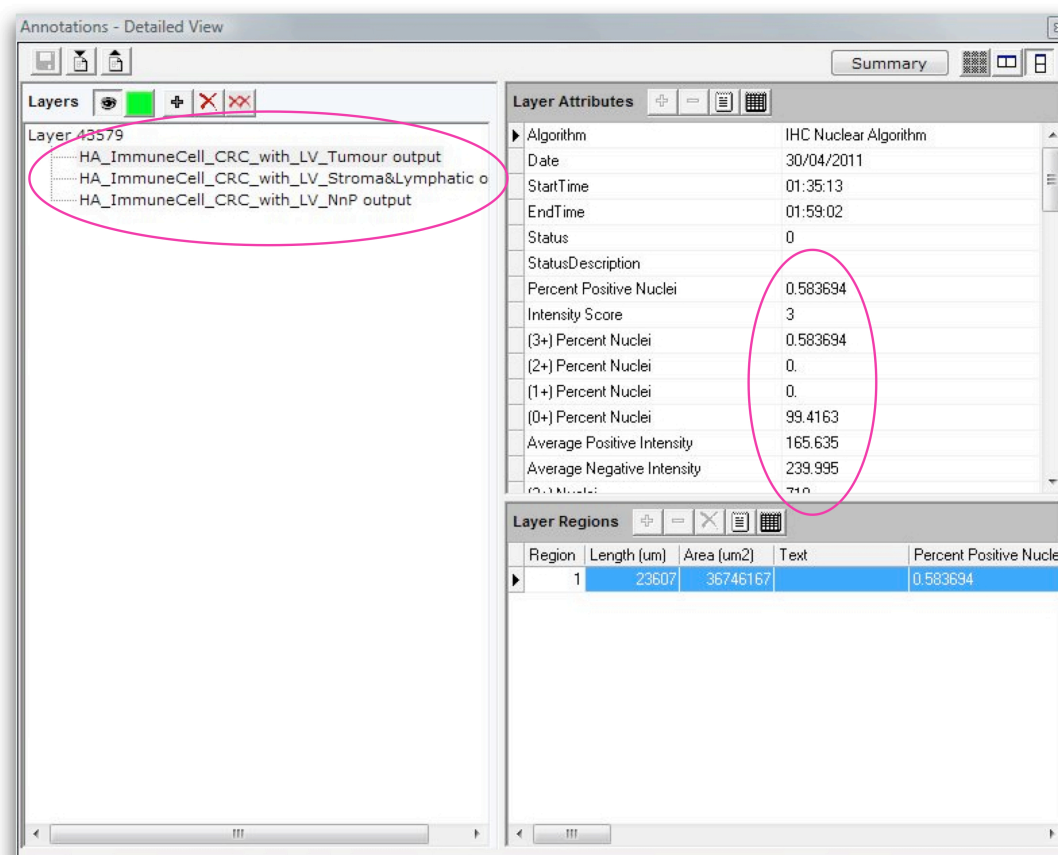


Figure 4.12 Example Genie™ Analysis Output

Genie™ Classifiers under-went pattern recognition training to identify areas of tissue. These then provided data analysis outputs, for example; 'HA_ImmuneCell_CRC_with_LV_Tumour' (colorectal or liver tumour tissue), 'HA_ImmuneCell_CRC_with_LV_Stroma&Lymphatic' (colorectal or liver stroma and lymphoid tissue) and 'HA_ImmuneCell_CRC_with_LV_NnP' (Non-neoplastic colorectal and liver tissue). Classifiers were then combined with a nuclear algorithm for each output and expressed as the number of percentage positive cells within that area.

Digitally acquired images were then marked up for analysis, highlighting the area of interest to reduce the background white space (Figure 4.13). Analysis was carried out and data exported into Microsoft Excel™.

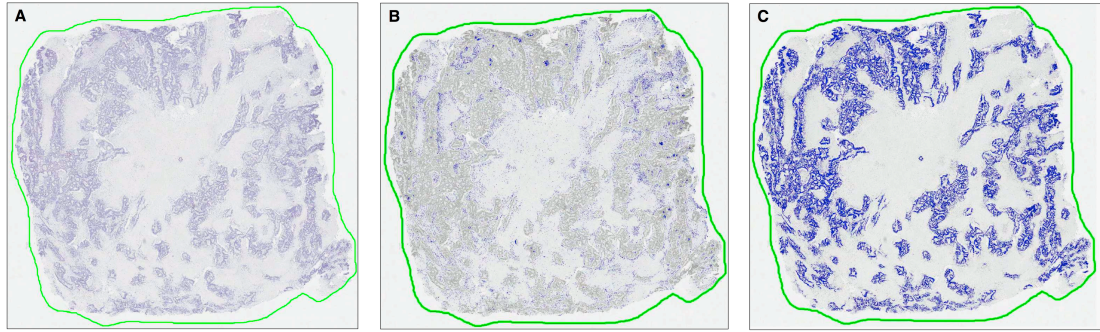


Figure 4.13 Genie™ Analysis of Stroma and Tumour

The area of interest was manually marked (green line) to reduce the amount of background white space. Genie™ Classifiers underwent pattern recognition training to identify areas of tissue and were then combined with a nuclear algorithm for each output, for example A) tissue alone B) stroma and C) colorectal liver metastatic tumour.

The distinct morphology of CRC tumour necessitated the generation of only a few variations of Genie™ classifiers for different sets of tumour samples. AstraZeneca are one of the few places in the United Kingdom to pilot this image analysis platform. The development of classifiers to distinguish human tumour, stroma and non-neoplastic tissue, is a novel achievement. Refined image analysis, coupled with this ability to characterise distinct human tissue components, could refine current pathological techniques. The classifiers were able to separate the designated regions with a high degree of accuracy. Example images of separating tumour from stroma can be seen in Figure 4.14.

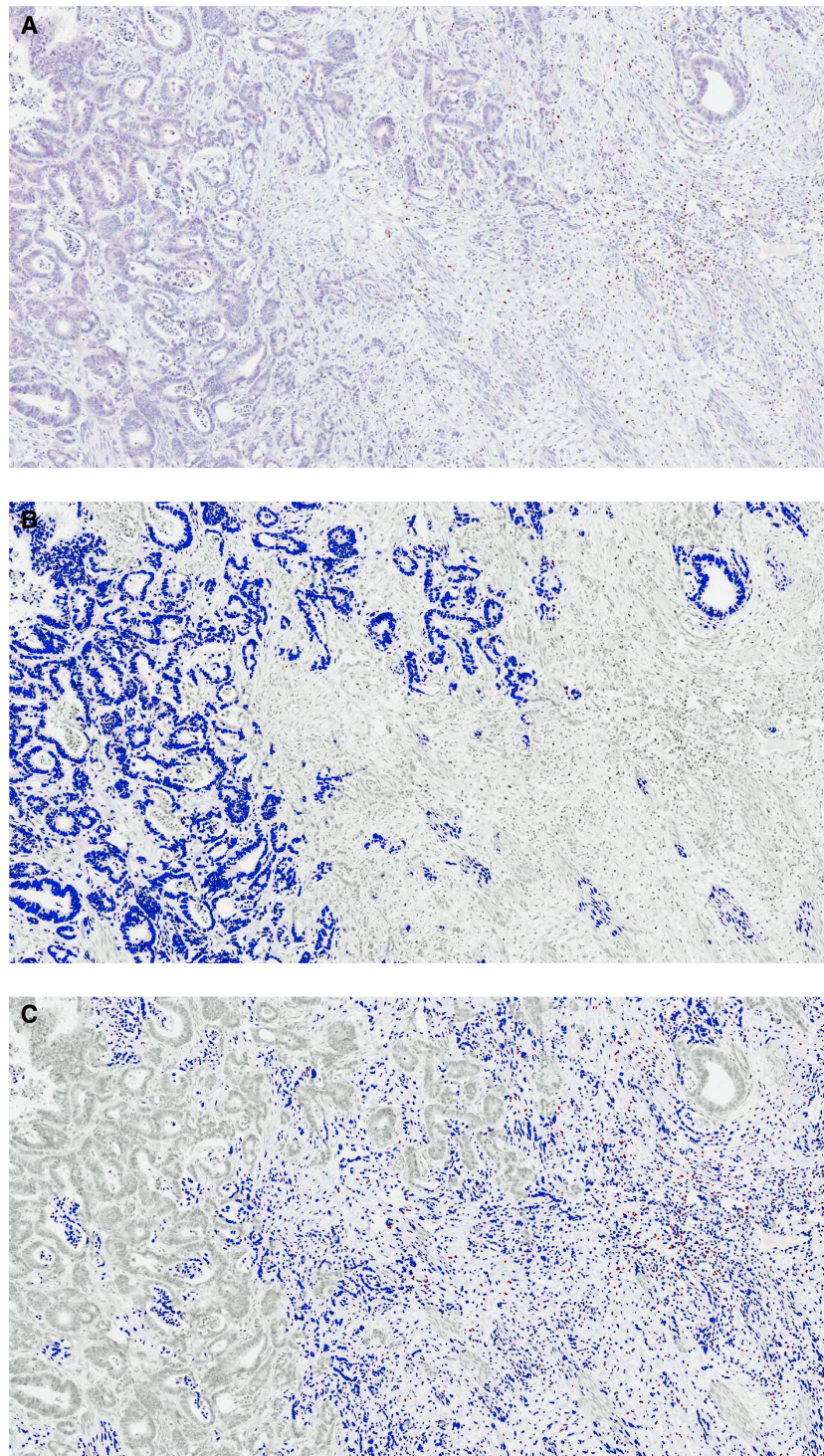


Figure 4.14 Genie™ Analysis of Foxp3 Algorithm in Stroma and Tumour

A) Digital images were acquired. Genie™ Classifiers were then used to distinguish the areas of B) tumour and C) stroma, combined with a nuclear algorithm to quantify the percentage positive number of immune cells (brown).

4.2.4. Immune Infiltrates in Colorectal Metastatic Liver Samples

It is becoming increasingly apparent that tumours contain various cells from the immune system, including Tregs, cytotoxic T cells, NK cells, macrophages, neutrophils, B lymphocytes, and DCs (Pages et al., 2008).

It was necessary to solidify the association between tumour progression and inflammation and to understand the interactions between tumour cells and immune infiltrates, that result in a balance between tumour promotion and tumour suppression. An increasing amount of evidence supports the idea that immune infiltration into the tumour microenvironment could influence clinical outcome and disease progression, regardless of the tumour stage.

4.2.4.1. Adaptive Immunity

4.2.4.1.1. CD8 Positive Cytotoxic T Cells

The prevalence of cytotoxic T cells was analysed immunohistochemically using a CD8 antibody. Initially, seven primary CRC tissue samples with patient matched metastatic liver samples were evaluated (Figure 4.15).

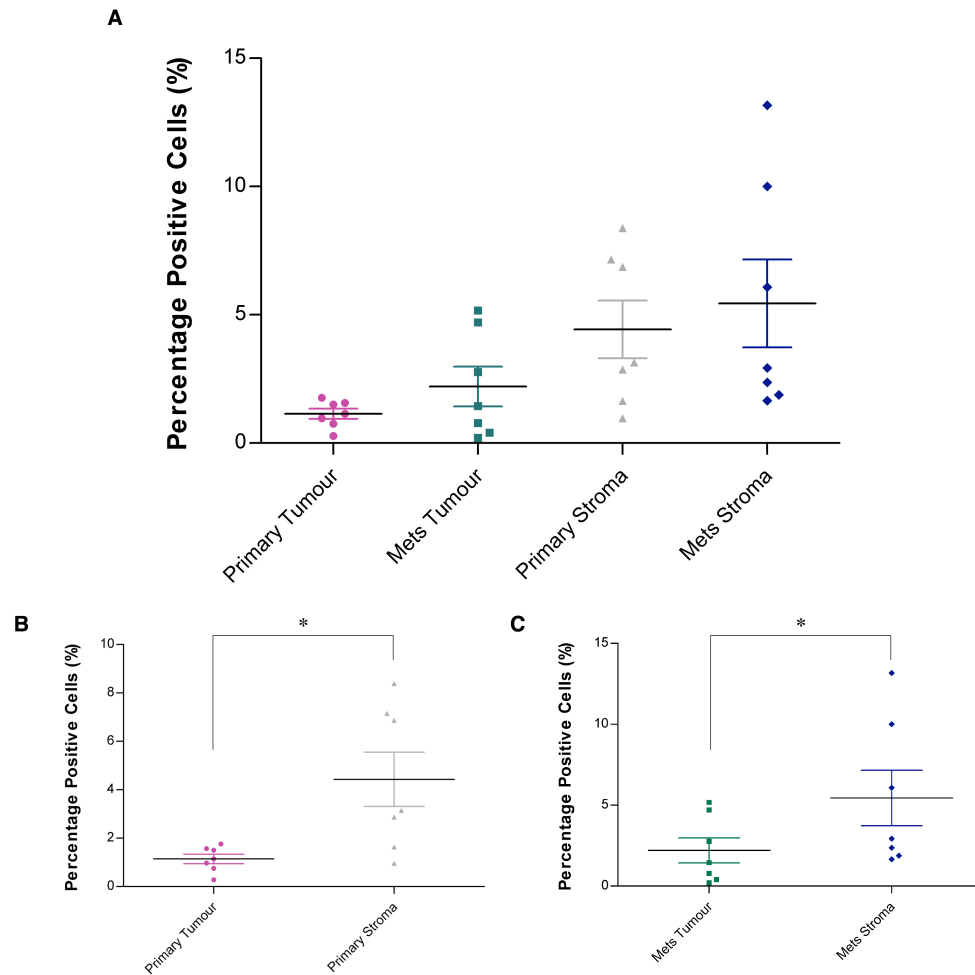


Figure 4.15 CD8 Cell Infiltrates in Primary CRC vs Metastatic Liver

Primary CRC and matched liver metastatic tissue was examined for CD8 cell infiltration using IHC techniques (mouse anti-human CD8 IgG2b, 0.5 μ g/ml). Digital images were acquired and Genie™ Classifiers were then used to distinguish the areas of tumour and stroma, combined with a nuclear algorithm to quantify the percentage positive number of CD8 cells. A) An overall assessment of the percentage positive CD8 cells in primary and metastatic disease was carried out. A direct comparison between the number of CD8 cells in the tumour and stroma for both B) primary and C) metastatic (met) tissue. (Paired t-test, normal distribution, * $p < 0.05$).

The percent of positive CD8 cells within the tumour and stroma of primary and secondary diseased tissue was compared. There was a significant ($p < 0.05$) elevation of CD8 CTLs within the stroma of both primary CRC and metastatic liver samples.

Previous studies have examined the CD8/CD3 T cell density ratio in relation to clinical outcome, where high proportions of CD8 cytotoxic T cells within the primary tumour was seen to be associated with reduced risk of relapse (Camus et al., 2009).

The primary (MET+) samples from Figure 4.15 were then compared to primary CRC samples that showed no metastatic development (MET-) ($n = 18$). This correlation was necessary to assess any differences in the prevalence of cytotoxic CD8 cells between a MET+ and MET- primary tissue phenotype (Figure 4.16).

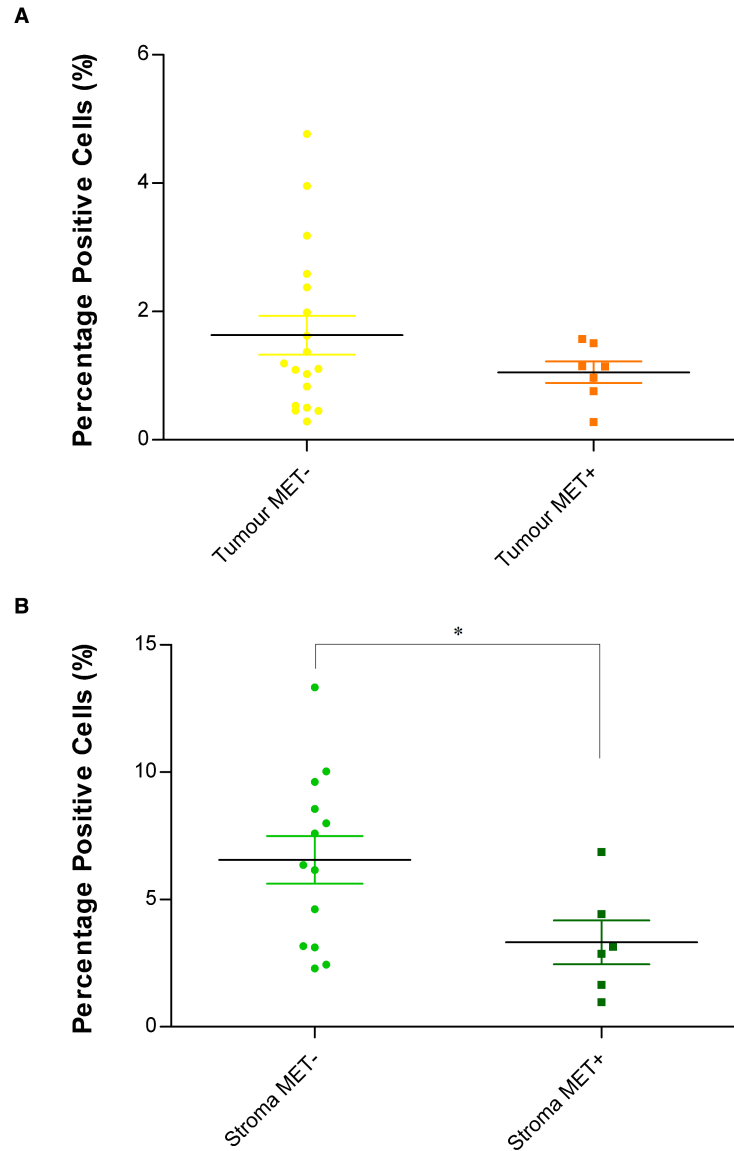


Figure 4.16 Comparison of CD8 Cells in MET+ and MET- Primary CRC Tissue

Primary CRC with no affiliated metastatic disease (MET-) and primary CRC that has since developed liver metastasis (MET+) were compared for CD8 cell infiltration using IHC techniques (mouse anti-human CD8 IgG2b, 0.5 µg/ml). Digital images were acquired and Genie™ Classifiers were then used to distinguish the areas of tumour and stroma. This was combined with a nuclear algorithm to quantify the percentage positive number of CD8 cells in the A) tumour and B) stroma. (Unpaired t-test, normal distribution, * $p < 0.05$).

MET⁺ and MET⁻ primary samples were evaluated for the percent of positive CD8 cells within the tumour (Figure 4.16A) and stroma (Figure 4.16B). Similar trends were observed for both tumour and stroma regions, where MET⁺ primary samples showed significantly lower levels of CD8 cell infiltration.

Data are in agreement with previous literature where MET⁺ patients showed significantly lower levels of CD3⁺CD8⁺ cells compared with MET⁻ patients (Camus et al., 2009). CD8⁺/CD4⁺ and CD8⁺/CD3⁺ cell ratios were also significantly higher in MET⁻ compared with MET⁺ patients (Camus et al., 2009).

Research suggests that primary CRC tissue with fewer CD8 infiltrates results in metastatic development. This is in accordance with previous research that highlighted that patients without recurrence had higher overall CD8 cell densities in primary tumours (Galon et al., 2006; Pages et al., 2008).

CRC liver metastatic samples with matched distant normal liver samples were then selected (n = 40) to enable a comparison between tumour, tumour adjacent non-neoplastic tissue and distant non-neoplastic samples (Figure 4.17)

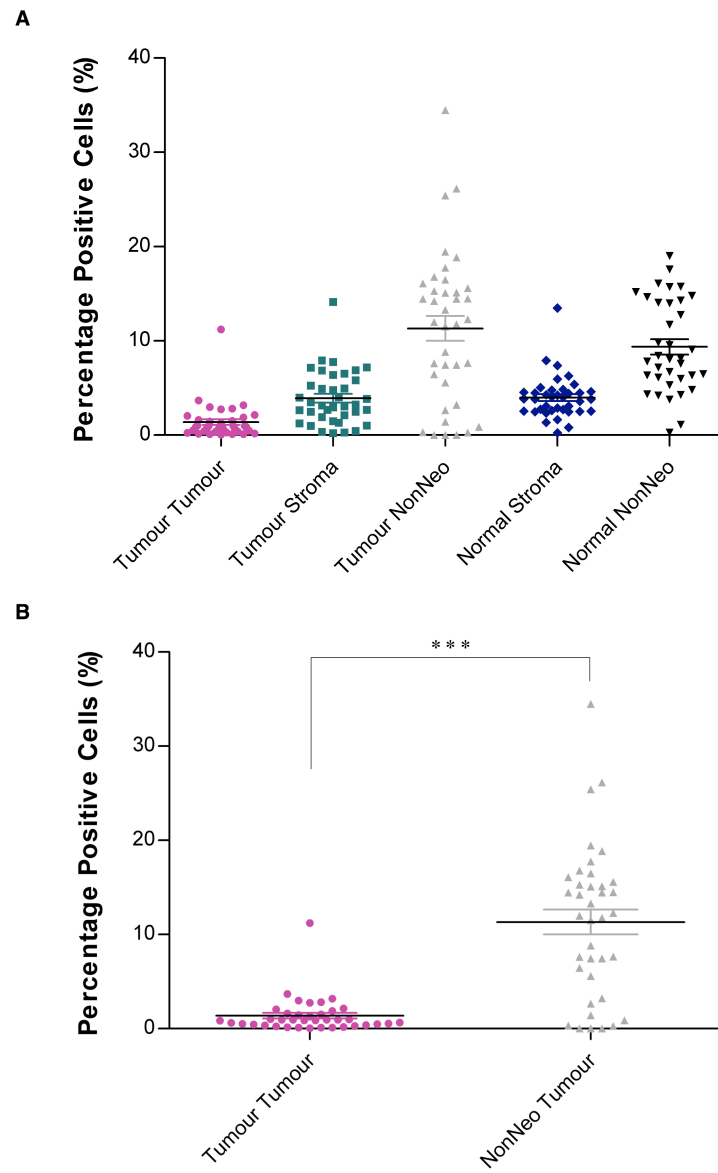


Figure 4.17 CD8 Cells in Liver Metastatic CRC and Matched Non-Neoplastic Tissue

The prevalence of CD8 cells was analysed immunohistochemically (mouse anti-human CD8 IgG2b, 0.5 μ g/ml). Digital images were acquired and Genie™ Classifiers were combined with a nuclear algorithm to quantify the percentage positive number of cells. A) Tumour (Tumour Tumour), tumour-associated stroma (Tumour Stroma) and tumour adjacent non-neoplastic (Tumour NonNeo) tissue was compared to matched distant normal stroma (Normal Stroma) and non-neoplastic (Normal NonNeo). B) A comparison between tumour adjacent non-neoplastic (NonNeo Tumour) and distant non-neoplastic (NonNeo Normal) tissue was achieved (Paired t-test, normal distribution, *** $p < 0.001$).

When investigating the location of CD8 cells, it became apparent that there was a significant increase in the number of CTLs within the non-neoplastic tissue at the tumour edge compared to distant non-neoplastic tissue or within the tumour itself ($p < 0.001$, Figure 4.17B). An example image of this is illustrated in Figure 4.18. In addition, the frequency of CD8 cells at the adjacent non-neoplastic area was higher ($p < 0.01$) than those observed within the stroma infiltrating the tumour. When comparing normal non-neoplastic tissue with tumour tissue the frequency of CD8 cells drops significantly ($p > 0.001$), perhaps indicating the inability of CD8 cells to penetrate into the CT.

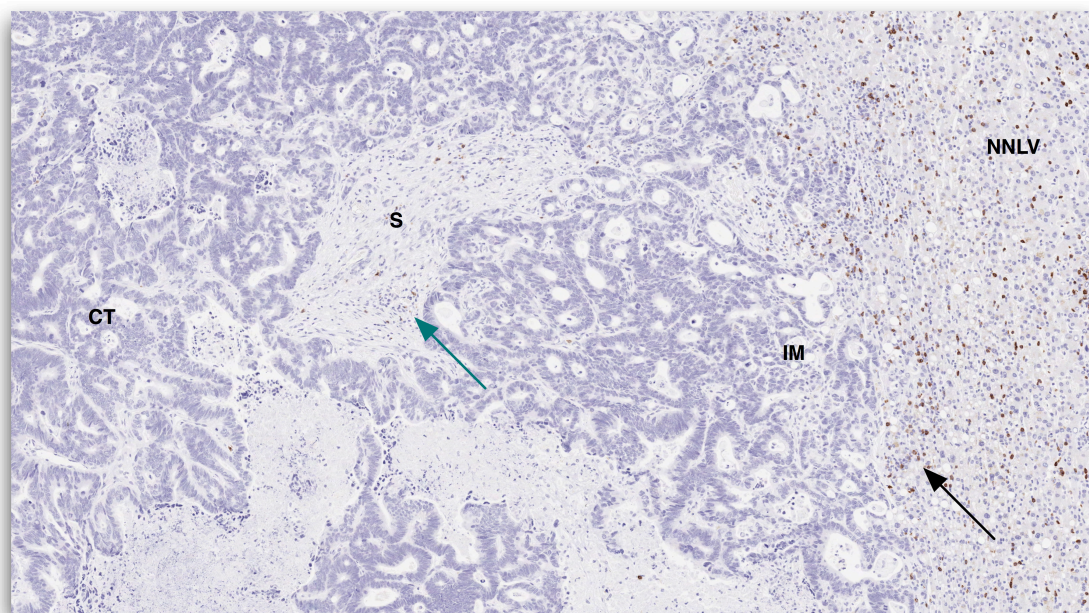


Figure 4.18 Example Image of CD8 Immune Cells in Liver Metastatic CRC

Liver metastatic CRC tissue was de-waxed and re-hydrated followed by a pH 6 citrate antigen retrieval step. Sections were blocked in 3 % H_2O_2 followed by a serum-free protein block. Mouse anti-human CD8 IgG2b (0.5 $\mu\text{g}/\text{ml}$) antibody was then incubated for 1 hour. Sections were incubated for 30 minutes in Mouse Envision HRP-linked polymer followed by two TBS-T wash steps. Liquid DAB was then added for 10 minutes before the sections were rinsed with water and counter-stained with Haematoxylin Gill III. Following dehydration in ethanol and clearing in xylene, sections were mounted with cover slips and left to air dry prior to visualisation. Image at x 20 original magnification. (CT, tumour centre; S, stroma; IM, invasive margin;>NNLV, non-neoplastic liver; green arrow, CD8 within the stroma; black arrow, CD8 within the>NNLV).

Numerous CD8 cells were observed in the non-neoplastic liver (NNLV) tissue at the tumour edge (Figure 4.18, black arrow). The number of CD8 cells at this invasive IM was significantly higher than those found at the CT, both within the tumour-associated stroma (Figure 4.18, green arrow) and in the tumour itself.

Previous studies have also examined the location of CD8 cells in the CT and at the IM of CRC patients. These studies have shown that patients without recurrence had higher overall CD8 cell densities (Galon et al., 2006; Pages et al., 2008).

The rationale for the elevation of CTLs at the tumour edge becomes an interesting debate. The author would like to propose two hypotheses. Firstly, the increased number of CD8 cells at the tumour edge may be providing a protective ‘blanket’ for the surrounding non-neoplastic tissue. Here the CTLs could be holding back the progression of tumour growth. This would tie in well with studies that show an elevation of CD8 cells results in reduced recurrence and a MET- phenotype. However, it could also be argued that the tumour may be producing a cocktail of chemokines and cytokines, preventing CD8 penetration into the CT and therefore resulting in reduced levels of tumour cytotoxicity. Perhaps what we are seeing is the result of a cytokine/chemokine chemical gradient extending from the tumours edge? Understanding ways to perforate this hypothesised impenetrable ‘buffer zone’ could lead to the development of a therapeutic solution.

Finally, primary and metastatic CRC samples were pooled to examine the occurrence of CD8 cells specifically between the tumour and stroma (Figure 4.19).

The frequency of CTLs was significantly higher in the stroma (Figure 4.19B, green arrow) compared to those infiltrating the tumour (Figure 4.19B, black arrow) ($p < 0.0001$).

4.2.4.1.2. *Foxp3* Positive Tregs

Alongside the level of infiltrating CTLs, the pervasiveness of Tregs was also investigated, through staining for Foxp3. Foxp3-positive staining was observed in colorectal tumour sections of various stages and differentiation. Initially, as with CD8 staining, seven primary CRC tissue samples with patient matched metastatic liver samples were evaluated to investigate the role of Tregs in CRC tumour progression (Figure 4.20).

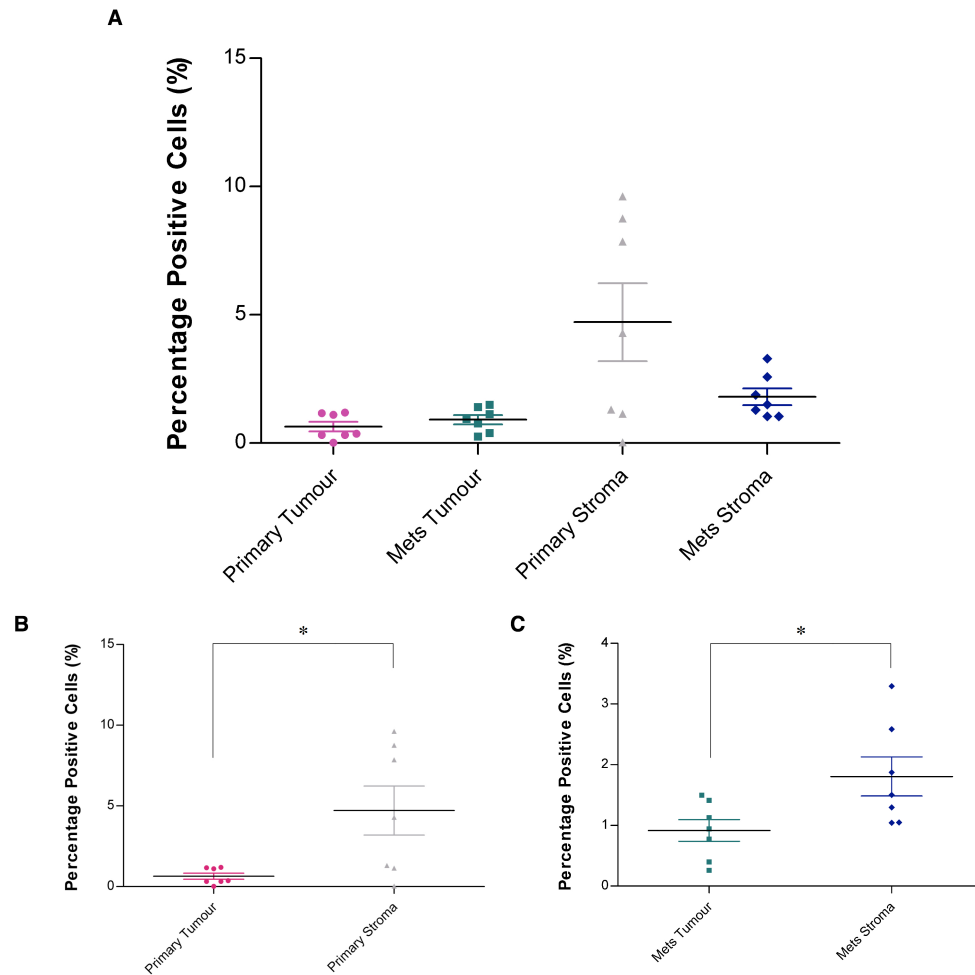


Figure 4.20 Foxp3 Cell Infiltrates in Primary CRC vs Matched Metastatic Liver

Primary CRC and matched liver metastatic tissue was examined for Treg infiltration into the tumour and stroma using IHC techniques (mouse anti-human Foxp3 IgG1, 5 μ g/ml). Digital images were acquired and Genie™ Classifiers were then used to distinguish the areas of tumour and stroma. This was combined with a nuclear algorithm to quantify the percentage positive number of Foxp3 Tregs. A) An overall assessment of the percentage positive Tregs in primary and metastatic disease was carried out. A direct comparison was made between the number of Tregs in the tumour and stroma for both B) primary and C) metastatic (met) tissue. (Paired t-test, * $p < 0.05$).

No significant differences were found when evaluating the frequency of Tregs between primary CRC and secondary liver disease (Figure 4.20A). However, as with CD8 analysis, Tregs were significantly elevated within the stromal areas compared to infiltrating the tumour itself (Figure 4.20B). This was true for both primary and secondary disease.

To further examine this correlation, primary MET+ and primary MET- samples were compared for Treg frequency (Figure 4.21).

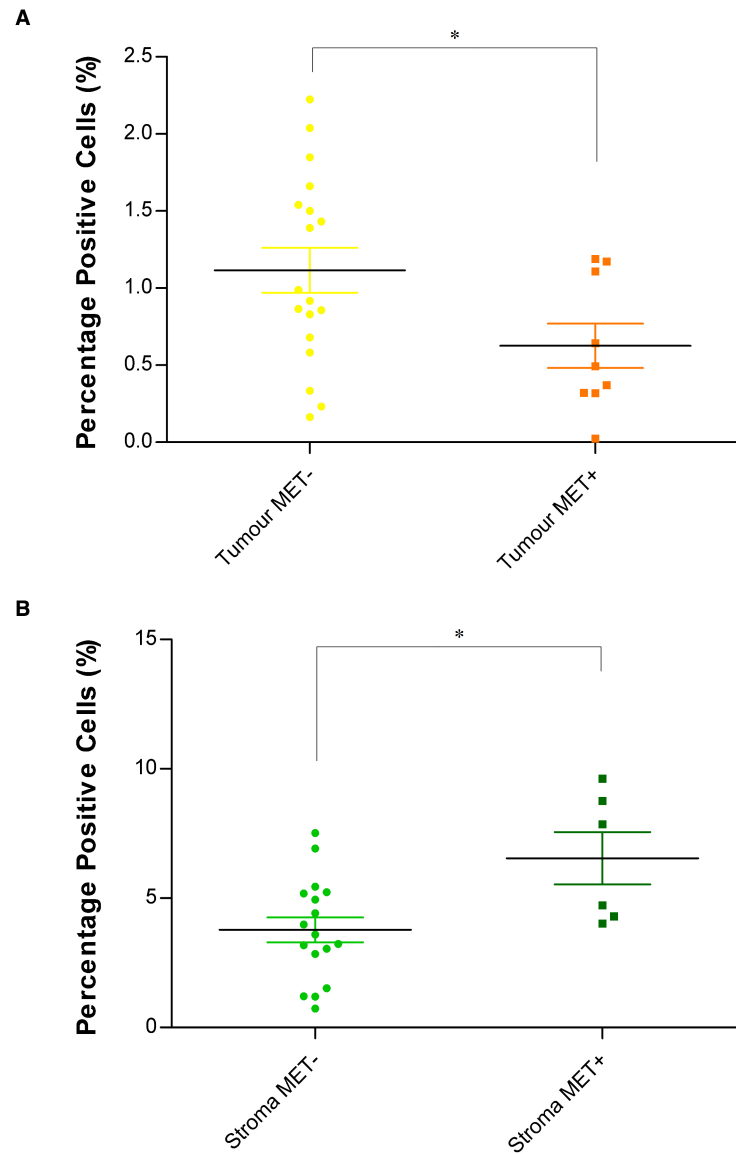


Figure 4.21 Comparison of Foxp3 Cells in MET+ and MET- Primary CRC Tissue

Primary CRC with no affiliated metastatic disease (MET-) and primary CRC that has since developed liver metastasis (MET+) were evaluated immunohistochemically (mouse anti-human Foxp3 IgG1, 5 µg/ml). Digital images were acquired and Genie™ Classifiers were then used to distinguish the areas of tumour and stroma. This was combined with a nuclear algorithm to quantify the percentage positive number of Foxp3 Tregs infiltration into the A) tumour and B) stroma. (Unpaired Mann-Whitney test, * $p < 0.05$).

Results demonstrated an inverse relationship between Tregs in the stroma and tumour of MET+ tissue. A decrease in the incidence of Tregs within tumour cell-rich regions was affiliated with a MET+ phenotype, whereas an increase Tregs within stromal-rich regions was associated with a MET+ phenotype.

The general consensus is that increased numbers of Tregs are associated with poor prognosis and tumour progression. However, here we showed that Tregs infiltrating the tumour are less frequent in patients who go on to develop metastatic disease (MET+). Some literature has suggested that Tregs may not always be associated with poor prognosis. For example, Salama *et al.*, reported an increase in Foxp3 density within the tumour was linked with better OS (Salama et al., 2009). In contrast, additional research has shown that patients with elevated Treg numbers showed reduced survival rates and the accumulation of Tregs was related to disease progression (Mizukami et al., 2008b; Wolf et al., 2005).

The current data are in conflict with some previous literature showing no significant difference in the number of Tregs (CD4⁺CD25^{hi}) between MET+ and MET- when analysed using large scale flow cytometry (Camus et al., 2009).

It is the author's opinion that analysis using large-scale flow cytometry loses the detail of location that has been demonstrated in this study and this is why a lack of significance was previously observed. By using IHC techniques, the precise location of Tregs can be compared, to a greater degree of accuracy. The current data also perhaps supports the previously conflicting publications on the prognostic

significance of Tregs. Are Tregs within the tumour associated with better prognosis, whilst Tregs within the stroma associated with a poor prognosis?

The question of the prognostic role of Tregs in human CRC appears to be complex and ambiguous. Curiel *et al.*, (2004) reported that the increase in Tregs correlated with tumour staging and reduced survival in ovarian carcinoma. Subsequent data are in agreement with this, in other solid tumours, such as NSCLC (Woo *et al.*, 2001), gastric (Mizukami *et al.*, 2008b) and hepatocellular carcinoma (Fu *et al.*, 2007). In contrast to this, data have accumulated suggesting that elevated Tregs may not always be linked with poor prognosis (Ladoire *et al.*, 2011a; Salama *et al.*, 2009). A recent study has proposed that tumour infiltrating Tregs are associated with favourable prognosis in patients with CRC, and Tregs are acting against a microbial driven response rather than by tumour antigens (Ladoire *et al.*, 2011a).

Galon's group found no association between Foxp3, CTLA-4, GITR, IL-10, TGF- β and the presence of intratumoural or distant metastasis (Pages *et al.*, 2008).

As with the CD8 cell analysis, metastatic CRC samples with matched distant non-neoplastic tissue were analysed for Treg infiltration (Figure 4.22).

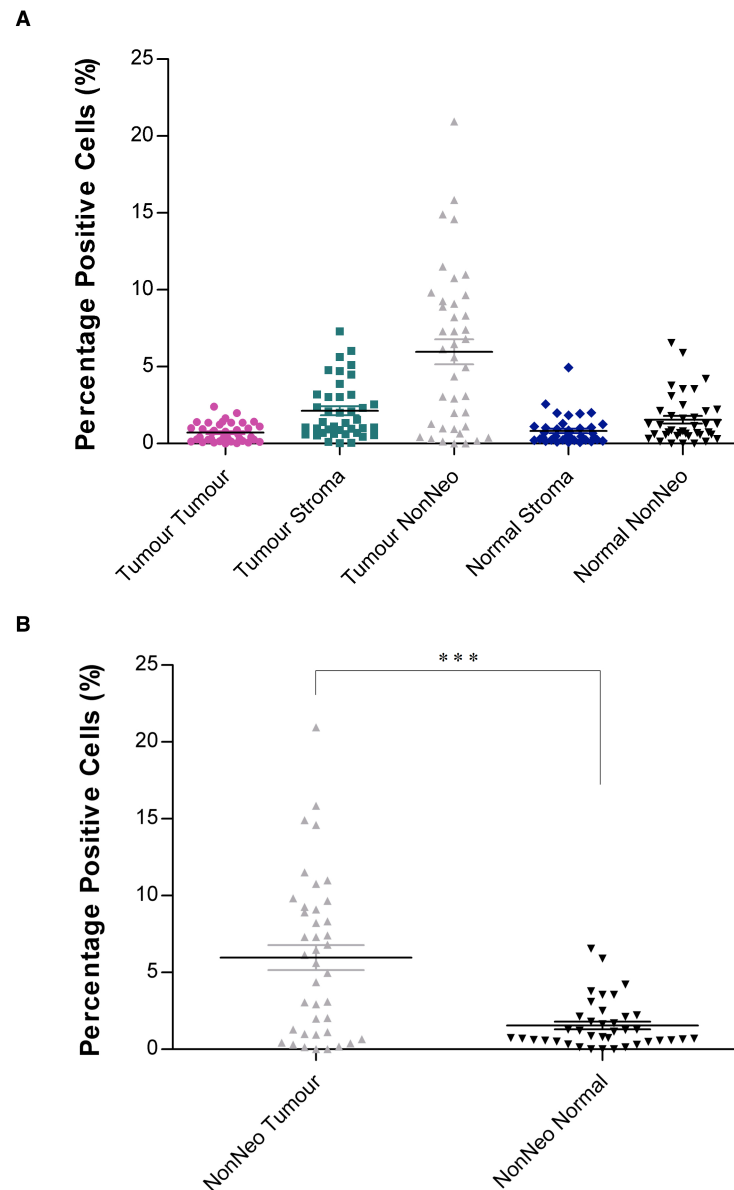


Figure 4.22 Foxp3 Cells in Liver Metastatic CRC and Matched Non-Neoplastic Tissue

The number of Tregs in metastatic CRC liver samples was analysed immunohistochemically (mouse anti-human Foxp3 IgG1, 5 μ g/ml). Digital images were acquired and Genie™ Classifiers were then used to distinguish the areas of tumour, stroma and tumour adjacent non-neoplastic (Tumour NonNeo) tissue, compared matched distant normal stroma and non-neoplastic (Normal NonNeo). B) A comparison between tumour adjacent non-neoplastic (NonNeo Tumour) and distant non-neoplastic (NonNeo Normal) tissue was achieved. (Paired t-test, *** $p < 0.001$).

Interestingly, the highest level of infiltrating Tregs was observed in the tumour adjacent non-neoplastic tissue. The frequency of Tregs here was significantly ($p > 0.001$) higher than those observed at the matched distant non-neoplastic samples (Figure 4.22B). Results are in agreement with previous literature showing elevated Tregs in tumour sections compared to normal tissue (Mizukami et al., 2008b).

In addition, this level of Treg infiltration at the tumour edge is very similar to that seen for CD8 cells. Amplified numbers of Tregs were found within the tumour adjacent non-neoplastic tissue, compared to those that had infiltrated the tumour ($p > 0.001$). An increase in Treg number could be responsible for an imbalance in the immune system, which would then favour unresponsiveness. This situation could lead to tumour cells escaping immune cell recognition (Colombo and Piconese, 2007). Tumour progression could therefore result from Treg-mediated suppression of the anti-tumour immune response, such as CTLs (Bui et al., 2006).

Interestingly, the numbers of Tregs within tumour stroma were higher ($p > 0.01$) than those observed within distant non-neoplastic stromal tissue (Figure 4.22A). It could be speculated that the level of Tregs is elevated because Tregs might be attracted to the tumour microenvironment and could be patrolling the tumour stromal 'streets', suppressing any immune cell that has accomplished tumour infiltration.

The similarities and co-localisation of Tregs and CD8 CTLs at the IM is demonstrated in Figure 4.23.

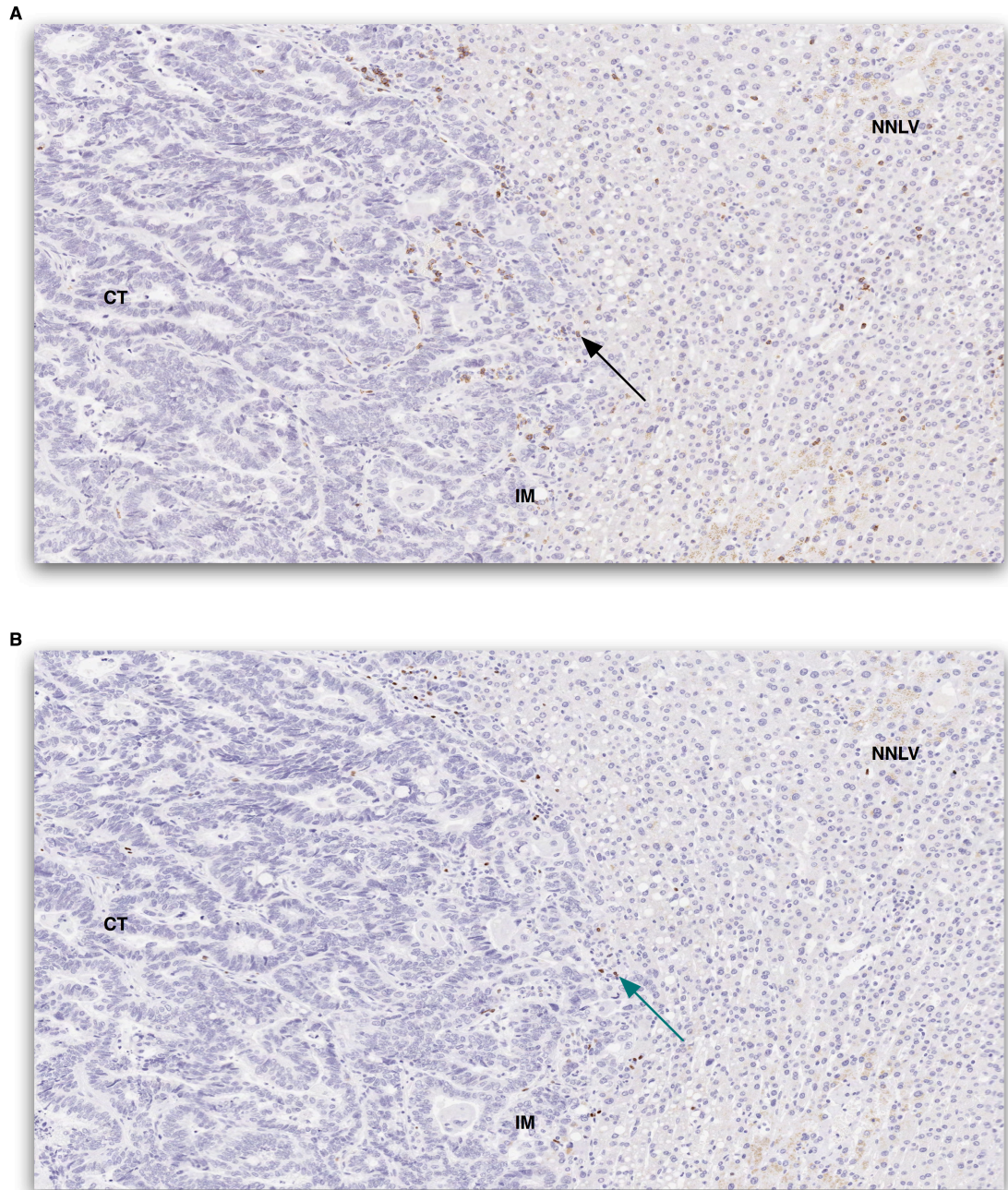


Figure 4.23 Example Image of CD8 and Foxp3 Cell Co-localisation at the Tumour Edge

Example images of liver metastatic CRC tissue stained with A) anti-human CD8 IgG2b (0.5 μ g/ml) or B) anti-human Foxp3 IgG1 (5 μ g/ml). Images at x 20 original magnification. (CT, tumour centre; IM, invasive margin;>NNLV, non-neoplastic liver; black arrow, example CD8 cell; green arrow, example co-localising Treg).

Sequential cutting of sections enabled a more detailed analysis of immune cell locations within subsequent sections. CD8 cells (Figure 4.23A, black arrow) were seen in very close proximity to Tregs (Figure 4.23A, green arrow).

Studies suggest that tumour-related factors mediate Treg trafficking into the tumour microenvironment, which could explain the elevated Tregs observed at the tumour edge. Chemotaxis experiments have demonstrated the ability of the macrophage-derived chemokine, CCL22, to induce Treg migration through its receptor CCR4 and impair anti-tumour immunity (Curiel et al., 2004). Tregs strongly express CCR4 on their surface and have been shown to also migrate in response to CCL17 via the same CCR4 receptor (Ishida and Ueda, 2006). The mechanism for CCL22 and CCL17 up-regulation has not yet been clarified, however, it has been suggested that the tumour microenvironment induces macrophages to secrete these chemokines (Mizukami et al., 2008a). Further to this, the tumour microenvironment could provide a favourable setting for Treg expansion due to the cocktail of chemokines, such as TGF- β , it produces (Yamaguchi et al., 2007).

Patients with elevated Treg levels show reduced survival rates and the accumulation of Tregs is debatably related to disease progression (Mizukami et al., 2008b; Wolf et al., 2005). Evidence suggests that depleting Tregs leads to rejection of transplanted tumours in mice models (Shimizu et al., 1999).

A direct comparison between Tregs within the tumour and those found in the stroma was achieved (Figure 4.24).

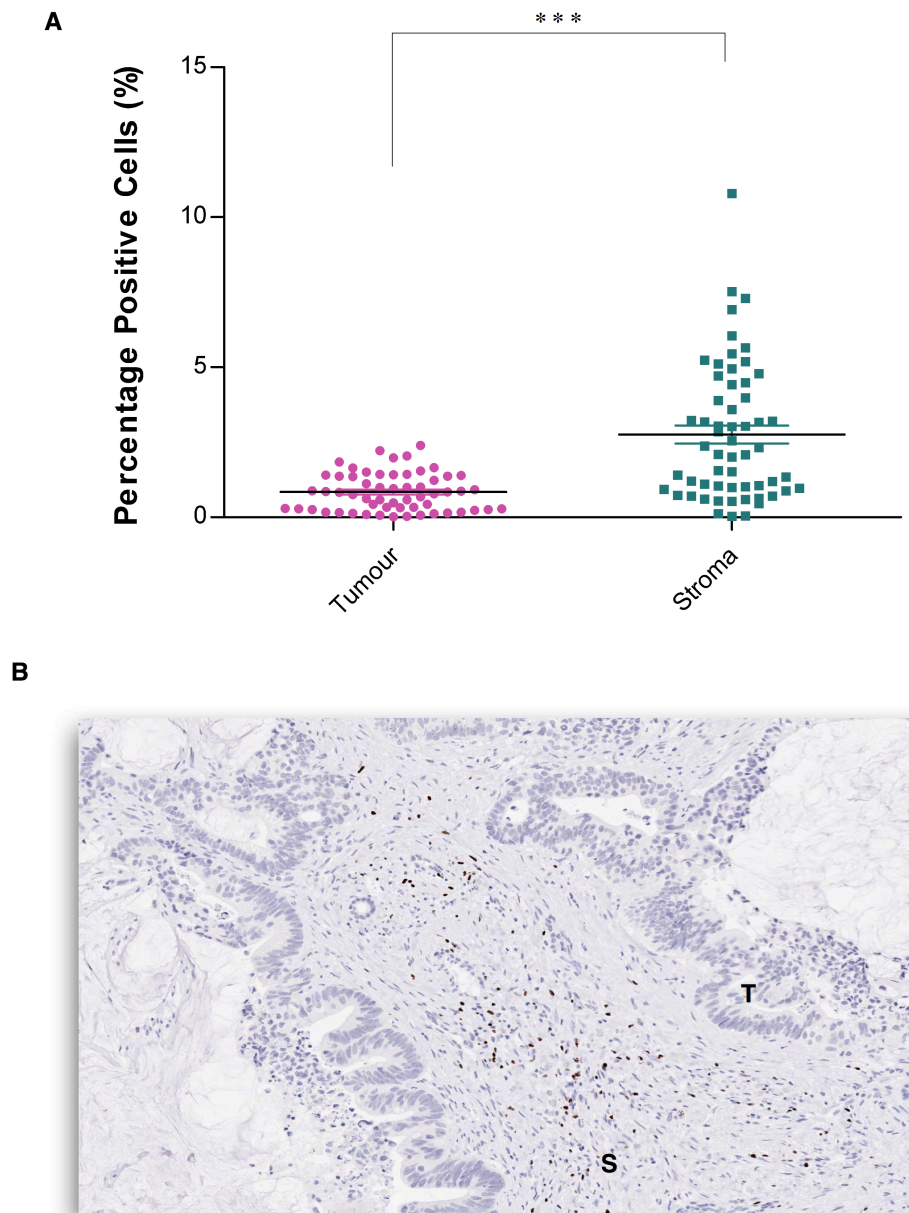


Figure 4.24 Overall Evaluation of Foxp3 Cells in Tumour and Stroma

The number of Tregs was analysed immunohistochemically (mouse anti-human Foxp3 IgG1, 5 μ g/ml). Digital images were acquired and Genie™ Classifiers were then used to distinguish areas of tumour and stroma. This was combined with a nuclear algorithm to quantify the percent positive Tregs. A) Primary CRC and CRC metastatic liver samples were pooled to compare the percentage positive Tregs between tumour and stroma. (Unpaired t-test, *** $p < 0.001$). B) A corresponding example image (at x 20 original magnification) of liver metastatic CRC tissue stained with anti-human Foxp3 (T, tumour; S, stroma).

As with CD8 cells, Tregs were seen to be significantly higher within the stroma than within the tumour itself ($p < 0.001$). An example image depicting this can be seen in Figure 4.24B, where Tregs reside predominantly within the stroma (S) and to a much lesser extent within regions of tumour (T).

The clinicopathologic significance of Tregs and CD8 cells during hepatocarcinogenesis has also been studied, where the prevalence of Tregs was suggested to be an unfavourable prognostic marker (Kobayashi et al., 2007). The infiltration of Tregs and CD8 cells in patients with metastatic liver tumours from primary CRC were evaluated. Analysis of the anti-tumour response (Tregs and CD8 T cells) in primary HCC ($n = 235$), intrahepatic metastatic foci ($n = 27$) and liver metastasis from primary CRC ($n = 59$) was evaluated. The frequency of Tregs was higher in primary tumours than metastatic. Tregs were elevated in HCC compared to non-tumour tissue or healthy liver samples, where low-Treg groups showed improved OS and DFS compared to high-Treg groups (Kobayashi et al., 2007).

4.2.4.2. Innate Immunity

4.2.4.2.1 CD68 Positive Macrophages

The current study then moved on to look at the occurrence of macrophages, using CD68 staining. The frequency of macrophages within primary and metastatic tissue was investigated (Figure 4.25).

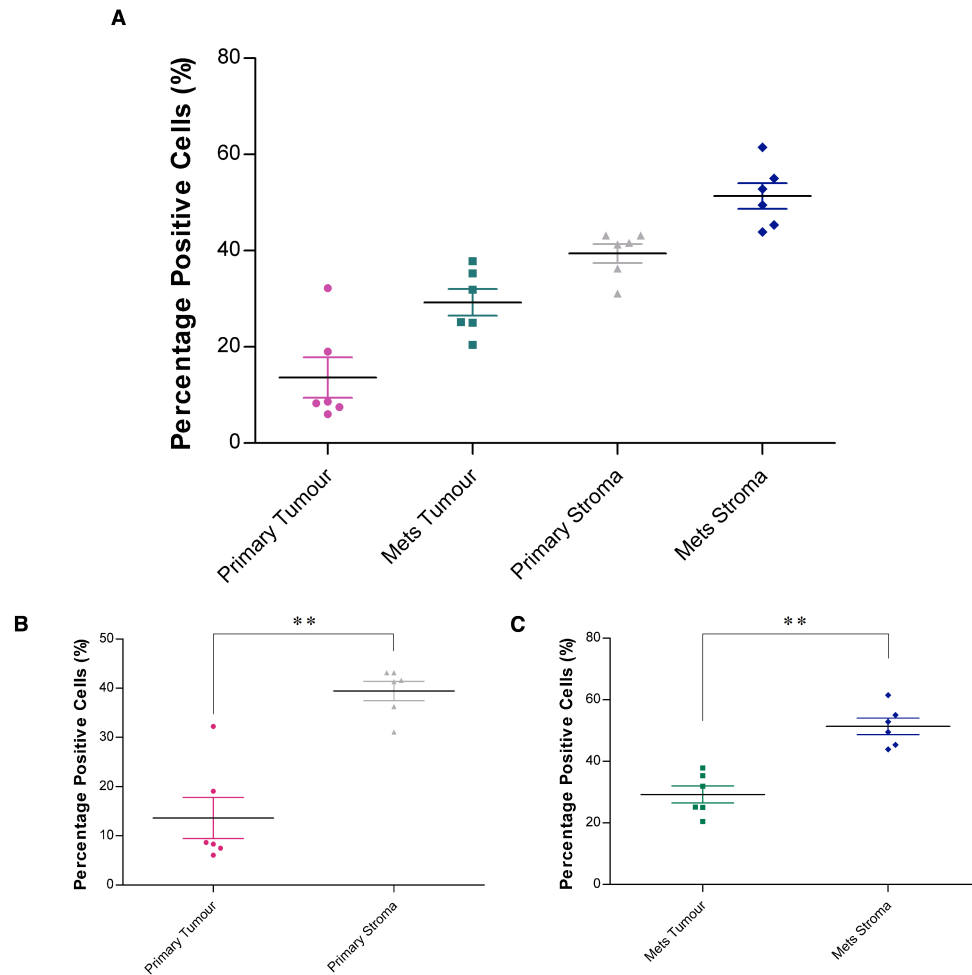


Figure 4.25 CD68 Macrophage Infiltrates in Primary CRC vs Metastatic Liver

Primary CRC and matched liver metastatic tissue was examined for CD68 cell infiltration into the tumour and stroma using IHC techniques (anti-human CD68 IgG1, 0.2 µg/ml). Digital images were acquired and Genie™ Classifiers were then used to distinguish areas of tumour and stroma and combined with a nuclear algorithm to quantify the percent positive CD68 cells. A) An overall assessment of the percentage positive CD68 cells in primary and metastatic disease was carried out. A direct comparison between the number of CD68 cells in the tumour and stroma for both B) primary and C) metastatic (met) tissue. (Paired t-test, ** $p < 0.01$).

When evaluating CD68, similar trends were observed for macrophages as those seen for CTLs and, to some extent, Tregs. An elevation in macrophage number was noted in the metastatic versus primary samples. This was true for numbers within tumour ($p < 0.01$) and stroma ($p < 0.05$) of metastatic tissue opposed to primary tissue (Figure 4.25A). In addition, macrophage infiltration was highest in stromal areas, in contrast to those seen within the tumour tissue, for both primary ($p < 0.01$) and metastatic ($p < 0.01$) disease (Figure 4.25B).

TAMs have been identified as regulators of tumour progression, via their ability to promote angiogenesis and metastatic development (Qian and Pollard, 2010). TAMs are derived from monocytes that are recruited largely by monocyte chemotactic protein (MCP) chemokines. TAMs have a dual function: IL-2 and IL-12 mediated neoplastic cell death, but also the production of angiogenic and lymphangiogenic growth factors renders them mediators of neoplastic progression (Coussens and Werb, 2002). Along with tumour cells, TAMs also produce IL-10, which dampens the anti-tumour response.

Further research explored the macrophage infiltration in primary MET⁺ and MET⁻ tissue (Figure 4.26).

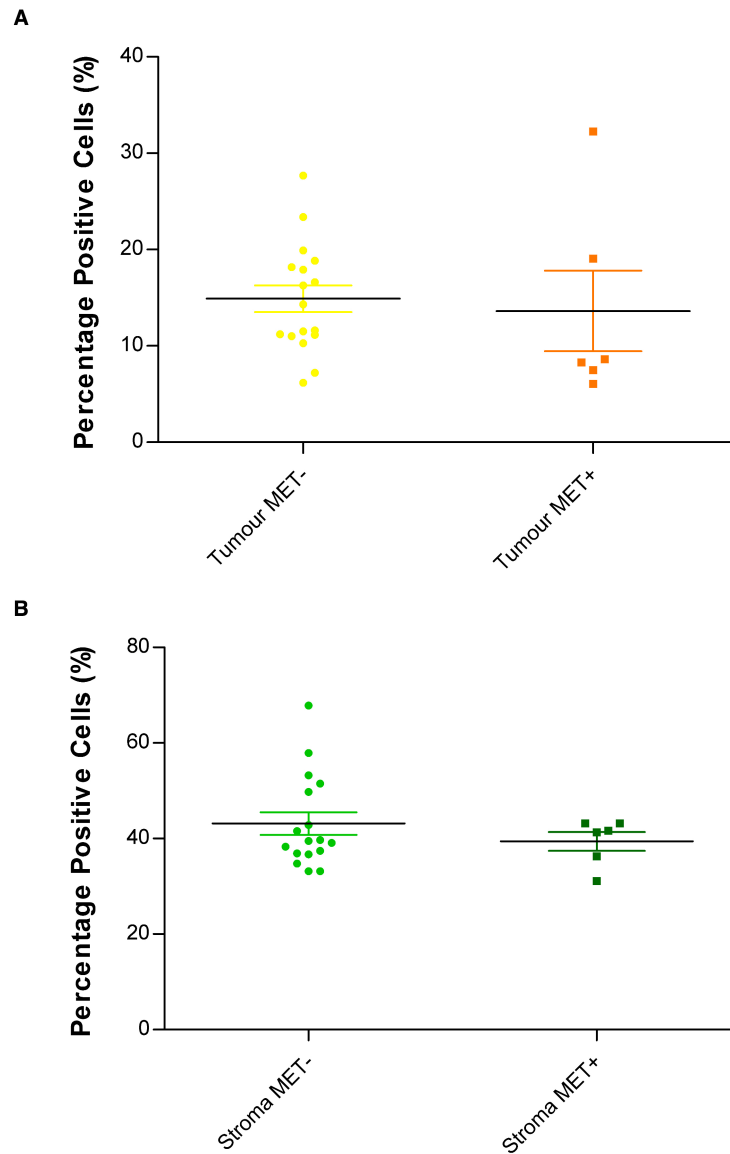


Figure 4.26 Comparison of CD68 Cells in MET+ and MET- Primary CRC Tissue

Primary CRC with no affiliated metastatic disease (MET-) and primary CRC that has since developed liver metastasis (MET+) were analysed using IHC techniques (anti-human CD68 IgG1, 0.2 µg/ml). Digital images were acquired and Genie™ Classifiers were used, combined with a nuclear algorithm to determine the number of percent positive CD68 cells in the A) tumour and B) stroma. (Unpaired t-test).

Interestingly, there was no statistical significance between macrophages in the tumour or stroma of MET+ versus MET- primary CRC tissue. This is in agreement with recently published data demonstrating that CD68⁺ cell density alone resulted in no correlation to survival or metastatic development (DeNardo et al., 2011). However, when combined with CD8 CTL analysis, it was shown that an inverse relationship occurred between macrophages and CTLs within the stroma of breast cancer tissue. Results alluded to a CD68^{high}/CD4^{high}/CD8^{low} pro-tumour phenotype, associated with reduced OS and relapse-free survival (RFS) (DeNardo et al., 2011).

Differences in the prognostic significance of TAMs could, in part, be explained by the fact that TAMs result in either pro-tumour or anti-tumour activities, depending on the cytokines to which they are exposed to (Ruffell et al., 2010). Cytokines, such as IFN- γ or TNF- α , result in TAM cytotoxicity, antigen presentation and the release of pro-inflammatory cytokines, whereas TAMs exposed to immunosuppressive cytokines promote angiogenesis and block CTL activity (Ruffell et al., 2010).

Within the current study, TAMs were examined in comparison to the frequency of macrophages observed at distant sites of non-neoplastic tissue (Figure 4.27).

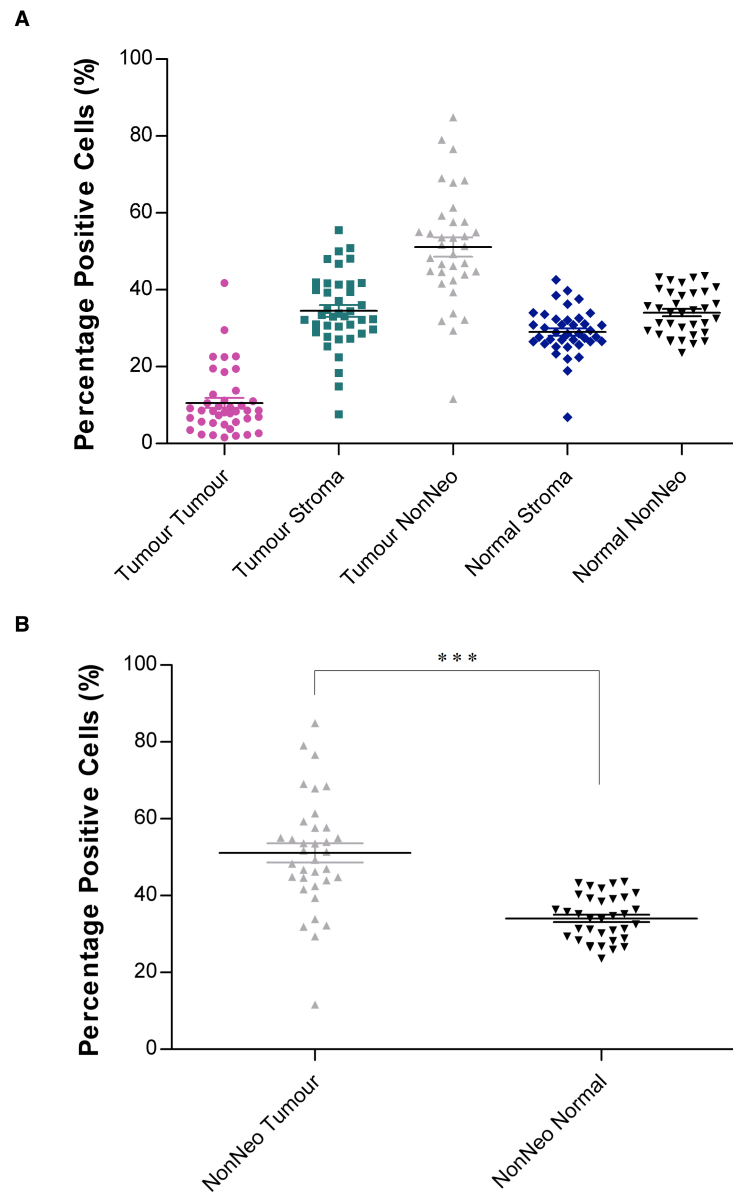


Figure 4.27 CD68 Cells in Liver Metastatic CRC and Matched Non-Neoplastic Tissue

CRC metastatic liver samples were analysed for CD68 cells immunohistochemically (anti-human CD68 IgG1, 0.2 μ g/ml). Digital images were acquired and Genie™ Classifiers were combined with a nuclear algorithm to quantify CD68 cells, looking at the difference between tumour, stroma and tumour adjacent non-neoplastic (Tumour NonNeo) tissue, compared to matched distant normal stroma and non-neoplastic (Normal NonNeo). B) A comparison between tumour adjacent non-neoplastic (NonNeo Tumour) and distant non-neoplastic (NonNeo Normal) tissue was achieved. (Paired t-test, *** $p < 0.001$).

A significant elevation of macrophage numbers was observed at the tumour IM and adjacent non-neoplastic tissue, when compared to distant non-neoplastic samples (Figure 4.27B). Previous research has revealed that the cytokine, CSF-1, plays a key role in recruitment and activation of macrophages (Tang et al., 1992). In addition, the number of macrophages at this IM site was also higher than those seen within the tumour ($p < 0.001$) and stroma ($p < 0.01$), very similar to the trends observed for CTLs and Tregs.

An example image illustrating the numbers of macrophages found at the tumour IM and adjacent non-neoplastic tissue is depicted in Figure 4.28.

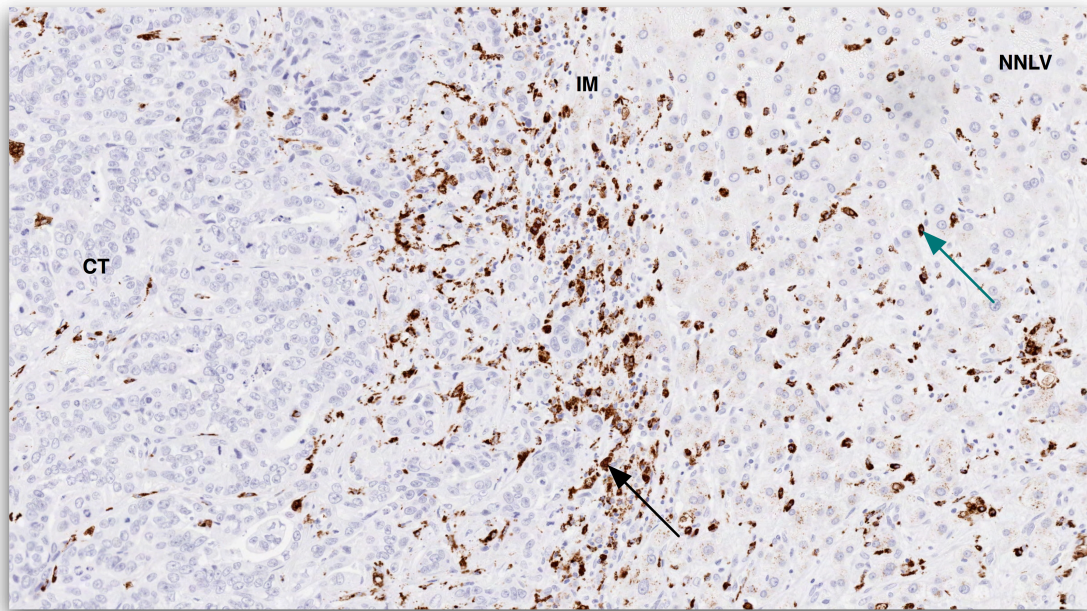


Figure 4.28 Example Image of Infiltrating CD68 Cells at the Tumour Edge

An example image of a CRC metastatic liver section stained with anti-human CD68 IgG1 (0.2 $\mu\text{g/ml}$). Black arrow, CD68 cell at the IM, green arrow, CD68 cell within adjacent NNLV tissue (CT, tumour centre; IM, invasive margin; NNLV, non-neoplastic liver). Image at x 20 original magnification.

The influx of macrophages to the tumour IM is very similar to that of Tregs and CD8 cells. This could be explained, in part, by the ability of macrophages to produce the chemokine CCL22. Cellular trafficking has been shown to occur between CCL22 and CCL17 and cells expressing the CCR4 receptor. Tregs strongly express CCR4 on their surface and so could migrate to the tumour microenvironment, influenced by this macrophage-derived chemokine (Curiel et al., 2004); (Mizukami et al., 2008a).

The frequency of macrophages within the tumour and stroma of primary and metastatic CRC tumour tissue was then scrutinised (Figure 4.29).

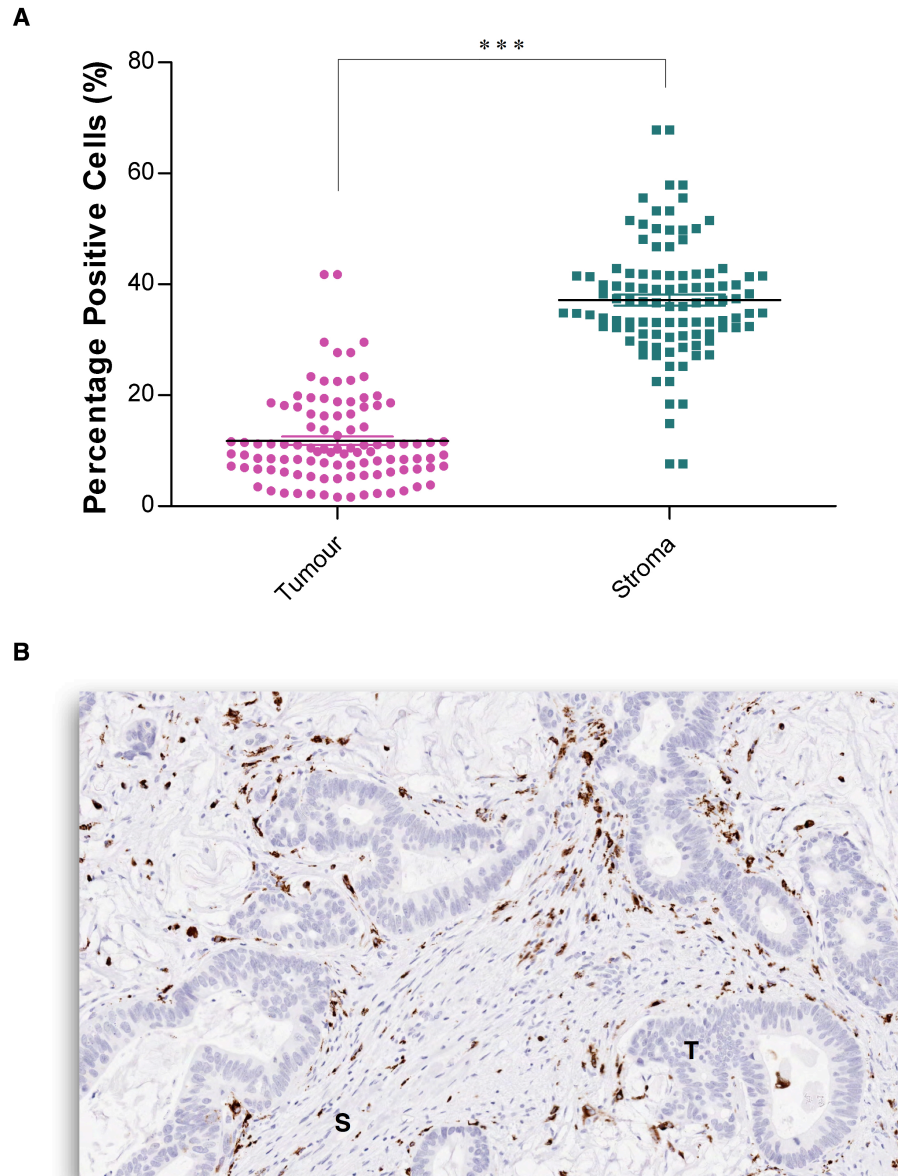


Figure 4.29 Overall Evaluation of CD68 Cells in Tumour and Stroma

Primary CRC and metastatic liver samples were pooled and analysed for CD68 cells immunohistochemically (anti-human CD68 IgG1, 0.2 μ g/ml). Digital images were acquired and Genie™ Classifiers were combined with a nuclear algorithm to quantify the number of positive CD68 cells. A) The percentage of positive CD68 cells was compared between tumour and stroma. (Unpaired t-test, *** $p < 0.001$). B) A corresponding example image of liver metastatic CRC tissue stained with anti-human CD68 IgG1 (0.2 μ g/ml). Image at x 20 original magnification (T, tumour; S, stroma).

Elevation of macrophages within the stroma was observed and is in agreement with previous literature, showing the stromal macrophages had the most significant impact on prognostic factors.

4.2.4.2.2. CD56 Positive NK Cells

To complete the set of immune markers studied, the frequency of CD56-positive NK cells was determined within primary CRC and matched liver metastatic samples (Figure 4.30).

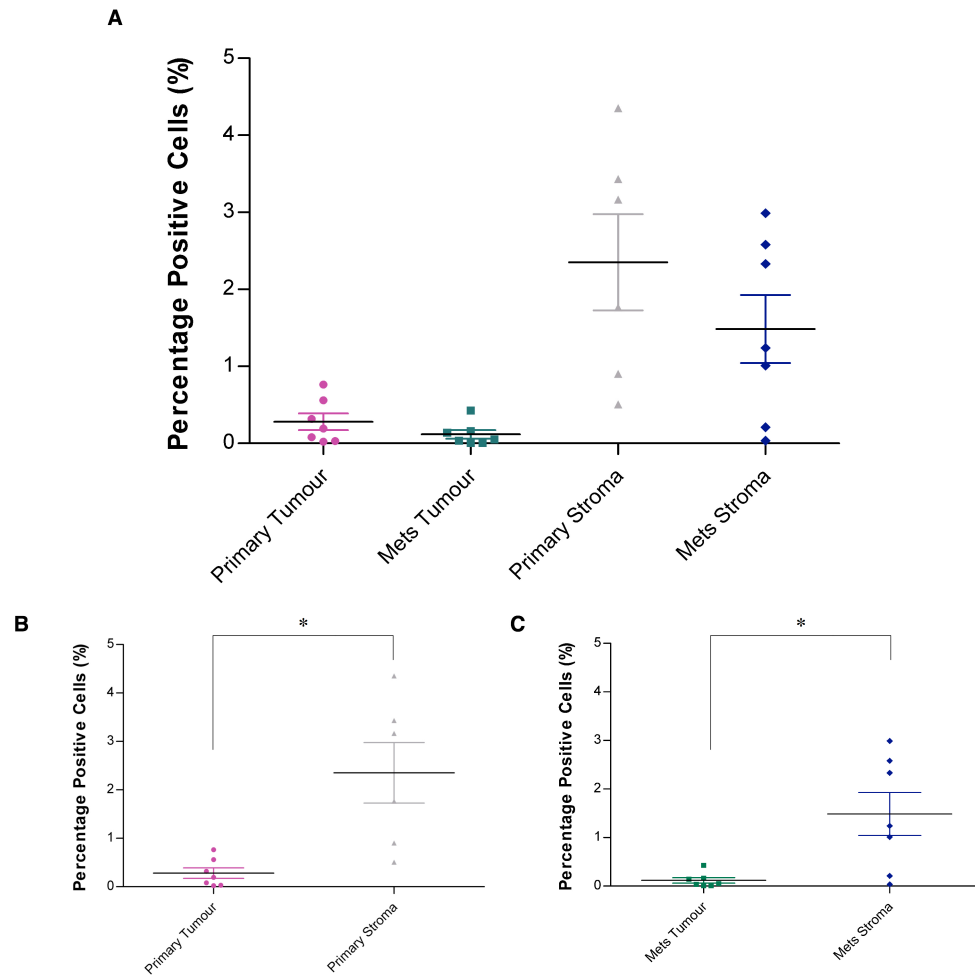


Figure 4.30 CD56 NK Cell Infiltrates in Primary CRC vs Metastatic Liver

Primary CRC and matched liver metastatic tissue were examined for NK cell infiltration using IHC techniques (anti-human CD56 IgG1, 0.5 µg/ml). Digital images were acquired and Genie™ Classifiers were combined with a nuclear algorithm to quantify the percentage of CD56 positive cells. A) An overall assessment of the percentage positive CD56 cells in primary and metastatic disease. A comparison between the number of NKs in the tumour and stroma of B) primary and C) metastatic (met) tissue. (Paired t-test, * $p < 0.05$).

As with previous immune infiltrates, the highest occurrence of NK cells was observed within the stroma of both primary and metastatic disease (Figure 4.30B). However, the author would like to draw the reader's attention to the scale bars used within this study. Although similar trends were observed for the location of NK cells, the percentage of positive CD56 cells was significantly lower than that of other immune infiltrates, such as CD8s, Tregs and macrophages.

A comparison between the number of NK cells within primary MET- and MET+ tissue was then accomplished (Figure 4.31).

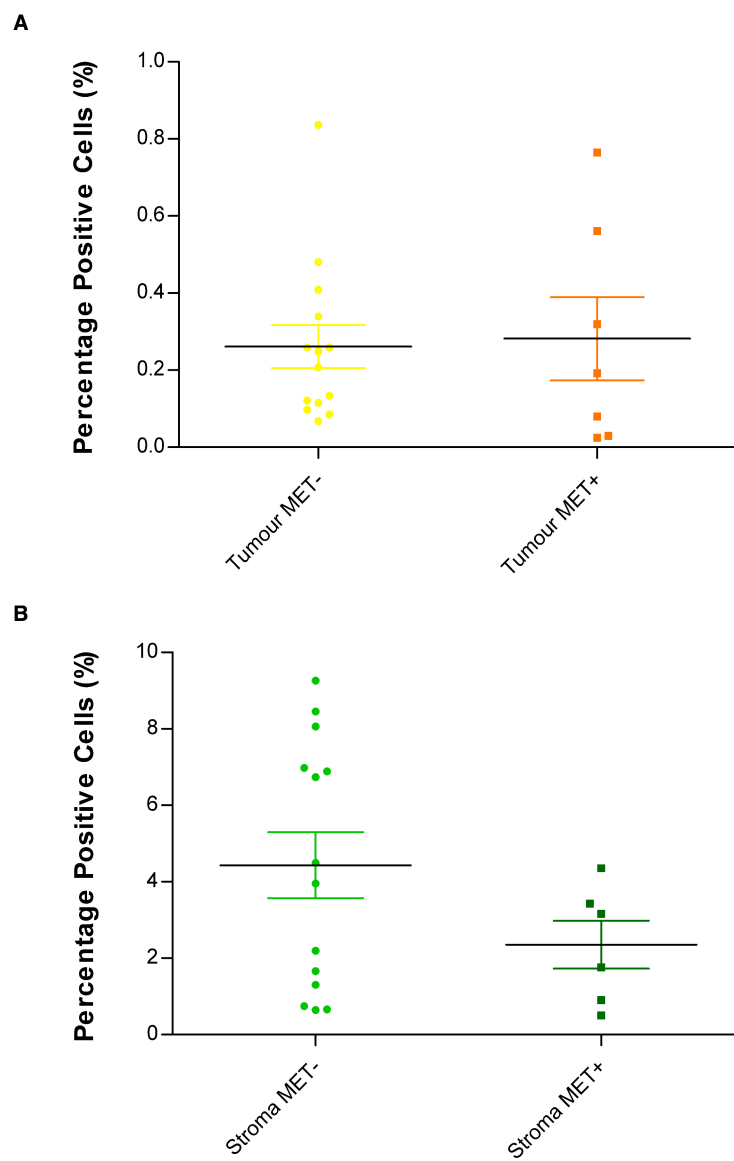


Figure 4.31 Comparison of CD56 Cells in MET+ and MET- Primary CRC Tissue

Primary CRC with no affiliated metastatic disease (MET-) and primary CRC that has since developed liver metastasis (MET+) were examined for NK cell infiltration using IHC techniques (anti-human CD56 IgG1, 0.5 µg/ml). Digital images were acquired and Genie™ Classifiers were used to distinguish areas of tumour and stroma. This was combined with a nuclear algorithm to quantify the percentage of CD56 positive cells. A) tumour and B) stroma were compared for CD56 cell infiltration.

A trend was observed within the stroma between MET- and MET+ CD56 cells, where primary tissue, which went on to develop metastatic disease, showed fewer NK cells (Figure 4.31B). Fewer NK cells would suggest a reduced level of tumour cell cytotoxicity and therefore favour disease progression and metastasis. However, no statistically significant difference was observed, possibly due to the low numbers.

Within the literature analysis of CD57 as an NK cell marker was associated with survival in CRC (Mlecnik et al., 2010a). Extensive work was achieved using a platform of techniques including gene expression, to identify immune-related genes associated with patient prognosis and absence of tumour recurrence. The phenotypes and locations of intratumoral immune cells were assessed for correlations with DFS.

CD56 NK cells were subsequently analysed within the tumour and compared to matched, distant, non-neoplastic samples (Figure 4.32).

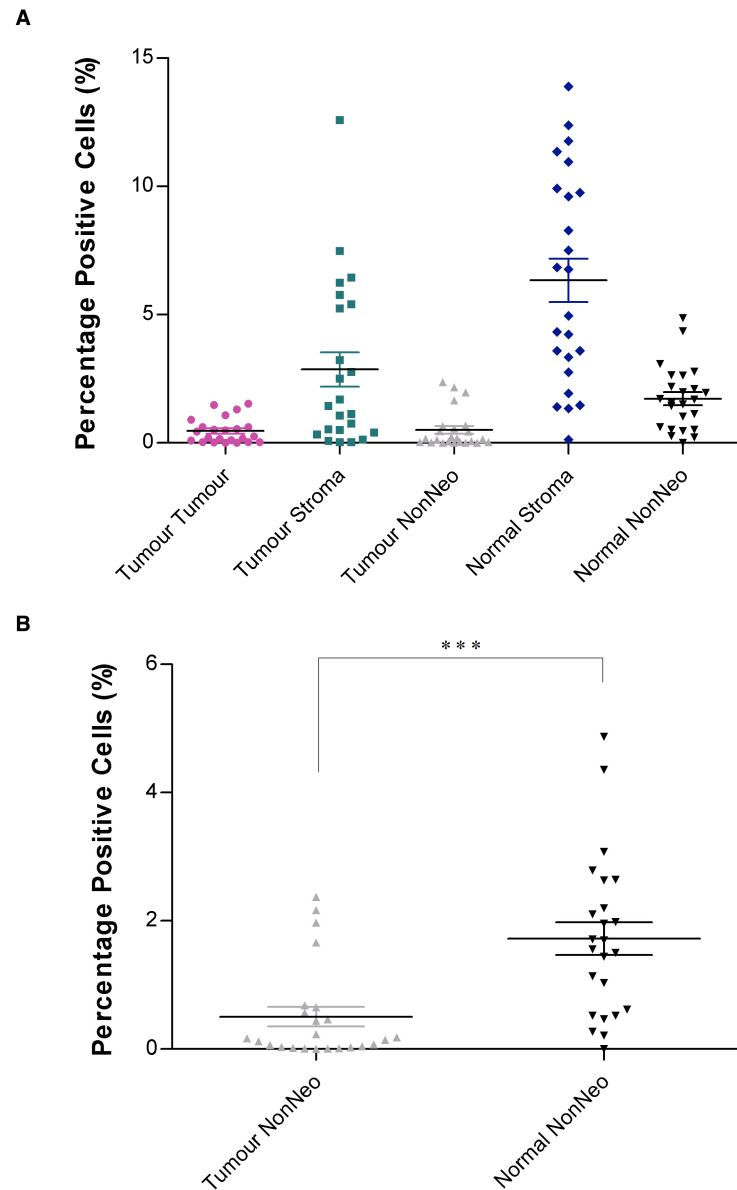


Figure 4.32 CD56 Cells in Liver Metastatic CRC and Matched Non-Neoplastic Tissue

Liver metastatic CRC samples were analysed immunohistochemically for CD56-positive cell infiltrates (anti-human CD56 IgG1, 0.5 μ g/ml). Digital images were acquired and Genie™ Classifiers were combined with a nuclear algorithm to quantify the percentage of CD56 positive cells, looking at the difference between tumour, stroma and tumour adjacent non-neoplastic (Tumour NonNeo) tissue, compared to matched distant normal stroma and non-neoplastic (Normal NonNeo) tissue. B) A comparison between tumour and tumour adjacent non-neoplastic (NonNeo Tumour) tissue was achieved. (Mann-Whitney test, *** $p < 0.001$).

The numbers of CD56-positive NK cells were compared between tumour adjacent non-neoplastic tissue and matched distant non-neoplastic samples (Figure 4.32B). A significant ($p < 0.001$) decrease in the prevalence of NK cells was observed at the tumour edge. This was also true when comparing distant stroma NK numbers to those seen in the stroma within the tumour ($p < 0.05$). This drop in NK cell numbers may result in limited NK-mediated tumour cell killing. No difference in numbers of NK cells was seen between the tumour edge and those infiltrating the tumour, possibly indicating a lack of anti-tumour NK cell activity.

The prevalence of NKs was then compared between the tumour and stroma of all CRC patients within the study (Figure 4.33).

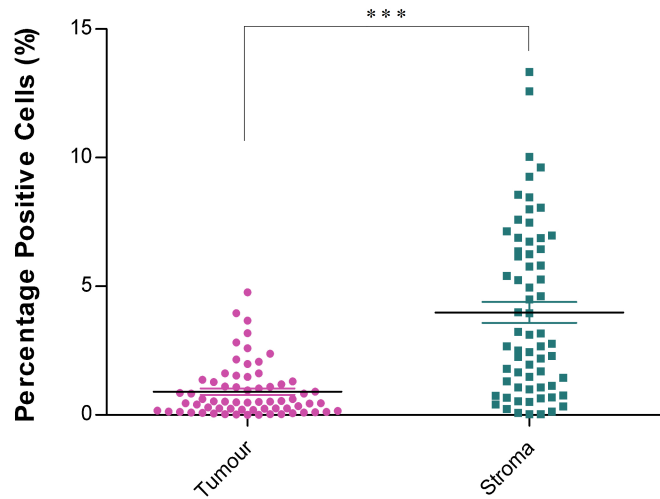


Figure 4.33 Overall Evaluation of CD56 Cells in Tumour and Stroma

Primary CRC and liver metastatic samples were pooled and examined for NK cell infiltration using IHC techniques (anti-human CD56 IgG1, 0.5 µg/ml). Digital images were acquired and Genie™ Classifiers were combined with a nuclear algorithm to quantify the percentage of CD56-positive cells. A) The number of percentage positive CD56 cells was compared between tumour and stroma. (Unpaired t-test, *** p < 0.001).

In agreement with the trend seen for previous immune infiltrates, there was a significant increase in the amount of NK cells within the stroma compared to those seen within the tumour itself (Figure 4.33).

4.2.4.3. Tumour Environment

4.2.4.3.1. CD31 Positive Vasculature Staining

Alongside immune infiltrates, various aspects of the tumour microenvironment were also analysed in this study.

Decades of research have been invested into studying the ability of tumours to induce the formation of new blood vessels, a key requirement to sustain solid tumour growth. Fundamental to that research was the discovery and subsequent understanding of the VEGF and its contribution to driving tumour angiogenesis (Ferrara, 2002).

Within this study, CD31 was used to analyse the distribution of blood vessels within and around the tumour and stroma, first comparing primary and metastatic tissue (Figure 4.34).

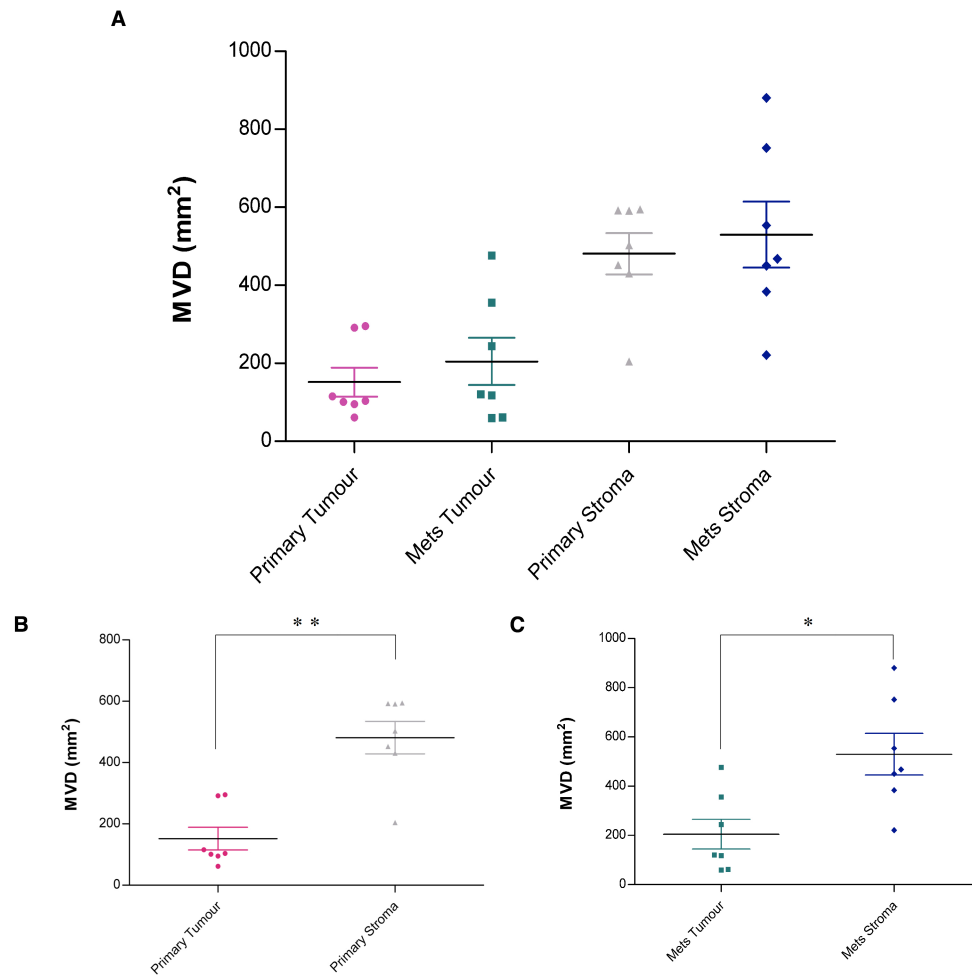


Figure 4.34 CD31 MVD in Primary CRC vs Metastatic Liver

Primary CRC and matched liver metastatic tissue was examined for microvessel density (MVD) by examining the number of vessels per unit area (mm²) within the tumour and stroma using IHC techniques (anti-hum CD31 IgG1, 0.27 µg/ml). Digital images were acquired and Genie™ Classifiers were combined with a nuclear algorithm to quantify the MVD. A) An overall assessment of the MVD in primary and metastatic disease was carried out. A direct comparison between the MVD in the tumour and stroma for both B) primary and C) metastatic (met) tissue was achieved (Mann-Whitney test, * $p < 0.05$, ** $p < 0.01$).

Anti-human CD31 was used to stain the vasculature within tissue samples. Image analysis was achieved as previously described, utilising the Genie pattern recognition software in association with a microvessel density (MVD) algorithm. MVD was calculated by examining the number of vessels per unit area (mm^2). There was no significant difference in the MVD between primary and metastatic disease, both within the tumour and stroma (Figure 4.34A). However, elevation in the number of vessels was observed infiltrating the stroma in primary ($p < 0.01$) and metastatic ($p < 0.05$) tissue (Figure 4.34B), compared with the tumour.

The vessel density was compared between MET+ and MET- primary CRC tissue (Figure 4.35).

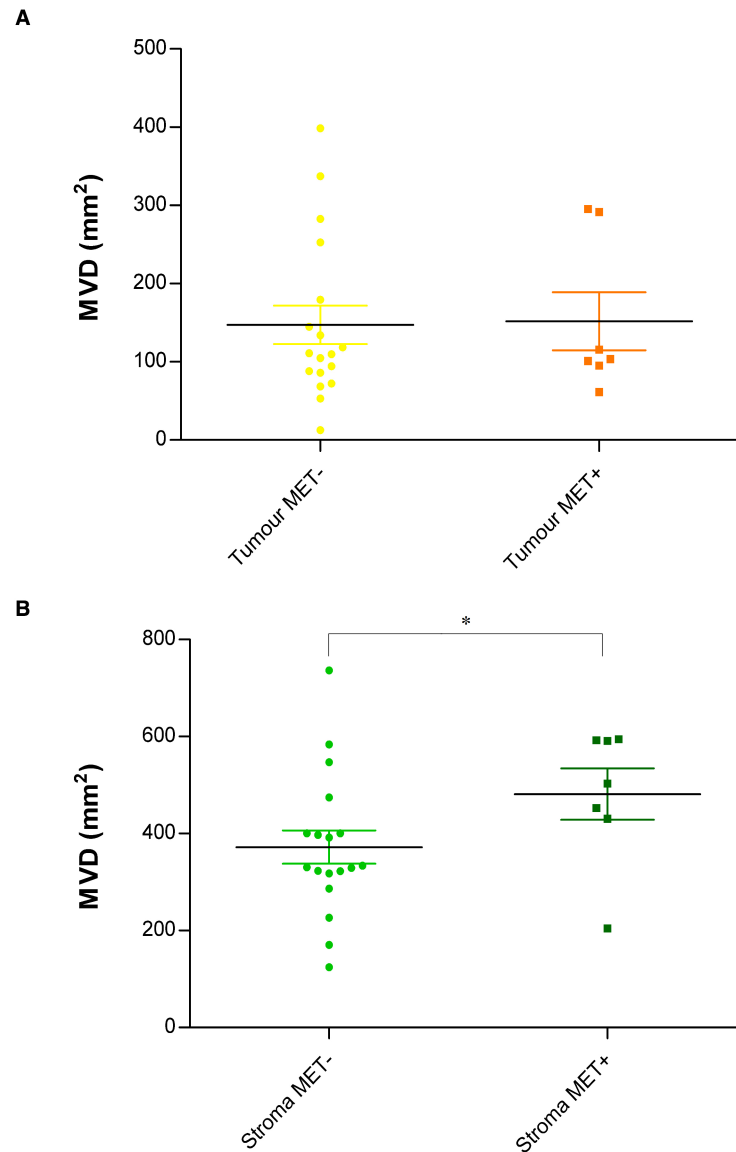


Figure 4.35 Comparison of CD31 MVD in MET+ and MET- Primary CRC Tissue

Primary CRC with no affiliated metastatic disease (MET-) and primary CRC that has since developed liver metastasis (MET+) were examined for the number of vessels per unit area (mm²) within the tumour and stroma using IHC techniques (anti-hum CD31 IgG1, 0.27 µg/ml). Digital images were acquired and Genie™ Classifiers were combined with a nuclear algorithm to quantify the microvessel density (MVD). MVD was compared in the A) tumour and B) stroma. (Mann-Whitney test, * p < 0.05).

The microvessel density was significantly higher in the stroma of MET+ primary tissue (Figure 4.35B). This reiterates previous data showing the importance of the vasculature system and angiogenesis in tumour progression. The formation of new blood vessels from pre-existing vasculature is key to tumour progression and metastasis of solid tumours (Yancopoulos et al., 2000). Angiogenesis is needed to supply nutrients and oxygen to the central tumour, and without adequate vascular supply solid tumours rarely grow beyond 1–2 mm (Lin et al., 2007).

CD31 was subsequently analysed in the tumour and surrounding non-neoplastic tissue and compared to distant non-neoplastic samples (Figure 4.36).

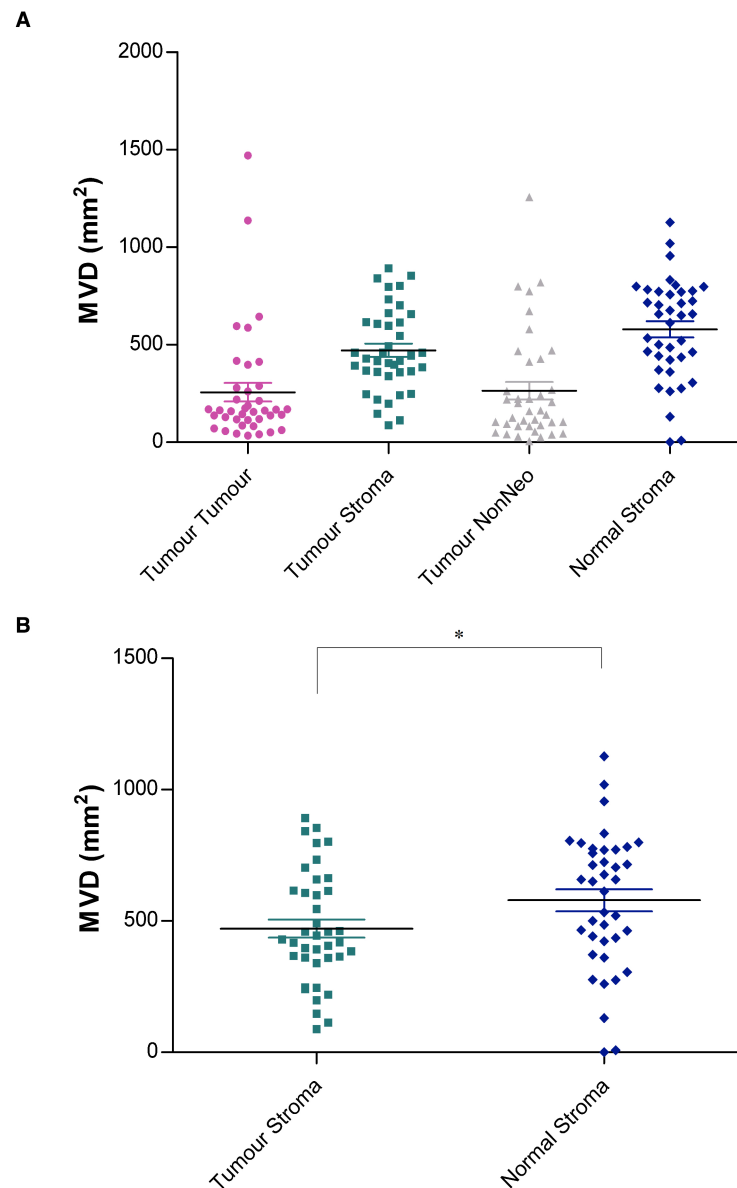


Figure 4.36 CD31 MVD in Liver Metastatic CRC and Matched Non-Neoplastic Tissue

Liver metastatic CRC samples were examined for the number of vessels per unit area (mm²) within the tumour and stroma using IHC techniques (anti-hum CD31 IgG1, 0.27 µg/ml). Digital images were acquired and Genie™ Classifiers were combined with a nuclear algorithm to quantify the microvessel density (MVD). The number of vessels per unit area was analysed in metastatic CRC samples, looking at the difference between tumour, stroma and tumour adjacent non-neoplastic (Tumour NonNeo) tissue, compared to the MVD in matched distant normal stroma and non-neoplastic (Normal NonNeo) tissue. B) A comparison between stroma within the tumour (Tumour Stroma) and tumour adjacent non-neoplastic (Tumour NonNeo) tissue was achieved. (Paired t test, *** p < 0.001).

The MVD was compared between tumour tissue and matched distant normal samples (Figure 4.36). The stroma within the tumour had significantly higher levels of vessels than those seen infiltrating the tumour ($p < 0.001$) or in the non-neoplastic adjacent tissue ($p < 0.001$). However, when comparing this number of tumour stromal vessels to stroma in distant non-neoplastic normal tissue, there were higher number of vessels in the non-neoplastic samples ($p < 0.05$, Figure 4.36B). This could simply be explained by the fact that the liver is a very well vascularised organ.

CD31 was used to establish the differences in MVD within the tumour and surrounding stroma of both primary and metastatic CRC (Figure 4.37).

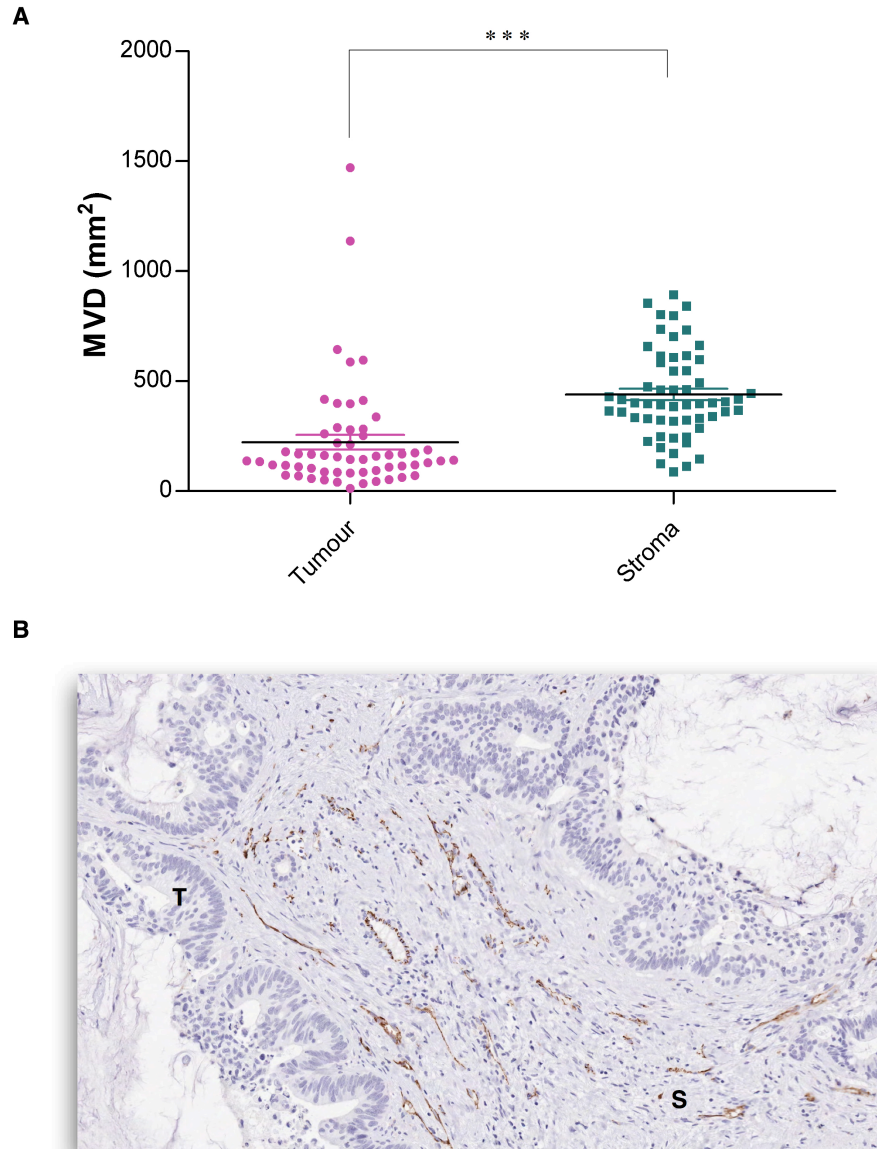


Figure 4.37 Overall Evaluation of MVD in Tumour and Stroma

Primary CRC and metastatic liver samples were pooled and examined for the number of vessels per unit area (mm²) within the tumour and stroma using IHC techniques (anti-human CD31 IgG1, 0.27 µg/ml). Digital images were acquired and Genie™ Classifiers were combined with a nuclear algorithm to quantify the microvessel density (MVD). A) The MVD was compared between tumour and stroma. (Unpaired t test, *** p < 0.001). B) A corresponding example image of liver metastatic CRC tissue stained with anti-human CD31 IgG1 (0.27 µg/ml). Image at x 20 original magnification (T, tumour; S, stroma).

The vasculature in and around the tumour was predominately within the stroma (Figure 4.37A). This is in agreement with previous data, indicating that intratumoural vessels are scarce in CRC. An example image of the elevated levels of stromal infiltrating vessels is seen in Figure 4.37B. This vascular localisation pattern, combined with corresponding α -SMA analysis (Section 4.2.3.9.) contributes to recognising CRC as having a stromal phenotype (Smith et al., 2010).

4.2.4.3.2. HIF-1 α Positive Hypoxia Staining

The formation of new blood vessels is essential to supply solid tumours with nutrients and oxygen to facilitate tumour growth. It is therefore sensible to suggest a relationship between the lack of adequate vascular supply and the levels of hypoxia (Dewhirst, 2009; Matsumoto et al., 2010; Vaupel and Mayer, 2007).

Hypoxia in tumours is caused by an imbalance in oxygen supply and demand, where regions of tumour are beyond the diffusion distance of oxygen. The level of hypoxia was evaluated using HIF-1 α in primary and matched secondary CRC diseased tissue (Figure 4.38).

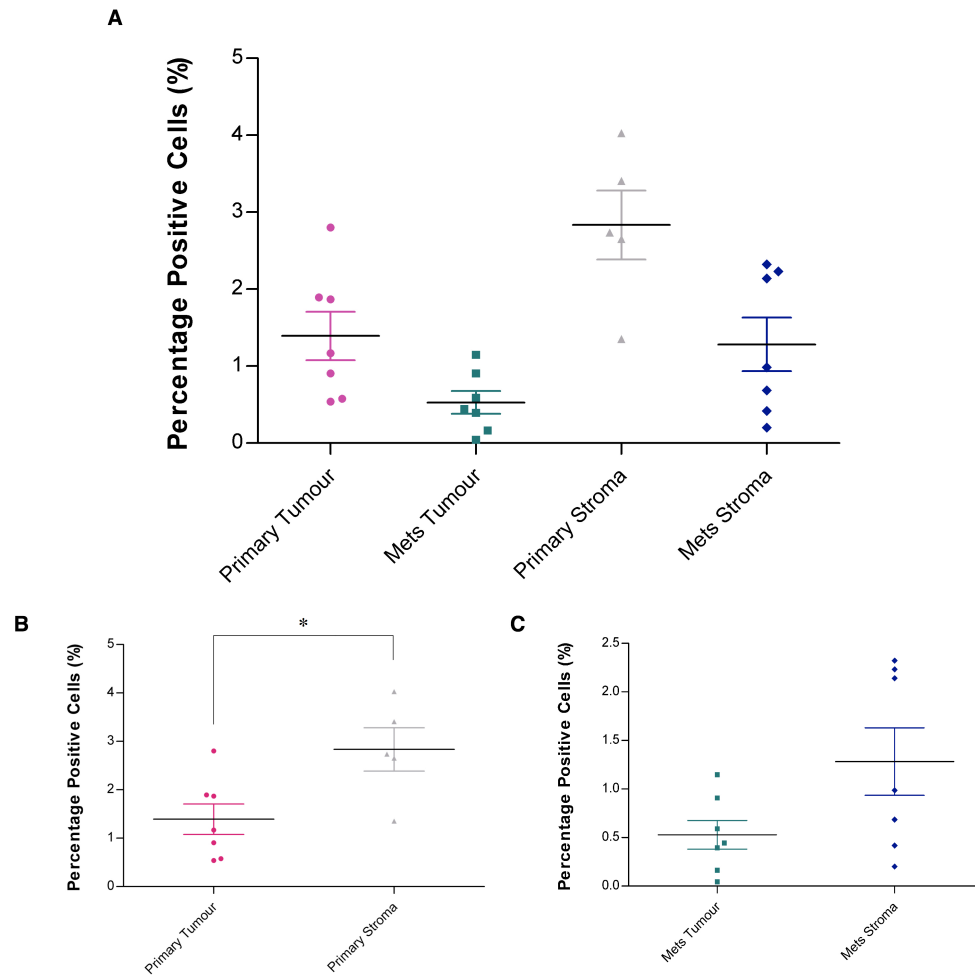


Figure 4.38 HIF-1 α in Primary CRC vs Metastatic Liver

Primary CRC and matched liver metastatic tissue was examined for hypoxia-inducible transcription factor-1 α (HIF-1 α) within the tumour and stroma using IHC techniques (anti-human HIF-1 α IgG1, 5 μ g/ml). Digital images were acquired and Genie™ Classifiers were combined with a nuclear algorithm to quantify the number of HIF-1 α -positive cells. A) An overall assessment of HIF-1 α in primary and metastatic disease was carried out. A direct comparison between hypoxia in the tumour and stroma for both B) primary and C) metastatic (met) tissue was achieved. (Mann-Whitney test, * $p < 0.05$).

Intratumoural hypoxia causes increased expression and activity of HIF-1 α and thus provides a good marker of hypoxic tissue. Overall, the percentage of positive HIF-1 α cells was relatively low, perhaps reflecting a stromal phenotype and well vascularised system. Surprisingly, an increase was observed in the primary stromal tissue compared to primary tumour (Figure 4.38B). This was unexpected as it was the author's opinion that the hypoxic cells would predominate throughout the tumour. HIF-1 α is widely expressed in normoxic cells but is normally rapidly degraded by the ubiquitin/proteasomal pathway (Semenza, 1999; Zhong et al., 2004). HIF-1 regulates the transcription of a broad range of genes that facilitate responses to a hypoxic environment, including regulation of angiogenesis, erythropoiesis, the cell cycle, metabolism and apoptosis.

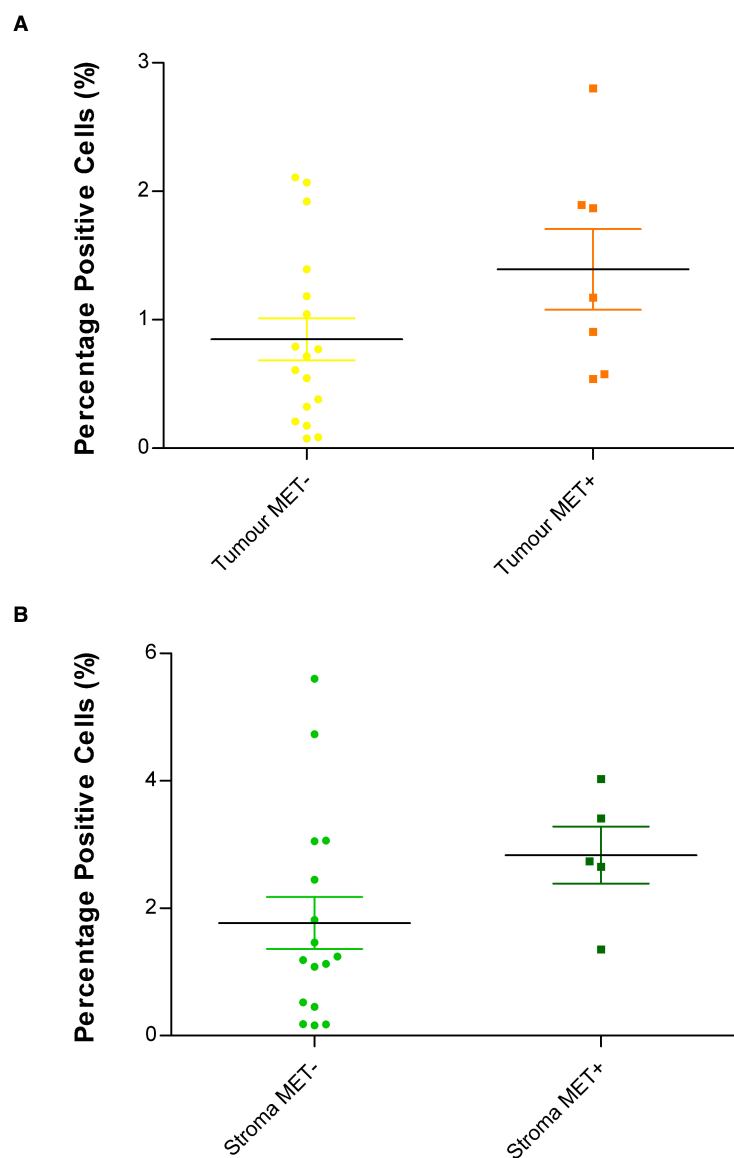


Figure 4.39 Comparison of HIF-1 α in MET+ and MET- Primary CRC Tissue

Primary CRC with no affiliated metastatic disease (MET-) and primary CRC that has since developed liver metastasis (MET+) were analysed for hypoxia-inducible transcription factor-1 α (HIF-1 α) using IHC techniques (anti-human HIF-1 α IgG1, 5 μ g/ml). Digital images were acquired and Genie™ Classifiers were combined with a nuclear algorithm to quantify the number of HIF-1 α positive cells in the A) tumour and B) stroma.

Although no statistical significance was observed between MET- and MET+ primary samples, a general trend was seen that MET+ tissue showed an elevation of tumoural and stromal HIF-1 α positive cells. Data are in agreement with the well published idea that hypoxia plays an important role in tumour progression, angiogenesis and metastasis (Dewhirst et al., 2008).

The frequency of HIF-1 α was then compared between tumour and adjacent non-neoplastic matched tissue (Figure 4.40).

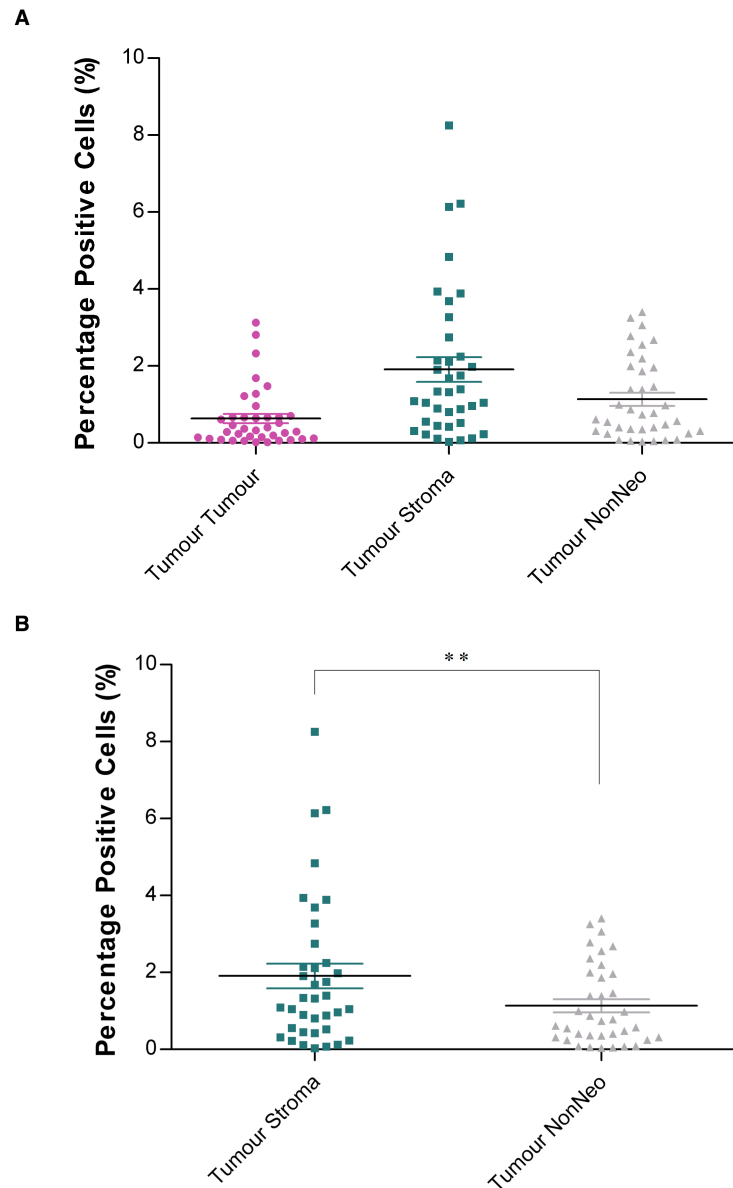


Figure 4.40 HIF-1 α in Liver Metastatic CRC and Matched Non-Neoplastic Tissue

The level of hypoxia-inducible transcription factor-1 α (HIF-1 α) was analysed immunohistochemically in liver metastatic CRC samples (anti-human HIF-1 α IgG1, 5 μ g/ml). Digital images were acquired and Genie™ Classifiers were combined with a nuclear algorithm to quantify the number of HIF-1 α -positive cells. A) The difference between tumour, stroma and tumour adjacent non-neoplastic (Tumour NonNeo) was examined. B) A comparison between the tumour (Tumour Stroma) and tumour adjacent non-neoplastic (Tumour NonNeo) tissue was achieved. (Paired t test, ** p < 0.01).

Levels of hypoxia were established and compared within the tumour infiltrating stroma and tumour adjacent non-neoplastic samples (Figure 4.40B). A significant increase was seen in the tumour-associated stroma ($p < 0.01$). The adjacent non-neoplastic tissue should show relatively low levels of hypoxia as the vasculature structures here should be intact.

Interestingly, hypoxic levels appeared elevated in the tumour infiltrating stroma compared to the tumour tissue itself ($p < 0.05$). This unexpected result was further investigated by comparing the difference between tumour and stroma levels of hypoxia in primary and metastatic tissue (Figure 4.41).

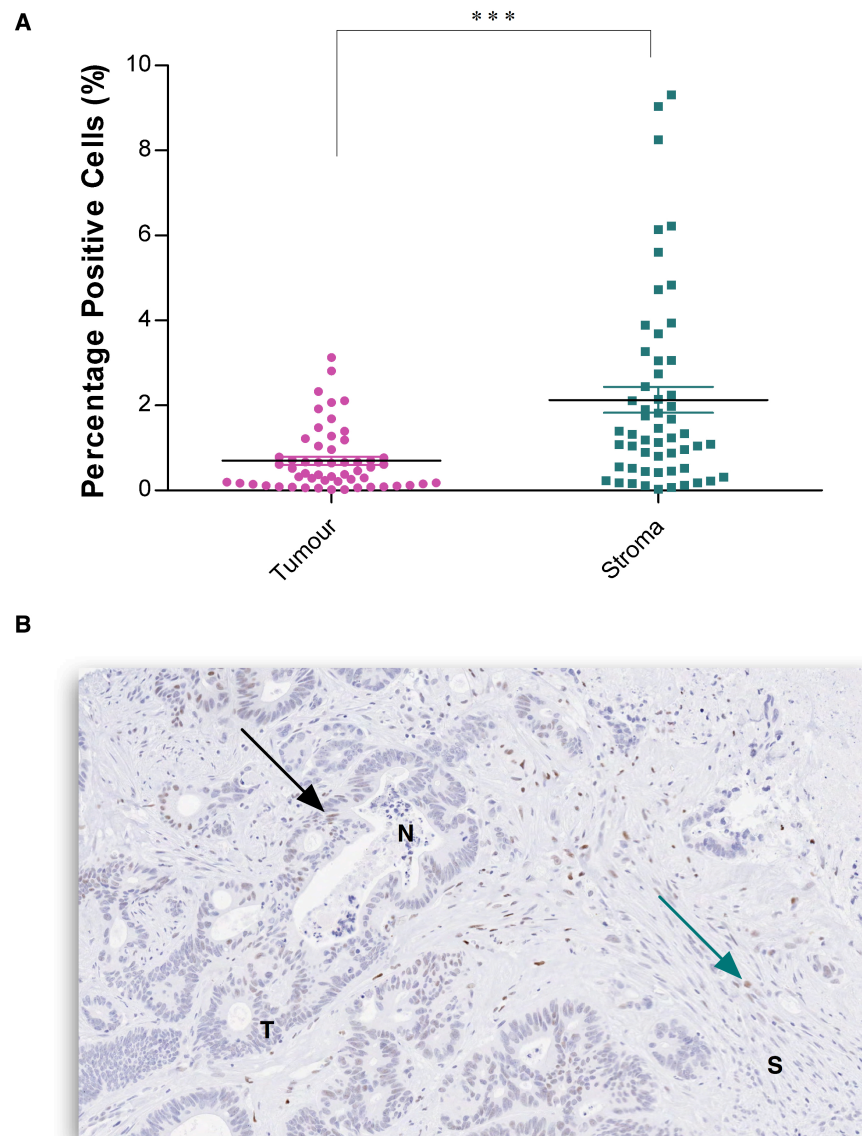


Figure 4.41 Overall Evaluation of Hypoxia in Tumour and Stroma

Primary CRC and CRC metastatic liver samples were pooled and examined for hypoxia-inducible transcription factor-1 α (HIF-1 α) within the tumour and stroma using IHC techniques (anti-human HIF-1 α IgG1, 5 μ g/ml). Digital images were acquired and Genie™ Classifiers were combined with a nuclear algorithm to quantify the number of HIF-1 α positive cells. A) The percentage of HIF-1 α positive cells was compared between tumour and stroma. (Mann-Whitney test, *** $p < 0.001$). B) A corresponding example image of liver metastatic CRC tissue stained with anti-human HIF-1 α IgG1 (5 μ g/ml). Image at x 20 original magnification (T, tumour; S, stroma; N, necrotic; black arrow, example hypoxic cell within the tumour; green arrow, example hypoxic cell within the stroma).

Data reiterates the trend previously observed that an increase in hypoxia was observed within the stroma versus tumour cells (Figure 4.41A). An example image shows HIF-1 α positive cells within the stroma (S) and tumour (T) (Figure 4.41B). In addition, an observation was made that the greatest levels of tumour cell hypoxia was observed adjacent to necrotic (N) regions (also illustrated in Figure 4.46). It is also noted that the intensity of the staining differs. The lower levels of HIF-1 α staining seen within the stroma could therefore be a result of HIF-1 α expression not yet degraded by the ubiquitin/proteasomal pathway (Semenza, 1999; Zhong et al., 2004).

4.2.4.3.3. CC-3 Positive Apoptotic Staining

Defects in apoptosis mechanisms have key roles in tumour progression, allowing neoplastic cells to survive beyond normal limitations, for example, hypoxia, oxidative stress and cell-to-cell contact restrictions. Protecting tumour cells by escaping apoptosis facilitates the accumulation of genetic alterations that result in deregulation of cell proliferation, differentiation and motility, favouring invasiveness and tumour progression (Reed, 2003).

The level of apoptosis was determined by CC-3 staining and assessed in primary and metastatic CRC samples (Figure 4.42).

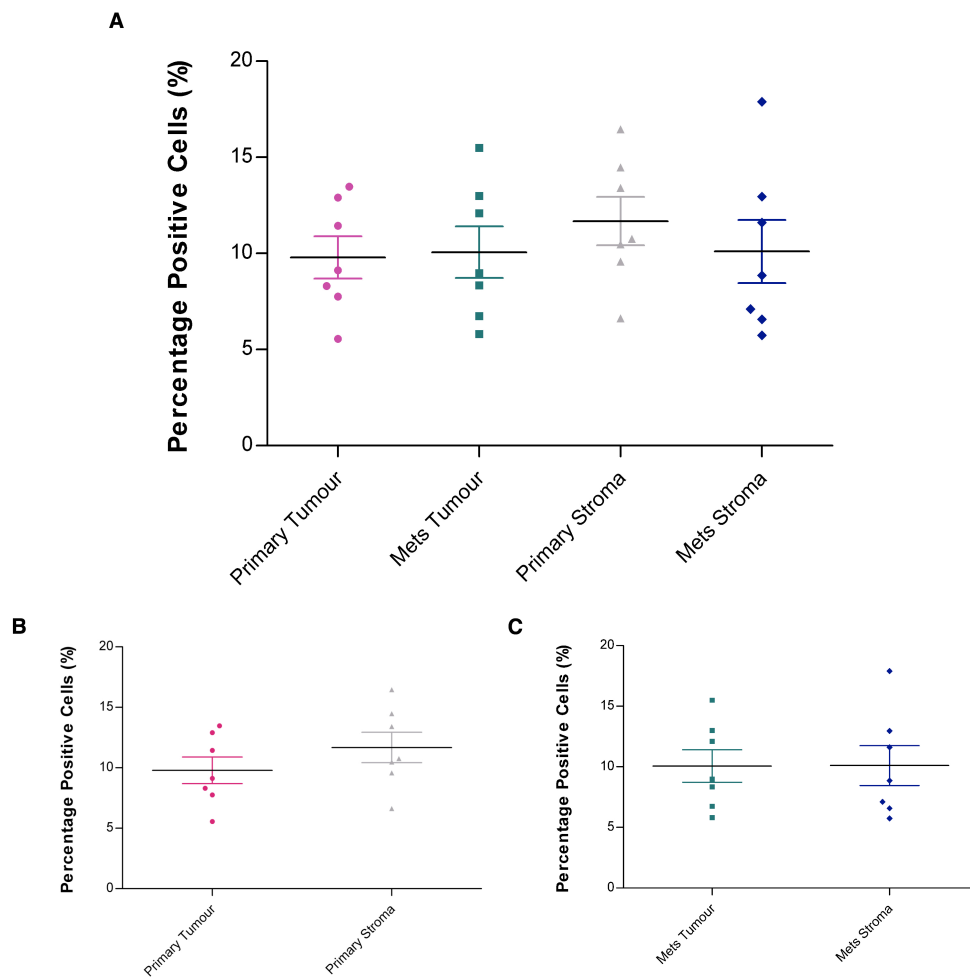


Figure 4.42 CC-3 in Primary CRC vs Metastatic Liver

Primary CRC and matched metastatic liver samples were examined for cleaved caspase-3 (CC-3) within the tumour and stroma using IHC techniques (anti-human CC-3 IgG1, 5 µg/ml). Digital images were acquired and Genie™ Classifiers were combined with a nuclear algorithm to quantify the number of CC-3 positive cells. A) An overall assessment of CC-3 in primary and metastatic disease was carried out. A direct comparison between the levels of apoptosis in the tumour and stroma for both B) primary and C) metastatic (met) tissue was achieved.

Similar levels of CC-3-positive apoptotic cells were observed throughout both primary and metastatic CRC tumours. Apoptosis and inflammation via tumour-released cytokines have been proposed to play a key role in CRC progression. TNF- α is a cytokine extensively researched for its ability to induce apoptosis. TNF- α expression in tumour cells is thought to facilitate immunological escape by inflammation-enhanced metastasis (Grimm et al., 2010b). In addition, it is thought that tumour cells expressing TNF- α can induce apoptosis in tumour infiltrating CD8 CTLs (Grimm et al., 2010a; Koyama et al., 2002).

The current study is a blanket screen of apoptosis within all cells throughout the tumour microenvironment, segregated via regions, but not necessarily cell type. This is perhaps a limitation of the current work as it becomes difficult to hypothesise the prognostic significance of apoptosis in combined cell populations. Based on the prevalence of immune cells within the stroma, one could speculate that apoptosis seen within this region could be indicative of immune cell death. Likewise, one could suggest that the level of apoptosis seen within the tumour region is most likely to reflect tumour cell death, as opposed to infiltrating immune cells.

The levels of apoptotic positive cells within the tumour and stroma were compared in MET+ and MET- primary tissues (Figure 4.43).

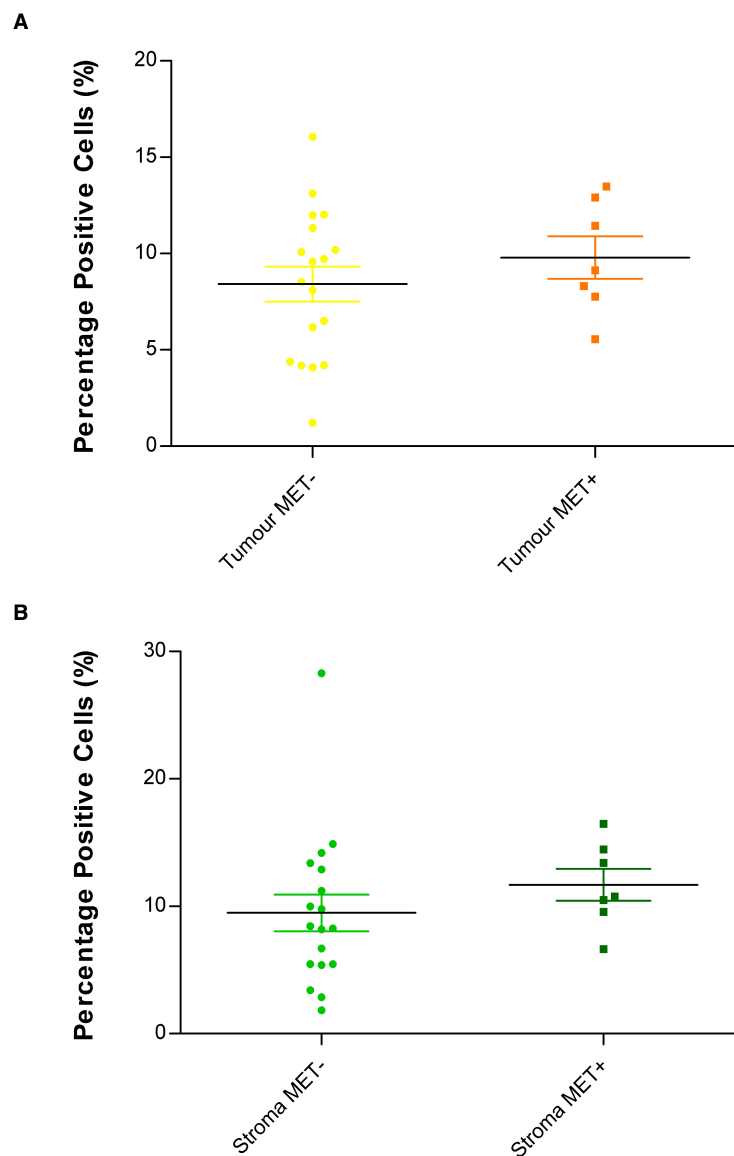


Figure 4.43 Comparison of CC-3 in MET+ and MET- Primary CRC Tissue

Primary CRC with no affiliated metastatic disease (MET-) and primary CRC that has since developed liver metastasis (MET+) were examined for cleaved caspase-3 (CC-3) within the tumour and stroma using IHC techniques (anti-human CC-3 IgG1, 5 μ g/ml). Digital images were acquired and Genie™ Classifiers were combined with a nuclear algorithm to quantify the number of CC-3-positive cells in the A) tumour and B) stroma.

Significant differences were not seen between MET⁺ and MET⁻ primary tissue samples (Figure 4.43). Based on the previously suggested assumptions that apoptotic cells within the tumour region were predominantly tumour cells, one would expect reduced tumour cell death to be associated with a MET⁺ phenotype. Defects in tumour cell apoptosis, and the ability to escape the restraints of normally controlled cell death, could facilitate metastasis by allowing epithelial cells to survive without attachment to the ECM (Frisch and Screaton, 2001).

In addition, defects in tumour apoptotic machinery could hinder the ability of immune infiltrates to undergo tumour cell killing.

The level of apoptosis seen in and around the tumour was then compared to that found at distant matched tissue (Figure 4.44).

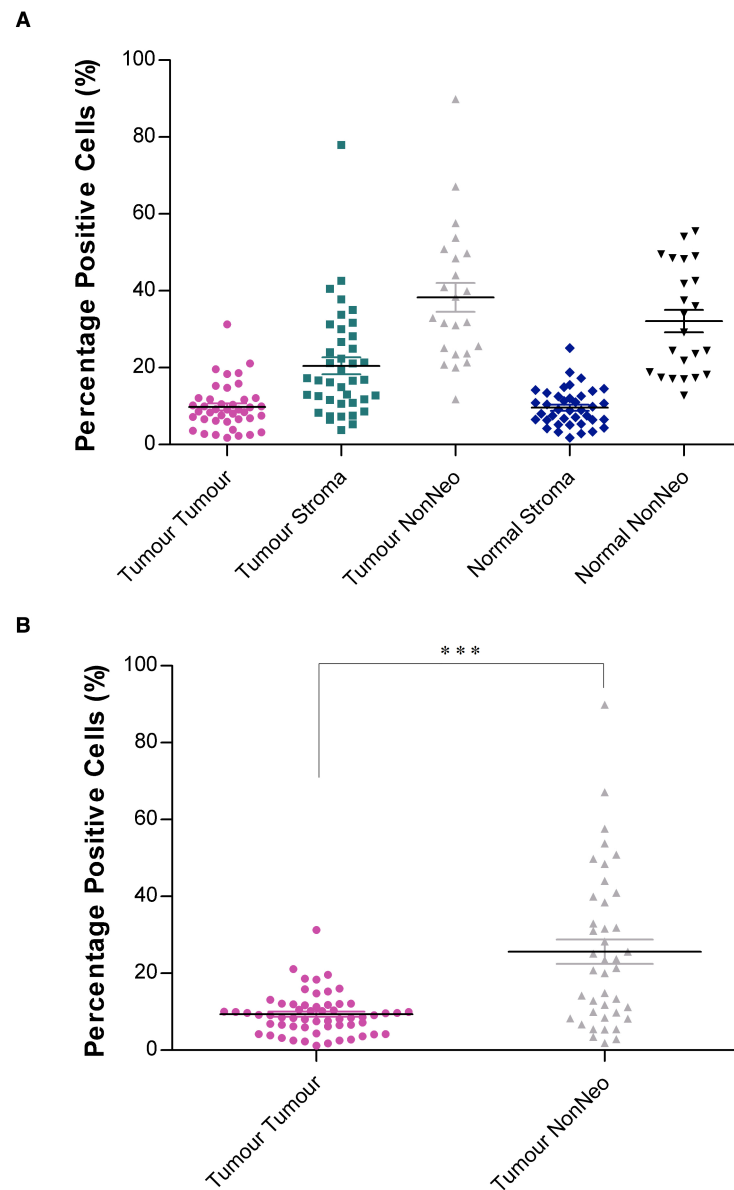


Figure 4.44 CC-3 in Liver Metastatic CRC and Matched Non-Neoplastic Tissue

The percentage of cleaved caspase-3 (CC-3) positive apoptotic cells was analysed immunohistochemically in liver metastatic CRC samples (anti-human CC-3 IgG1, 5 μ g/ml). Digital images were acquired and Genie™ Classifiers were combined with a nuclear algorithm to quantify the number of CC-3-positive cells, investigating A) the difference between tumour, stroma and tumour adjacent non-neoplastic (Tumour NonNeo) tissue, compared to matched distant normal stroma and non-neoplastic (Normal NonNeo). B) A comparison between tumour (Tumour Tumour) and tumour adjacent non-neoplastic (NonNeo Tumour) tissue was achieved. (Paired t-test, *** $p < 0.001$).

Tumour adjacent non-neoplastic tissue showed significantly higher levels of apoptosis than that seen within the tumour (Figure 4.44B). Previously in the current study, the accumulation of immune cells, such as CTLs (Figure 4.23A), at the IM and tumour adjacent non-neoplastic tissue, has been highlighted. The same region subsequently showed the highest levels of apoptosis, greater than those observed within the tumour-associated stroma ($p < 0.01$) and the tumour itself ($p < 0.001$). These results possibly suggest that adjacent non-neoplastic tissue, and the immune cells within it, is undergoing high levels of cell death. This is in accordance with research indicating that tumour cells expressing TNF- α can induce apoptosis in tumour-infiltrating CD8 CTLs (Grimm et al., 2010a).

Analysis of apoptosis was then achieved in tumour versus stroma regions (Figure 4.45).

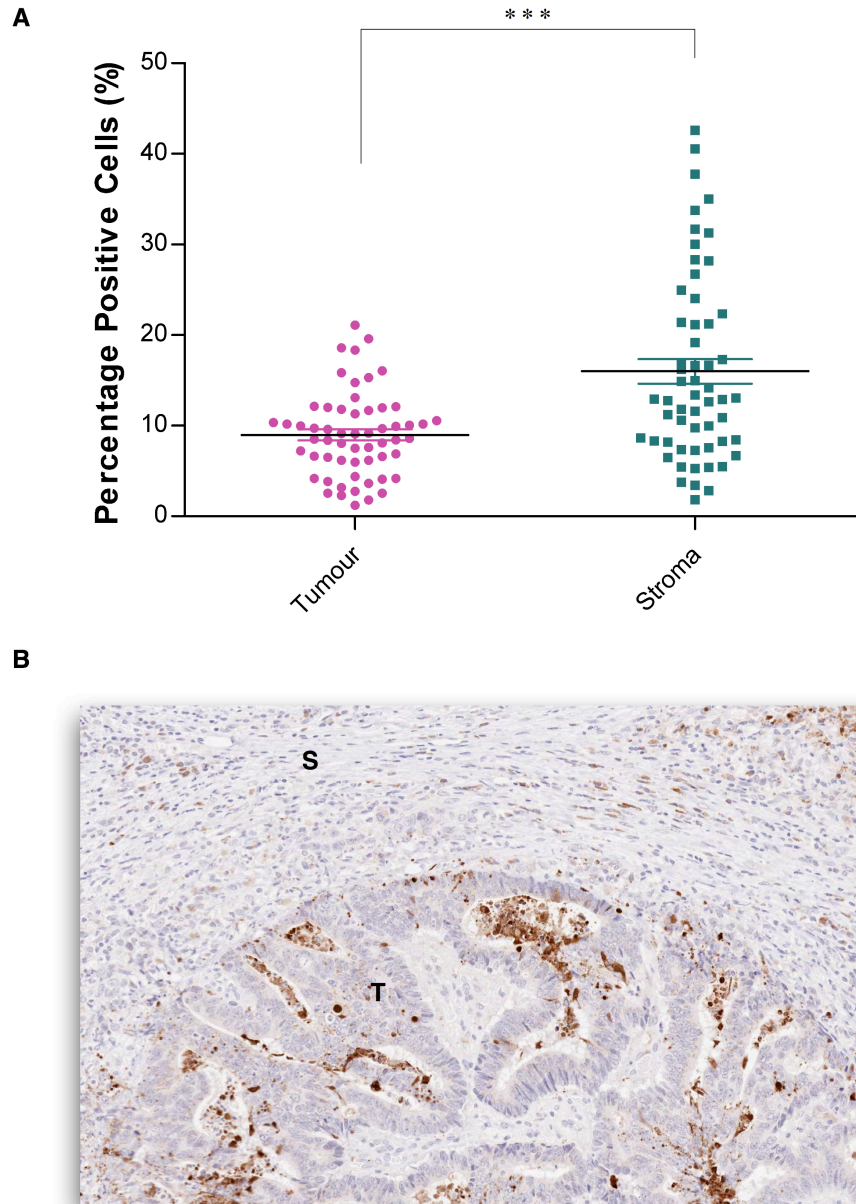


Figure 4.45 Overall Evaluation of Apoptosis in Tumour and Stroma

Primary CRC and liver metastatic samples were pooled and examined for cleaved caspase-3 (CC-3) positive apoptotic cells using IHC techniques (anti-human CC-3 IgG1, 5 μ g/ml). Digital images were acquired and Genie™ Classifiers were combined with a nuclear algorithm to quantify the number of CC-3-positive cells, A) investigating CC-3 expression between tumour and stroma (unpaired t-test, *** $p < 0.001$). B) A corresponding example image of liver metastatic CRC tissue stained with anti-human CC-3 IgG1 (5 μ g/ml). Image at x 20 original magnification (T, tumour; S, stroma).

A higher level of apoptosis activity was observed within the stromal regions when compared to tumour (Figure 4.45A). It is well established that the cellular and non-cellular stromal components of the tumour microenvironment, such as myofibroblasts and ECM proteins, contribute to the anti-apoptotic protection of tumour cells (Sebens and Schafer, 2011).

The prevalence of apoptotic cells within the tumour microenvironment was compared and contrasted to areas of hypoxia and necrosis. It was hypothesised that areas of hypoxia would see subsequent elevated levels of apoptosis and necrotic regions. Example images are illustrated in Figure 4.46.

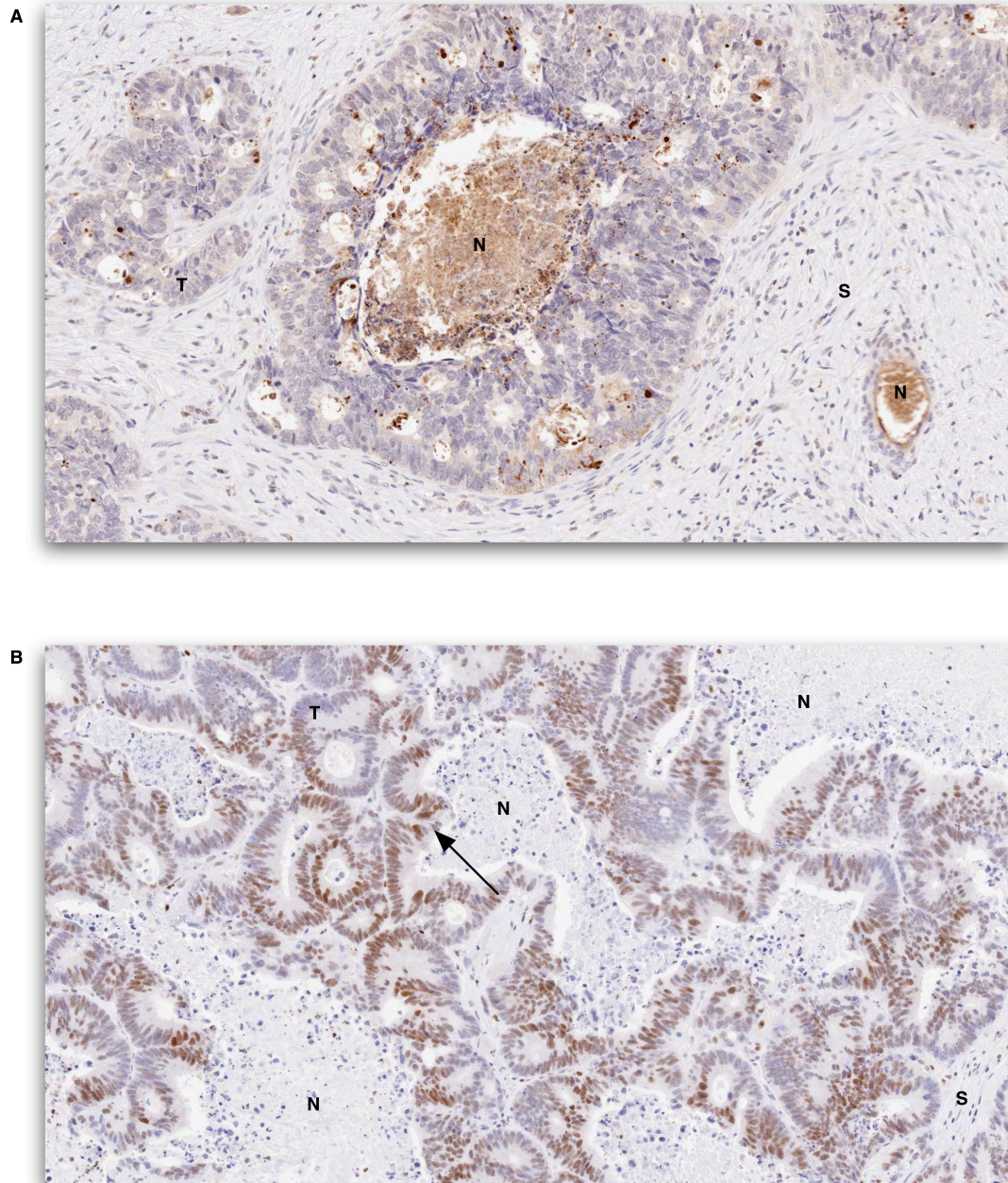


Figure 4.46 Example Images of Hypoxic and Apoptotic Areas of Necrosis

Example images of liver metastatic CRC samples analysed immunohistochemically for apoptosis using cleaved caspase-3 (anti-human CC-3 IgG1, 5 μ g/ml) and hypoxia by hypoxia-inducible transcription factor-1 α (anti-human HIF-1 α IgG1, 5 μ g/ml). Digital images were acquired and Genie™ Classifiers were combined with a nuclear algorithm to quantify the number of A) CC-3- and B) HIF-1 α -positive cells. Images at x 20 original magnification (T, tumour; S, stroma; N, necrotic).

Levels of apoptosis within the tumour region were strongly affiliated to the central, necrotic (N) areas (Figure 4.46A). In addition, it was noticed that these necrotic areas were associated with adjacent hypoxic cells (Figure 4.46B, black arrow).

4.2.4.3.4 Ki67 Positive Proliferation Staining

Ki67 was used to assess the level of proliferation within the tumour and stroma of primary and metastatic CRC samples (Figure 4.47).

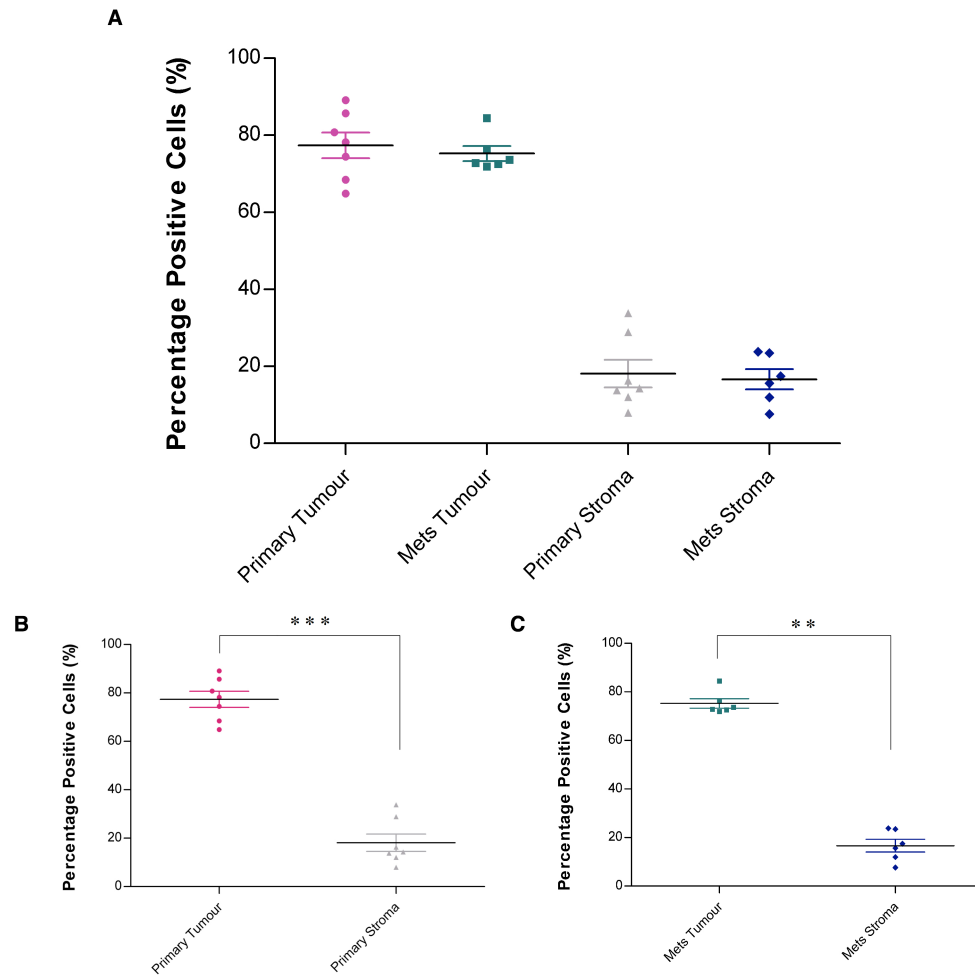


Figure 4.47 Ki67 in Primary CRC vs Metastatic Liver

Primary CRC and matched liver metastatic tissue were examined for the proliferation marker, Ki67 using IHC techniques (anti-human Ki67 IgG1, 0.35 μ g/ml). Digital images were acquired and Genie™ Classifiers were combined with a nuclear algorithm to quantify the number of Ki67-positive cells. A) An overall assessment of percentage positive proliferating cell in primary and metastatic disease was carried out. A direct comparison between proliferation in the tumour and stroma for both B) primary and C) metastatic (met) tissue was achieved. (Paired t test, ** $p < 0.01$, *** $p < 0.001$).

The level of proliferation was significantly higher in the tumour compared to that seen in the stroma of both primary and metastatic samples. No difference in proliferation was observed within these regions when comparing primary and metastatic disease (Figure 4.47A). The percentage of Ki67-positive proliferating cells reached near 80 % within the tumour of both primary and met samples.

The level of proliferation was investigated in primary CRC tissue of a MET⁺ or MET⁻ phenotype (Figure 4.48).

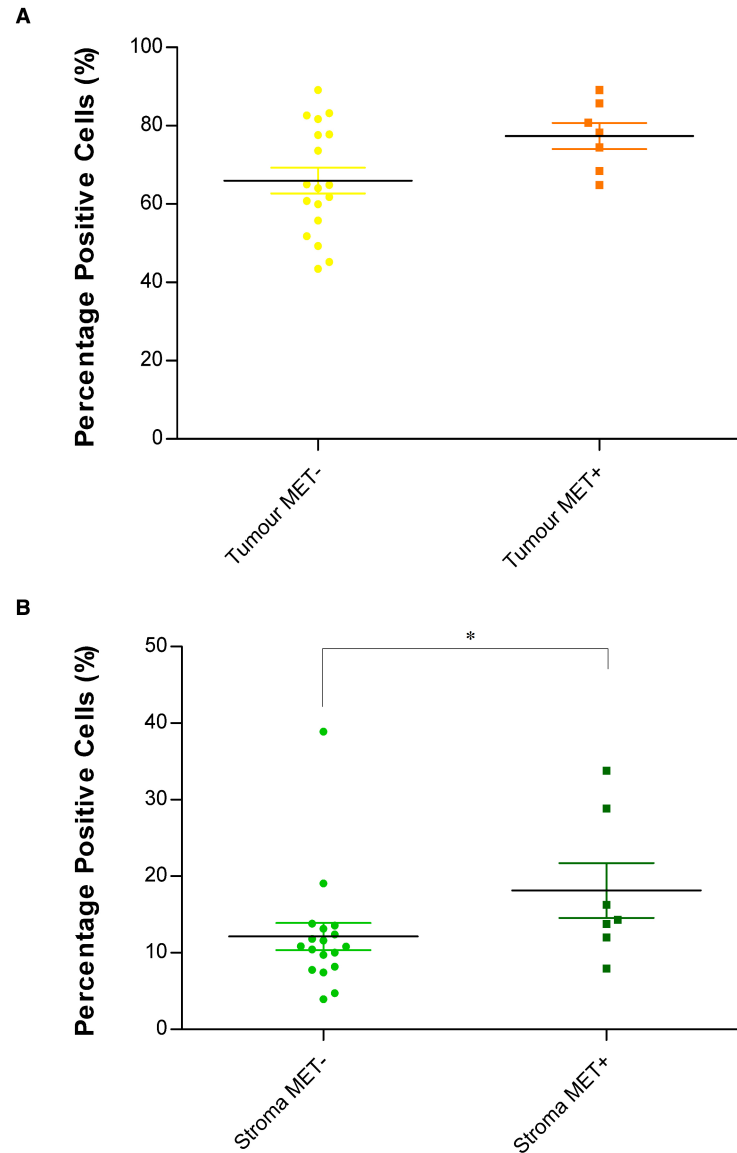


Figure 4.48 Comparison of Proliferation in MET+ and MET- Primary CRC Tissue

Primary CRC with no affiliated metastatic disease (MET-) and primary CRC that has since developed liver metastasis (MET+) were examined for the proliferation marker, Ki67 using IHC techniques (anti-human Ki67 IgG1, 0.35 µg/ml). Digital images were acquired and Genie™ Classifiers were combined with a nuclear algorithm to quantify the number of Ki67-positive cells in A) tumour and B) stroma. (Mann-Whitney test, * p < 0.01).

Although an increase in tumour proliferation was observed in MET+ CRC primary tissue, no significant correlation was determined (Figure 4.48A). When researching the differences in proliferating stromal cells, a significant ($p < 0.05$) increase was seen in tissue that went on to develop metastatic disease (Figure 4.48B).

The level of proliferation was compared in and around the tumour and adjacent non-neoplastic tissue (Figure 4.49).

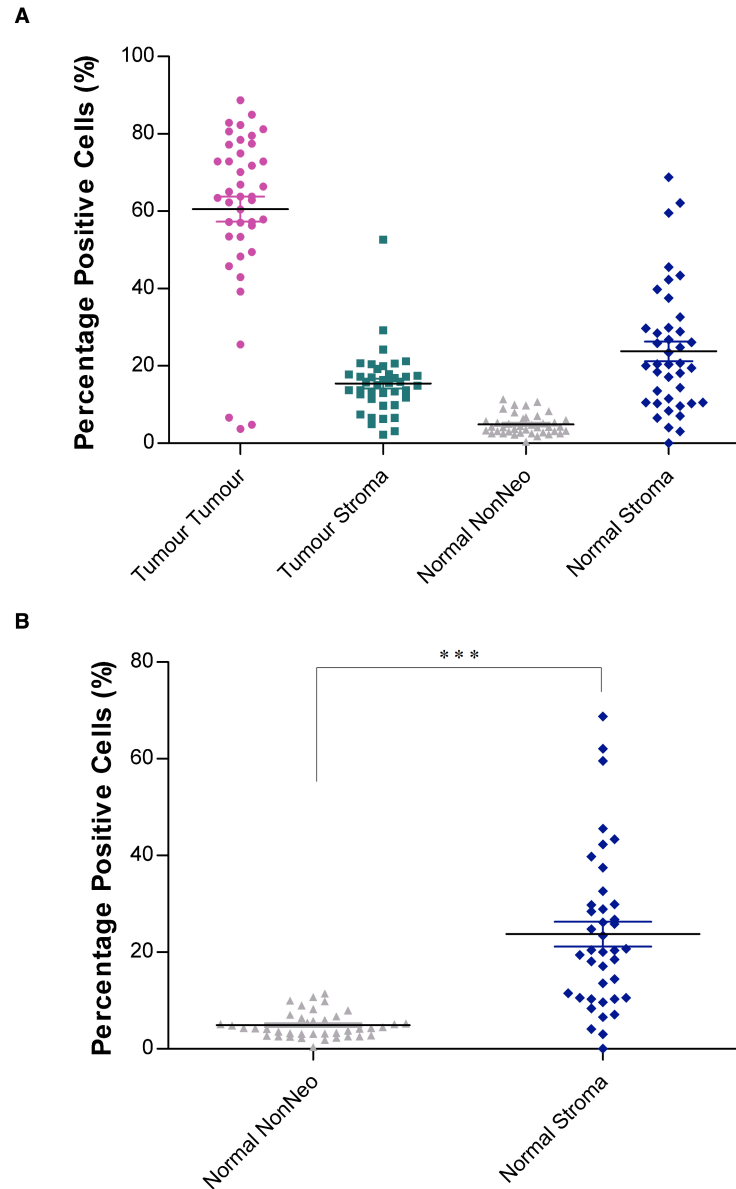


Figure 4.49 Ki67 in Liver Metastatic CRC and Matched Non-Neoplastic Tissue

Liver metastatic CRC samples were examined for the proliferation marker, Ki67 using IHC techniques (anti-human Ki67 IgG1, 0.35 $\mu\text{g/ml}$). Digital images were acquired and Genie™ Classifiers were combined with a nuclear algorithm to quantify the number of Ki67-positive cells, looking at the difference between tumour and tumour stroma tissue, compared to matched distant normal stroma and non-neoplastic (Normal NonNeo). B) A comparison between distant non-neoplastic and stroma tissue was achieved. (Wilcoxon test, *** $p < 0.001$).

The number of Ki67-positive cells in the tumour was significantly higher ($p < 0.001$) compared to that seen in distant non-neoplastic tissue (Figure 4.49A). This shows the highly proliferative phenotype of the neoplastic tissue. Interestingly, the proliferation seen in normal stroma showed no significant difference compared to that seen infiltrating the tumour (Figure 4.49). Under normal, non-neoplastic conditions the cells within the stroma show significantly higher ($p < 0.001$) levels of proliferation than observed in non-neoplastic tissue (Figure 4.49B). This relationship is completely inverted in a neoplastic setting, where the tumour cell replication was significantly more frequent than observed in the tumour associated stroma ($p < 0.001$).

This tumour-stroma relationship is further illustrated in Figure 4.50.

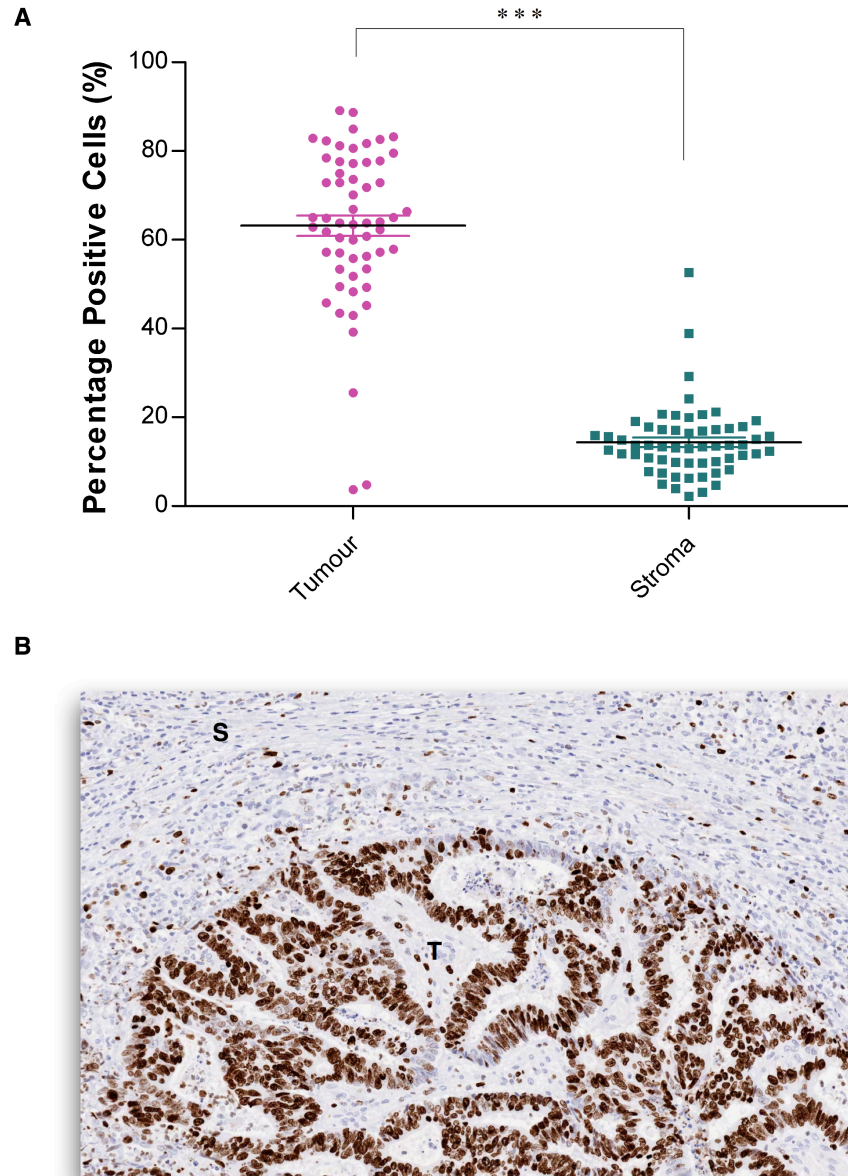


Figure 4.50 Overall Evaluation of Proliferation in Tumour and Stroma

Primary CRC and liver metastatic samples were pooled and examined immunohistochemically for the proliferation marker, Ki67 (anti-human Ki67 IgG1, 0.35 $\mu\text{g/ml}$). Digital images were acquired and Genie™ Classifiers were combined with a nuclear algorithm to quantify the number of Ki67-positive cells between A) tumour and stroma (Mann-Whitney test, *** $p < 0.001$). B) A corresponding example image of liver metastatic CRC tissue stained with anti-human Ki67 IgG1 (0.35 $\mu\text{g/ml}$). Image at x 20 original magnification (T, tumour; S, stroma).

The significant elevation in proliferation observed in tumour cells is illustrated in the pooled primary and metastatic patient cohort (Figure 4.50A). In addition, an example image is exemplified in Figure 4.50B. The image selected is the same area as that shown in Figure 4.45B stained with the apoptotic marker CC-3. The correlation between evading tumour cell death and uncontrolled proliferation is well documented within the literature to be a key contributor to tumour progression. These two images represent the tipping of this normally well-regulated and balanced environment.

4.2.4.3.5. α -SMA Stromal Staining

Irrespective of their origin, tumours are heterogeneous cellular entities; whose growth depends on reciprocal interactions between neoplastic cells and their non-neoplastic microenvironment. The stroma entity plays a pivotal role in many stages of carcinogenesis including proliferation, invasion, angiogenesis, metastasis and also drug resistance. The importance of the stroma has been demonstrated within this study and therefore further tumour/stroma phenotyping was achieved.

A Genie™ algorithm was established to determine the distribution and coverage of stroma compared to that of the tumour (Figure 4.51).

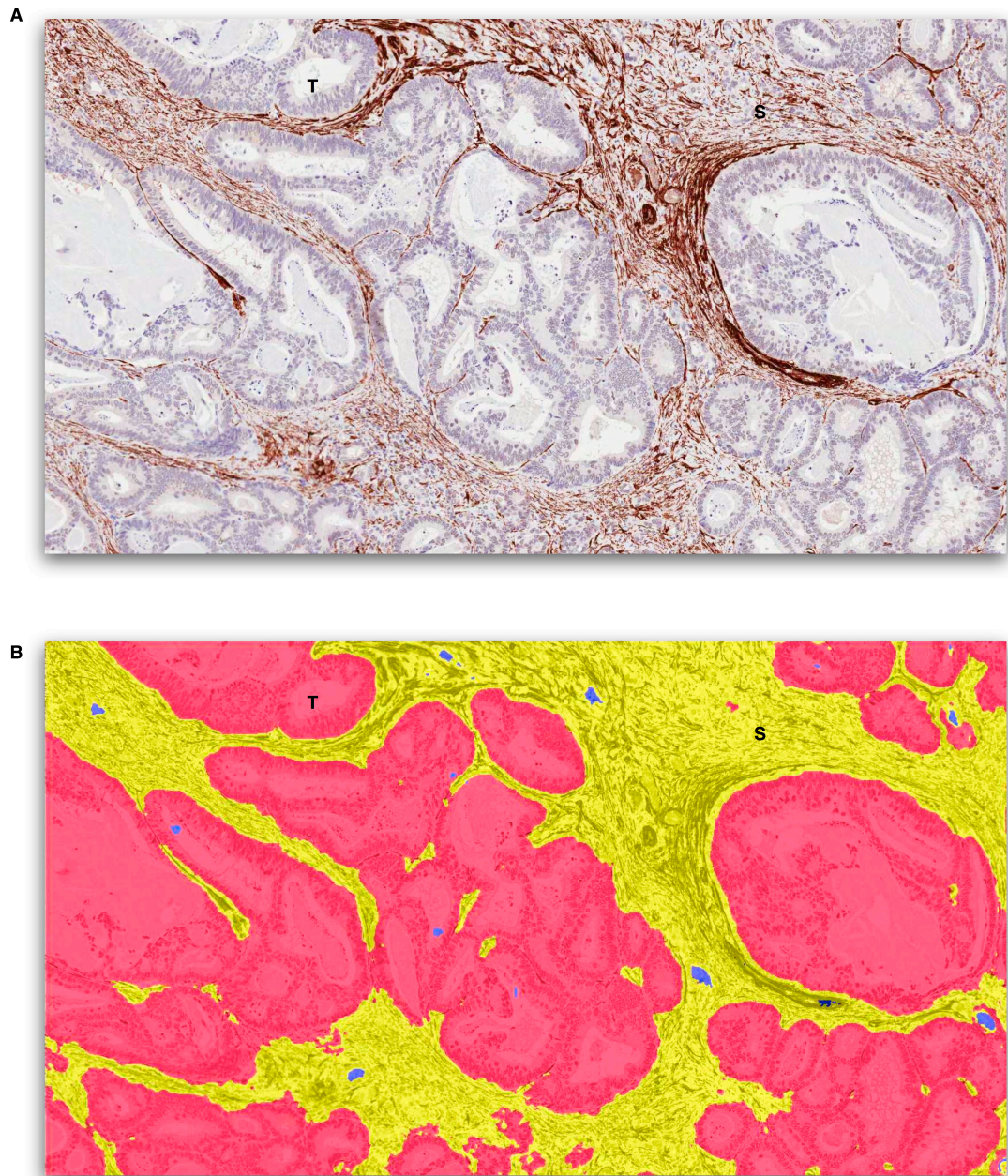


Figure 4.51 Example Images of α -SMA Staining and Genie™ Analysis

A) Example image of liver metastatic CRC tissue stained α -smooth muscle actin (α -SMA) used to aid in the identification of stroma. Sections were stained immunohistochemically (anti-human α -SMA IgG2a, 2 μ g/ml). B) Digital images were acquired (at x 20 original magnification) and Genie™ Classifiers were used to distinguish tumour (T, red) stroma (S, yellow) and glass (blue).

A Genie™ algorithm was constructed to analyse the percentage coverage of stroma, tumour and glass (Figure 4.51). The algorithm utilised α -SMA as a stromal marker. Regions of glass (blue) were excluded, except for any regions of white within the tumour cells. Primary and metastatic CRC has a very globular tumour phenotype where the tumour cells often grow in circular structures, encapsulating areas of white space. The entirety of these structures was used to depict the area of tumour coverage, not just the surrounding tumour cells.

The algorithm was then run across different CRC samples and the percentage coverage compared (Figure 4.52).

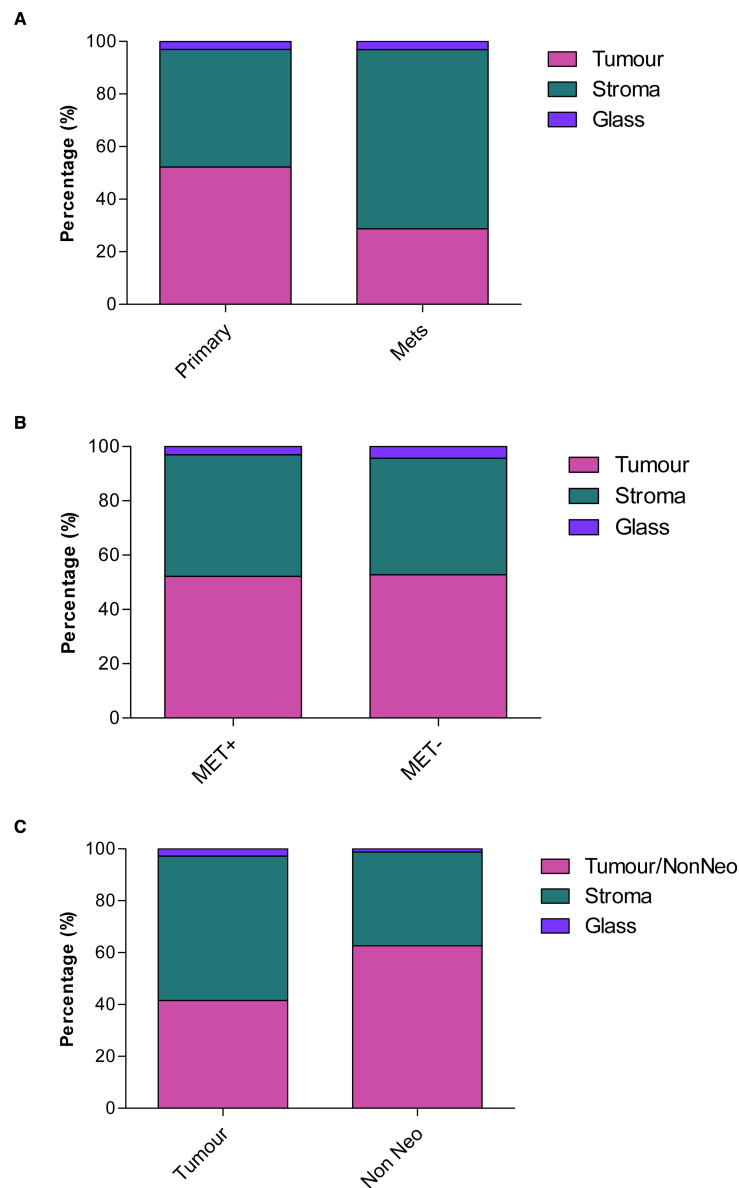


Figure 4.52 Percentage Area of Tumour and Stroma

Liver metastatic tissue was examined immunohistochemically for α -smooth muscle actin (α -SMA) to aid in the identification of stroma (anti-human α -SMA IgG2a, 2 μ g/ml). Digital images were acquired and Genie™ Classifiers were used to distinguish areas of tumour or non-neoplastic tissue (pink), stroma (green) and glass (blue) and expressed as a percentage of area covered. A) A comparison between primary CRC and matched liver metastatic tissue. B) Primary CRC with no affiliated metastatic disease (MET⁻) and primary CRC that has since developed liver metastasis (MET⁺) were compared. C) Primary and metastatic tumours were combined and compared to distant non-neoplastic (Non Neo) tissue.

The percentage coverage of tumour (pink) and stroma (green) was compared between primary and metastatic CRC samples (Figure 4.52A). The metastatic tissue had larger percentage coverage of stroma compared to the primary tissue. No difference was observed between primary tissue with a MET⁺ or MET⁻ phenotype (Figure 4.52B). Additionally, when comparing tumour samples to adjacent non-neoplastic tissue, the tumour samples had elevated levels of stroma to that seen in a non-neoplastic sample (Figure 4.52C).

Given the extensive amount of tumour-promoting, stroma-derived factors that facilitate tumour initiation, progression and metastasis, the stroma is likely to influence therapeutic outcome. A large repertoire of molecules and receptors orchestrate the interactions between tumour cells and their microenvironment. These include: cellular adhesion molecules, such as L1CAM and CD44; chemokines, for example CXCL12; and also various integrins and ECM receptors. It has been suggested that these could provide suitable targets to overcome drug- and chemoresistance (Sebens and Schafer, 2011).

The interactions orchestrated between stromal cells and tumour cells have been well studied; however, the author would like to suggest a focus on investigating the cross-talk between tumour-associated stroma and immune infiltrates. It has been shown that CAFs are pro-inflammatory during early stages of tumour progression and promote macrophage infiltration, angiogenesis and tumour growth (Erez et al., 2010). In addition, it is thought that CAFs can polarise different immune cells and modify their infiltration (Grum-Schwensen et al., 2010; Liao et al., 2009).

4.3. CONCLUSIONS AND FUTURE WORK

The frequency of a selection of immune cells was assessed immunohistochemically in CRC primary and liver metastatic patients. In addition, aspects of the tumour microenvironment were also studied and correlations with immune cells were subsequently made.

4.3.1. Immunohistochemistry Optimisation

Staining protocol optimisation was a fundamental requirement of this chapter, ensuring correct antibody specificity and that results were representative of the clinical setting. Careful marker selection, immune cell isolation, FACS analysis, positive and negative cell pellets, method development and key tissue selection all contributed to successful staining optimisation.

Automated IHC staining procedures combined with novel developments in image analysis facilitated rigorous and systematic quantification of immune cell infiltrates. Advancement in these areas has enabled a refined pathological approach to accurately determine immune cell densities and their distribution throughout tumour and stroma.

4.3.2. Adaptive Immunity

When investigating the prevalence of CD8 cells, a significant link between tumour and stroma tissue was apparent. An example of this relationship is shown in Figure 4.53A, showing the linear trend between the frequency of CD8 cells within primary

tumour and primary stroma ($p = 0.000243$, $r = 0.76$, $r^2 = 0.58$). This reiterates the importance of the tumour microenvironment and the impact of the stroma. Elevated levels of CD8 CTLs within the stroma may facilitate the infiltration of CD8 cells into the tumour and result in a better prognosis. In addition, the frequency of CD31 staining in the tumour stroma was also strongly correlated with the number of CD8 cells observed in both the primary tumour (Figure 4.53B, $p = 0.0112$, $r = 0.58$, $r^2 = 0.34$) and in the primary tumour stroma (Figure 4.53C, $p = 0.0178$, $r = 0.55$, $r^2 = 0.3$). Perhaps the increase of vasculature results in increased infiltration of CD8 cells.

When evaluating CRC tissue, there was a significant increase in the number of CTLs at the tumour edge compared to the number infiltrating the tumour and tumour-associated stroma, perhaps indicating the inability of CD8 cells to penetrate into the CT. Previous studies have shown that high levels of CD8 infiltrates are associated with survival in CRC (Mlecnik et al., 2010a). Further analysis of metastatic tissue showed a linear relationship between the numbers of CD8 cells found at the tumour-adjacent non-neoplastic tissue and those seen infiltrating the tumour stroma (Figure 4.53D, $p = 0.0000578$, $r = 0.37$, $r^2 = 0.06$). Are we observing a slow moving ‘traffic jam’ of CD8 cells trying to infiltrate the tumour?

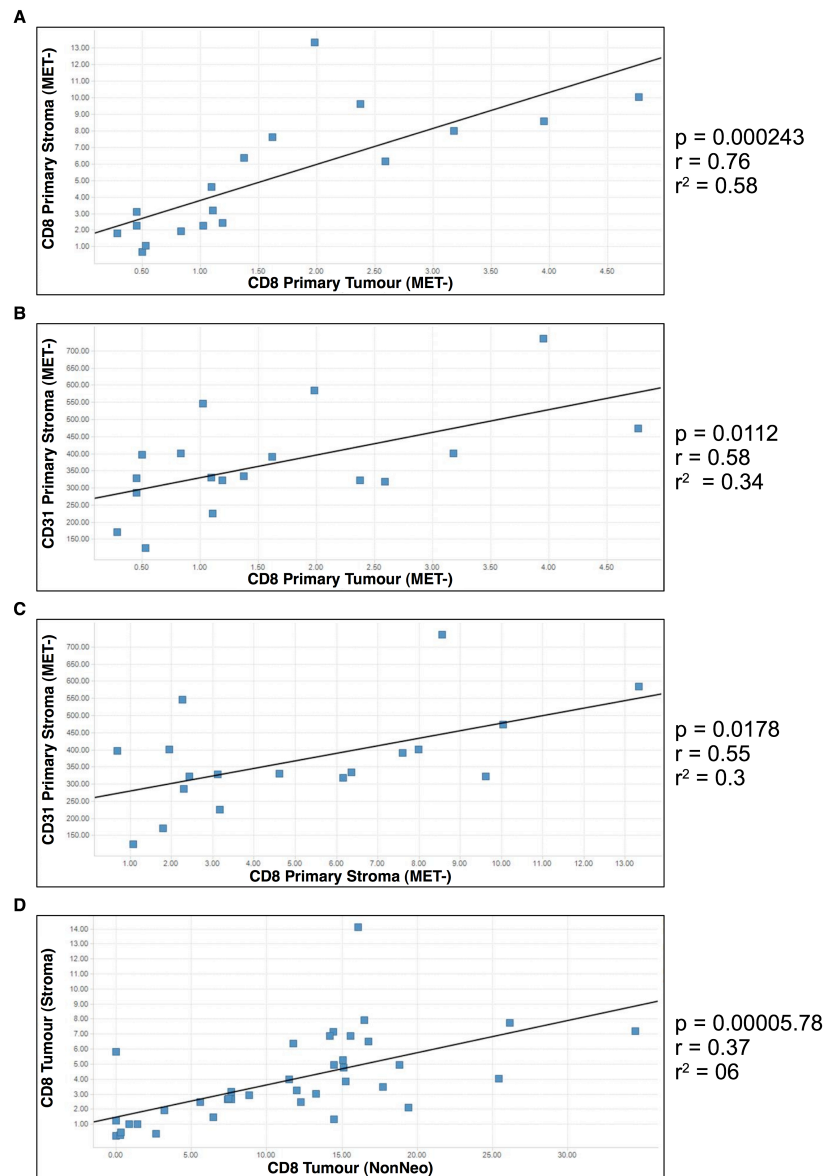


Figure 4.53 Concluding Statistical Correlations Observed for CD8 Cells

Primary CRC with no affiliated metastatic disease (MET-, A–C) and liver metastatic CRC (D) samples were evaluated immunohistochemically as previously described. Spotfire statistical analysis was then used to compare A) CD8 cells between primary tumour and primary tumour-associated stroma ($p = 0.000243$, $r = 0.76$, $r^2 = 0.58$). B) CD31 stained vasculature within primary stroma compared to CD8 cell frequency in primary tumour ($p = 0.0112$, $r = 0.58$, $r^2 = 0.34$) or with C) tumour-associated stroma ($p = 0.0178$, $r = 0.55$, $r^2 = 0.3$). D) A comparison in liver metastatic CRC samples between CD8 cells within the tumour-associated stroma and those seen in the tumour-adjacent non-neoplastic tissue ($p = 0.00005.78$, $r = 0.37$, $r^2 = 0.06$).

Tregs showed similar trends to CD8 cells in that they were significantly elevated within the stromal areas compared to infiltrating the tumour itself. This was true for both primary and secondary disease. Interestingly, the highest level of infiltrating Tregs was observed in the tumour-adjacent non-neoplastic tissue, compared to those that had infiltrated the tumour, which is very similar to that seen for CD8 cells. Further analysis revealed a linear relationship between the number of CD8 cells found at the tumour edge and the number of Tregs within the tumour tissue (Figure 4.54A, $p = 0.0487$, $r = 0.33$, $r^2 = 0.11$). Are Tregs and the cytokines they produce, in combination with the tumour microenvironment, contributing to trafficking of CD8 cells to the tumour edge? Tregs present at the IM were also strongly associated with increases of Tregs infiltrating the tumour-associated stroma (Figure 4.54B, $p = 0.000000000989$, $r = 0.80$, $r^2 = 0.64$). Further to this, elevations of Tregs within the tumour and tumour-associated stroma, correlated with reduced levels of tumour cell killing (Figure 4.54C, $p = 0.0117$, $r = -0.40$, $r^2 = 0.16$ and Figure 4.54D, $p = 0.0272$, $r = -0.35$, $r^2 = 0.13$). This demonstrates the impact of elevated Tregs within the tumour on the anti-tumour response. Previous studies have shown elevated Tregs in HCC compared to non-tumour tissue or healthy liver samples, where low-Treg groups showed improved OS and DFS compared to high-Treg groups (Kobayashi et al., 2007). In addition, the prevalence of Tregs was higher in primary than metastatic tumours (Kobayashi et al., 2007).

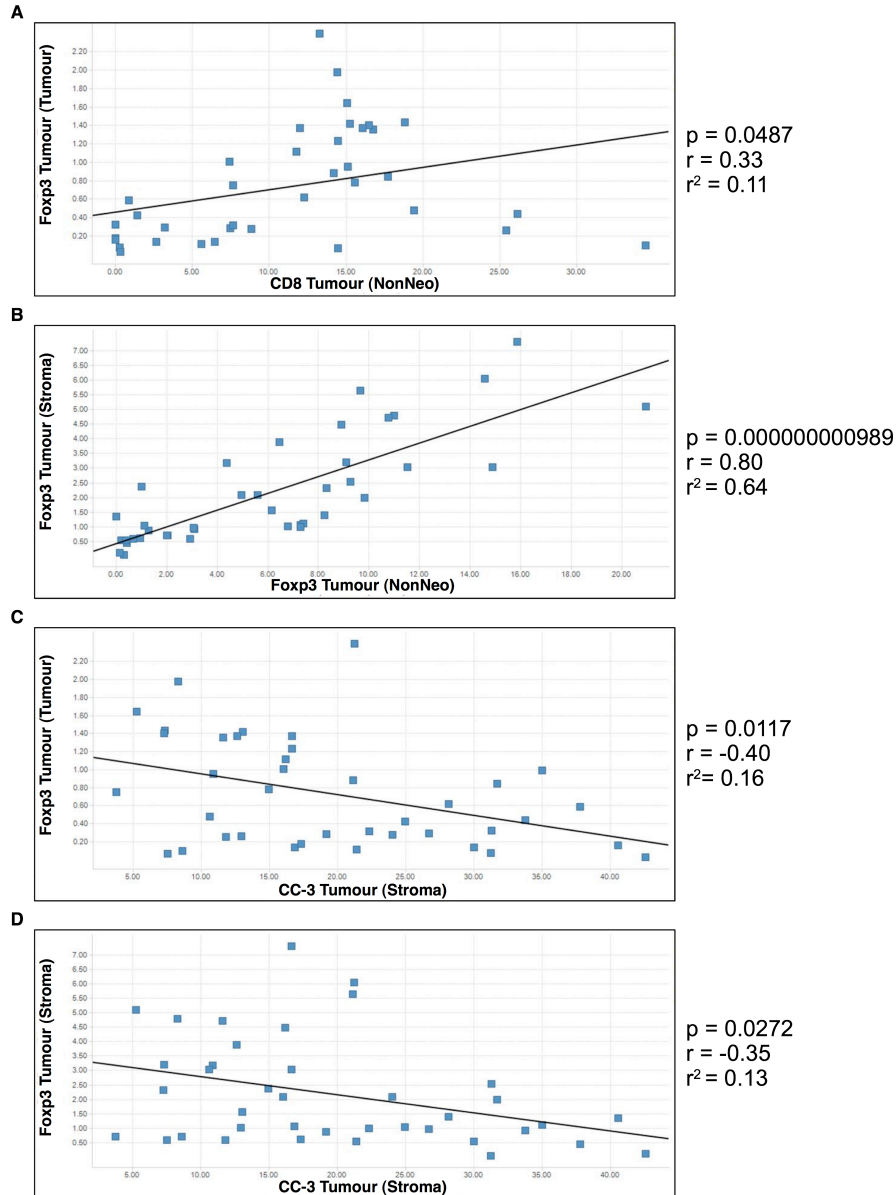


Figure 4.54 Concluding Statistical Correlations Observed for Tregs

Liver metastatic CRC samples were evaluated immunohistochemically as previously described. Spotfire statistical analysis was then used to compare A) Tregs within the tumour and CD8 cells at the tumour-adjacent non-neoplastic tissue ($p = 0.0487$, $r = 0.33$, $r^2 = 0.11$). B) Tregs between the tumour-associated stroma and tumour-adjacent non-neoplastic tissue ($p = 0.000000000989$, $r = 0.80$, $r^2 = 0.64$). C) The level of CC-3 positive tumour-associated stroma cell death was compared to the frequency of Tregs within the tumour ($p = 0.0117$, $r = -0.40$, $r^2 = 0.16$) or D) between the frequency of Tregs within the tumour-associated stroma ($p = 0.0272$, $r = -0.35$, $r^2 = 0.13$).

Further analysis was achieved to conclude the overall relationship between infiltrating CD8 cells and Tregs, in combination with tumour cell proliferation (Figure 4.55). The ratio of CD8 to Treg cells was calculated and compared between the tumour and stroma of primary CRC and liver metastatic samples. A significant relationship was observed, highlighting the link between the ratio of CD8:Tregs in the tumour and stroma ($p = 0.00000204$). Low infiltration of CD8 and Tregs in the stroma was associated with low numbers seen in the tumour. In addition, the CD8:Treg ratio was associated with the proliferation of the tumour cells. Ki67 was used as a marker for proliferation, where a spectrum of colour depicted the proliferation state from high (bright red), medium (purple) to low (blue). A low ratio of CD8:Treg cells was associated with higher levels of tumour proliferation.

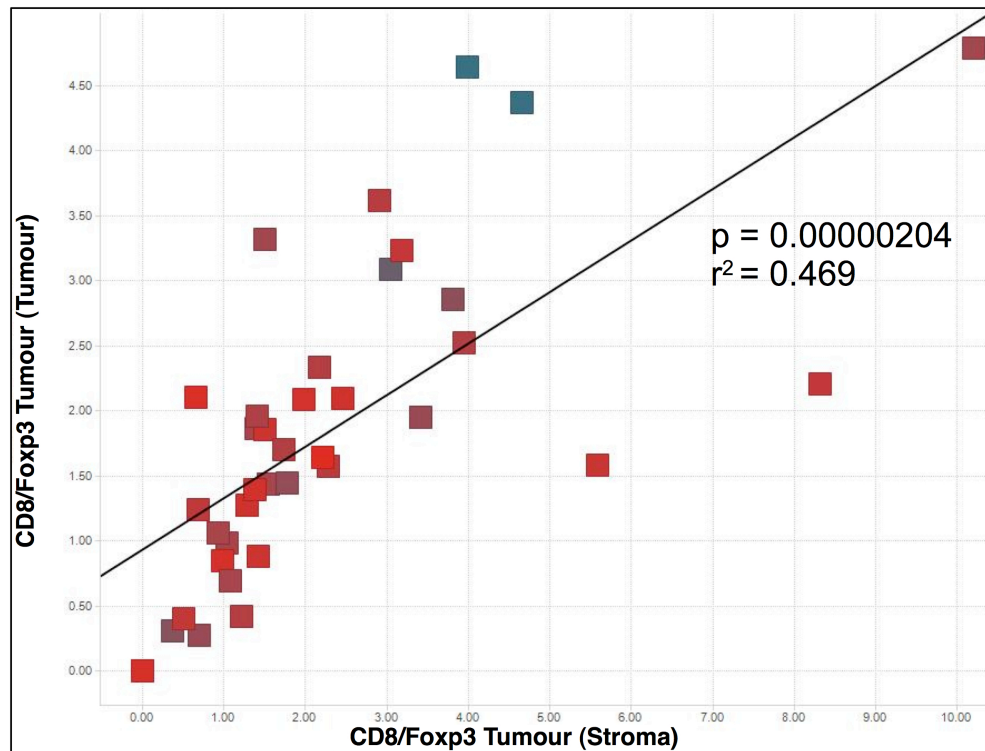


Figure 4.55 Statistical Correlation Between CD8/Treg Cell Ratio in the Tumour and Stroma, Linked with Tumour Proliferation

Primary CRC and liver metastatic CRC samples were evaluated immunohistochemically for CD8 and Foxp3 cell infiltrates as previously described. Spotfire statistical analysis was then used to compare the ratio of CD8:Tregs in the tumour (x axis) and the stroma (y axis). This was also correlated to the degree of tumour proliferation, within the same samples, measured by the proliferation marker Ki67 using IHC techniques. The range of Ki67 staining was coloured from blue (low proliferation) to red (high proliferation). ($p = 0.00000204$, $r^2 = 0.469$).

4.3.3. Innate Immunity

When evaluating CD68, similar trends were observed for macrophages as those seen for CTLs and, to some extent, Tregs. Macrophage infiltration within tumour-associated stroma correlated with the numbers seen within tumour tissue (Figure 4.56A, $p = 0.00000351$, $r = 0.88$, $r^2 = 0.77$). In addition, the increase in numbers of macrophages found at the tumour edge correlated with an increase in numbers infiltrating the tumour-associated stroma (Figure 4.56B, $p = 0.00149$, $r = 0.53$, $r^2 = 0.28$).

A linear relationship was observed between increases in TAMs within the stroma and increased levels of tumour cell death (Figure 4.56C, $p = 0.0273$, $r = 0.53$, $r^2 = 0.29$). This could be a result of IL-2- and IL-12-mediated tumour cell death. In agreement with this anti-tumour macrophage activity, increased TAM frequency was linked to a decrease in tumour cell proliferation (Figure 4.56D, $p = 0.0112$, $r = -0.60$, $r^2 = 0.36$).

Results appear to demonstrate the anti-tumour properties of TAMs; however, the importance of pro-tumour activities of TAMs is also recognised. Future research within this area could distinguish the M1/M2 phenotype of the macrophages present at the tumour microenvironment, thus providing further understanding of their prognostic significance.

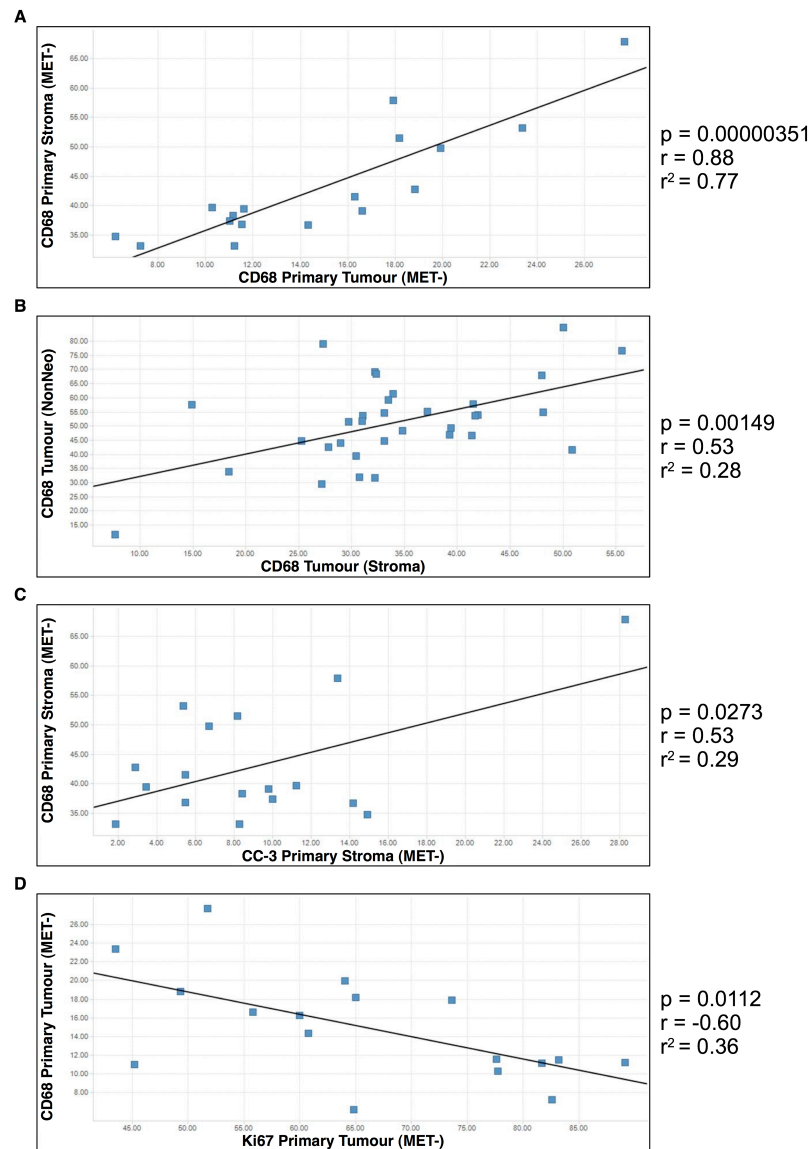


Figure 4.56 Concluding Statistical Correlations Observed for Macrophages

Primary CRC with no affiliated metastatic disease (MET-, A, C, D) and liver metastatic CRC (B) samples were evaluated immunohistochemically as previously described. Spotfire statistical analysis was then used to compare A) CD68 positive macrophages within the tumour and tumour-associated stroma ($p = 0.00000351$, $r = 0.88$, $r^2 = 0.77$). B) The frequency of CD68 cells in metastatic tumour-adjacent non-neoplastic tissue was compared with matched tumour-associated stroma ($p = 0.00149$, $r = 0.53$, $r^2 = 0.28$). C) Macrophages in tumour-associated stroma were compared with the level of CC-3-positive tumour-associated stroma cell death ($p = 0.0273$, $r = 0.53$, $r^2 = 0.29$). D) The number of macrophages in the tumour were compared with CC-3-positive tumour cell death ($p = 0.0112$, $r = -0.60$, $r^2 = 0.36$).

As with previous immune infiltrates, the highest occurrence of NK cells was observed within the stroma of both primary and metastatic disease. However, although similar trends were observed for the location of NK cells, the percentage of positive CD56 cells was significantly lower than that of other immune infiltrates, such as CD8s, Tregs and macrophages. The existence of fewer NK cells would suggest a reduced level of tumour cell cytotoxicity and therefore favour disease progression and metastasis. These counterintuitive clinical results were surprising and would have significant influence on the development of a tumour microenvironment model (Chapter 6). Future work should aim to understand the chemokines, cytokines and cellular interactions that orchestrate the limited numbers of NK cells in and around CRC tumours.

A tumour cell-centric view of cancer progression fails to include the importance of the tumour microenvironment and the immune infiltrates within it. Research has alluded to the importance of the stroma. During tumour progression, the surrounding microenvironment co-evolves into an activated state that facilitates tumour growth. Further understanding of this dynamic situation is empirical to address remaining questions and discover potential targeting opportunities.

The question of the prognostic role of Tregs in human CRC appears to be complex and ambiguous. The overall significant findings of this chapter, along with possible positive and negative contributing prognostic factors, are summarised diagrammatically in Figure 4.57.

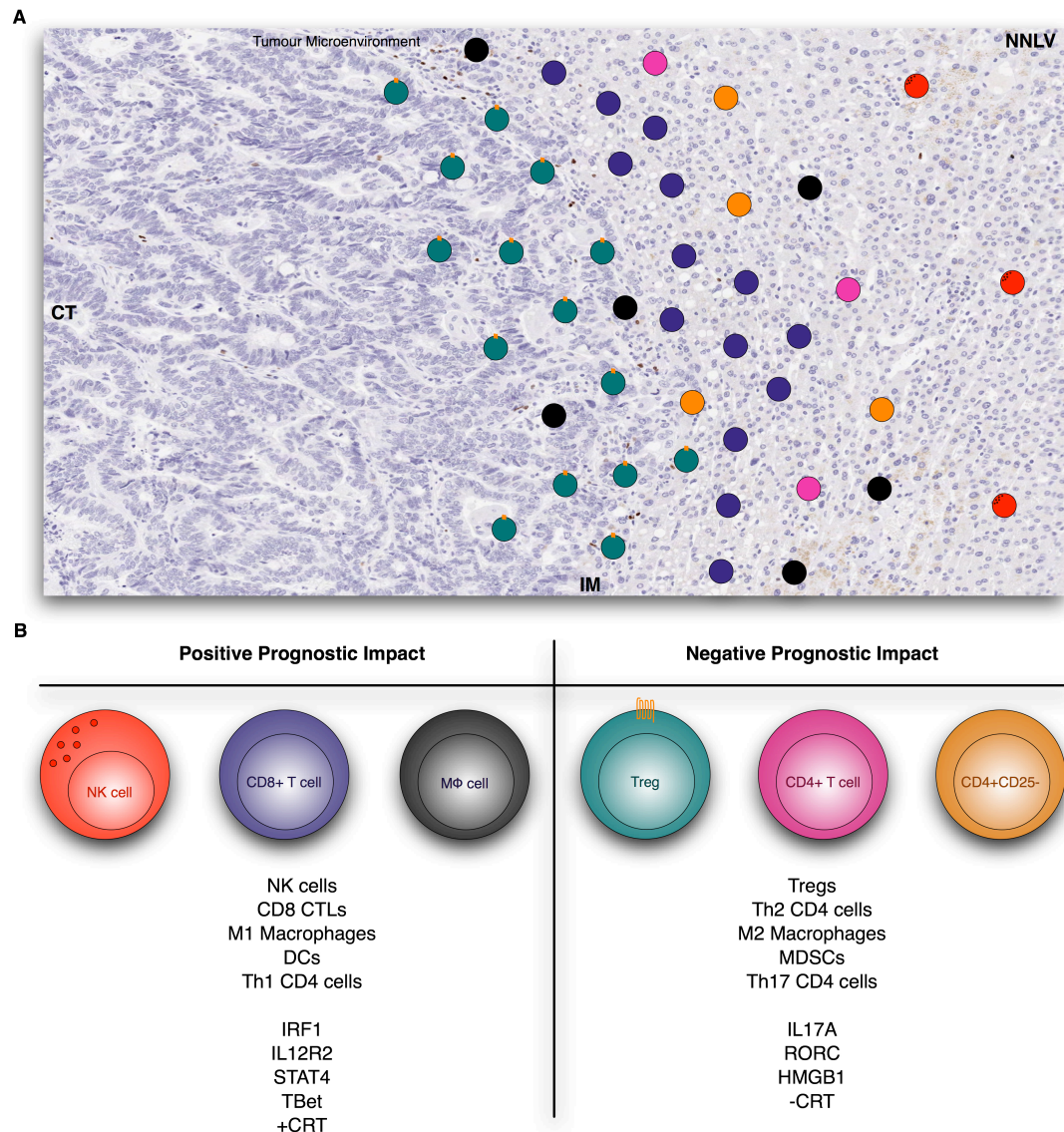


Figure 4.57 Diagrammatic Summary of Current Findings and Prognostic Factors within Literature.

A) An example image of the invasive margin (IM) of liver metastatic CRC tissue stained using IHC techniques, with representative cartoon immune cells demonstrating research findings. (CT, centre of tumour, NNLV, non-neoplastic liver). B) Differentiation of the positive and negative prognostic factors in CRC. (NK, natural killer; CTLs, cytotoxic T lymphocytes; DCs, dendritic cells; MDSCs, myeloid-derived suppressor cells; IRF1, interferon regulatory factor 1; IL-12R 2, interleukin-12 receptor 2; STAT4, signal transducer and activator of transcription 4 gene; Tbet, T cell-associated transcription factor; CRT, Calreticulin; IL-17A, interleukin-17A; RORC, retinoic acid-related orphan receptor C; HMGB1, high-mobility group protein B1).

An understanding of the underlying mechanisms responsible for immune cell infiltration is an important area of research and could add to a positive or negative prognostic impact. The expression of genes associated with pro-inflammatory cells, such as IL-17A and the Th17-specific transcription factor ROR.C have a negative prognostic impact in CRC. In addition, the high-mobility group protein B1 (HMGB1), a chromatin-binding protein released during cell stress, predicts poor survival. Calreticulin (CRT), required for loading of class I MHC proteins, is translocated to the cell surface during stress. An absence of CRT expression has a negative prognostic impact. In contrast, CRT cell-surface expression and the expression of IRF1, IL-12R.2, STAT4 and Tbet genes, are all associated with a positive prognosis (Fridman et al., 2011).

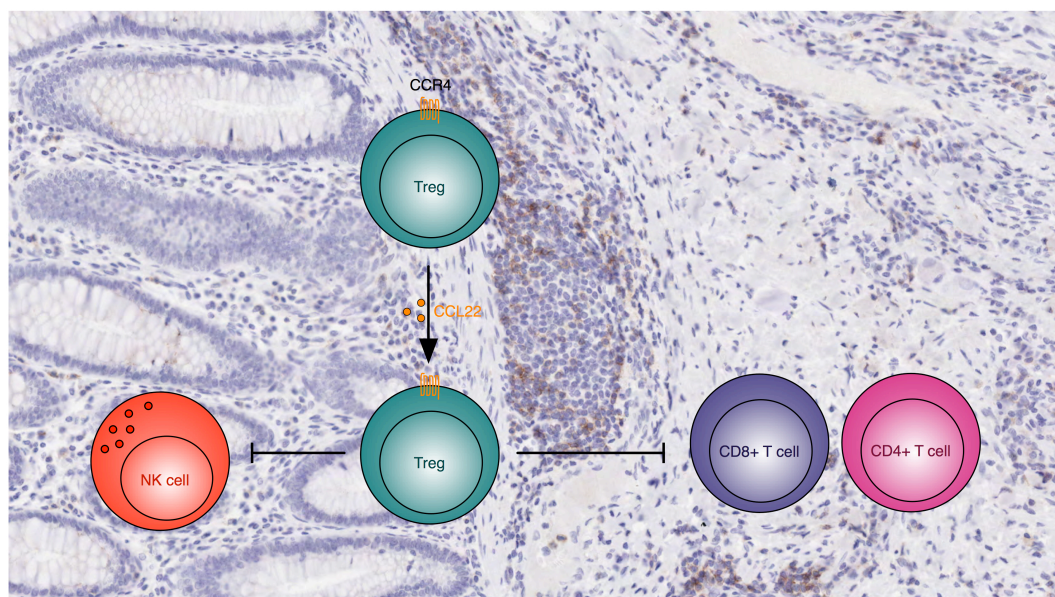
Additional future work could include looking at the changes in immune cell infiltrate pre and post chemotherapy treatment. A post-chemotherapy phenotype of CD8⁺ high and Foxp3⁺ low was associated with improved RFS and OS (Ladoire et al., 2011b). Perhaps a post-chemotherapy induced anticancer immune response is the deciding factor in DFS and OS.

Summary: Access to state-of-the-art imaging platforms and methodologies has enabled a refined pathological approach to accurately determine immune cell densities and their distribution throughout tumour- and stroma-rich regions. A significant increase in the prevalence of CD8 CTLs, Foxp3 Tregs, CD68 macrophages and CD56 NK cells was observed in the stroma of primary and metastatic CRC, compared to infiltration of the tumour. A direct comparison

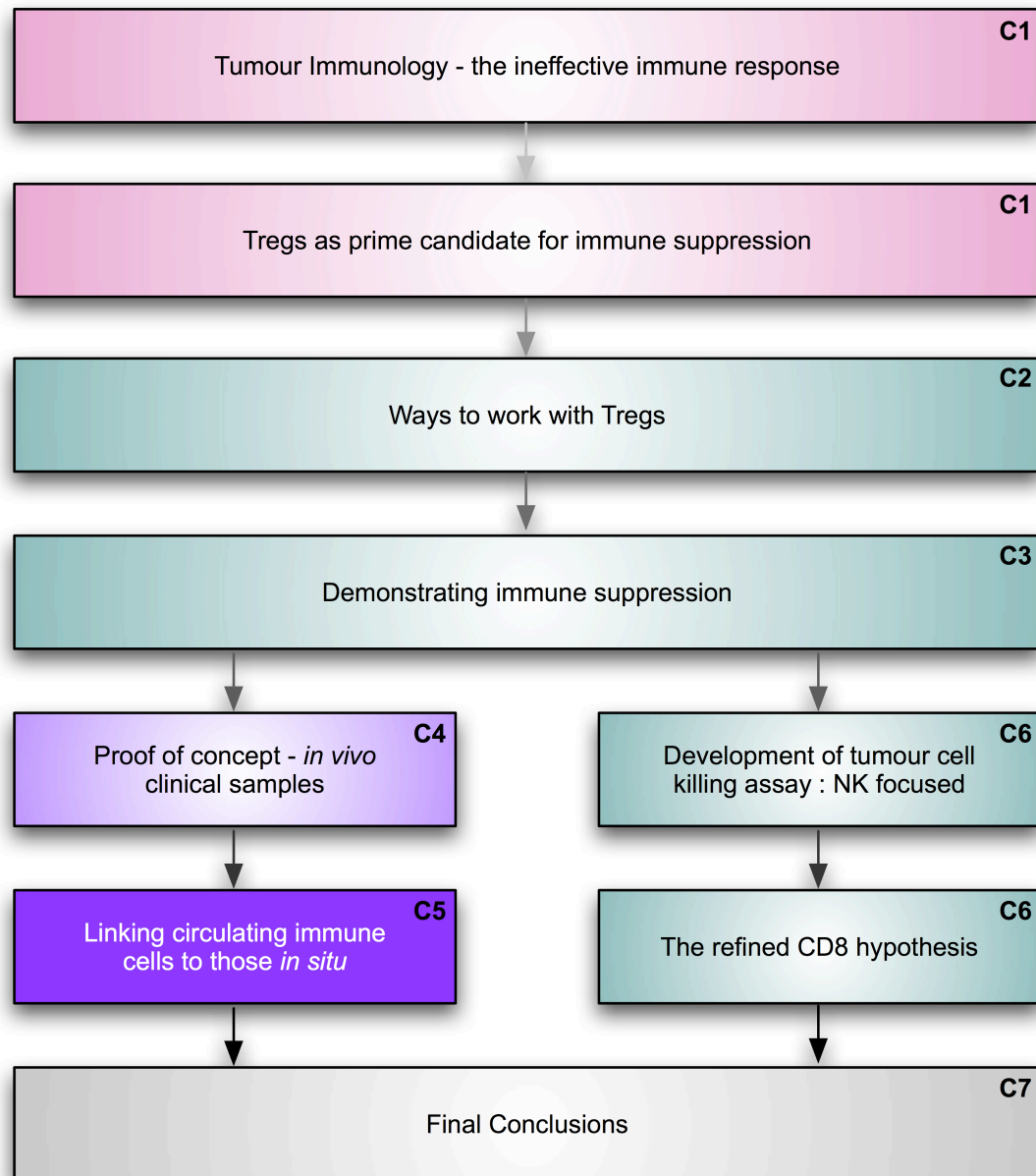
between non-metastatic primary CRC (MET-) and primary CRC that resulted in metastasis (MET+) was conducted. Elevated Tregs and reduced numbers of CD8 cells were observed in MET+ compared to MET- samples. Within MET+ tissue, immune infiltrates were elevated in adjacent non-neoplastic tissue, compared to distant non-neoplastic samples. This study adds to the ongoing discussion on the role of immune cells in metastatic development. A metastatic phenotype has been alluded to, where elevation of Tregs and low density CTLs, within primary tumour, is associated with metastasis. Accumulating evidence points to a critical role of immune infiltrates in allowing metastatic development, where Tregs may support tumour growth by suppressing the host anti-tumour immune response.

5. CHAPTER FIVE

A Link Between in Situ and Circulating Treg



Chronological Framework of Thesis Progression



■ Literature ■ *In vitro* ■ *Ex vivo* **C1** Chapter 1

The comparison of Treg accumulation between cancer patients and healthy volunteers was a fundamental requirement of this PhD to begin to understand the involvement of Tregs in actively suppressing the anti-tumour immune response and influencing survival rates and disease progression. Immunological mechanisms have been intensely studied in CRC. However, the prognostic significance of infiltrating Foxp3⁺ regulatory T cells, CD56⁺ NK cells, and CD8⁺ cytotoxic lymphocyte cells in primary and liver-metastatic colon tumour tissue remains unclear.

The aim of this chapter was to analyse the level of regulatory T cells in peripheral blood of primary and liver-metastatic patients and to investigate whether any correlation existed between this and infiltrating Foxp3⁺ regulatory T cells ‘in situ’.

5.1. METHODOLOGY

5.1.1. Patient Treg Suppression Assay

Tregs were isolated and a suppression assay set up as described in section 3.1.1. [Methyl-³H]-thymidine (TRA120 aqueous solutions 37 mBq, 1 mCi, B499 185 Gbq/mmol 5 Ci/mmol, Amersham) at 0.5 µCi per well was added for the final 18 hours of a day 5 assay. Plates were harvested on day 5 and, following the addition of scintillation fluid (MicroscintTM PerkinElmer, Cat 6013611), were left to dry at 37 °C in a humidified atmosphere containing 5 % v/v CO₂ for 2 hours prior to being read on a Microplate Scintillation & Luminiscence Counter (TopCount NXTTM, Packard).

5.1.2. Whole Blood FACS Analysis

Approximately 1–4 ml of whole blood (WB) was either provided as anonymous blood samples from patients undergoing liver resection or taken from healthy volunteers as previously described. 100 µl of WB was transferred to a FACS tube and incubated with anti-human CD25-PE, anti-human CD4-Pcy5, and anti-human CD3-ECD for 30 minutes. Red blood cells were then lysed using 500 µl of OptiLyse C (Beckman Coulter, A11895) and incubated for 10 minutes. Cells were then centrifuged for 5 minutes at $250 \times g$ and the supernatant removed. Cells were then fixed by adding 2.5 % v/v formaldehyde in PBS incubated for 15 minutes at room temperature. Cells were centrifuged for 5 minutes at $250 \times g$ and the supernatant removed. If intracellular staining was required, the samples were permeabilised in 500 µl of permeabilising buffer (0.1 % w/v saponin in PBS) and then anti-human Foxp3-FITC antibody added for 30 minutes. Cells were washed in 1 ml PBS, and centrifuged at $250 \times g$ for 5 minutes prior to the addition of 100 µl FLOW-COUNT™ Fluorospheres (Beckman Coulter, 7547053) and 500 µl of PBS to allow cell counting. Cells were analysed on a Beckman Coulter FC 500 flow cytometer using the ‘Absolute Count’ algorithm to provide a read out of cells/µl of WB.

5.1.3. *In vitro* Immunohistochemistry Antibody Staining Assay

Sections were dewaxed and rehydrated using a Leica Autostainer XL. Following this, where appropriate, antigen retrieval was performed using a pressure vessel in a RHS2 Microwave Rapid Histoprocessor (Milestone). The appropriate target retrieval

solution was added, pH6 (Dako, S1699), pH8 EDTA or pH9 (Dako, S2367). Slides were heated to 110 °C for 5 minutes and then cooled under running water for 15 minutes. The Autostainer 720 (Lab Vision) was then used to perform all antibody stains, washes and block steps, where antibodies were made up in PBS-0.05% Tween. Once the pre-treatment had been completed, the section was marked with an upper and lower boundary, using a waterproof pen (Dako, S2002) and pre-rinsed in TBS-T. 3% H₂O₂ was applied for 10 minutes at room temperature to block endogenous peroxidase activity. Slides were washed twice in TBS-T. Avidin block (Vector Labs, SP-2001) was applied for 20 minutes followed by a TBS-T wash. Biotin Block (Vector Labs, SP-2001) was applied for 20 minutes followed by an additional TBS-T wash. Slides were incubated for 20 minutes with serum-free protein block (Dako, X0909), which was then blown off the slides (a wash step was not performed at this stage). Sections were incubated with primary antibody for 60 minutes. The current study used the following antibodies at the corresponding optimised concentrations: mouse anti-human Foxp3 IgG1 (5 µg/ml, Clone 236A/E7, Abcam 20034), mouse anti-human CD8 IgG2b (0.5 µg/ml, Clone 4B11, Leica NCL-CD8-4B11), mouse anti-human CD56 IgG1 (0.5 µg/ml, Clone 1B6, Leica NCL-L-CD56-1B6), mouse anti-human Ki67 IgG1 (0.35 µg/ml, Clone MIB-1, Dako M7240), mouse anti-human CD68 IgG1 (0.2 µg/ml, Clone PG-M1, Dako M0876), rabbit anti-human CD31 (0.27 µg/ml, CHG-CD31-PI, AstraZeneca in house), rabbit anti-human cleaved caspase-3 (5 µg/ml, Clone D175, Cell Signalling Technology 9661), mouse anti-human α-SMA IgG2a (2 µg/ml, Clone 1A4, Sigma A2547) and mouse anti-human HIF-1α, IgG1 (5 µg/ml, Clone 54, Becton Dickinson 610950). Following primary antibody

incubation, slides were washed twice in TBS-T. Slides were incubated with corresponding secondary antibody; Vector Elite ABC kit (PK6101) or Mouse Envision HRP-linked polymer (Dako, K4001) for 30 minutes. Slides were washed twice in TBS-T and then incubated with avidin-biotinylated antibody (Vector Elite ABC kit) for 30 minutes. Slides were washed twice in TBS-T and then incubated in DAB (D/K3468) solution for 10 minutes. Slides were rinsed twice in distilled water and removed from the autostainer. Sections were counterstained with Carazzi's Haematoxylin Gill III (Surgipath, 01540BBE) then dehydrated in ethanol and cleared using xylene on the Leica Autostainer XL. Slides were then mounted using Premier Cover Glass slips (24 mm × 50 mm, Surgipath®) with Histomount™ (National Diagnostics, HS-103) on a Leica CV5030 and left to dry before viewing on a Leica DM4000B microscope.

5.1.4. Image Analysis

Analysis of IHC images was achieved using a ScanScope digital scanner (Aperio Technologies Ltd.) and images were taken at x 20 original magnification. Images were viewed and organised using ImageScope viewer and Spectrum operating system. Each scanned image was annotated for analysis to exclude areas of glass, dark background staining or poor sample quality. Genie™ pattern recognition software was used for the automated quantitative assessment of immune infiltrates within specific regions of tissue. Genie™ classifiers were generated for the separation of areas of tumour, stroma, lymphatic aggregates, non-neoplastic tissue and glass (as previously described in section 4.2.3).

5.1.5. Tissue Samples and Ethics

Samples were supplied by the GIMARK study tissue holdings (Division of Pre-Clinical Oncology, University of Nottingham) and given ethical approval by Nottingham Research Ethics Committee 1, REC reference 08/H0403/37, first granted in 2008. The SCS tissue bank supplies all tissues for the GIMARK study and this is also a University of Nottingham tissue bank operating under current ethical approval REC ref 10/H0405/6. All samples were acquired with ethical approval and written informed consent, patient information is summarised in Table 5.1.

Table 5.1 A Summary of the Tissue Used

1. Metastatic CRC with matched peripheral blood samples (n = 40)

CRC liver metastatic tissue with patient matched peripheral blood samples to investigate correlations between immune infiltrates within tumour and circulating immune cells

Abbreviation	Tissue	Females	Average Age at Study (years)	Males	Average Age at Study (years)	n = Total	Tissue Source
Patient	Liver metastatic patient blood	13	67.46	12	67.17	25	QMC
Health	Healthy volunteer blood	9	50.56	6	53.86	15	QMC
Tumour	Liver metastatic tumour tissue	13	67.46	12	67.17	25	QMC
Stroma	Liver metastatic tumour-associated stroma tissue	13	67.46	12	67.17	25	QMC
Cells/ul WB	Matched liver metastatic patient blood	13	67.46	12	67.17	25	QMC

(QMC; Queens Medical Centre Hospital, Nottingham)

5.1.6. Method of Statistical Analysis

Data were collated into certain groups and graphically expressed as the mean, where error bars depicted SD. Further analysis was then carried out to quantify any trends in the data, using Prism® 5 software and Spotfire® programmes. Paired data underwent a t-test to determine any significant differences. If the data assumed a normal distribution pattern, a paired or unpaired t-test was carried out. If the data did not assume a normal distribution pattern, a ranked method was selected. For paired rank testing a Wilcoxon test was carried out. For unpaired rank testing a Mann-Whitney analysis was used.

5.2. RESULTS AND DISCUSSION

5.2.1. Examining Tregs in CRC Liver Metastatic Patients

There is accumulating evidence showing an increase in the prevalence of Tregs in cancer patients. Elevated levels of Tregs are seen in the PB of pancreas cancer patients (Liyanage et al., 2002). Research has also shown significant increases in the proportions of CD4⁺CD25⁺ T cells in PB of patients with epithelial malignancies (Wolf et al., 2003), gastrointestinal cancers (Sasada et al., 2003) and patients with NSCLC and late-stage OVC (Woo et al., 2001).

Further investigation into the pervasiveness of Tregs and other immune cells in CRC patients was required to solidify the hypothesis that inflammation is an influencing factor in tumour progression, and to explore links between circulating immune cells

and those found at the tumour site. The current research was carried out on anonymous blood samples from patients undergoing liver resection.

Isolation of Tregs from patients was problematic due to restrictions on the availability of the blood from surgery (late afternoon) and subsequent length of the isolation procedure. It was therefore necessary to store the whole blood overnight prior to Treg isolation. In addition to this, it was only possible to collect a maximum of 18 ml of blood per patient, which was subject to change on a patient-to-patient basis. Despite these difficulties, a proliferation suppression assay was set up with Tregs isolated from patient blood as previously described, to investigate the suppressive ability of Tregs from liver metastatic patients against PHA stimulated effector cells (Figure 5.1).

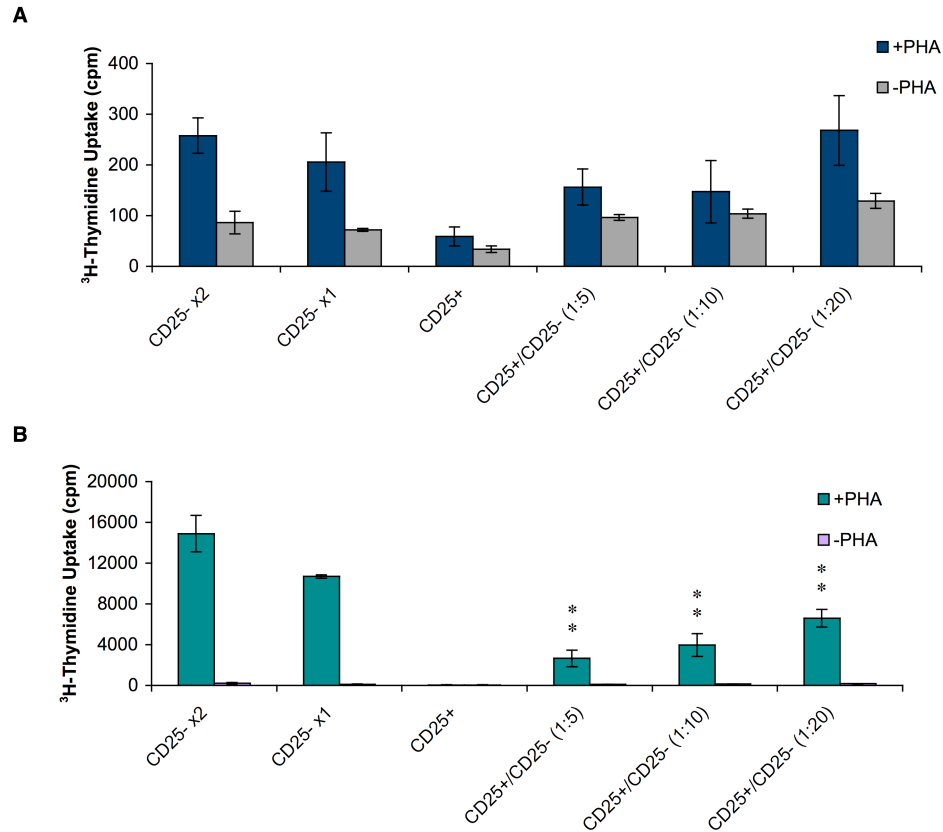


Figure 5.1 Metastatic Liver Patient Treg Suppression of PHA Stimulated Effector Cells, via 3H-Thymidine Incorporation

CD4⁺CD25⁺ Tregs and CD4⁺CD25⁻ effector cells were isolated from 18 ml blood from a consenting metastatic liver patient. CD4⁺CD25⁻ cells, stimulated with 10 µg/ml PHA were plated at 5 x 10⁴ cells per well. CD4⁺CD25⁺ cells were then added at 0:2, 0:1, 1:0, 1:5, 1:10 and 1:20 Treg:effector cell ratios. Cells were cultured at 37 °C in a humidified atmosphere containing 5 % v/v CO₂ for 96 hours. 0.5 µCi of [Methyl-3H]-thymidine was added per well and incubated for the final 18 hours of the assay before harvesting. Scintillation fluid was added prior to reading on a Microplate Scintillation Counter. Data are a mean of triplicates from a single plate (± SD) and is representative of n = 3 experiments. A) Patient sample compared to B) healthy donor. Results were evaluated using Prism 5 and statistically analysed using a one way ANOVA and Tukey's multiple comparison post-test (** p < 0.001, * p < 0.05).

The effect of Tregs from the liver metastatic patient was compared to that of a healthy donors. However, due to time restrictions the patient blood was left overnight and the healthy donor blood was used immediately. The proliferative response of T cells from the liver metastatic patient was much reduced. Although the response of effector cells in the presence of Treg cells was reduced, it was not significant. It is possible that reduced proliferation, observed across the entire experiment, was due to leaving the blood overnight prior to use. Further work looking at healthy donor blood left overnight would help to identify the reason for this drop in proliferation.

Due to the aforementioned problems of limited volumes of patient blood and the timings of receiving the samples, it was necessary to develop a more efficient assay to determine true Treg numbers in a shorter amount of time. A technique was developed to determine Treg numbers using whole blood (WB) FACS analysis staining for CD4, CD3, CD25 and Foxp3. Assay optimisation was crucial as WB FACS staining is problematic. Previous groups have developed WB FACS surface staining techniques (Qiu et al., 2009); however, WB FACS analysis of internal markers, such as Foxp3, have not been published.

WB FACS analysis requires lysis of the red blood cells. This is a very destructive step and has a huge impact on the robustness of the cells of interest. Protocol optimisation is illustrated in Figure 5.2, where the destructive nature of this reagent is demonstrated in the ‘spray’ of cells in the FSC/SSC plots (Figure 5.2A). To minimise these effects and improve the protocol, additional fixative steps were

subsequently introduced. This was successful and resulted in little, if any, disruption to the cells of interest. It was therefore possible to gate accurately on the lymphocyte population. The results of assay optimisation can be seen in Figure 5.2, where the final assay method (Figure 5.2C) results in approximately 11 % CD4⁺CD25⁺Foxp3⁺ Tregs, which correlates with previous research (Rudge et al., 2006). The final stage of assay optimisation was to incorporate a cell counting element. Fluorescent beads at a known concentration were introduced into the system, which allowed specific calculations to be carried out for cell populations (Figure 5.2C). The final read out for this assay was cells/μl WB.

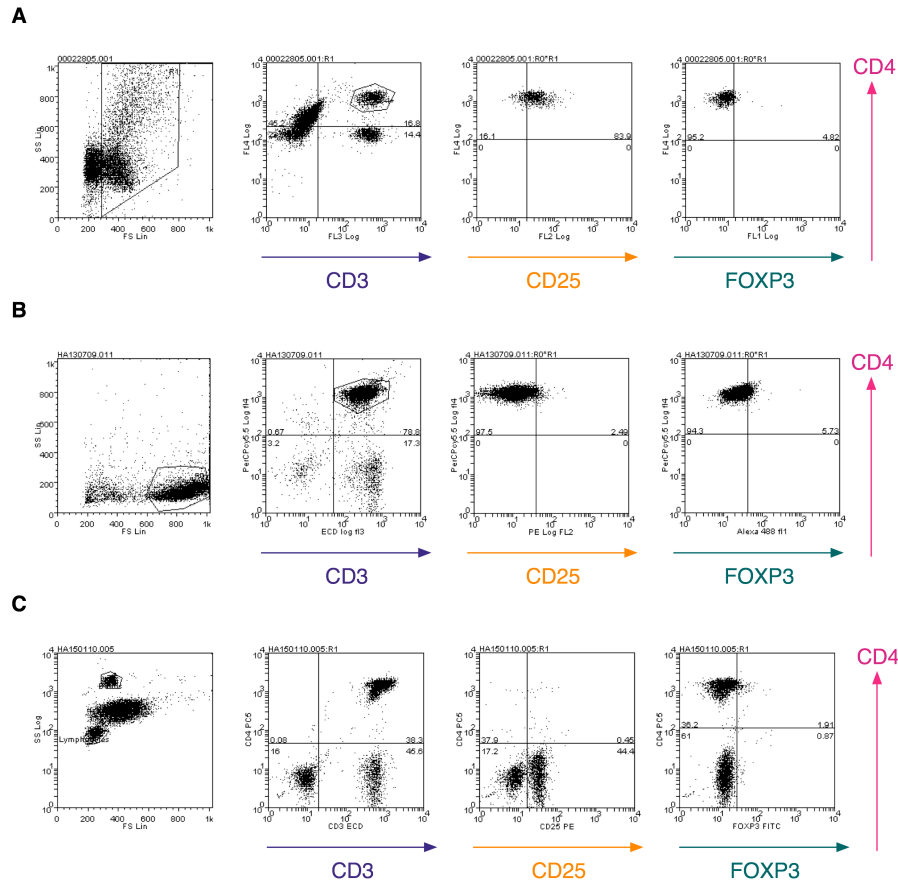


Figure 5.2 Optimisation of Whole Blood FACS Analysis Protocol

100 μ l of whole blood (WB) was incubated with 5 μ l PeCy5 anti-CD4, ECD anti-CD3 and PE anti-CD25 for 10 minutes. Various conditions were then tried to attain clear populations and good intracellular staining. A) FACSlyse was added for 10 minutes before washing twice in PBS (1 % FCS). B) Cells were fixed in 4 % formaldehyde prior to FACSlyse for 10 minutes. C) Optilyse was added for 10 minutes followed by fixation in 4 % formaldehyde. Cells were then permeabilised followed by intracellular staining using 5 μ l Alexa 488 anti-human FOXP3 for 30 minutes. Fluorescent cell counting beads were also added once the protocol was optimised to allow cell count per μ l of WB. Data were acquired on a Beckman Coulter FC 500 flow cytometer and analysed using Weasel software.

Following successful assay optimisation, a screen of Tregs/ μ l of WB was carried out in 19 liver metastatic cancer patients and was compared to healthy volunteers (Figure 5.3).

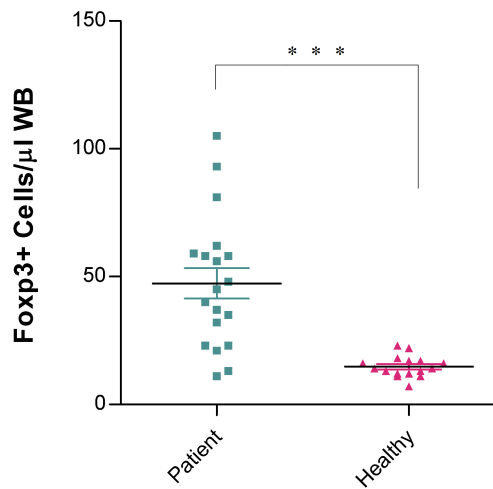


Figure 5.3 Whole Blood FACS Analysis of Fxp3⁺ Tregs in CRC Metastatic Patients Compared to Healthy Volunteers

100 μ l of whole blood (WB) was incubated with 5 μ l PeCy5 anti-CD4, ECD anti-CD3 and PE anti-CD25 for 10 minutes. Optilyse was added for 10 minutes followed by fixation in 4 % formaldehyde. Cells were then permeabilised and intracellular stained with 5 μ l Alexa 488 anti-human Fxp3 for 30 minutes. Fluorescent cell counting beads were added (960/ μ l) to allow Treg count per μ l of WB analysis and a direct comparison between CRC hepatic metastatic (patient) and healthy aged-matched volunteers (healthy). Data were acquired on a Beckman Coulter FC 500 flow cytometer and analysed using Weasel software. Statistical analysis was achieved using the unpaired t-test where *** $p < 0.0001$ and error bars depict \pm SD.

A significant ($p < 0.0001$) elevation in the number of circulating Tregs in CRC liver metastatic patients was observed when compared to healthy volunteers (Figure 5.3). This is in agreement with previous accumulating evidence showing significant increases in the proportions of $CD4^+CD25^+$ T cells in the PB of patients with NSCLC, OVC (Woo et al., 2001), and gastric and oesophageal cancer patients (Mizukami et al., 2008a).

Additional research has shown that spontaneous T cell responses against a variety of TAAs have been detected in the peripheral blood of CRC patients; however, no survival benefit was observed (Nagorsen et al., 2005). This lack of effect may be the immunosuppressive effect of elevated peripheral blood (PB) and tumour-infiltrating Tregs. Tumour cells use Tregs to suppress desired anti-tumour immune responses and protect themselves from immune attack (Wang, 2006).

5.2.2. Additional Immune Cells in CRC Liver Metastatic Patients

The inverse relationship and prognostic significance of Tregs and $CD8^+$ CTLs is becoming increasingly documented within the literature. The current study subsequently examined the same patient cohort for levels of $CD3^+CD8^+$ CTLs (Figure 5.4).

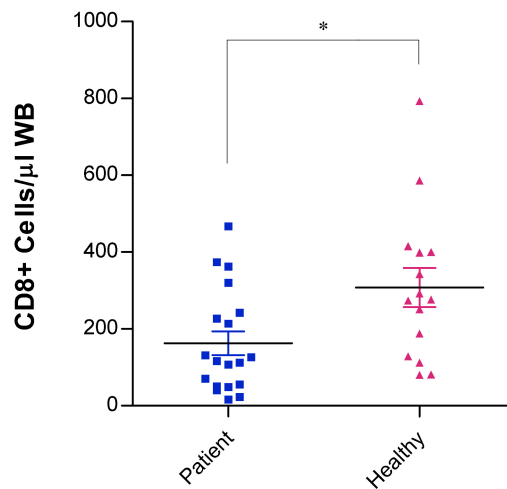


Figure 5.4 Whole Blood FACS Analysis of CD8⁺ Cells in CRC Metastatic Patients Compared to Healthy Volunteers

100 μ l of whole blood (WB) was incubated with 5 μ l PE anti-CD4, ECD anti-CD3 and FITC anti-CD8 for 10 minutes. Optilyse was added for 10 minutes followed by fixation in 4 % formaldehyde. Fluorescent cell counting beads were added (960/ μ l) to allow CD8 cell count per μ l of WB analysis and a direct comparison between CRC hepatic metastatic (patient) and healthy aged-matched volunteers (healthy). Data were acquired on a Beckman Coulter FC 500 flow cytometer and analysed using Weasel software. Statistical analysis was achieved using the unpaired t-test where * $p < 0.05$ and error bars depict \pm SD.

A significant ($p < 0.05$) difference between healthy volunteers and CRC liver metastatic patients was observed. Patients suffering from CRC had reduced levels of CD8⁺ CTLs compared to healthy individuals.

This is in agreement with recently published data that demonstrated that CD8^{low} cell density resulted a pro-tumour phenotype, associated with reduced OS and RFS (DeNardo et al., 2011).

Previous research evaluated the prognostic significance of the numbers of CD8 cells in the peripheral blood of patients with CRC. Peripheral CD8 counts were a significant ($p < 0.05$) independent prognostic indicator of OS; patients with higher CD8 levels had longer OS than those with lower CD8 frequencies (Qiu et al., 2009).

The prevalence of NK and NKT cells was then scrutinised to explore any additional trends in circulating immune cells within CRC patients (Figure 5.5).

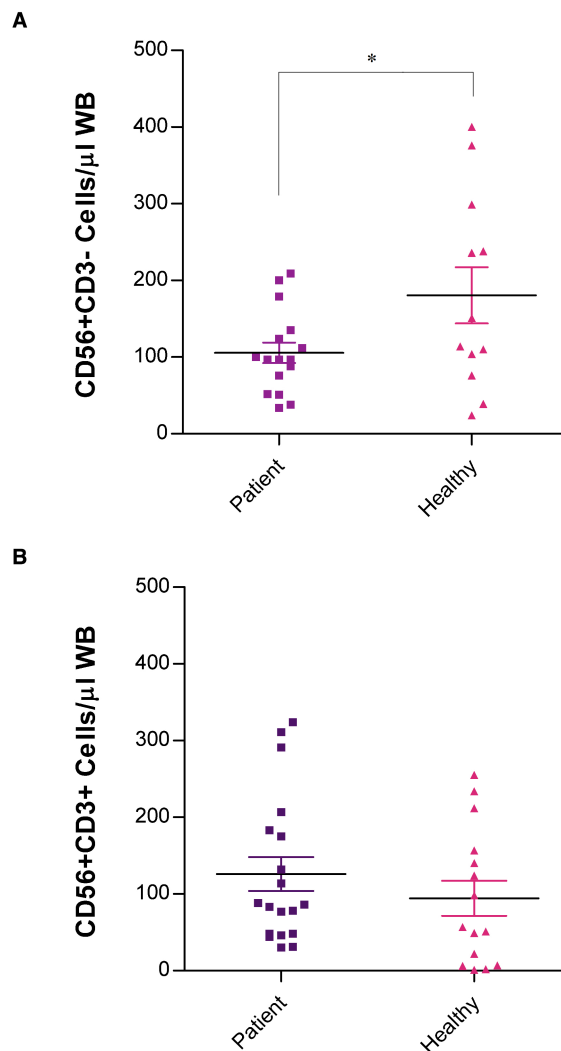


Figure 5.5 Whole Blood FACS Analysis of CD56⁺CD3⁻ NK Cells and CD56⁺CD3⁺ NKT Cells in CRC Metastatic Patients Compared to Healthy Volunteers

100 μ l of whole blood (WB) was incubated with 5 μ l PeCy5 anti-CD56 and ECD anti-CD3 PE for 10 minutes. Optilyse was added for 10 minutes followed by fixation in 4 % formaldehyde. Fluorescent cell counting beads were added (960/ μ l) to cell count per μ l of WB analysis and a direct comparison between CRC hepatic metastatic (patient) and healthy aged-matched volunteers (healthy). A) CD56⁺CD3⁻ cells were gated to determine NK cells/ μ l WB or B) gated on CD56⁺CD3⁺ to establish NKT cells/ μ l WB. Data were acquired on a Beckman Coulter FC 500 flow cytometer and analysed using Weasel software (unpaired t-test, * $p < 0.05$).

The frequency of CD56⁺CD3⁻ NK cells (Figure 5.5A) and CD56⁺CD3⁺ NKT cells (Figure 5.5B) was assessed in both patient and healthy volunteer groups. Reduced numbers of circulating NK cells was observed within the patient population compared to volunteers ($p < 0.05$). Circulating NKT cells showed no significant difference between the two groups. This lack of significance with NKT cells conflicts with previous research on diffuse large B-cell lymphoma, which reported elevated NKT cell numbers. In addition, research suggested a link between decreased NKT numbers with tumour burden and a more aggressive disease (Hus et al., 2011).

The current study has shown significant differences in circulating immune cells within the peripheral blood of CRC patients versus healthy volunteers. However, questions remained unanswered such as: are these trends mimicked at the local tumour site?

To determine whether these trends in circulating immune cells resulted in any differences *in situ*, matched patient tumour tissue was examined immunohistochemically. A similar study to that of chapter 4 was carried out; however, limited tissue availability meant that it was only possible to successfully stain for two markers; Foxp3 and CD8 were chosen.

Matched patient tumour tissue was examined for Tregs by Foxp3 IHC staining and subsequently compared to corresponding levels of circulating Tregs (Figure 5.6).

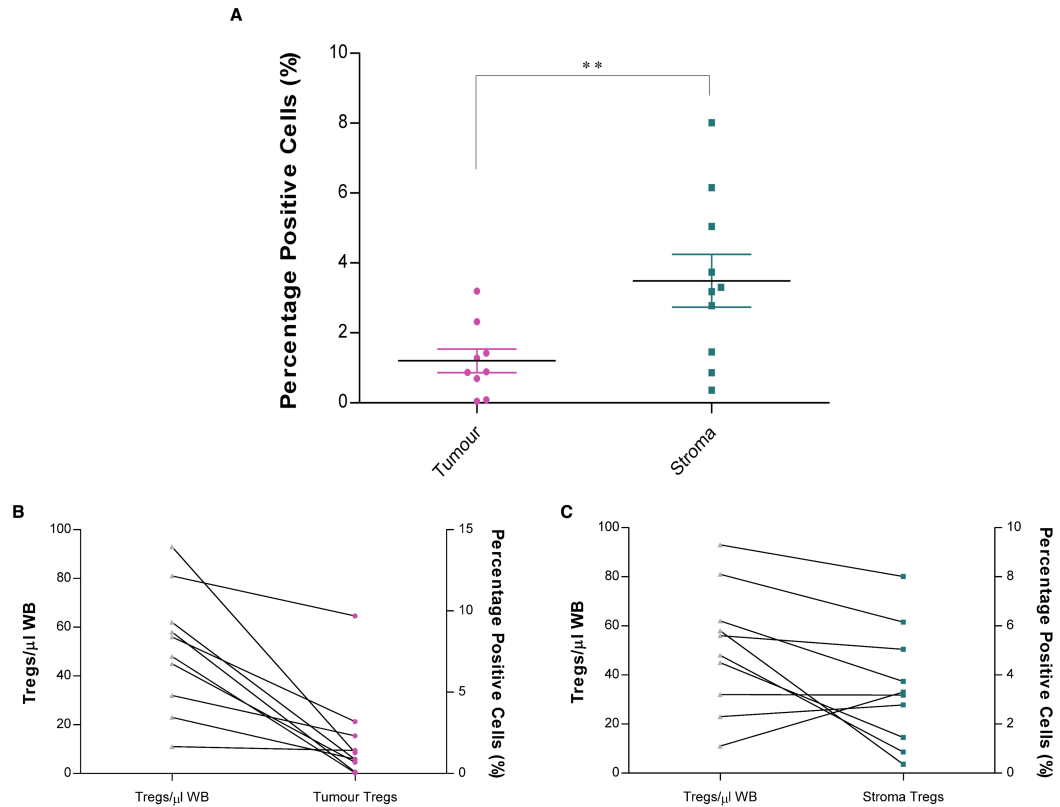


Figure 5.6 IHC Study of Tumour and Stromal Tregs in CRC Metastatic Patients, linked to Matched Whole Blood FACS Analysis

A) Liver metastatic CRC tissue was examined for Treg infiltration into the tumour and stroma using IHC techniques, stained with anti-human Foxp3 IgG1 (5 μ g/ml). Digital images were acquired and Genie™ Classifiers were combined with a nuclear algorithm to quantify the number of Foxp3-positive Tregs in tumour and stroma (unpaired t-test, ** $p < 0.01$). These IHC results from B) tumour or C) stroma were directly compared to patient matched circulating Treg numbers. Here, 100 μ l of whole blood (WB) was incubated with 5 μ l PeCy5 anti-CD4, ECD anti-CD3 and PE anti-CD25 for 10 minutes. Optilyse was added for 10 minutes followed by fixation in 4 % formaldehyde. Cells were then permeabilised and intracellular stained with 5 μ l Alexa 488 anti-human Foxp3 for 30 minutes. Fluorescent cell counting beads were added (960/ μ l) to allow Treg count per μ l of WB analysis.

A similar trend was observed to that seen in previous IHC studies: the number of Tregs was significantly elevated in the stroma of CRC liver metastatic patients compared to the numbers seen within the tumour itself (Figure 5.6A). The frequency of Tregs/ μ l of blood evaluated in Figure 5.3 was then linked to the number of Tregs seen at the tumour microenvironment of matched patient samples. Specifically, Tregs/ μ l WB were contrasted with Tregs in the tumour (Figure 5.6B) and those found in the stroma (Figure 5.6B). A direct relationship was noticed between elevation of Tregs in the blood and the numbers of Tregs found at the tumour site. Data were expressed linearly to further evaluate this association (Figure 5.7).

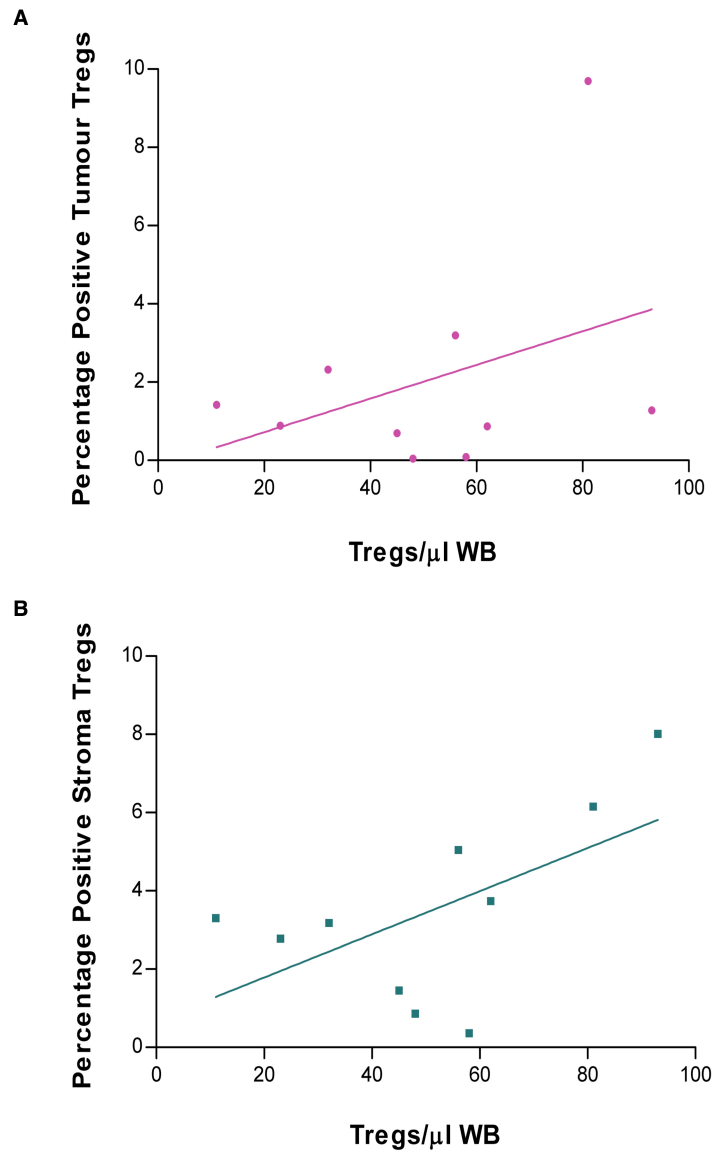


Figure 5.7 The Relationship Between Circulating Tregs and their Prevalence at the Tumour Site.

The correlation between IHC Treg analysis and peripheral blood work was evaluated using linear regression. The number of percentage positive Tregs within the A) tumour or B) stroma, evaluated by IHC, were expressed against the number of Tregs/ μ l whole blood (WB) from matched CRC liver metastatic patient samples. A trend line was calculated from the line of best fit.

Linear regression was used to evaluate the relationship between circulating Tregs and those observed within the tumour (Figure 5.7A). A distinct correlation was seen, where increased levels of Tregs within the PB was associated with increased levels of Tregs seen within the tumour ($r^2 = 0.1424$). A similar trend was also observed when comparing Tregs/ μ l WB to those present within the stroma (Figure 5.7B, $r^2 = 0.3338$).

Previously published research has presented evidence to suggest a relationship between improved OS and a reduction in circulating Tregs in patients with metastatic castration-resistant prostate cancer (Vergati et al., 2011).

To determine whether similar trends were seen with CTLs, further IHC was carried out within the same cohort of patients and the number of percentage positive CD8 cells within the tumour and stroma was established (Figure 5.8).

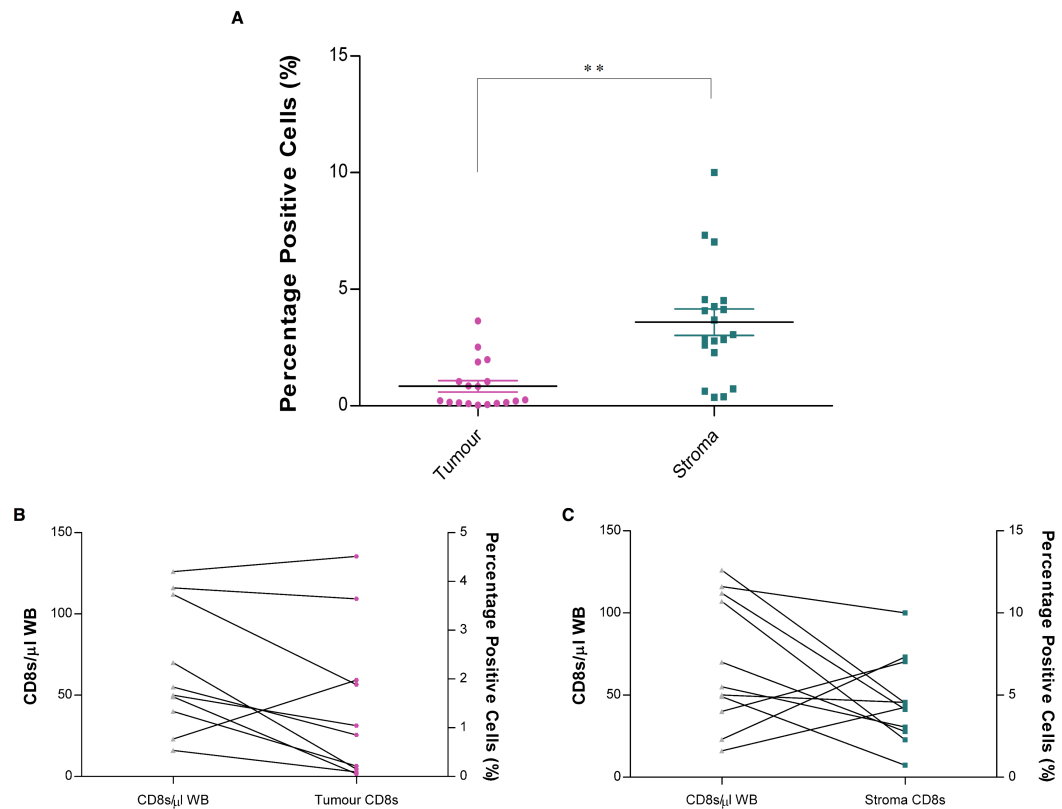


Figure 5.8 IHC Study of Tumour and Stromal CTLs in CRC Metastatic Patients, linked to Matched Whole Blood FACS Analysis

A) Liver metastatic CRC tissue was examined for CD8 CTL infiltration into the tumour and stroma using IHC techniques, stained with anti-human CD8 IgG2b (0.5 $\mu\text{g/ml}$). Digital images were acquired and Genie™ Classifiers were combined with a nuclear algorithm to quantify the number of CD8-positive CTLs in tumour and stroma (unpaired t-test, ** $p < 0.01$). These IHC results from B) tumour or C) stroma were directly compared to patient matched circulating CD8 cell numbers. Here, 100 μl of whole blood (WB) was incubated with 5 μl PE anti-CD4, ECD anti-CD3 and FITC anti-CD8 for 10 minutes. Optilyse was added for 10 minutes followed by fixation in 4 % formaldehyde. Fluorescent cell counting beads were added (960/ μl) to allow CD8 cell count per μl of WB analysis.

The prevalence of CD8 cells within the tumour and stroma was evaluated and significantly higher frequencies of CTLs were detected in the stroma (Figure 5.8A). The number of percentage positive CD8 cells in the tumour or stroma was then compared to the frequency in matched patient PB (Figure 5.8B and C). The relationships were further analysed using linear regression (Figure 5.9).

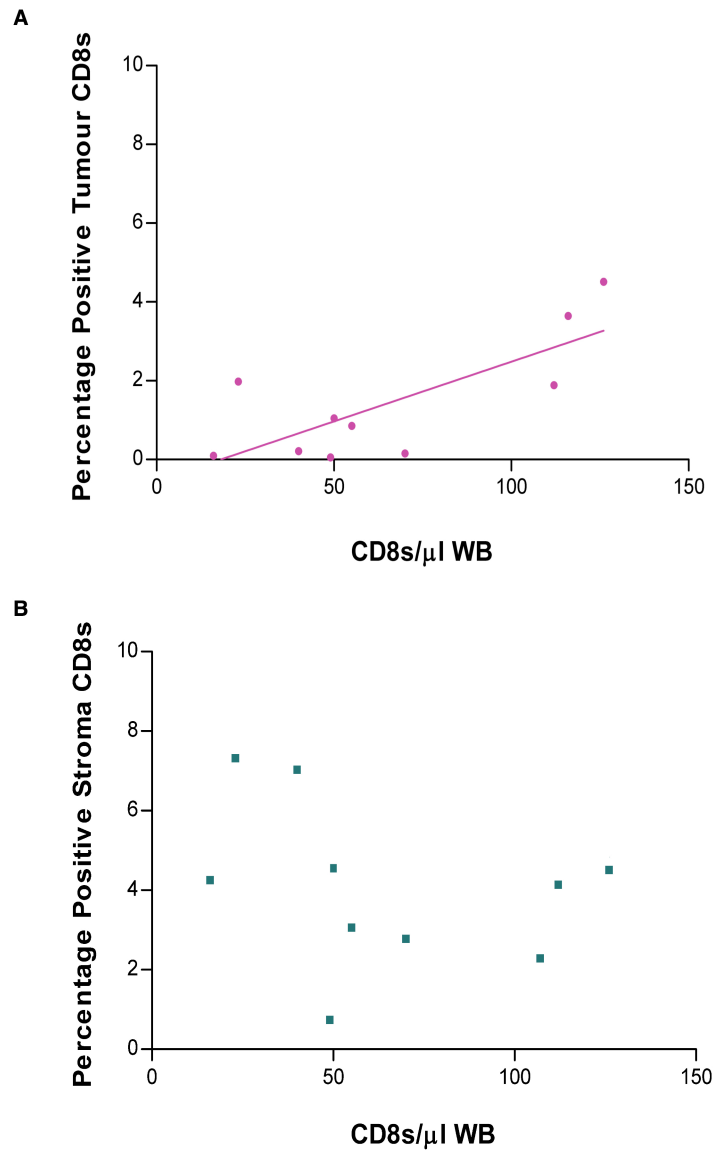


Figure 5.9 The Relationship Between Circulating CTLs and their Prevalence at the Tumour Site

The correlation between IHC CD8 analysis and peripheral blood work was evaluated using linear regression. The number of percentage positive CD8 CTLs within the tumour, evaluated by IHC, were expressed against the number of CD8s/ μ l whole blood (WB) from matched CRC liver metastatic patient samples. A trend line was calculated from the line of best fit.

A direct correlation was observed between the number of CD8 cells within the PB and the frequency within the tumour of matched patient tissue (Figure 5.9A, $r^2 = 0.5775$). No significant correlation was observed when evaluating the tumour-associated stroma.

5.3. CONCLUSION AND FUTURE WORK

5.3.1. Examining Tregs in CRC Liver Metastatic Patients

Accumulating evidence shows an increase in the prevalence of Tregs in pancreas cancer patients (Liyanage et al., 2002), epithelial malignancies (Wolf et al., 2003), gastrointestinal cancers (Sasada et al., 2003) and patients with NSCLC and late-stage OVC (Woo et al., 2001). Further investigation into the pervasiveness of Tregs and other immune cells in CRC patients was required to solidify the hypothesis that inflammation is an influencing factor in tumour progression, and to explore links between circulating immune cells and those found at the tumour site.

Due to the aforementioned problems with patient blood samples, a more efficient WB FACS analysis method was successfully developed to determine true Treg numbers. Assay optimisation, built on previously published techniques (Qiu et al., 2009), allowed development of WB FACS analysis of internal markers, such as Foxp3. Following successful assay optimisation, a screen of Tregs/ μ l of WB was carried out in 19 liver metastatic cancer patients and compared to healthy volunteers. A significant elevation in the number of circulating Tregs in CRC liver metastatic

patients was observed, compared to healthy volunteers. Tumour cells use Tregs to suppress the anti-tumour immune response and protect themselves from immune attack (Wang, 2006), perhaps facilitated by elevated circulating PB Tregs.

5.3.2. Additional Immune Cells in CRC Liver Metastatic Patients

The same patient cohort was examined for levels of $CD3^+CD8^+$ cells and patients suffering from CRC were found to have reduced levels of $CD8^+$ CTLs compared to healthy individuals. This inverse relationship of Tregs and $CD8^+$ CTLs is becoming increasingly documented within the literature, where $CD8^{low}$ cell density was associated with a pro-tumour phenotype, reduced OS and lower RFS (DeNardo et al., 2011). Numbers of PB $CD8$ cells in CRC was an independent prognostic indicator of OS; patients with higher $CD8$ levels had longer OS than those with lower $CD8$ frequencies (Qiu et al., 2009).

The frequency of $CD56^+CD3^-$ NK cells and $CD56^+CD3^+$ NKT cells was then scrutinised to explore any additional trends in circulating immune cells within CRC patients. The frequency of circulating NK cells was lower within the patient population than in volunteers. However, in contradiction to recent publications, NKT cells showed no significant difference between the two groups (Hus et al., 2011).

To determine whether these trends in circulating immune cells resulted in any differences *in situ*, matched patient tumour tissue was examined immunohistochemically for Foxp3 and $CD8$. The number of Tregs/ μ l WB was

evaluated against the frequency of Tregs in the tumour and tumour-associated stroma. A direct linear relationship was observed; increased levels of Tregs within the PB were associated with increased levels of Tregs seen within the tumour and stroma. In addition, a direct correlation was observed between the number of CD8 cells within the PB and the frequency within the tumour of matched patient tissue.

Results have shown a significant difference in the prevalence of immune cells in the peripheral blood of CRC liver metastatic and healthy volunteers. Within the blood, CRC patients exhibited a Treg^{high}CD8^{low}NK^{low} phenotype when compared to age-matched healthy controls. Previous studies have evaluated the prognostic importance of immune infiltrates at the tumour microenvironment. The link between circulating immune cells and those found *in situ* could provide a valuable prognostic tool.

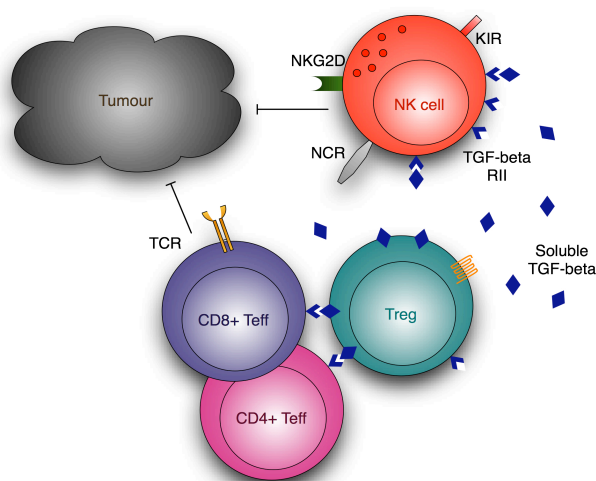
The current study, however, fails to answer the ‘*chicken or the egg*’-like question. Which came first, amplified numbers of circulating immune cells or elevated tumour infiltrates? In addition, the question still remains: can tumours traffic these immune cells into its local microenvironment, from such distant locations? Also, would you see the same association between *in situ* and circulating immune cells in patients not presenting metastatic disease? Additional research is therefore greatly warranted.

It appears that most tumours are associated with tumour-promoting innate immune response, involving macrophages, while B and T cells are involved in a less efficient anti-tumour immune response. Tumour cells exploit infiltrating immune cells for their own benefit.

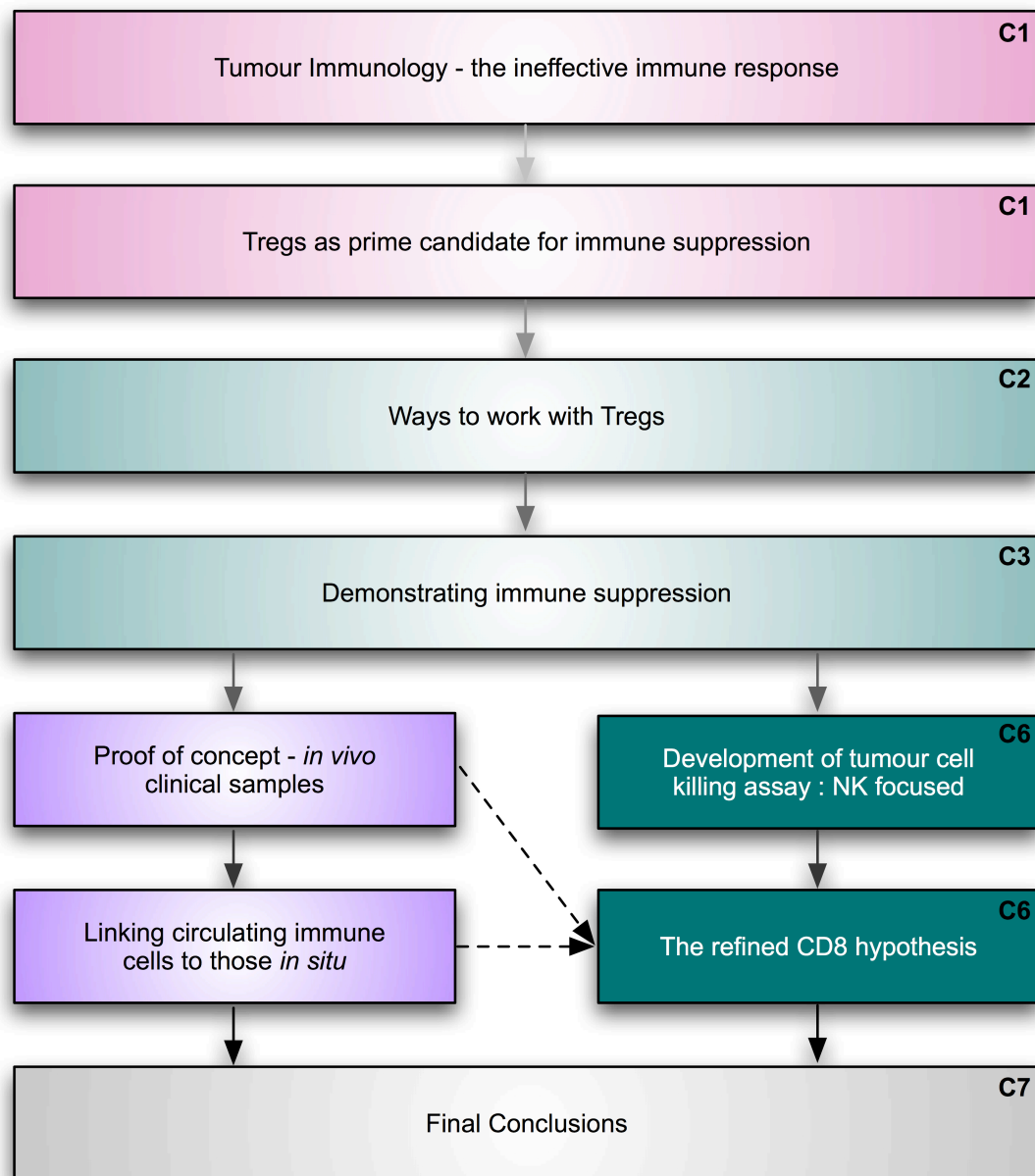
Summary: *The comparison of Treg accumulation between cancer patients and healthy volunteers was a fundamental requirement of this PhD. The aim of this chapter was to analyse the level of Tregs in peripheral blood of primary and liver-metastatic patients and to investigate whether any correlation existed between this and infiltrating Foxp3⁺ regulatory T cells 'in situ'. Within peripheral blood, CRC patients exhibited a Treg^{high}CD8^{low}NK^{low} phenotype when compared to age matched healthy volunteers.*

6. CHAPTER SIX

Building an *in vitro* Model and Interrogating the System



Chronological Framework of Thesis Progression



This PhD study has established that Tregs could be key players in CRC tumour progression. Previous chapters have demonstrated the prevalence of Tregs in and around the tumour. In addition, the study determined a correlation between Tregs and patients with a MET⁺ phenotype. Key to these data were the finding that Tregs co-localised to various effector cells. Although research into Treg biology is intensifying, many questions remain unanswered. In order to progress the study further and understand tumour-Treg-immune cell interactions, it was necessary to construct a realistic 'ex vivo' model. The rationale for this model was to gain an insight into the role of Tregs within the tumour microenvironment and suppression of anti-tumour immunity. Due to the time constraints of a PhD, this work was undertaken in parallel with chapters 4 and 5. Chapter 6 aimed to investigate research interactions between CD4⁺CD25⁺ Tregs and a candidate for Treg mediated suppression. The original contender selected was CD3⁺CD56⁺ NK cells. In addition, the model encompassed further levels of complexity, incorporating tumour cells. Despite several mechanisms of suppression being suggested, the effects of regulatory T cells on tumour-killing cells, such as natural killer cells, remain ambiguous. It is becoming widely acknowledged that inhibiting Treg function in cancer patients may contribute to the success of new immunotherapies. This in vitro model would therefore be employed to screen for Treg targets. This compilation of assays could provide a platform on which to validate lead antibodies produced against the selected Treg target.

6.1. METHODOLOGY

6.1.1 K562 Cell Killing Assay

K562 tumour cells were re-suspended at 2×10^7 cells per ml in PBS and 5(6)-Carboxyfluorescein diacetate N-succinidyl ester (CFSE, Sigma, Cat 2188) was added at a final concentration of $2.5 \mu\text{M}$. Cells were incubated for 8 minutes with vortexing every 2 minutes. Cells were then centrifuged for 4 minutes at $300 \times g$ and the supernatant removed. Cells were re-suspended in 10% v/v FBS RPMI and transferred to a new tube. This step was repeated three times. Stained cells were recounted using Trypan blue exclusion. CFSE stained K562 cells were seeded at 1×10^4 cells per well in a 96-well round bottom Nunc Tissue Culture Plate (Nuclon™ Surface, Cat 163320). Isolated PBMCs from a healthy donor (as previously described) were then added (100 μl) at 1:0, 1:3, 1:10 and 1:30 K562:PBMC cell ratios. Cells were cultured at 37°C in a humidified atmosphere containing 5 % v/v CO_2 for 6 hours. Cells were then stained with 100 μl 1:10 v/v propidium iodide (PI) for 15 minutes, to assess cell viability before being analysed using FACS.

6.1.2 NKG2D and TGF- β RII FACS Analysis

PBMCs were isolated as previously described. 1×10^6 cells were transferred to FACS tubes and washed in 1 ml PBS by centrifugation at $250 \times g$ for 5 minutes. 5 μl of anti-human TGF- β RII primary antibody (R&D Systems, AF-241-NA) was incubated for 20 minutes followed by two PBS wash steps. Additional antibodies, such as anti-human CD8-FITC, anti-human CD3-Alexa 647, anti-human CD3-ECD,

anti-human CD4-ECD, anti-human CD56-PC5, and anti-human NKG2D-PE (Beckman Coulter, A08934), were also used in different required combinations. Cells were washed twice in PBS before incubating, where appropriate, with TGF- β RII secondary donkey anti-goat IgG-PE (R&D Systems, F0107) for 20 minutes at room temperature, protected from light. Cells were then fixed by adding 1 ml of 2.5 % v/v formaldehyde in PBS and incubated for 15 minutes. A final wash step in PBS preceded analysis on a Beckman Coulter FC 500 flow cytometer and data were analysed using Weasel software.

6.1.3 ULBP-2 and MICA FACS Analysis

Various tumour cell lines were re-suspended at 1×10^6 cells per ml in PBS. 200 μ l of this cell suspension was centrifuged for 5 minutes at $300 \times g$ and the supernatant removed. Cells were re-suspended in 1% v/v BSA PBS and left on ice to block for 30 minutes. 10 μ l of monoclonal anti-human MICA (R&D Systems, MAB1300) and ULBP-2 (R&D Systems, MAB1298) primary antibodies at 25 μ g/ml were incubated for 30 minutes on ice. Cells were then washed twice in BSA-PBS before incubating with 10 μ l of secondary goat F(ab')₂ anti-mouse IgG (Fc γ)-FITC antibody (Beckman Coulter, PN IM1619) at 25 μ g/ml, kept on ice and in the dark. Two final wash steps in BSA-PBS preceded analysis on a Beckman Coulter FC 500 flow cytometer and data were analysed using Weasel software.

6.1.4 NK Cell Isolation

NK cell isolation was achieved using an EasySep® Human CD56 selection kit (EasySep®, 18055) and carried out according to the manufacturer's instructions. In brief, PBMCs were isolated as previously described (Section 2.1.2) and re-suspended at 1×10^8 cells per ml in isolation buffer (PBS w/o Ca/Mg, 0.1 % BSA, 2 mM EDTA). EasySep® Positive Selection Cocktail was added at 100 µl/ml of cells, mixed and incubated at room temperature for 15 minutes. This cocktail contained a combination of mAbs, bound in bispecific tetrameric antibody complexes (TACs), directed against CD56 and dextran. EasySep® Magnetic Nanoparticles were then added at 50 µl/ml of cells, mixed and incubated for 10 minutes. These nanoparticles were a suspension of magnetic dextran iron particles in water. The cell suspension was increased to 2.5 ml by adding isolation buffer and then placed into the Purple EasySep® Magnet and incubated for 5 minutes. Following this, the magnet and tube were inverted together, in one continuous motion, pouring of the supernatant fraction. The magnetically labelled NK cells remain inside the tube, held by the magnetic field. The tube was removed from the magnet and the separation process repeated a further two times by adding an additional 2.5 ml of isolation buffer. Following this the tube was removed from the magnet to elute the NK cells, which were then re-suspended in the appropriate media, ready for use.

6.1.5 Soluble TGF- β Human FlowCytomix Kit

The levels of TGF- β were quantified using a FlowCytomix™ bead-based Multiple Analyte Detection Kit (eBioscience®, BMS8420FF, 58729005). This is a fluorescent bead immunoassay, utilising similar science as the ELISA technique. Samples were first diluted 1:10 with Assay Buffer and acidified by adding 20 μ l of 1N HCl and incubated at room temperature for 1 hour, followed by the addition of 20 μ l 1N NaOH. Similar to an ELISA, a standard curve was prepared using 3 μ l of standard mixture provided, with 57 μ l of assay buffer, titrated into seven standard dilutions at 1:3. Beads coated with TGF- β -specific antibodies were then prepared (1:20 reagent dilution buffer) and 10 μ l added to 10 μ l of sample per tube. 20 μ l of a biotin-conjugated secondary antibody was added to bind to the TGF- β captured by the first antibodies (1:20 reagent dilution buffer), mixed and incubated at room temperature for 2 hours in the dark. 400 μ l of assay buffer was added to each tube, centrifuged for 5 minutes at $200 \times g$ and the supernatant removed. This wash step was repeated, followed by addition of Streptavidin-PE, which emits a signal when bound to the biotin conjugate. 0.7 μ l of Streptavidin-PE mixture and 19.3 μ l of assay buffer were added per tube, mixed and incubated at room temperature for 1 hour, in the dark. Following this, 400 μ l of assay buffer was added to each tube, centrifuged for 5 minutes at $200 \times g$ and the supernatant removed. This wash step was repeated prior to analysis on a Beckman Coulter FC 500 flow cytometer and data were analysed using FlowCytomix Pro 2.3 Software.

6.1.6. Method of Statistical Analysis

Data points were in triplicate and graphically expressed as the mean, where error bars depicted SD. Further analysis was then carried out to quantify any trends in the data, using Prism® 5 software. To analyse the repeat measured data within this chapter a one way ANOVA was firstly implemented to determine any significant differences. A Tukey's multiple comparison post-test was then implemented to further distinguish p values between data groups.

6.2. RESULTS AND DISCUSSION

NK cells play an important role in the innate immune system, as they are cytotoxic towards tumour cells via the granule exocytosis and the Fas-Fas-L pathway. Granule exocytosis utilises perforin to traffic granzyme A and B to the cytosol of appropriate targets, where they induce cell death by cleavage of critical substrates (Figure 6.1).

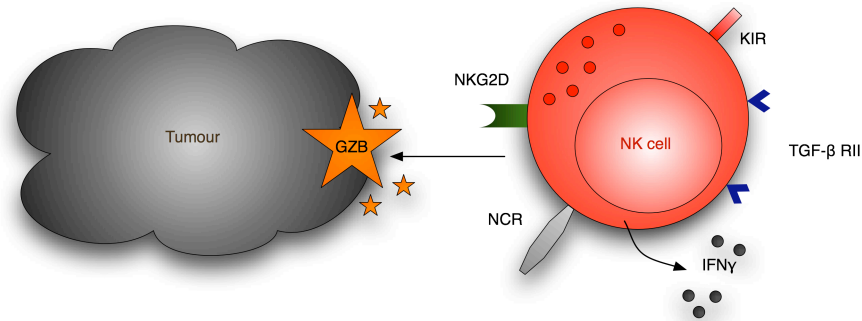


Figure 6.1 Diagrammatic Representation of Natural Killer Cell and Tumour Interaction

Natural Killer (NK) cells are cytotoxic towards tumour cells via release of Interferon- γ (IFN- γ) and tumour necrosis factor- α (TNF- α). A network of cell surface receptors, including members of the NK Groups 2 (NKG2) family, killer cell immunoglobulin-like receptors (KIRs) and natural cytotoxicity receptors (NCRs) including NKp46, NKp30 and NKp44, orchestrate tumour cell target recognition. This initiates a cascade of intracellular events in the target tumour cell involving rapid induction of reactive oxygen species, caspase activation, loss of mitochondrial membrane potential and DNA fragmentation, leading to target cell death. (GZB, granzyme B; TGF- β RII, transforming growth factor- β receptor II).

Following target recognition, NK cells rapidly secrete large amounts of IFN- γ , TNF- α , CCL3, CCL4 and CCL5 that influence innate and adaptive immune responses (Ghiringhelli et al., 2006; Zimmer et al., 2008). Tumour cell recognition by NK cells is dictated by a balance between inhibitory signals mediated by MHC class I molecules and activating signals triggered by specific ligands. The MIC-NKG2D system is an example of an activating signal that participates in the control of epithelial tumours. However, in cancer patients, tumour-mediated shedding of MICs can occur resulting in reduced NK cell activation (Ghiringhelli et al., 2005).

Multiple checkpoints exist to prevent inappropriate activation of damaging mechanisms, including TGF- β , which down-regulates cell-surface expression of activating NK receptors and so limits their killing activities (Moretta et al., 2005). Cell surface expression of TGF- β receptors on NK cells makes them vulnerable to control by soluble TGF- β . Therefore, under certain pathological conditions that increase exposure to TGF- β , NK cells may under-express activating receptors. Signals from soluble or cell-associated TGF- β within a tumour microenvironment can therefore suppress NK cell killing, enabling tumour escape (Moretta et al., 2005). Within a tumour site, the cytokine profile is typically immunosuppressive and the level of TGF- β is likely to be elevated. Sources of TGF- β within the tumour microenvironment include tumour cells, stromal cells, migratory hematopoietic cells and Tregs. In addition, macrophages have been incriminated in tumour progression and one contributory factor might be the release and activation of latent TGF- β (Wahl et al., 2006).

Therefore, it is suggested that NK cell surface expression of TGF- β receptors may facilitate Treg-mediated, cell-contact dependent, down regulation of the NK cell-activating receptor NKG2D (Ghiringhelli et al., 2005; Moretta et al., 2005; Zimmer et al., 2008). Figure 6.2 illustrates this hypothesis and highlights the basic components for the proposed *in vitro* model.

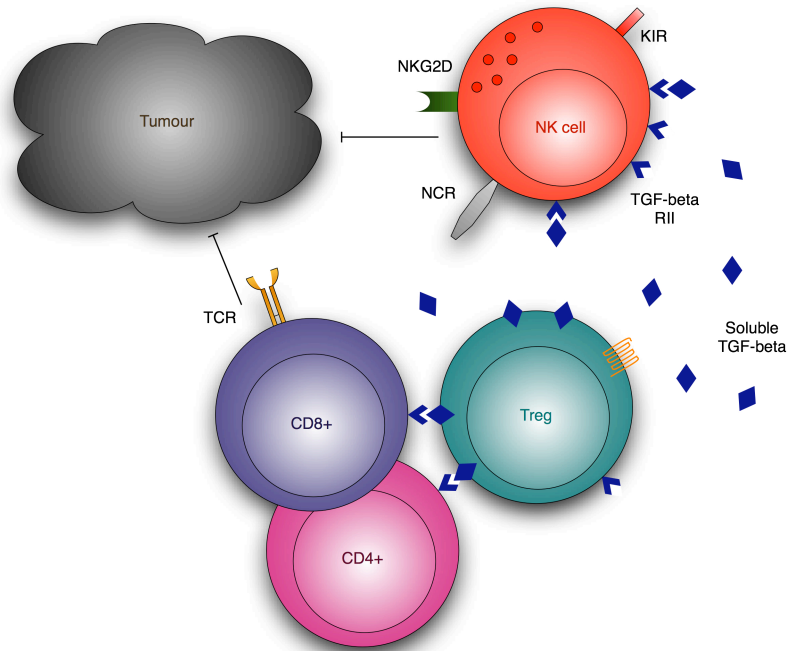


Figure 6.2 Diagrammatic Representation of Treg Suppression of Natural Killer Cells and Tumour Interaction

Cell surface expression of transforming growth factor- β receptor II (TGF- β RII) on natural killer (NK) cells makes them vulnerable to control by soluble TGF- β . Signals from soluble or cell-associated TGF- β within a tumour microenvironment cause under-expression of activating NK receptors, therefore suppress NK cell killing, enabling tumour escape. It is suggested that NK cell surface expression of TGF- β receptors functions to facilitate Treg-mediated cell-contact dependent down regulation of the NK cell-activating receptor NKG2D. Thus, Tregs are able to inhibit NK cell effector functions and resting NK cell proliferation, resulting in reduced cytotoxicity towards tumour targets. (TCR, T cell receptor; NKG2D, NK Group 2 member D; KIR, killer cell immunoglobulin-like receptor; NCR, natural cytotoxicity receptor).

It is speculated that Tregs are able to inhibit NK cell effector functions and resting NK cell proliferation, resulting in reduced cytotoxicity towards tumour targets (Zimmer et al., 2008). Studies have shown that Tregs impair NK cell activation in cancer patients (Ghiringhelli et al., 2005). Both human and murine *in vitro* and *in vivo* systems have shown Tregs potently suppress NK cell responses, including the NK cell-mediated control of tumour expansion (Ghiringhelli et al., 2005).

NK cells have been shown to kill MHC class I-deficient (MHC I-) tumour cell lines (Smyth et al., 2000). *In vivo* studies have demonstrated that NK-deficient mice have problems clearing MHC I- tumour cells and chemically induced tumours are more susceptible in mice depleted of NK cells (Kim et al., 2000).

An *in vitro* model, investigating the suppressive ability of Tregs on NK cell killing activity and interactions with effector cells will improve understanding of the role of Tregs within the tumour microenvironment and suppression of anti-tumour immunity.

6.2.1. K562 Cell Killing Assay with PBMCs

The first step in constructing a Treg:effector:NK cell suppression model is the development of a reliable cell killing assay. Preliminary studies involved looking at the K562 cell line, derived from a chronic myelogenous leukaemia (CML) patient in blast crisis (Klein et al., 1976). K562 cells are subject to NK cell killing as they lack the MHC complex required to inhibit NK cell activity. This cell line was used initially to develop this work looking at cell killing by PBMCs.

CFSE labelling was used to distinguish the K562 cells from co-cultured unlabelled PBMCs. Cells were co-cultured for 6 hours and then counter-stained with PI to assess cell viability (Figure 6.3A).

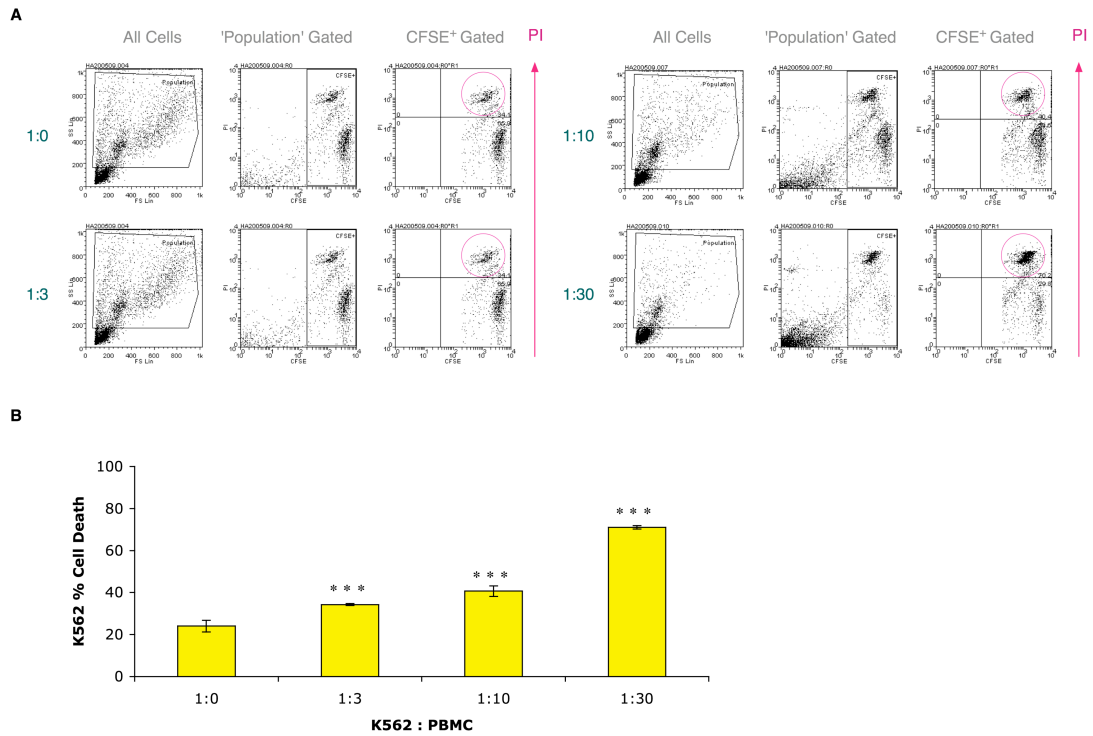


Figure 6.3 FACS Analysis of K562 Cell Killing Assay with PBMCs

K562 cells at 2×10^7 cells per ml were stained with $2.5 \mu\text{M}$ CFSE, 8 minutes. Cells were then re-suspended in 10 % v/v FBS RPMI and washed three times prior to cell counting. CFSE stained K562 cells were seeded at 1×10^4 cells per well with isolated PBMCs at 1:0, 1:3, 1:10 and 1:30 (K562:PBMC cell ratios). Cells were cultured at 37°C in a humidified atmosphere containing 5 % v/v CO_2 for 6 hours and then counter-stained with $100 \mu\text{l}$ propidium iodide (PI) for 15 minutes to assess cell viability. A) Cells were analysed using FACS, gated to initially remove cell debris ('Population') and then to evaluate CFSE positive cells only. B) Cell killing was expressed as a percentage of PI+ to PI- cells. Data are a mean of triplicates from a single plate (\pm SD) and is representative of three different experiments, statistically analysed using a one way ANOVA and Tukey's multiple comparison post-test (***) $p < 0.001$).

The total cell population was first gated to remove debris and then subsequently further gated to remove CFSE-negative PBMC cells. FACS analysis was then set to quantify a consistent number of events within the CFSE positive region (K562 cells), to prevent variations in PBMC events from influencing the results. Cell walls of viable cells are impermeable to PI; however, necrotic cells lose their integrity and become permeable. The incorporation of PI can therefore be used as a measure of cell viability. This assay was repeated three times and cell-killing activity expressed as a percentage of CFSE⁺PI⁺ (dead K562s) cells to CFSE⁺PI⁻ (viable K562s) (Figure 6.3B).

Increasing numbers of PBMCs resulted in elevated levels of CFSE⁺PI⁺, dead K562 cells. A background of 24.04 % was observed with no PBMCs present, which significantly increased to 71.07 % with 1:30 K562:PBMC cell ratios (Figure 6.3B).

This assay was repeated with varying K562:PBMC cell ratios to determine the optimum killing conditions (Figure 6.4).

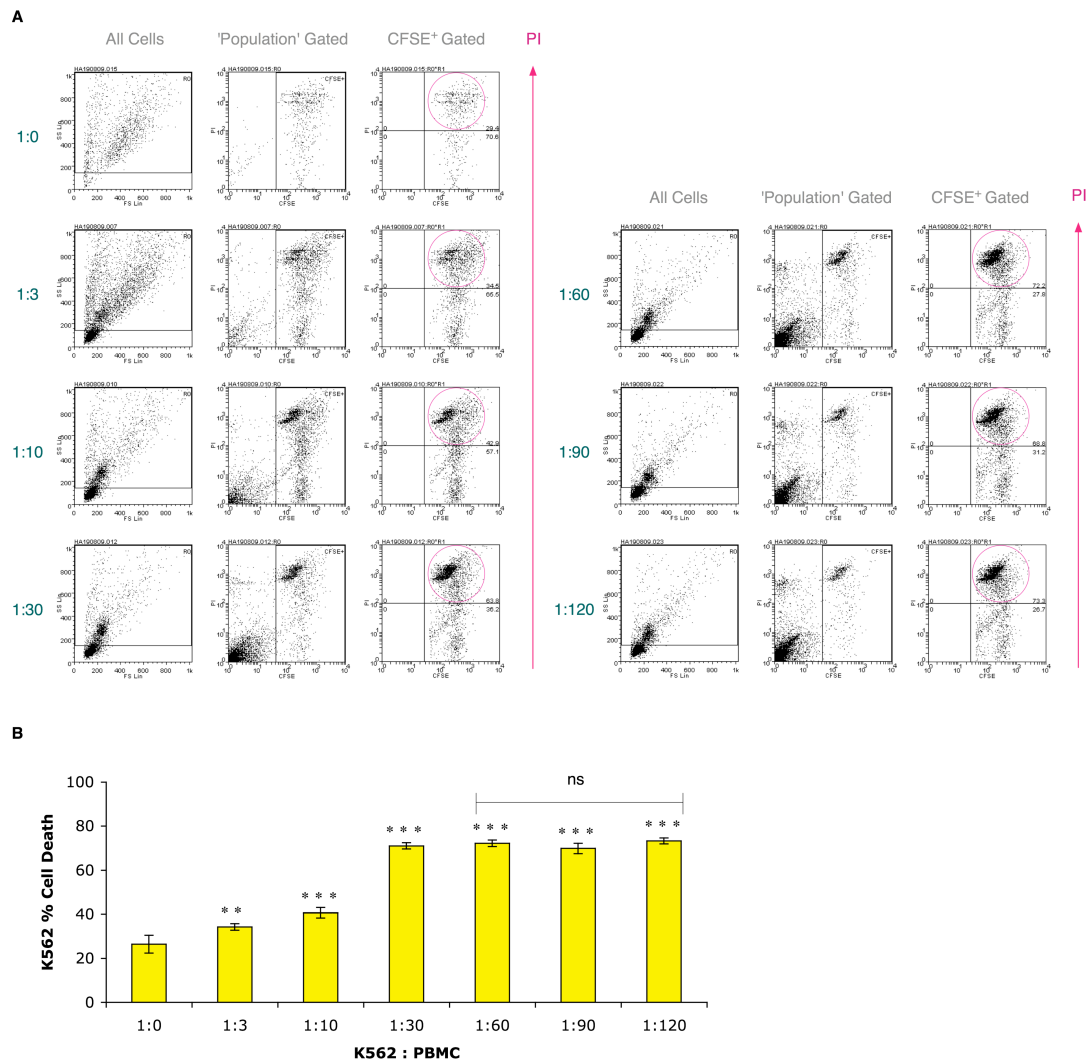


Figure 6.4 Extended K562 Cell Killing Assay with PBMCs

K562 cells at 2×10^7 cells per ml were stained with $2.5 \mu\text{M}$ CFSE for 8 minutes. Cells were then re-suspended in 10 % v/v FBS RPMI and washed three times prior to cell counting. CFSE stained K562 cells were seeded at 1×10^4 cells per well with isolated PBMCs at 1:0, 1:3, 1:10, 1:30, 1:60, 1:90 and 1:120 (K562:PBMC cell ratios). Cells were cultured at 37°C in a humidified atmosphere containing 5 % v/v CO_2 for 6 hours and then counter-stained with $100 \mu\text{l}$ propidium iodide (PI) for 15 minutes to assess cell viability. A) Cells were analysed using FACS, gated to initially remove cell debris ('Population') and then to evaluate CFSE positive cells only. B) Cell killing was expressed as a percentage of PI+ to PI- cells. Data are a mean of triplicates from a single plate (\pm SD) and is representative of three different experiments, statistically analysed using a one way ANOVA and Tukey's multiple comparison post test (** $p < 0.01$; *** $p < 0.001$; ns, no significant difference).

This FACS data were then expressed as a percentage of K562 cell death (Figure 6.4B). As described previously, an increase in cell death was observed when the ratio of PBMCs was elevated to 1:30. A plateau was then seen at higher ratios, where an increase in PBMC cell number did not influence the percentage of K562 cell death (Figure 6.4B).

To allow time for Treg isolation during day 1, followed by an overnight cell-killing assay, it was essential to extend the killing assay. A time course was therefore prepared to determine the effect of extended incubation times (Figure 6.5).

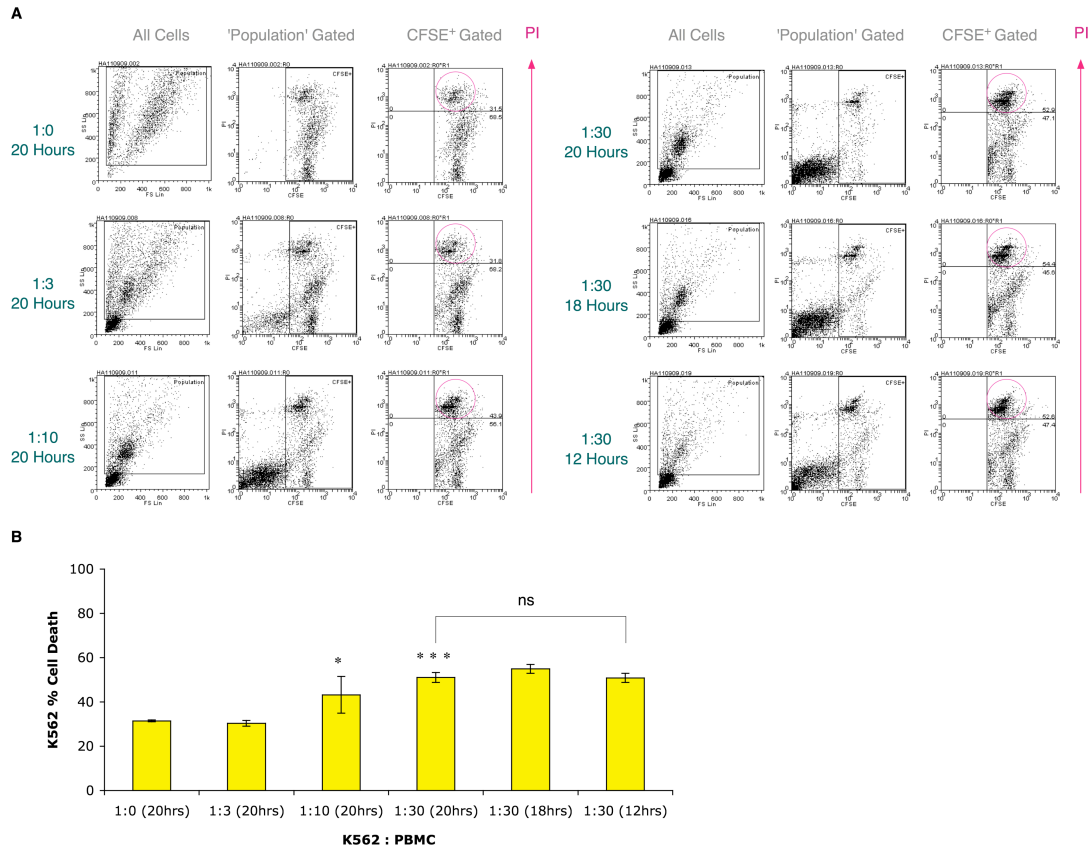


Figure 6.5 Extended K562 Cell Killing Assay with PBMCs

K562 cells at 2×10^7 cells per ml were stained with $2.5 \mu\text{M}$ CFSE for 8 minutes. Cells were then re-suspended in 10 % v/v FBS RPMI and washed three times prior to cell counting. CFSE-stained K562 cells were seeded at 1×10^4 cells per well with isolated PBMCs at 1:0, 1:3, 1:10, 1:30, 1:60, 1:90 and 1:120 (K562:PBMC cell ratios). Cells were cultured at 37°C in a humidified atmosphere containing 5 % v/v CO_2 for 12, 18 or 20 hours and then counter-stained with $100 \mu\text{l}$ propidium iodide (PI) for 15 minutes to assess cell viability. A) Cells were analysed using FACS, gated to initially remove cell debris ('Population') and then to evaluate CFSE positive cells only. B) Cell killing was expressed as a percentage of PI+ to PI- cells. Data are a mean of triplicates from a single plate (\pm SD) and is representative of three different experiments, statistically analysed using a one way ANOVA and Tukey's multiple comparison post test (* $p < 0.05$; *** $p < 0.001$; ns, no significant difference).

Prolonging the cell killing assay at the required 1:30 K562:PBMC ratio made very little difference to the percentage of cell death (Figure 6.5). Assay optimisation was therefore complete and a reliable cell-killing assay established (future work will now not include the detailed FACS analysis figures). This assay was then used to determine the effect on cell killing when a Treg population was introduced into the system.

Isolated Tregs and PBMCs from the same donor were co-cultured with CFSE stained K562s and incubated for 16 hours prior to determining the K562 percentage cell death via PI staining (Figure 6.6). No significant suppression of cell killing was observed. It was speculated that this was due to skewed Treg:PBMC cell ratios with the presence of the K562 cells.

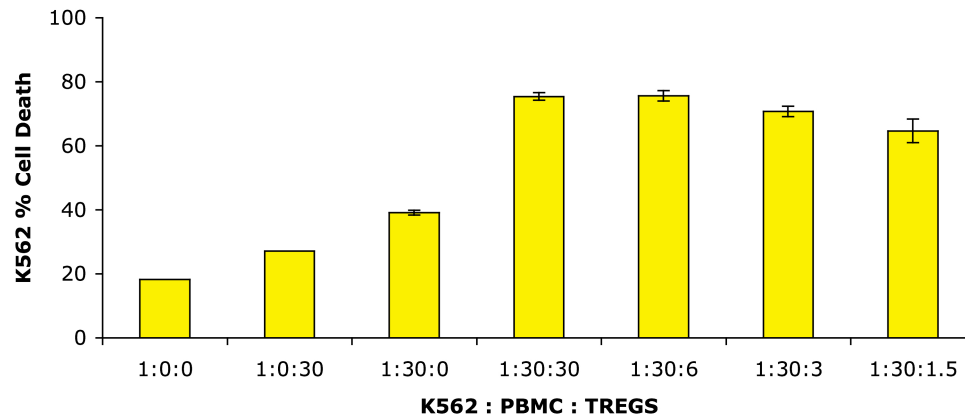


Figure 6.6 Failure of Treg Mediated Suppression of K562 Cell Killing Assay with PBMCs

K562 cells at 2×10^7 cells per ml were stained with 2.5 μ M CFSE for 8 minutes. Cells were then re-suspended in 10 % v/v FBS RPMI and washed three times prior to cell counting. Expanded Tregs and donor matched isolated PBMCs were incubated at the indicated ratios with CFSE-stained K562 cells and cultured at 37 °C in a humidified atmosphere containing 5 % v/v CO₂ for 16 hours. Cells were counter-stained with 100 μ l propidium iodide (PI) for 15 minutes to assess cell viability and analysed using FACS, gated on CFSE positive cells, then cell killing expressed as a percentage of PI+ to PI- cells. Data are a mean of triplicates from a single plate (\pm SD).

A 4 hour pre-incubation step for the Tregs and PBMCs was then introduced, prior to adding the K562 target cells (Figure 6.7).

A significant reduction in the percentage of K562 cell killing was observed when Tregs were introduced at a 1:30:60 K562:PBMC:Treg cell ratio (Figure 6.7). This significant suppression was not observed when the Tregs were replaced with the same number of CD25⁺ effector control cells. This confirmed that Tregs were having a suppressive effect on a population of cells within PBMCs that would normally cause the cell killing activity. At this stage it was speculated that this was against NK cells.

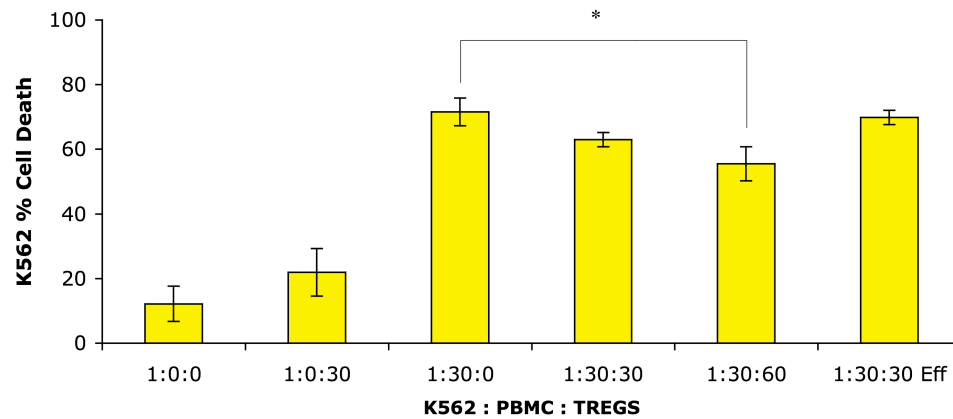


Figure 6.7 Treg Mediated Suppression of K562 Cell Killing Assay with PBMCs

K562 cells at 2×10^7 cells per ml were stained with 2.5 μ M CFSE for 8 minutes. Cells were then re-suspended in 10 % v/v FBS RPMI and washed three times prior to cell counting. Isolated Tregs and PBMCs were pre-incubated at the indicated ratios for 4 hrs. Isolated effector cells (Eff) from the same donor replaced Tregs as a control. CFSE-stained K562 cells were then introduced and cultured at 37 °C in a humidified atmosphere containing 5 % v/v CO₂ for 12 hours. Cells were counter-stained with 100 μ l propidium iodide (PI) for 15 minutes to assess cell viability and analysed using FACS, gated on CFSE-positive cells, then cell killing expressed as a percentage of PI+ to PI- cells. Data are a mean of triplicates from a single plate (\pm SD) and is representative of three different experiments, statistically analysed using a one way ANOVA and Tukey's multiple comparison post-test (* p < 0.05).

6.2.2. FACS Investigation of Model Markers on PBMCs

To confirm the details of the proposed model, it was essential to investigate the key components using specific cell markers to determine the expression on single cell populations. This enabled a more complex understanding of the functional role of each cell population and how it contributed to the suppression of tumour cell killing.

A network of cell surface receptors, including members of the NKG2 family, KIR family and NCRs, orchestrate tumour target cell recognition. These receptors collaborate with cytokine receptors to coordinate the recognition and disposal of dangerous cells, whilst avoiding normal autologous cells. Specifically, the cell surface receptor NKG2D plays a key role in coordinating the recognition and disposal of tumour cells and so an understanding of its distribution on different cell populations was important (Figure 6.8).

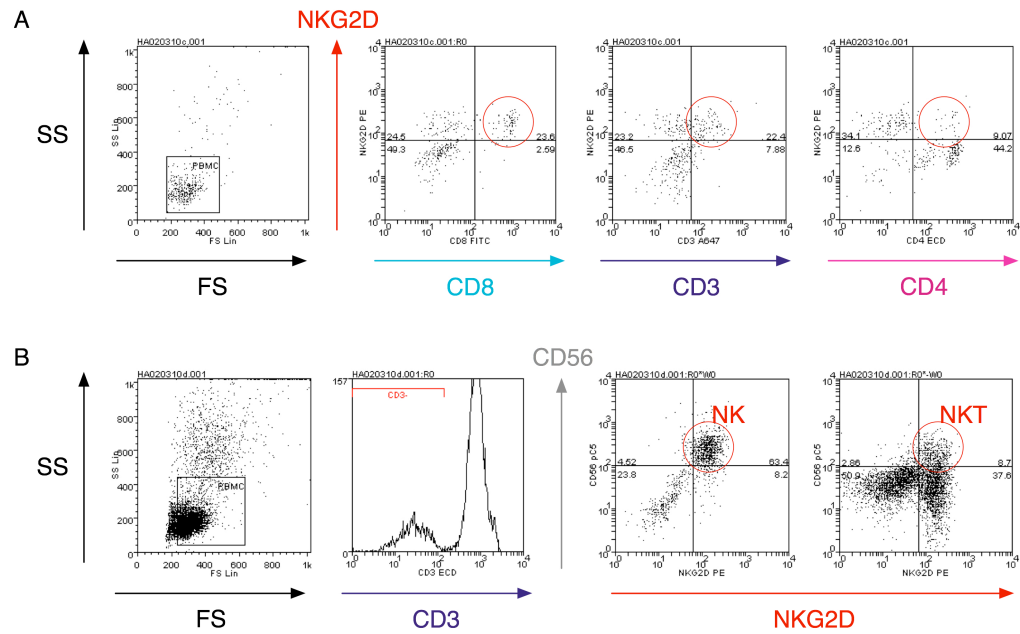


Figure 6.8 Investigation of NKG2D Expression

1×10^6 isolated PBMCs were washed in PBS and incubated with A) 5 μ l FITC anti-CD8, PE anti-NKG2D, Alexa647 anti-CD3 and ECD anti-CD4 or B) pC5 anti-CD56, PE anti-NKG2D, and ECD anti-CD3 for 20 minutes. Cells were washed and fixed for 15 minutes. Data were acquired immediately on a Beckman Coulter FC 500 flow cytometer and analysed using Weasel software.

NKG2D was seen to be expressed on CD3 and CD8 cells, and to a lesser extent on CD4 cells (Figure 6.8A). More detailed FACS analysis was required to distinguish the different subdivisions of cells expressing NKG2D.

CD56 is a known marker for NK and NKT cell populations (Whiteside and Herberman, 1990). CD56 was used against NKG2D after gating positively or negatively for CD3 cell populations. Data highlighted that NKG2D is expressed on CD56⁺CD3⁻ NK cells and also CD56⁺CD3⁺ NKT cells (Figure 6.8B).

It is hypothesised that NK cell surface expression of TGF- β receptors may function to facilitate Treg-mediated, down-regulation of NKG2D. The expression TGF- β RII was therefore investigated (Figure 6.9).

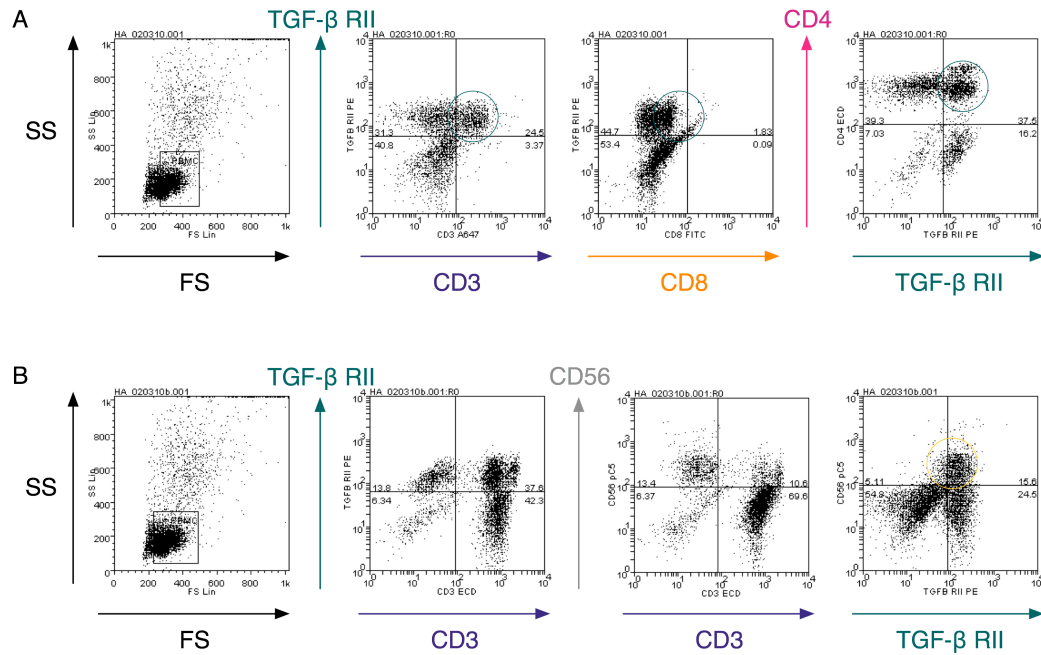


Figure 6.9 Investigation of TGF- β RII Expression

1×10^6 isolated PBMCs were washed in PBS and incubated with primary TGF- β RII antibody for 20 minutes. Cells were then washed twice in PBS and incubated with 5 μ l A) ECD anti-CD4, Alexa 647 anti-CD3 and FITC anti-CD8 or B) ECD anti-CD3 and PeCy5 anti-CD56 for 20 minutes. Following two further wash steps, cells were incubated with secondary TGF- β RII antibody for 20 minutes and fixed for 15 minutes. Data were acquired immediately on a Beckman Coulter FC 500 flow cytometer and analysed using Weasel software.

FACS analysis revealed co-staining of TGF- β RII with CD3⁺ cells, CD4⁺ cells and also CD8⁺ cells. To further distinguish these cell populations, the NK cell marker CD56 was then introduced (Figure 6.9B).

TGF- β RII was seen on cells that express CD56, confirming that NK cells have TGF- β RII. Gating the cell population on CD3 enabled segregation of NK and NKT cells, where both were seen to express TGF- β RII. The cell surface expression of TGF- β receptors on NK cells could render them vulnerable to control by soluble TGF- β . Therefore, under certain pathological conditions known to increase exposure to TGF- β , NK cells may under-express activating receptors, such as NKG2D. Signals from soluble or cell-associated TGF- β within a tumour microenvironment may therefore suppress NK cell killing, enabling tumour escape. Within a tumour site, the cytokine profile is typically immunosuppressive and the level of TGF- β is likely to be elevated. Sources of TGF- β within the tumour microenvironment include tumour cells, stromal cells, migratory haematopoietic cells and Tregs.

6.2.3. K562 Cell Killing Assay with NK Cells

NK cells were isolated from 50 ml of healthy blood as described in section 6.1.4. The EasySep® human CD56 positive selection kit is designed to isolate CD56⁺ NK and NKT cells from PBMCs. The kit utilises tetrameric antibody complexes and dextran-coated magnetic particles combined with a human fc receptor antibody to minimise non-specific binding. The process is summarised in Figure 6.10.

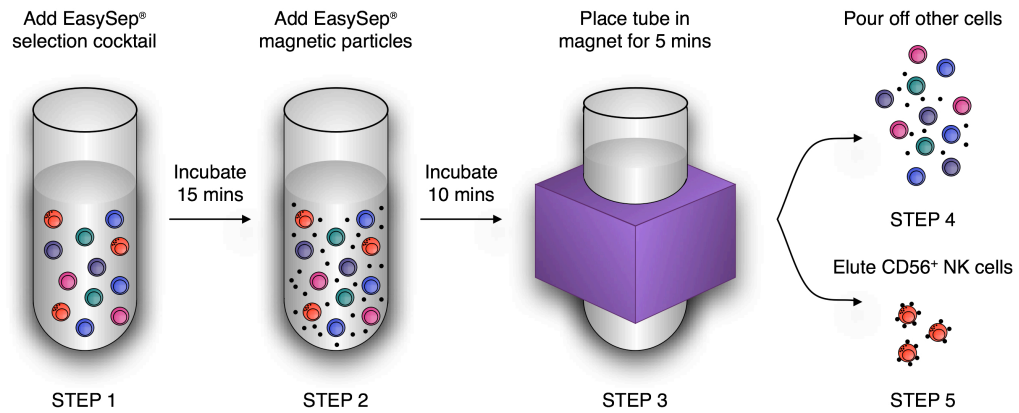


Figure 6.10 Diagrammatic Representation of the EasySep® Human NK Isolation Procedure

Step 1 involves adding EasySep® antibody selection cocktail to peripheral blood mononuclear cells (PBMCs), isolated from 50 ml human blood. Magnetic nanoparticles are then added, mixed and incubated in step 2. This cell suspension is then placed into the purple EasySep® magnet and incubated for 5 minutes. The magnet and tube are inverted together, in one continuous motion, pouring off the supernatant (Step 4). The magnetically labelled NK cells remain inside the tube, held by the magnetic field. To elute the NK cells, the tube is simply removed from the magnet (step 5).

Isolated NK cells were co-cultured with CFSE-stained K562 cells at increasing ratios to establish their cytotoxic function (Figure 6.11). A significant increase in the percentage of K562 cell death was observed when NK cell ratios were elevated to 1:3 (64.0 %), 1:10 (83.4 %) and 1:30 (89.8 %) K562:NK cell ratios. In this assay, NK cells were isolated based on a CD56-positive selection only. Due to this, the population would therefore also include CD56⁺CD3⁻ NK, CD56⁺CD3⁺ NKT, CD56⁺CD8⁺ cell types. A CD56⁻ control was included and showed elevated levels (36.9 %) of cytotoxic activity compared to effector cells (data not shown) and background levels of K562 cell death (1:0 ratio, 4.5 %). This demonstrates other cytotoxic T cells that would perhaps contribute to tumour-cell killing; however, those populations were outside the scope of the current study.

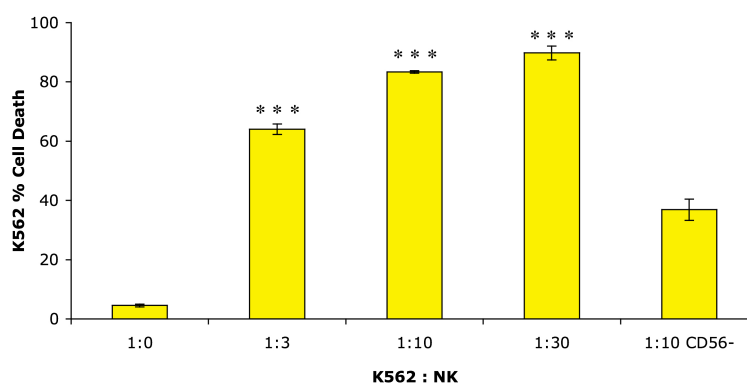


Figure 6.11 K562 Cell Killing Assay with Isolated NK Cells

K562 cells at 2×10^7 cells per ml were stained with $2.5 \mu\text{M}$ CFSE for 8 minutes. Cells were then re-suspended in 10 % v/v FBS RPMI and washed three times prior to cell counting. CFSE stained K562 cells were seeded at 1×10^4 cells per well with isolated CD56+ natural killer (NK) cells at 1:0, 1:3, 1:10 and 1:30 (K562:NK cell ratios). Isolated CD56- cells were included as a control. Cells were cultured at 37°C in a humidified atmosphere containing 5 % v/v CO_2 for 16 hours and then counter-stained with $100 \mu\text{l}$ propidium iodide (PI) for 15 minutes to assess cell viability. Cells were analysed using FACS, gated on CFSE positive cells, then cell killing expressed as a percentage of PI+ to PI- cells. Data are a mean of triplicates from a single plate (\pm SD) and is representative of three different experiments, statistically analysed using a one way ANOVA and Tukey's multiple comparison post-test (***) ($p < 0.001$).

As NK cells were isolated based on CD56-positive selection, further FACS analysis was achieved to determine the percentage breakdown of various other cell populations included (Figure 6.12).

FACS analysis revealed a relatively high percentage of CD8 cells within the population. Also, by gating on CD3 positive or CD3 negative it was possible to determine the amount of NK versus NKT cells present (Figure 6.12).

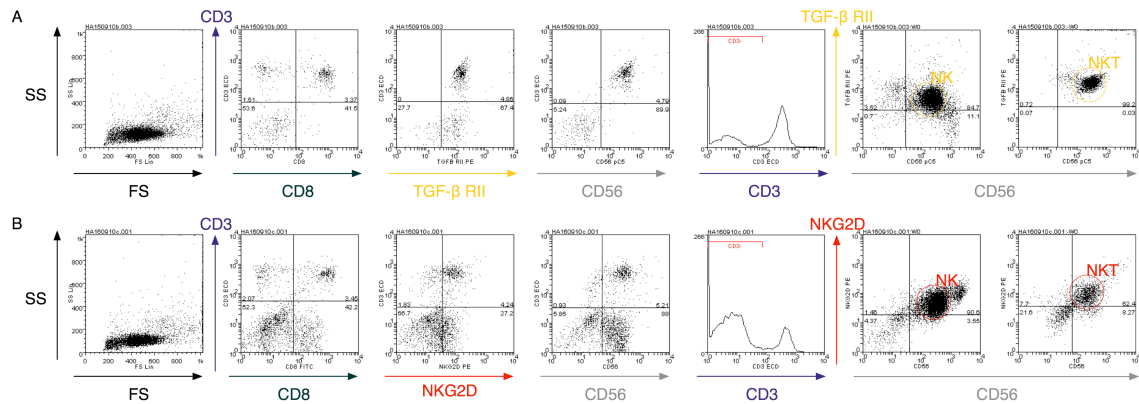


Figure 6.12 FACS Analysis of Isolated NK Cells

NK cells were isolated from 50 ml healthy human blood and 1×10^6 cells were removed for FACS analysis. A pre-titrated volume of surface antibodies was added: ECD anti-CD3, FITC anti-CD8, PeCy5 anti-CD56 with A) PE anti-TGF- β RII or B) PE anti-NKG2D. Cells were then fixed and permeabilised. Data were acquired on a Beckman Coulter FC 500 flow cytometer and analysed using Weasel software. NK and NKT analysis was carried out on CD3+/- gating.

Flow cytometer data confirmed the expression of NKG2D receptor on CD3⁻ NK and CD3⁺ NKT cell populations (Figure 6.12). In addition, cell surface expression of the TGF- β receptor II (TGF- β RII) on CD56⁺ NK cells was observed, which potentially makes them vulnerable to control by soluble TGF- β .

The effect of introducing Tregs into the system was then determined. This was established by isolating both NK cells and Tregs on the same day, from the same donor. Tregs and NK cells were then pre-incubated at various ratios before adding K562 tumour cells and observing the cytotoxicity of the NK cells (Figure 6.13).

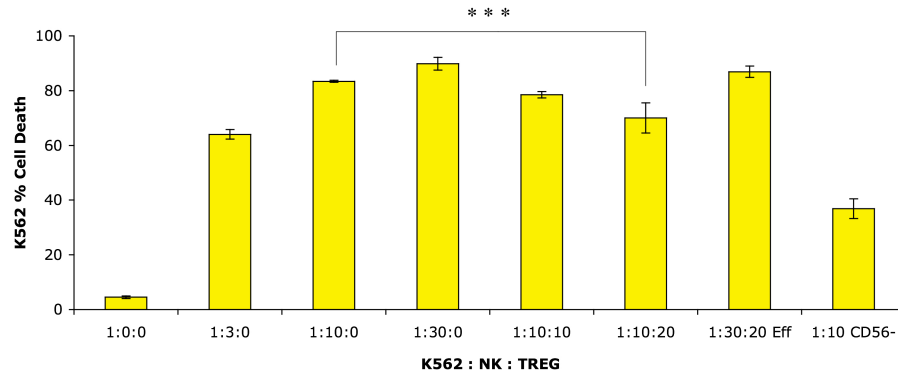


Figure 6.13 Treg Mediated Suppression of K562 Cell Killing Assay with NK Cells Isolated from the same Donor

K562 cells at 2×10^7 cells per ml were stained with 2.5 μ M CFSE for 8 minutes. Cells were then re-suspended in 10 % v/v FBS RPMI and washed three times prior to cell counting. Isolated Tregs and CD56+ natural killer (NK) cells were pre-incubated at the indicated ratios for 4 hours. Isolated effector (Eff) and CD56- cells were also included as controls. CFSE stained K562 cells were then introduced and cultured at 37 °C in a humidified atmosphere containing 5 % v/v CO₂ for 12 hours. Cells were counter-stained with 100 μ l propidium iodide (PI) for 15 minutes to assess cell viability and analysed using FACS, gated on CFSE positive cells, then cell killing expressed as a percentage of PI+ to PI- cells. Data are a mean of triplicates from a single plate (\pm SD) and is representative of three different experiments, statistically analysed using a one way ANOVA and Tukey's multiple comparison post-test (***) $p < 0.001$).

Tregs significantly reduced the tumour cell killing activity of the NK cells (Figure 6.13). At the highest ratio of NK cells to K562 cells (1:10), the percentage cell killing was 83.4 %. This was significantly reduced to 70 % when Tregs were introduced into the system at a 1:10:20 cell ratio ($p < 0.001$). To determine whether the NK cells were orchestrating target cell killing of K562 cells via the NKG2D receptor, a neutralising NKG2D antibody was studied (Figure 6.14).

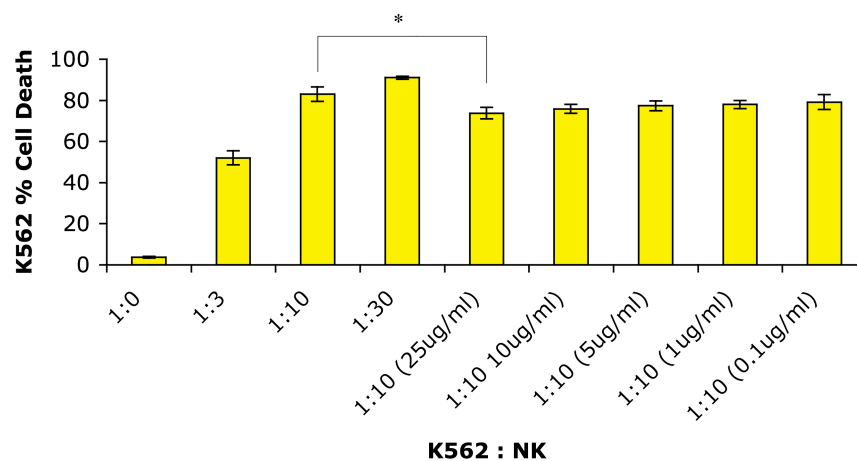


Figure 6.14 The Effect of a Neutralising anti-NKG2D Antibody on NK Cell Killing of K562 Cells

K562 cells at 2×10^7 cells per ml were stained with $2.5 \mu\text{M}$ CFSE for 8 minutes. Cells were then re-suspended in 10 % v/v FBS RPMI and washed three times prior to cell counting. Isolated NK cells were pre-incubated with various concentrations of a neutralising NKG2D antibody for 30 minutes. CFSE stained K562 cells were seeded at 1×10^4 cells per well with NK cells at 1:0, 1:3, 1:10 and 1:30 (K562:NK cell ratios). Cells were cultured at 37°C in a humidified atmosphere containing 5 % v/v CO_2 for 6 hours and then counter-stained with $100 \mu\text{l}$ propidium iodide (PI) for 15 minutes to assess cell viability. Cells were analysed using FACS, gated on CFSE-positive cells, then cell killing expressed as a percentage of PI+ to PI- cells. Data are a mean of triplicates from a single plate (\pm SD) and is representative of three different experiments, statistically analysed using a one way ANOVA and Tukey's multiple comparison post-test (* $p < 0.05$).

Here isolated NK cells were pre-incubated with a titration of neutralising NKG2D antibody (nNKG2D) prior to co-culture with K562 cells. A significant reduction in NK cell killing capability was observed with 25 µg/ml of nNKG2D antibody. The titration of nNKG2D was introduced into the 1:10 K562:NK cell ratio and resulted in a reduction from 83.0 % to 73.7 % at the top concentration of 25 µg/ml. This window of suppression resulting from blocking the NKG2D pathway is relatively small. To ensure the antibody was fully functional, FACS analysis of NKG2D expression was carried out on isolated NK cells incubated with varying amounts of nNKG2D (Figure 6.15).

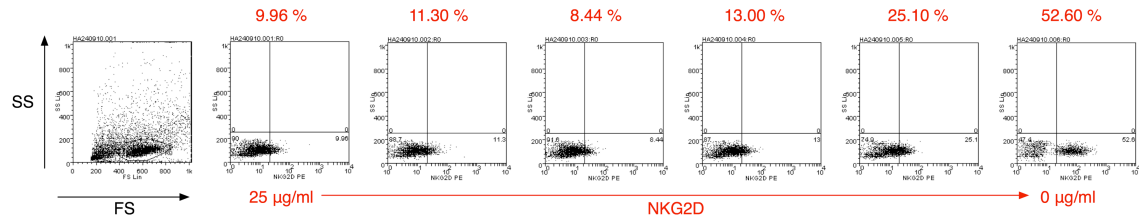


Figure 6.15 FACS Analysis of Isolated NK Cells with Neutralising anti-NKG2D Antibody

NK cells were isolated from 50 ml healthy human blood and 1×10^6 cells were removed for FACS analysis. Cells were pre-incubated with a titration of neutralising anti-NKG2D antibody for 30 minutes. PE anti-NKG2D surface antibody was added before cells were fixed. Data were acquired on a Beckman Coulter FC 500 flow cytometer and analysed using Weasel software.

Results show a dose-dependent level of expression of NKG2D. NKG2D expression drops to 9.96 % when NK cells are incubated with 25 µg/ml of antibody compared to a normal level of approximately 52.6 %. This FACS analysis confirmed the neutralising antibody was working well. The small window of effect is therefore interesting and could be due to a number of reasons. It is known that various other recognition receptors and ligands contribute to the cell killing activity of NK cells, for example, NKp46, NKp30 and NKp44.

To further understand the mechanisms of cell killing in this system and to test the TGF- β -focused hypothesis, an additional antibody was also investigated to neutralise the TGF- β receptor II (nTGF- β RII). Again, this was introduced into the K562:NK:Treg assay system (Figure 6.16).

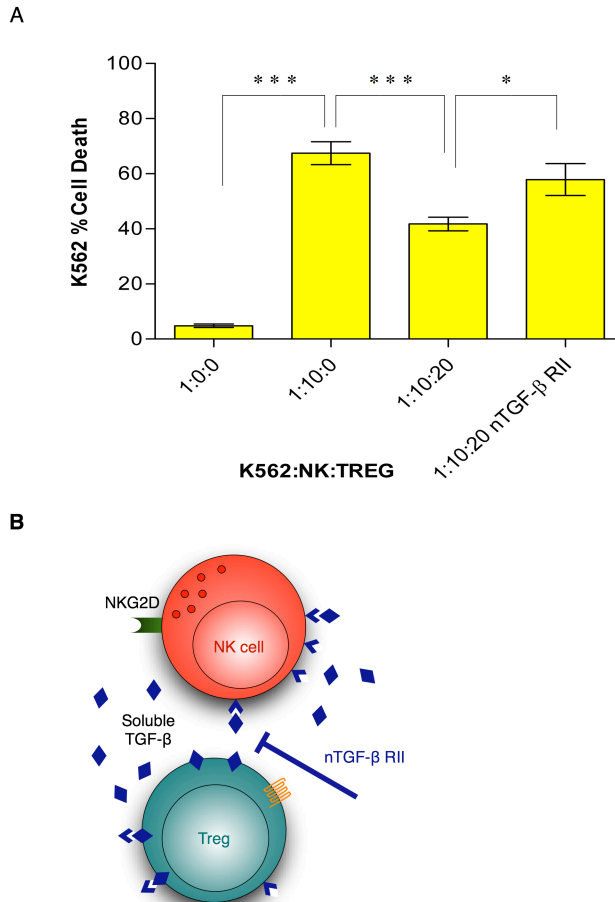


Figure 6.16 Treg Mediated Suppression of K562 NK Cell Killing is Abrogated by Neutralising TGF- β RII Antibody

A) K562 cells at 2×10^7 cells per ml were stained with 2.5 μ M CFSE for 8 minutes. Cells were then re-suspended in 10 % v/v FBS RPMI and washed three times prior to cell counting. Neutralising TGF- β RII antibody (nTGF- β RII, 50 μ g/ml) was pre-incubated with isolated CD56⁺ natural killer (NK) cells (1 hour) before adding Tregs isolated from the same donor (4 hours). CFSE stained K562 cells were then introduced and cultured at 37 °C in a humidified atmosphere containing 5 % v/v CO₂ for a further 16 hours. Cells were counter-stained with 100 μ l propidium iodide (PI) for 15 minutes to assess cell viability and analysed using FACS, gated on CFSE positive cells, then cell killing expressed as a percentage of PI⁺ to PI⁻ cells. Data are a mean of triplicates from a single plate (\pm SD) and is representative of three different experiments, statistically analysed using a one way ANOVA and Tukey's multiple comparison post-test (* $p < 0.05$, *** $p < 0.001$). B) Diagrammatic representation of the rationale behind the assay.

At a 1:10 K562:NK cell ratio, 67.5 % of K562 cell killing was achieved, which was reduced to 41.6 % when Tregs were introduced into the assay. This suppressive ability of Tregs was significantly abrogated by pre-incubating the NK cells with nTGF- β RII, returning the percentage of K562 cell death to 57.9 % (Figure 6.16). Data are in agreement with literature suggesting a link between membrane-tethered TGF- β and cell-to-cell contact dependent Treg suppression mechanisms (Nakamura et al., 2004; Nakamura et al., 2001).

Many components within the tumour microenvironment have been shown to contribute to the elevated levels of soluble TGF- β . Sources of TGF- β within the tumour microenvironment include tumour cells, stromal cells and migratory haematopoietic cells (Liu et al., 2007).

It remains unclear whether Tregs are capable of directly producing TGF- β themselves, or if they induce bystander cells to do so (Nakamura et al., 2004; Nakamura et al., 2001). The ability of Tregs to produce soluble TGF- β was therefore studied by evaluating the concentration of TGF- β present in the supernatants of *ex vivo* isolated Tregs (Figure 6.17).

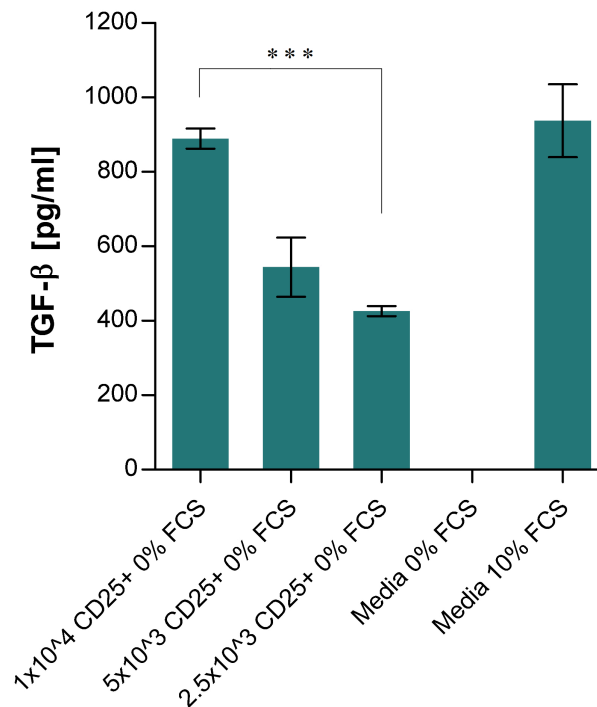


Figure 6.17 Treg Production of Soluble TGF-β

CD4⁺CD25⁺ Tregs were isolated from 50 ml blood from a consenting healthy volunteer. Cells were cultured in 0 % FCS Media at 37 °C in a humidified atmosphere containing 5 % v/v CO₂ for 72 hours. The levels of TGF-β were quantified using FlowCytomix™. Samples were firstly acidified prior to adding TGF-β specific beads. 20 µl of biotin-conjugated secondary antibody was added, mixed and incubated for 2 hours. Samples were washed twice followed by addition of Streptavidin-PE, mixed and incubated for 1 hour. Finally samples were washed prior to analysis on a Beckman Coulter FC 500 flow cytometer and data were analysed using FlowCytomix Pro 2.3 Software. Samples were compared against a standard curve (1:3) and results evaluated using Prism® 5. Data are a mean of triplicates from a single plate (± SD), statistically analysed using a one way ANOVA and Tukey's multiple comparison post-test (***) p < 0.001).

The level of TGF- β was determined using FlowCytomix™ detection kit. Originally, supernatants were analysed from suppression experiments (Figure 3.3); however, preliminary experiments revealed that media containing FCS affected the results. To overcome this problem, Tregs were isolated as previously described and incubated for 72 hours in serum free media (Figure 6.17). Wells containing 1×10^4 Tregs per ml resulted in an increased concentration of TGF- β (889.6 $\mu\text{g/ml}$), which was significantly higher than wells with 5×10^3 Tregs (544.3 $\mu\text{g/ml}$) and 2.5×10^3 Tregs (426.4 $\mu\text{g/ml}$). Data suggest that the soluble TGF- β analysed is being produced by the Tregs present.

Given the reported ability of TGF- β to inhibit lymphocyte cytotoxicity, the production of TGF- β by Tregs when co-cultured with NK cells was investigated. An understanding of whether TGF- β was responsible for the suppression of NKG2D-mediated NK cell cytotoxicity of ligand-expressing tumour targets was required.

To further determine the implications of elevated levels of TGF- β within the tumour microenvironment and to clarify that TGF- β is a key player in the suppression mechanisms of NK-mediated tumour cell killing, Tregs were removed from the assay and replaced with a known concentration (10 ng/ml) of soluble TGF- β (sTGF- β) (Figure 6.18).

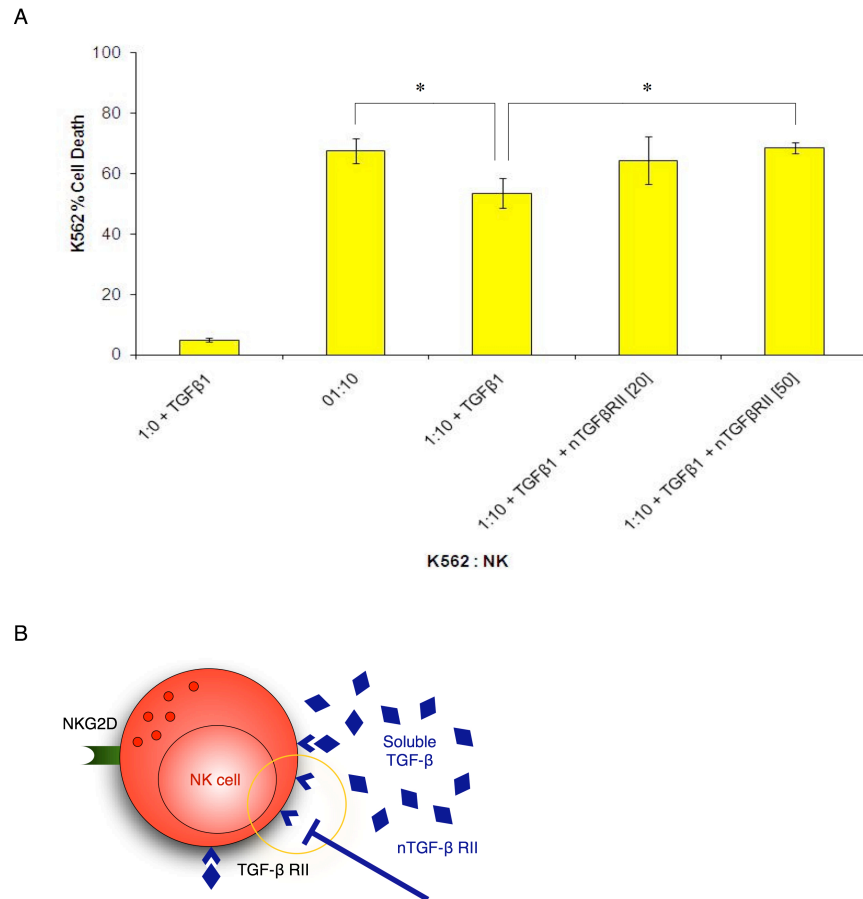


Figure 6.18 TGF- β 1 Mediated Suppression of K562 NK Cell Killing is Abrogated by Neutralising TGF- β RII Antibody

A) K562 cells at 2×10^7 cells per ml were stained with 2.5 μ M CFSE for 8 minutes. Cells were then re-suspended in 10 % v/v FBS RPMI and washed three times prior to cell counting. Neutralising TGF- β RII antibody (nTGF- β RII, 20 or 50 μ g/ml) was pre-incubated with isolated CD56⁺ natural killer (NK) cells for 1 hour. Soluble TGF- β 1 was then introduced at a final concentration of 10 ng/ml and incubated for 4 hours. CFSE-stained K562 cells were introduced and cultured at 37 °C in a humidified atmosphere containing 5 % v/v CO₂ for a further 16 hours. Cells were counter-stained with 100 μ l propidium iodide (PI) for 15 minutes to assess cell viability and analysed using FACS, gated on CFSE-positive cells, then cell killing expressed as a percentage of PI+ to PI- cells. Data are a mean of triplicates from a single plate (\pm SD) and is representative of three different experiments, statistically analysed using a one way ANOVA and Tukey's multiple comparison post-test (* $p < 0.05$). B) Diagrammatic representation of the rationale behind the assay.

A similar trend to introducing Tregs was observed, where sTGF- β significantly suppressed NK cell killing from 67.5 % to 53.4 % ($p < 0.05$). nTGF- β RII antibody at 50 $\mu\text{g/ml}$ returns K562 cell killing to 68.5 % ($p < 0.05$). TGF- β specific antibodies have been shown to prevent suppression *in vitro* and CD25⁺ Treg are not able to suppress CD8⁺ cells lacking the TGF- β receptor (Chen et al., 2005). However the data presented here is inconsistent with previous studies that have suggested that only surface bound TGF- β is functional during attempts to transfer suppression on NK cell cytotoxicity by using the supernatants of activated Tregs (Smyth et al., 2006). The author would like to suggest that both membrane-tethered and close proximity sTGF- β are having a significant impact. Research suggests that Tregs are functioning in a TGF- β -dependent manner. Data are in agreement with research showing TGF- β 1 causes a strong down-regulation of the surface expression of NKp30 and inhibition of NK-mediated recognition and killing of DCs (Castriconi et al., 2003).

To specifically examine the effects of TGF- β on NKG2D expression, isolated CD56⁺ NK cells were cultured with a titration of sTGF- β and the NKG2D expression determined using FACS analysis (Figure 6.19).

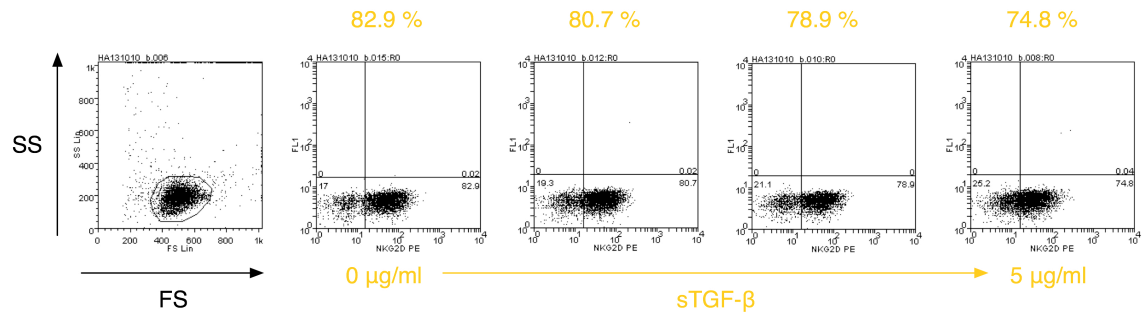


Figure 6.19 FACS Analysis of NKG2D Expression on Isolated NK Cells with increasing amounts of Soluble TGF- β

NK cells were isolated from 50 ml healthy human blood and 1×10^6 cells were removed for FACS analysis. Cells were pre-incubated with a titration of soluble TGF- β overnight. PE anti-NKG2D surface antibody was added before cells were fixed. Data were acquired on a Beckman Coulter FC 500 flow cytometer and analysed using Weasel software.

A reduction in NKG2D expression levels can be seen when NK cells were cultured with increasing amounts of sTGF- β (Figure 6.19). In comparison to previous research, the drop in NKG2D expression is relatively small. This could be due to differences in incubation times as previous studies have incubated isolated NK cells with sTGF- β for 7 days compared to the 4 or 16 hours investigated during this study (Castriconi et al., 2003).

Internal analysis of all the aforementioned cytokines would also be very interesting, and would provide an insight into their origin within the suppressive environment.

6.2.4. Evaluating TGF- β in CRC Liver Metastatic Patients

Previous studies have demonstrated an inverse linear relationship between plasma TGF- β 1 and the level of NKG2D on NK cells in lung cancer patients (Lee et al., 2004a).

Studies demonstrate that TGF- β -specific antibodies prevent suppression *in vitro* and Tregs are not able to suppress CD8⁺ cells that lack the TGF- β receptor (Chen et al., 2005). Due to the TGF- β -focused hypothesis within this study, it was decided to investigate the level of TGF- β in CRC liver metastatic patient blood (Figure 6.20).

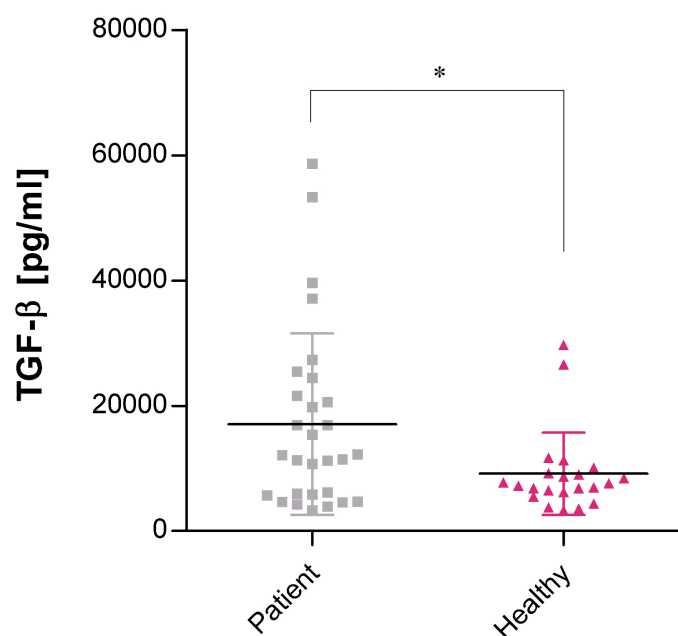


Figure 6.20 Concentration of Soluble TGF- β in Blood of CRC Liver Metastatic Patients Compared to Healthy Volunteers

The plasma from previous blood donors was analysed for the concentration of TGF- β using FlowCytomix™. Samples were firstly acidified prior to adding TGF- β specific beads. 20 μ l of biotin-conjugated secondary antibody was added, mixed and incubated for 2 hours. Samples were washed twice followed by addition of Streptavidin-PE, mixed and incubated for 1 hour. Finally, samples were washed prior to analysis on a Beckman Coulter FC 500 flow cytometer and data were analysed using FlowCytomix Pro 2.3 Software. Samples were compared against a standard curve (1:3) and were results evaluated using Prism® 5. Data were statistically analysed using an unpaired t test (\pm SD, * $p < 0.05$).

29 CRC liver metastatic patients had a mean sTGF- β concentration of 17.1 $\mu\text{g/ml}$ compared to a mean of 9.1 $\mu\text{g/ml}$ in healthy volunteers. Results suggest that CRC metastatic liver patients have higher levels of sTGF- β in their PB. Further analysis comparing the sTGF- β concentration to matched patient Tregs/ μl WB showed no significant correlation. The elevated levels of sTGF- β within the patient cohort can therefore not be explained by elevated numbers of circulating Tregs at this time; however, within a tumour site the cytokine profile is typically immunosuppressive and the level of TGF- β is likely to be elevated.

6.2.5. FACS Investigation of Tumour Markers

Engagement of NKG2D by its ligand (NKG2DL) results in activation of NK cell killing and cytokine secretion or co-stimulation of CTLs. NKG2D is a receptor for the stress-inducible and tumour-associated MHC class I chain-related proteins A (MICA) and B (MICB); and members of the cytomegalovirus UL16 binding proteins (ULBP) family ULBP1-4 and REA1G. NKG2DL are up-regulated in tumours which should render the tumour cells sensitive to NKG2D-dependent cell killing. MIC molecules are expressed in association with cell stress, infection or malignant transformation. *In vitro*, cell stress-inducible MIC molecules are expressed by many tumour cell lines and up-regulated upon infection with human *Escherichia coli* (Groh et al., 1999).

Here, nine cancer cell lines were analysed for their expression of MICA and ULBP-2 (Figure 6.21).

Control/ULBP-2/MICA

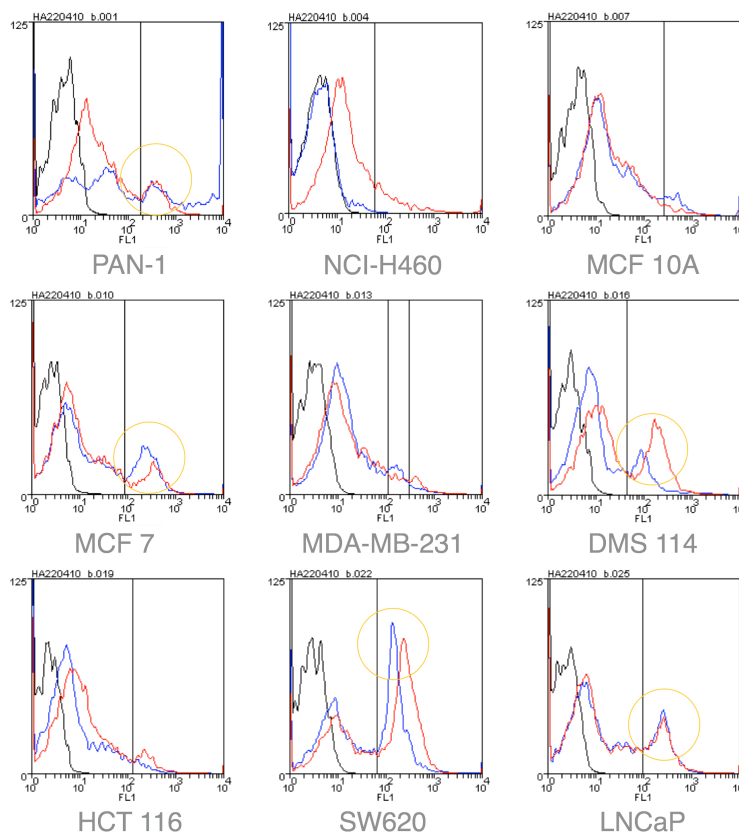


Figure 6.21 FACS Analysis Investigating the Expression of MICA and ULBP-2 on a Selection of Tumour Cell Lines

A suspension of 1×10^6 cells/ml was washed and blocked in PBS-BSA and then incubated with anti-MICA or anti-ULBP-2 at 25 μ g/ml for 30 minutes. Cells were washed twice before incubating for 30 minutes with secondary FITC antibody. MICA (blue) and ULBP-2 (red) expression was compared against a control of unstained cells for each cell line. Data were acquired on a Beckman Coulter FC 500 flow cytometer and analysed using Weasel software.

Data showed high levels of expression on SW-620 cells for both MICA and ULBP-2. PAN-1, MCF-7, DMS 114 and LNCaP also showed expression of these ligands to a lesser extent. It is interesting to observe that most cell lines have a mixed expressing population, perhaps indicative of ligand up/down-regulation at differing stages of the cell cycle.

Expression of NKG2DL on NK-resistant tumour lines has been shown to mediate tumour elimination (Cerwenka et al., 2000), and ectopic expression of NKG2D ligands causes rejection of tumour cells by NK and CTLs in syngeneic mice (Maccalli et al., 2009). This illustrates the relevance of NKG2D signalling in immunosurveillance against tumours. However, tumours have developed multiple ways to evade the NKG2D-mediated immune response. Literature illustrates that tumour cells release soluble MIC molecules to adjust to the NKG2D-mediated tumour immune surveillance (Groh et al., 1999). Tumour cells shed NKG2DL, resulting in increased levels in the peripheral blood of cancer patients.

6.3. CONCLUSIONS AND FUTURE WORK

6.3.1. Cell Killing Assay

The development of a reliable cell killing assay was an essential starting point for this chapter to provide the foundations for constructing a Treg:effector:NK cell suppression model. The K562 cell line provided a dependable tumour cell line, easily subjective to NK cell-mediated killing as they lacked the MHC complex required to

inhibit NK cell activity. This was in agreement with previous research demonstrating the ability of NK cells to kill MHC I-deficient tumour cell lines (Smyth et al., 2000). The replacement of PBMCs in preliminary studies with isolated NK cells and further introduction of Tregs was a fundamental requirement to begin to understand the interactions between Tregs and NK cells in the tumour environment. Tregs suppressed the cell killing ability of NK cells in agreement with *in vivo* studies showing Treg impairment of NK cell activation in cancer patients (Ghiringhelli et al., 2005). Both human and murine *in vitro* and *in vivo* systems have shown Tregs potently suppress NK cell responses, including the NK cell-mediated control of tumour expansion (Ghiringhelli et al., 2005).

6.3.2. Investigation of Model Key Players

Flow cytometer data confirmed the expression of NKG2D receptor on CD3⁻ NK and CD3⁺ NKT cell populations. The involvement of NKG2D in orchestrating NK cell-mediated tumour killing was tested *in vitro* using an nNKG2D antibody. High concentrations of the nNKG2D antibody significantly reduced NK cytotoxicity. In addition, cell surface expression of TGF- β RII on CD56⁺ NK cells was observed, which potentially makes them vulnerable to control by sTGF- β . This hypothesis was tested by introducing a nTGF- β RII antibody into a K562:NK:Treg cell killing assay to block TGF- β signalling. The suppressive ability of Tregs was abrogated with the addition of nTGF- β RII antibody. It was demonstrated that Tregs produce a small quantity of sTGF- β . Also, sTGF- β was shown to suppress NK cell-mediated killing of K562 cells, which was also recovered by nTGF- β RII antibody. Data illustrates

that under certain pathological conditions known to increase exposure to TGF- β , NK cells may under-express NKG2D. Signals from soluble or cell-associated TGF- β within a tumour microenvironment may result in suppression of NK cell-mediated killing, enabling tumour escape.

Results have contributed to further developments regarding the Treg-NK interactions at the tumour microenvironment (Figure 6.22).

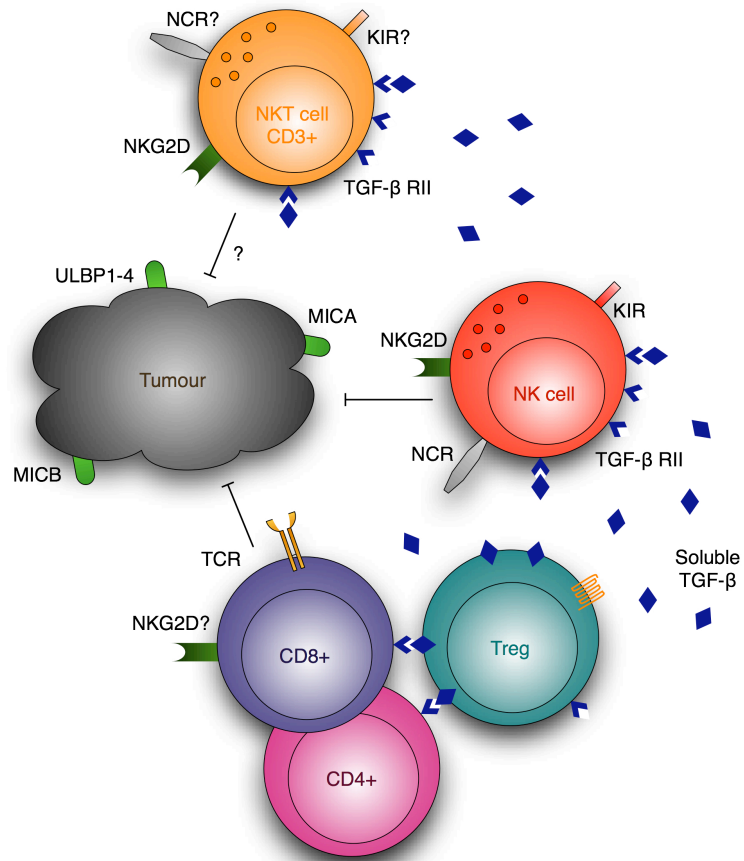


Figure 6.22 Further Developed Diagrammatic Representation of Treg Suppression of Natural Killer Cells and Tumour Interaction

Cell surface expression of tumour growth factor- β (TGF- β) on NK cells makes them vulnerable to control by soluble TGF- β . NK cell surface expression of TGF- β receptor II (TGF- β RII) functions to facilitate Treg mediated cell-contact dependent down-regulation of the NK cell-activating receptor NKG2D. Thus, Tregs are able to inhibit NK cell interaction with tumour ligands such as MHC class I chain-related proteins A (MICA) and B (MICB) and also members of the cytomegalovirus UL16 binding proteins (ULBP) family such as ULBP1-4 and REA1G, reducing cytotoxicity towards tumour targets.

6.3.3. Refined Hypothesis

The low frequency of NK cells found within the tumour, at the tumour IM and also within the tumour microenvironment illustrated in chapter 4, raised concerns with regards to developing a NK cell-mediated tumour-killing model. NK cells are an efficient tumour cell killing entity, therefore the work described in chapter 6 remains to be of significant value and could possibly contribute to further research, developing ways to increase NK cell presence at the tumour microenvironment and improve tumour cell death. However, the prevalence of CD8 CTLs within the tumour microenvironment did not go unnoticed. Without the time constraints of the current study, the author would refine the tumour model and begin to investigate the role and contribution of CD8 cells, in parallel to further developing NK cell directed research. Preliminary data have been accomplished, developing CD8 isolation techniques and investigating the expression of NKG2D (Figure 6.23).

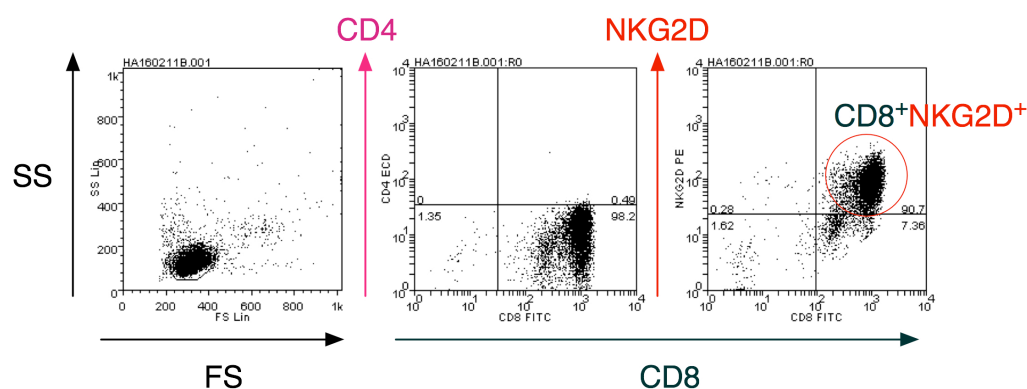


Figure 6.23 NKG2D FACS Analysis of Isolated CD8 Cells

CD8 cell isolation was achieved using an EasySep[®] Human CD8 Positive Selection Kit (EasySep[®], 18053) and carried out according to the manufacturer's instructions. CD8 cells were isolated from 50 ml healthy human blood and 1×10^6 cells were removed for FACS analysis. Cells were incubated with a pre-titrated volume of surface antibodies; PeCy5 anti-CD4, FITC anti-CD8 and PE anti-NKG2D. Cells were then fixed and data were acquired on a Beckman Coulter FC 500 flow cytometer and analysed using Weasel software.

CD8 cell isolation was successfully achieved from 50 ml of healthy blood as described in section 7.1.1. The EasySep® human CD8 positive selection kit is designed to isolate CD8⁺ cells and utilises tetrameric antibody complexes and dextran-coated magnetic particles combined with a human Fc receptor blocker to minimise non-specific binding. CD8⁺ cells were isolated to a 98.2 % purity, as evaluated using FACS analysis (Figure 6.23). Isolated CD8 cells were then assessed for the expression of NKG2D. Approximately 90.7 % of CD8⁺ cells were also positive for NKG2D receptor expression. These results are in agreement with previous FACS analysis of NKG2D expression on PBMCs showing a CD8⁺NKG2D⁺ cell population (Figure 6.8).

Further work investigated the effects of incubating isolated CD8 cells with a titration of sTGF- β (Figure 6.24).

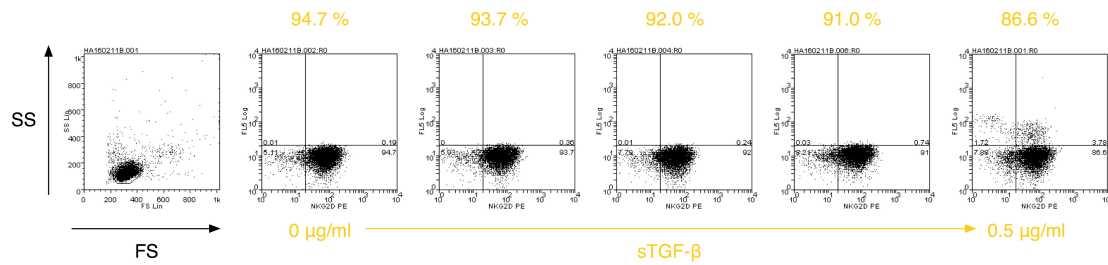


Figure 6.24 FACS Analysis of NKG2D Expression on Isolated CD8 Cells with increasing amounts of Soluble TGF- β

CD8 cell isolation was achieved using an EasySep® Human CD8 Positive Selection Kit (EasySep®, 18053) and carried out according to the manufacturer's instructions. CD8 cells were isolated from 50 ml healthy human blood and 1×10^6 cells were removed for FACS analysis. Cells were pre-incubated with a titration of soluble TGF- β overnight. PE anti-NKG2D surface antibody was added before cells were fixed. Data were acquired on a Beckman Coulter FC 500 flow cytometer and analysed using Weasel software.

As shown in Figure 6.24, isolated CD8 cells expressed lower levels of NKG2D receptor when pre-incubated with sTGF- β . In the absence of sTGF- β , approximately 94.7 % of CD8 cells expressed detectable levels of NKG2D. This value decreased when cells were incubated with a titration of sTGF- β , dropping to approximately 86.6 % at top concentrations of 0.5 μ g/ml. Results were similar to those seen when NK cells were incubated with sTGF- β (Figure 6.19).

Preliminary results demonstrate that CD8 cells express NKG2D and that this expression is susceptible to sTGF- β mediated down-regulation. Data are in agreement with previous literature demonstrating that NKR's can also be expressed by T cells (Correia et al., 2011). Studies have shown that CD8 cells can express both activating and inhibiting NKR's, including KIR members, NKG2D and NKp46. Thus, modifying T cell function could be possible by altering the TCR threshold by changing the expression of activating or inhibitory NKR's. Whilst little is known about the environmental signals that trigger NKR acquisition by CD8 cells, recent studies have suggested that IL-15 is a key player (Correia et al., 2011). CD8+CD56+ T cells cultured with IL-15 resulted in NK-like cytotoxicity. Meresse et al demonstrated that, in the presence of IL-15, CD8 cells acquired the ability to kill NKG2DL-bearing target cells (Meresse et al., 2004).

Is it possible that the presence of NKG2D receptor on effector cells of innate (NKs) and adaptive (CD8s) immune systems could link innate and adaptive immune responses? Over-expression of NKG2DL on tumour cells results in tumour

regression, perhaps by NK cell activation combined with a potent co-stimulatory signal to NKG2D expressing CD8 cells.

6.3.4. Future Work

Future work could involve working with a cytokine-induced killing (CIK) population. This involves culturing PBMCs with IL-1 α , anti-CD3, IFN- γ and IL-2 to push the cells towards a phenotypically cell killing population (Li et al., 2007). In addition, a variety of agents, generally referred to as biologic response modifiers, are known to increase the activation, proliferation, or cytotoxicity of NK cells, including IL-2, IL-12 and IFN- α . Cytokine-induced NK cell activation may be responsible for anti-tumour effectiveness of cytokine-based immunotherapy, possibly an area of future interest.

Expansion of a human-NK-92 cell line could also be investigated (Tam et al., 2003), with the idea to possibly replace freshly isolated NK cells and thus allow more elaborate assays, not restricted by limited cell numbers.

Additional research could include the use of cortisol, an adrenocortical hormone that suppresses the immune system and directly inhibits NK cell activity. Further to this, prolactin is an immunostimulatory hormone that has been shown to directly increase NK cell cytotoxicity (Mavoungou et al., 2005). It has been suggested that the increase in NK cell cytolytic activity observed after prolactin treatment correlates with an increase in surface expression of NCRs, including NKp30, NKp44 and

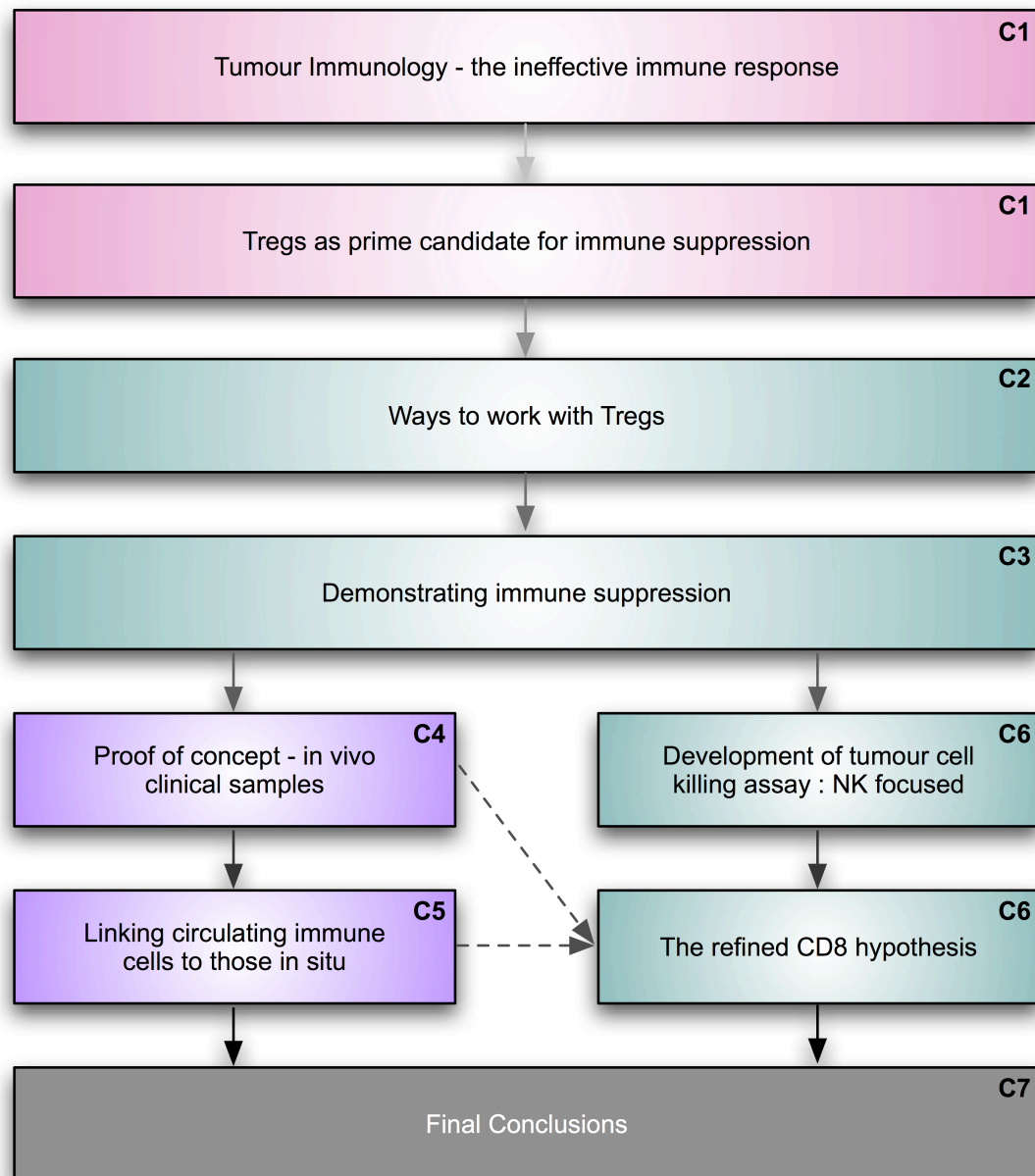
NKp46 (Mavoungou et al., 2005). Indoleamine 2,3-dioxygenase (IDO) is a powerful enzyme with suggested immunomodulatory effects. IDO-generated tryptophan-derived catabolites such as L-kynurenine have been reported to prevent up-regulation of NKp46 and NKG2D and therefore as a consequence impair NK cell killing activity (Della Chiesa et al., 2006). Further development and knowledge of the aforementioned hormones and enzymes could result in advances in NK cell-mediated anti-tumour therapies.

Literature suggests that tumour cells release soluble MIC molecules and shed NKG2D ligands in order to modulate and evade NKG2D-mediated tumour immune surveillance (Groh et al., 1999). As with the elevated levels of sTGF- β in CRC liver metastatic patients, it would be interesting to investigate whether a difference is observed in the concentration of MICA or ULBP2 present in circulating peripheral blood.

***Summary:** The development of an in vitro human Treg suppression model, investigating NK cell tumour killing, could be used to improve knowledge of tumour microenvironment and suppression of anti-tumour immunity. Preliminary studies have developed a cell-killing assay and shown that K562 cells are susceptible to cell killing by NK and possibly CD8 cells.*

CHAPTER 7 – FINAL CONCLUSIONS

Chronological Framework of Thesis Progression



■ Literature ■ In vitro ■ Ex vivo **C1** Chapter 1

Construction of a realistic ex vivo model was achieved in chapter 6, where research was carried out in parallel with chapters 4 and 5. The current chapter aims to draw final conclusions and closing remarks.

7.1. FINAL CONCLUSIONS

During the preparation of this thesis, Hanahan and Weinberg published an updated version of their iconic ‘Hallmarks of Cancer’ (Hanahan and Weinberg, 2011). The next generation and emerging hallmarks include ‘avoiding immune destruction’ and ‘tumour-promoting inflammation’. The importance of the immune system in perhaps all cancers is becoming readily acknowledged. The ability of the immune system to inadvertently support other cancer-promoting hallmarks, resulting in tumour-promoting consequences of inflammatory responses, is becoming widely appreciated (Cavallo et al., 2011).

Compelling evidence suggests that inflammation can have a counterintuitive effect on all phases of carcinogenesis. For example: inducing DNA instability and mutation in tumour-initiating cells; supplying growth factors to sustain tumour proliferation; releasing survival factors that limit tumour cell death; proangiogenic factors; ECM-modifying molecules to facilitate angiogenesis, invasion and metastasis; and inductive signals that initiate EMT. In addition to the infiltrating pro-inflammatory immune cells, other cell types, including epithelial cells, endothelial cells, fibroblasts, and stromal cells, may play a role in contributing to the inflammation by secreting and responding to pro-inflammatory factors such as the aforementioned cytokines, chemokines, growth factors, and proteases.

The concept that inflammation is associated with neoplasia was first proposed by Rudolff Virchow in 1863. Centuries later, a wealth of evidence has accumulated to support the hypothesis that organs subjected to chronic inflammation can provide the perfect milieu in which tumours thrive. There is now a general consensus that inflammation and immune cells play a critical role in tumorigenesis. Reprogramming of the immune microenvironment in tumours is a promising strategy for improving the efficacy of standard anticancer treatments.

It is now widely acknowledged that inhibiting Treg function in cancer patients may contribute to the success of new therapies, specifically immunotherapies (Colombo and Piconese, 2007). Evidence suggests that depleting Tregs leads to rejection of transplanted tumours in mouse models (Shimizu et al., 1999).

The current study has investigated ways to work with Tregs, looking at their isolation procedure, mechanisms of suppression and possible methods for expansion. The involvement of Tregs at the tumour microenvironment was studied within clinical colorectal cancer samples. Data have confirmed the importance of immune infiltrates in and around the tumour. A novel method of image analysis was implemented and facilitated quick and objective immune cell quantification in precise tumour- and stroma-rich regions. This detailed analysis has alluded to a CD8-low Treg-high liver metastatic phenotype within primary CRC tissue. Such a powerful image analysis platform could potentially revolutionise traditional pathological techniques, whereby the TNM staging system could be replaced with an immune score as a more accurate

indicator of patient prognosis. In addition, correlations have been made between circulating immune cells in peripheral blood and those seen *in situ*.

Finally, the mechanism by which NK (and CD8) cells are prevented from orchestrating tumour cell killing has been proposed. The importance of TGF- β has been highlighted where Tregs can suppress NK cell-mediated tumour cell killing via down regulation of NKG2D receptor expression. An understanding of this mechanism could provide potential therapeutic targets in an immunotherapy directed strategy.

A final diagrammatic summary of the current study is depicted in Figure 7.1.

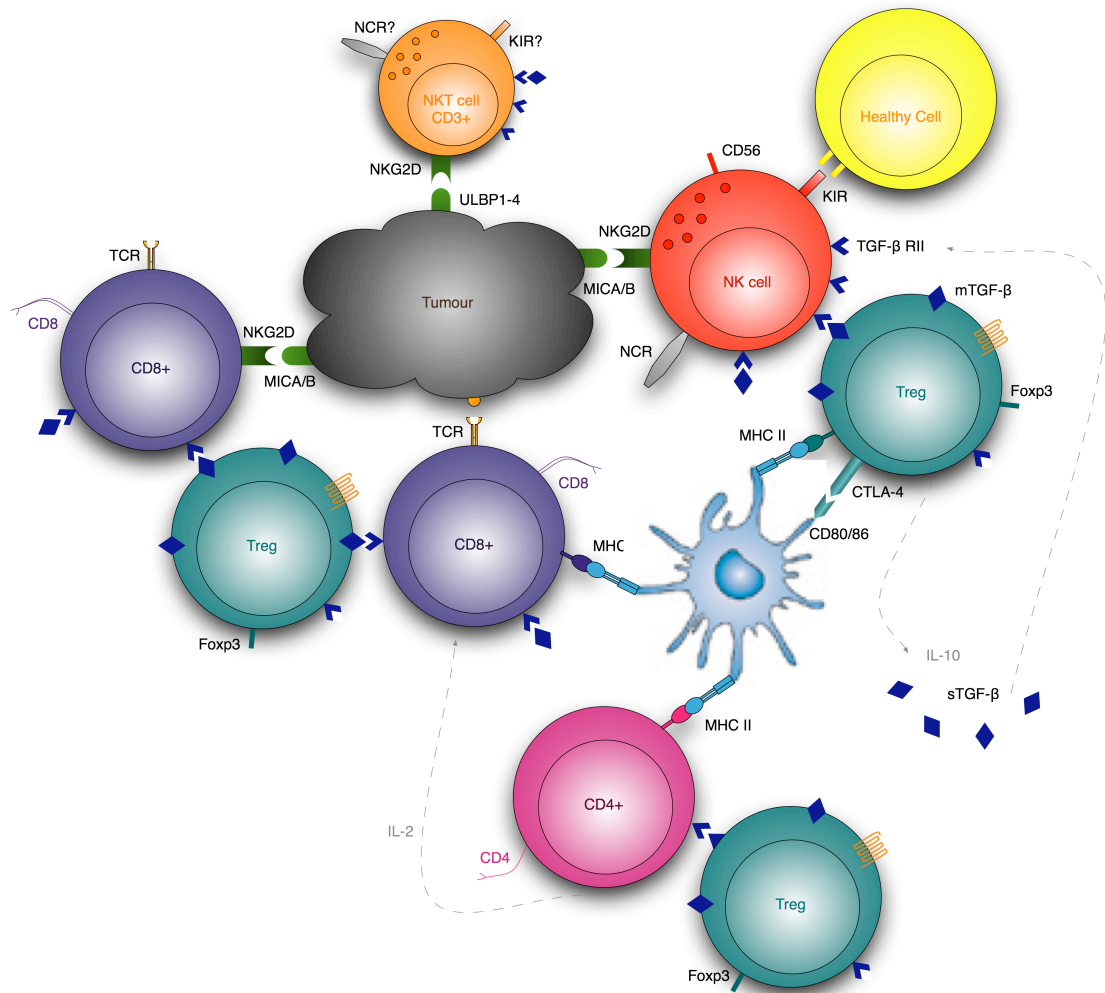


Figure 7.1 Concluding Diagrammatic Representation of Immune Cell Interactions within the Tumour Microenvironment

Cell-surface expression of tumour growth factor- β receptor II (TGF- β RII) on natural killer (NK), natural killer T (NKT) and CD8 cells, makes them vulnerable to control by soluble TGF- β (sTGF- β). In addition, this could facilitate Treg-mediated cell-contact dependent down-regulation of NKG2D receptor. Thus, Tregs are able to inhibit NK cell and CD8 cell interactions with tumour ligands such as MHC class I chain-related proteins A (MICA) and B (MICB) and also members of the cytomegalovirus UL16 binding proteins (ULBP) family such as ULBP1-4 and REA1G, reducing cytotoxicity towards tumour targets. (TCR, T cell receptor; KIR, killer cell immunoglobulin-like receptor; NCR, natural cytotoxicity receptor; mTGF- β RII, membrane-tethered transforming growth factor- β receptor II).

Overall a detailed understanding of the host immune system and tumour cells has been achieved, which will facilitate the advancement of future anti-cancer focused research. The development of this current model could therefore provide a platform to screen possible Treg targets. Initial studies could use siRNA and then progress to an antibody-directed therapeutic approach. This compilation of assays would provide a platform to validate lead antibodies produced against the selected Treg target.

CHAPTER 8 – APPENDIX

8.1. ACHIEVEMENTS

8.1.1. Papers In Preparation

Title TBC, similar to: Elevated stromal Foxp3⁺ regulatory T cells combined with low density CD8⁺ cytotoxic T cells are associated with colorectal metastatic tumour progression. H.K. Angell, X. Huan, S. Mistry, M. Cumberbatch, N. Gray, C. Womack, S.A. Watson, R.W. Wilkinson, D.I. Pritchard. To be submitted to: TBC

Title TBC. H.K. Angell, X. Huan, S. Mistry, M. Cumberbatch, N. Gray, C. Womack, S.A. Watson, R.W. Wilkinson, D.I. Pritchard. To be submitted to: TBC.

Title TBC, similar to: Foxp3⁺ regulatory T cells suppress CD56⁺ natural killer cell-mediated tumour killing in a transforming growth factor- β dependent manner. H.K. Angell, S.A. Watson, R.W. Wilkinson, D.I. Pritchard. To be submitted to: TBC.

8.1.2. Published Abstracts

Blood Sweat and Tregs. Angell H, Blount DG, Watson SA, Wilkinson RW, Pritchard DI. Journal of Pharmacy and Pharmacology 62(10): 1491-1492.

Immunological Regulation in the Tumour Microenvironment. Angell H, Blount DG, Watson SA, Wilkinson RW, Pritchard DI. Journal of Pharmacy and Pharmacology 62(10): 1221-1222.

Blood Sweat and Tregs: Immunological regulation in the tumour microenvironment. Angell H, Blount D, Watson S, Wilkinson R, Pritchard D. Immunology 131(suppl. 1):58.

8.1.3. Oral Presentations

Accepted at NCRI Cancer Conference, 2011, Liverpool

Elevated stromal Foxp3⁺ regulatory T cells combined with low density CD8⁺ cytotoxic T cells are associated with colorectal metastatic tumour progression. H.K. Angell, X. Huan, S. Mistry M. Cumberbatch, N. Gray, C. Womack, S.A. Watson, D.I. Pritchard, R.W. Wilkinson.

UKPharmSci Conference, Nottingham

Immunological Regulation in the Tumour Microenvironment. [Angell H](#), Blount DG, Watson SA, Wilkinson RW, Pritchard DI.

UKPharmSci Conference, Nottingham

Blood Sweat and Tregs. [Angell H](#), Blount DG, Watson SA, Wilkinson RW, Pritchard DI.

8.1.4. Awards

- **Richard Hambro Award, NCRI 2011**
- **AstraZeneca Scientific Innovations Award 2011**
- **NCRI Cancer conference, Liverpool**; National Cancer Research Institute 'Passport and Networking' prize 2010.

8.1.5. Posters

British Association of Cancer Research/ The Royal Society of Medicine, London

Immunological Regulation in the Tumour Environment. [Angell H](#), Blount DG, Watson SA, Grabowska AM, Wilkinson RW, Pritchard DI.

Bioengineering and Synthetic Biology, Oxford

Injectable hyperbranched materials with thermal-responsive and photocrosslinkable properties for tissue engineering applications. Tai H, Wang W, Birkin N, Howard D, [Angell H](#), Heath F, Endruweit A, Rose F, Alexander C, Shakesheff K, Howdle S.

The EACR Special Conference; Inflammation and Cancer, Berlin

Immunological Regulation in the Tumour Environment. [Angell HK](#), Blount DG, Watson SA, Grabowska AM, Wilkinson RW, Pritchard DI.

UKPharmSci Conference, Nottingham

Blood Sweat and Tregs: Immunological Regulation in the Tumour Microenvironment II. [Angell H](#), Blount DG, Watson SA, Wilkinson RW, Pritchard DI.

UKPharmSci Conference, Nottingham

Immunological Regulation in the Tumour Microenvironment. Angell H, Blount DG, Watson SA, Wilkinson RW, Pritchard DI.

NCRI Cancer Conference, Liverpool

Blood Sweat and Tregs: Immunological Regulation in the Tumour Microenvironment II. Angell H, Blount DG, Watson SA, Wilkinson RW Pritchard DI.

BSI Annual C

ongress, Liverpool

Blood Sweat and Tregs: Immunological Regulation in the Tumour Microenvironment II. Angell H, Blount DG, Watson SA, Wilkinson RW Pritchard DI.

Accepted at NCRI Cancer Conference, 2011, Liverpool

Elevated stromal Foxp3+ regulatory T cells combined with low density CD8+ cytotoxic T cells are associated with colorectal metastatic tumour progression. H.K. Angell, X. Huan, S. Mistry, M. Cumberbatch, N. Gray, C. Womack, S.A. Watson, D.I. Pritchard, R.W. Wilkinson.

Accepted at NCRI Cancer Conference, 2011, Liverpool

Foxp3+ regulatory T cells suppress CD56+ natural killer cell-mediated tumour killing in a transforming growth factor- β dependent manner. H.K. Angell, S.A. Watson, R.W. Wilkinson, D.I. Pritchard.

Accepted at NCRI Cancer Conference, 2011, Liverpool

Quantitative assessment of tumour infiltrating lymphocytes using GenieTM pattern recognition software for the separate analysis of tumour versus stroma in head and neck squamous cell carcinoma (HNSCC) improves biomarker reproducibility. X. H. Yap, H. K. Angell, N. Gray, C. Womack, R. W. Wilkinson, M. Cumberbatch.

8.2. REFERENCES

- Allavena, P., A. Sica, C. Garlanda, and A. Mantovani. 2008. The Yin-Yang of tumor-associated macrophages in neoplastic progression and immune surveillance. *Immunol Rev.* 222:155-61.
- Anderberg, C., H. Li, L. Fredriksson, J. Andrae, C. Betsholtz, X. Li, U. Eriksson, and K. Pietras. 2009. Paracrine signaling by platelet-derived growth factor-CC promotes tumor growth by recruitment of cancer-associated fibroblasts. *Cancer Res.* 69:369-78.
- Antons, A.K., R. Wang, K. Oswald-Richter, M. Tseng, C.W. Arendt, S.A. Kalams, and D. Unutmaz. 2008. Naive precursors of human regulatory T cells require FoxP3 for suppression and are susceptible to HIV infection. *J Immunol.* 180:764-73.
- Apostolou, I., and H. von Boehmer. 2004. In vivo instruction of suppressor commitment in naive T cells. *J Exp Med.* 199:1401-8.
- Baecher-Allan, C., J.A. Brown, G.J. Freeman, and D.A. Hafler. 2001. CD4+CD25^{high} regulatory cells in human peripheral blood. *J Immunol.* 167:1245-53.
- Baecher-Allan, C., and D.A. Hafler. 2006. Human regulatory T cells and their role in autoimmune disease. *Immunol Rev.* 212:203-16.
- Baecher-Allan, C., E. Wolf, and D.A. Hafler. 2006. MHC class II expression identifies functionally distinct human regulatory T cells. *J Immunol.* 176:4622-31.
- Battaglia, M., A. Stabilini, B. Migliavacca, J. Horejs-Hoeck, T. Kaupper, and M.G. Roncarolo. 2006. Rapamycin promotes expansion of functional CD4+CD25+FOXP3+ regulatory T cells of both healthy subjects and type 1 diabetic patients. *J Immunol.* 177:8338-47.
- Beyer, M., and J.L. Schultze. 2006. Regulatory T cells in cancer. *Blood.* 108:804-11.
- Bhowmick, N.A., E.G. Neilson, and H.L. Moses. 2004. Stromal fibroblasts in cancer initiation and progression. *Nature.* 432:332-7.
- Bluestone, J.A., and A.K. Abbas. 2003. Natural versus adaptive regulatory T cells. *Nat Rev Immunol.* 3:253-7.
- Bresatz, S., T. Sadlon, D. Millard, H. Zola, and S.C. Barry. 2007. Isolation, propagation and characterization of cord blood derived CD4⁺ CD25⁺ regulatory T cells. *J Immunol Methods.* 327:53-62.
- Brown, D.C., and K.C. Gatter. 2002. Ki67 protein: the immaculate deception? *Histopathology.* 40:2-11.
- Bui, J.D., R. Uppaluri, C.S. Hsieh, and R.D. Schreiber. 2006. Comparative analysis of regulatory and effector T cells in progressively growing versus rejecting tumors of similar origins. *Cancer Res.* 66:7301-9.

- Byeon, S.E., W.S. Choi, E.K. Hong, J. Lee, M.H. Rhee, H.J. Park, and J.Y. Cho. 2009. Inhibitory effect of saponin fraction from *Codonopsis lanceolata* on immune cell-mediated inflammatory responses. *Arch Pharm Res.* 32:813-22.
- Camps, J.L., S.M. Chang, T.C. Hsu, M.R. Freeman, S.J. Hong, H.E. Zhau, A.C. von Eschenbach, and L.W. Chung. 1990. Fibroblast-mediated acceleration of human epithelial tumor growth in vivo. *Proc Natl Acad Sci U S A.* 87:75-9.
- Camus, M., M. Tosolini, B. Mlecnik, F. Pages, A. Kirilovsky, A. Berger, A. Costes, G. Bindea, P. Charoentong, P. Bruneval, Z. Trajanoski, W.H. Fridman, and J. Galon. 2009. Coordination of intratumoral immune reaction and human colorectal cancer recurrence. *Cancer Res.* 69:2685-93.
- Castriconi, R., C. Cantoni, M. Della Chiesa, M. Vitale, E. Marcenaro, R. Conte, R. Biassoni, C. Bottino, L. Moretta, and A. Moretta. 2003. Transforming growth factor beta 1 inhibits expression of NKp30 and NKG2D receptors: consequences for the NK-mediated killing of dendritic cells. *Proc Natl Acad Sci U S A.* 100:4120-5.
- Cavallo, F., C. De Giovanni, P. Nanni, G. Forni, and P.L. Lollini. 2011. 2011: the immune hallmarks of cancer. *Cancer Immunol Immunother.* 60:319-26.
- Cerwenka, A., A.B. Bakker, T. McClanahan, J. Wagner, J. Wu, J.H. Phillips, and L.L. Lanier. 2000. Retinoic acid early inducible genes define a ligand family for the activating NKG2D receptor in mice. *Immunity.* 12:721-7.
- Chen, M.L., M.J. Pittet, L. Gorelik, R.A. Flavell, R. Weissleder, H. von Boehmer, and K. Khazaie. 2005. Regulatory T cells suppress tumor-specific CD8 T cell cytotoxicity through TGF-beta signals in vivo. *Proc Natl Acad Sci U S A.* 102:419-24.
- Colombo, M.P., and S. Piconese. 2007. Regulatory-T-cell inhibition versus depletion: the right choice in cancer immunotherapy. *Nat Rev Cancer.* 7:880-7.
- Correia, M.P., A.V. Costa, M. Uhrberg, E.M. Cardoso, and F.A. Arosa. 2011. IL-15 induces CD8+ T cells to acquire functional NK receptors capable of modulating cytotoxicity and cytokine secretion. *Immunobiology.* 216:604-12.
- Coussens, L.M., and Z. Werb. 2002. Inflammation and cancer. *Nature.* 420:860-7.
- Curiel, T.J., G. Coukos, L. Zou, X. Alvarez, P. Cheng, P. Mottram, M. Evdemon-Hogan, J.R. Conejo-Garcia, L. Zhang, M. Burow, Y. Zhu, S. Wei, I. Kryczek, B. Daniel, A. Gordon, L. Myers, A. Lackner, M.L. Disis, K.L. Knutson, L. Chen, and W. Zou. 2004. Specific recruitment of regulatory T cells in ovarian carcinoma fosters immune privilege and predicts reduced survival. *Nat Med.* 10:942-9.
- de la Rosa, M., S. Rutz, H. Dorninger, and A. Scheffold. 2004. Interleukin-2 is essential for CD4+CD25+ regulatory T cell function. *Eur J Immunol.* 34:2480-8.
- Della Chiesa, M., S. Carlomagno, G. Frumento, M. Balsamo, C. Cantoni, R. Conte, L. Moretta, A. Moretta, and M. Vitale. 2006. The tryptophan catabolite L-kynurenine

- inhibits the surface expression of NKp46- and NKG2D-activating receptors and regulates NK-cell function. *Blood*. 108:4118-25.
- DeNardo, D.G., D.J. Brennan, E. Rexhepaj, B. Ruffell, S.L. Shiao, S.F. Madden, W.M. Gallagher, N. Wadhwani, S.D. Keil, S.A. Junaid, H.S. Rugo, E. Hwang, K. Jirstrom, B.L. West, and L.M. Coussens. 2011. Leukocyte Complexity Predicts Breast Cancer Survival and Functionally Regulates Response to Chemotherapy. *Cancer Discovery*. 1:OF52-OF65.
- Dewhirst, M.W. 2009. Relationships between cycling hypoxia, HIF-1, angiogenesis and oxidative stress. *Radiat Res*. 172:653-65.
- Dewhirst, M.W., Y. Cao, and B. Moeller. 2008. Cycling hypoxia and free radicals regulate angiogenesis and radiotherapy response. *Nat Rev Cancer*. 8:425-37.
- Dunn, G.P., A.T. Bruce, H. Ikeda, L.J. Old, and R.D. Schreiber. 2002. Cancer immunoediting: from immunosurveillance to tumor escape. *Nat Immunol*. 3:991-8.
- Dvorak, H.F. 1986. Tumors: wounds that do not heal. Similarities between tumor stroma generation and wound healing. *N Engl J Med*. 315:1650-9.
- Erez, N., M. Truitt, P. Olson, S.T. Arron, and D. Hanahan. 2010. Cancer-Associated Fibroblasts Are Activated in Incipient Neoplasia to Orchestrate Tumor-Promoting Inflammation in an NF-kappaB-Dependent Manner. *Cancer Cell*. 17:135-47.
- Fearon, E.R., and B. Vogelstein. 1990. A genetic model for colorectal tumorigenesis. *Cell*. 61:759-67.
- Ferrara, N. 2002. VEGF and the quest for tumour angiogenesis factors. *Nat Rev Cancer*. 2:795-803.
- Figuerola-Tentori, D., S. Querol, I.A. Dodi, A. Madrigal, and R. Duggleby. 2008. High purity and yield of natural Tregs from cord blood using a single step selection method. *J Immunol Methods*. 339:228-35.
- Fontenot, J.D., M.A. Gavin, and A.Y. Rudensky. 2003. Foxp3 programs the development and function of CD4+CD25+ regulatory T cells. *Nat Immunol*. 4:330-6.
- Fridman, W.H., J. Galon, F. Pages, E. Tartour, C. Sautes-Fridman, and G. Kroemer. 2011. Prognostic and predictive impact of intra- and peritumoral immune infiltrates. *Cancer Res*. 71:5601-5.
- Frisch, S.M., and R.A. Screaton. 2001. Anoikis mechanisms. *Curr Opin Cell Biol*. 13:555-62.
- Fu, J., D. Xu, Z. Liu, M. Shi, P. Zhao, B. Fu, Z. Zhang, H. Yang, H. Zhang, C. Zhou, J. Yao, L. Jin, H. Wang, Y. Yang, Y.X. Fu, and F.S. Wang. 2007. Increased regulatory T cells correlate with CD8 T-cell impairment and poor survival in hepatocellular carcinoma patients. *Gastroenterology*. 132:2328-39.
- Galon, J., A. Costes, F. Sanchez-Cabo, A. Kirilovsky, B. Mlecnik, C. Lagorce-Pages, M. Tosolini, M. Camus, A. Berger, P. Wind, F. Zinzindohoue, P. Bruneval, P.H. Cugnenc, Z. Trajanoski, W.H. Fridman, and F. Pages. 2006. Type, density, and

- location of immune cells within human colorectal tumors predict clinical outcome. *Science*. 313:1960-4.
- Galon, J., W.H. Fridman, and F. Pages. 2007. The adaptive immunologic microenvironment in colorectal cancer: a novel perspective. *Cancer Res*. 67:1883-6.
- Gershon, R.K., R.L. Carter, and K. Kondo. 1967. On concomitant immunity in tumour-bearing hamsters. *Nature*. 213:674-6.
- Gershon, R.K., and K. Kondo. 1971. Infectious immunological tolerance. *Immunology*. 21:903-14.
- Ghiringhelli, F., C. Menard, F. Martin, and L. Zitvogel. 2006. The role of regulatory T cells in the control of natural killer cells: relevance during tumor progression. *Immunol Rev*. 214:229-38.
- Ghiringhelli, F., C. Menard, M. Terme, C. Flament, J. Taieb, N. Chaput, P.E. Puig, S. Novault, B. Escudier, E. Vivier, A. Lecesne, C. Robert, J.Y. Blay, J. Bernard, S. Caillat-Zucman, A. Freitas, T. Tursz, O. Wagner-Ballon, C. Capron, W. Vainchenker, F. Martin, and L. Zitvogel. 2005. CD4+CD25+ regulatory T cells inhibit natural killer cell functions in a transforming growth factor-beta-dependent manner. *J Exp Med*. 202:1075-85.
- Gilboa, E. 1999. How tumors escape immune destruction and what we can do about it. *Cancer Immunol Immunother*. 48:382-5.
- Gobert, M., I. Treilleux, N. Bendriss-Vermare, T. Bachelot, S. Goddard-Leon, V. Arfi, C. Biota, A.C. Doffin, I. Durand, D. Olive, S. Perez, N. Pasqual, C. Faure, I. Ray-Coquard, A. Puisieux, C. Caux, J.Y. Blay, and C. Menetrier-Caux. 2009. Regulatory T cells recruited through CCL22/CCR4 are selectively activated in lymphoid infiltrates surrounding primary breast tumors and lead to an adverse clinical outcome. *Cancer Res*. 69:2000-9.
- Grimm, M., M. Kim, A. Rosenwald, B. von Rahden, I. Tsaur, E. Meier, U. Heemann, C.T. Germer, M. Gasser, and A.M. Waaga-Gasser. 2010a. Tumour-mediated TRAIL-Receptor expression indicates effective apoptotic depletion of infiltrating CD8+ immune cells in clinical colorectal cancer. *Eur J Cancer*. 46:2314-23.
- Grimm, M., M. Lazariotou, S. Kircher, A. Hofelmayr, C.T. Germer, B.H. von Rahden, A.M. Waaga-Gasser, and M. Gasser. 2010b. Tumor necrosis factor-alpha is associated with positive lymph node status in patients with recurrence of colorectal cancer - indications for anti-TNF-alpha agents in cancer treatment. *Anal Cell Pathol (Amst)*. 33:151-63.
- Groh, V., R. Rhinehart, H. Secrist, S. Bauer, K.H. Grabstein, and T. Spies. 1999. Broad tumor-associated expression and recognition by tumor-derived gamma delta T cells of MICA and MICB. *Proc Natl Acad Sci U S A*. 96:6879-84.

- Groh, V., J. Wu, C. Yee, and T. Spies. 2002. Tumour-derived soluble MIC ligands impair expression of NKG2D and T-cell activation. *Nature*. 419:734-8.
- Grum-Schwensen, B., J. Klingelhofer, M. Grigorian, K. Almholt, B.S. Nielsen, E. Lukanidin, and N. Ambartsumian. 2010. Lung metastasis fails in MMTV-PyMT oncomice lacking S100A4 due to a T-cell deficiency in primary tumors. *Cancer Res*. 70:936-47.
- Guerra, N., Y.X. Tan, N.T. Joncker, A. Choy, F. Gallardo, N. Xiong, S. Knoblaugh, D. Cado, N.M. Greenberg, and D.H. Raulet. 2008. NKG2D-deficient mice are defective in tumor surveillance in models of spontaneous malignancy. *Immunity*. 28:571-80.
- Hanahan, D., and R.A. Weinberg. 2000. The hallmarks of cancer. *Cell*. 100:57-70.
- Hanahan, D., and R.A. Weinberg. 2011. Hallmarks of cancer: the next generation. *Cell*. 144:646-74.
- Huang, X., J. Zhu, and Y. Yang. 2005. Protection against autoimmunity in nonlymphopenic hosts by CD4⁺ CD25⁺ regulatory T cells is antigen-specific and requires IL-10 and TGF-beta. *J Immunol*. 175:4283-91.
- Hus, I., E. Staroslawska, A. Bojarska-Junak, A. Dobrzynska-Rutkowska, A. Surdacka, P. Wdowiak, M. Wasiak, M. Kusz, A. Twardosz, A. Dmoszynska, and J. Rolinski. 2011. CD3(+)/CD16(+)/CD56(+) cell numbers in peripheral blood are correlated with higher tumor burden in patients with diffuse large B-cell lymphoma. *Folia Histochem Cytobiol*. 49:183-7.
- Imai, T., M. Nagira, S. Takagi, M. Kakizaki, M. Nishimura, J. Wang, P.W. Gray, K. Matsushima, and O. Yoshie. 1999. Selective recruitment of CCR4-bearing Th2 cells toward antigen-presenting cells by the CC chemokines thymus and activation-regulated chemokine and macrophage-derived chemokine. *Int Immunol*. 11:81-8.
- Ishida, T., and R. Ueda. 2006. CCR4 as a novel molecular target for immunotherapy of cancer. *Cancer Sci*. 97:1139-46.
- Itoh, M., T. Takahashi, N. Sakaguchi, Y. Kuniyasu, J. Shimizu, F. Otsuka, and S. Sakaguchi. 1999. Thymus and autoimmunity: production of CD25⁺CD4⁺ naturally anergic and suppressive T cells as a key function of the thymus in maintaining immunologic self-tolerance. *J Immunol*. 162:5317-26.
- Kasproicz, D.J., P.S. Smallwood, A.J. Tzgnik, and S.F. Ziegler. 2003. Scurfin (FoxP3) controls T-dependent immune responses in vivo through regulation of CD4⁺ T cell effector function. *J Immunol*. 171:1216-23.
- Kiessling, R., E. Klein, H. Pross, and H. Wigzell. 1975. "Natural" killer cells in the mouse. II. Cytotoxic cells with specificity for mouse Moloney leukemia cells. Characteristics of the killer cell. *Eur J Immunol*. 5:117-21.
- Kim, S., K. Iizuka, H.L. Aguila, I.L. Weissman, and W.M. Yokoyama. 2000. In vivo natural killer cell activities revealed by natural killer cell-deficient mice. *Proc Natl Acad Sci U S A*. 97:2731-6.

- Klein, E., H. Ben-Bassat, H. Neumann, P. Ralph, J. Zeuthen, A. Polliack, and F. Vanky. 1976. Properties of the K562 cell line, derived from a patient with chronic myeloid leukemia. *Int J Cancer*. 18:421-31.
- Kobayashi, N. 1985. Malignant neoplasms in registered cases of primary immunodeficiency syndrome. *Jpn J Clin Oncol*. 15 Suppl 1:307-12.
- Kobayashi, N., N. Hiraoka, W. Yamagami, H. Ojima, Y. Kanai, T. Kosuge, A. Nakajima, and S. Hirohashi. 2007. FOXP3+ regulatory T cells affect the development and progression of hepatocarcinogenesis. *Clin Cancer Res*. 13:902-11.
- Koyama, S., N. Koike, and S. Adachi. 2002. Expression of TNF-related apoptosis-inducing ligand (TRAIL) and its receptors in gastric carcinoma and tumor-infiltrating lymphocytes: a possible mechanism of immune evasion of the tumor. *J Cancer Res Clin Oncol*. 128:73-9.
- Kuniyasu, Y., T. Takahashi, M. Itoh, J. Shimizu, G. Toda, and S. Sakaguchi. 2000. Naturally anergic and suppressive CD25(+)CD4(+) T cells as a functionally and phenotypically distinct immunoregulatory T cell subpopulation. *Int Immunol*. 12:1145-55.
- Ladoire, S., F. Martin, and F. Ghiringhelli. 2011a. Prognostic role of FOXP3+ regulatory T cells infiltrating human carcinomas: the paradox of colorectal cancer. *Cancer Immunol Immunother*.
- Ladoire, S., G. Mignot, S. Dabakuyo, L. Arnould, L. Apetoh, C. Rebe, B. Coudert, F. Martin, M.H. Bizollon, A. Vanoli, C. Coutant, P. Fumoleau, F. Bonnetain, and F. Ghiringhelli. 2011b. In situ immune response after neoadjuvant chemotherapy for breast cancer predicts survival. *J Pathol*. 224:389-400.
- LeBedis, C., K. Chen, L. Fallavollita, T. Boutros, and P. Brodt. 2002. Peripheral lymph node stromal cells can promote growth and tumorigenicity of breast carcinoma cells through the release of IGF-I and EGF. *Int J Cancer*. 100:2-8.
- Lee, J.C., K.M. Lee, D.W. Kim, and D.S. Heo. 2004a. Elevated TGF-beta1 secretion and down-modulation of NKG2D underlies impaired NK cytotoxicity in cancer patients. *J Immunol*. 172:7335-40.
- Lee, M.K.t., D.J. Moore, B.P. Jarrett, M.M. Lian, S. Deng, X. Huang, J.W. Markmann, M. Chiaccio, C.F. Barker, A.J. Caton, and J.F. Markmann. 2004b. Promotion of allograft survival by CD4+CD25+ regulatory T cells: evidence for in vivo inhibition of effector cell proliferation. *J Immunol*. 172:6539-44.
- Levental, K.R., H. Yu, L. Kass, J.N. Lakins, M. Egeblad, J.T. Erler, S.F. Fong, K. Csiszar, A. Giaccia, W. Weninger, M. Yamauchi, D.L. Gasser, and V.M. Weaver. 2009. Matrix crosslinking forces tumor progression by enhancing integrin signaling. *Cell*. 139:891-906.

- Levings, M.K., R. Sangregorio, and M.G. Roncarolo. 2001. Human cd25(+)cd4(+) t regulatory cells suppress naive and memory T cell proliferation and can be expanded in vitro without loss of function. *J Exp Med.* 193:1295-302.
- Li, H., J.P. Yu, S. Cao, F. Wei, P. Zhang, X.M. An, Z.T. Huang, and X.B. Ren. 2007. CD4 +CD25 + regulatory T cells decreased the antitumor activity of cytokine-induced killer (CIK) cells of lung cancer patients. *J Clin Immunol.* 27:317-26.
- Liao, D., Y. Luo, D. Markowitz, R. Xiang, and R.A. Reisfeld. 2009. Cancer associated fibroblasts promote tumor growth and metastasis by modulating the tumor immune microenvironment in a 4T1 murine breast cancer model. *PLoS One.* 4:e7965.
- Lin, E.Y., J.F. Li, G. Bricard, W. Wang, Y. Deng, R. Sellers, S.A. Porcelli, and J.W. Pollard. 2007. Vascular endothelial growth factor restores delayed tumor progression in tumors depleted of macrophages. *Mol Oncol.* 1:288-302.
- Liu, V.C., L.Y. Wong, T. Jang, A.H. Shah, I. Park, X. Yang, Q. Zhang, S. Lonning, B.A. Teicher, and C. Lee. 2007. Tumor evasion of the immune system by converting CD4+CD25- T cells into CD4+CD25+ T regulatory cells: role of tumor-derived TGF-beta. *J Immunol.* 178:2883-92.
- Liu, Z., K. Geboes, P. Hellings, P. Maerten, H. Heremans, P. Vandenberghe, L. Boon, P. van Kooten, P. Rutgeerts, and J.L. Ceuppens. 2001. B7 interactions with CD28 and CTLA-4 control tolerance or induction of mucosal inflammation in chronic experimental colitis. *J Immunol.* 167:1830-8.
- Liyanage, U.K., T.T. Moore, H.G. Joo, Y. Tanaka, V. Herrmann, G. Doherty, J.A. Drebin, S.M. Strasberg, T.J. Eberlein, P.S. Goedegebuure, and D.C. Linehan. 2002. Prevalence of regulatory T cells is increased in peripheral blood and tumor microenvironment of patients with pancreas or breast adenocarcinoma. *J Immunol.* 169:2756-61.
- Long, M., S.G. Park, I. Strickland, M.S. Hayden, and S. Ghosh. 2009. Nuclear factor-kappaB modulates regulatory T cell development by directly regulating expression of Foxp3 transcription factor. *Immunity.* 31:921-31.
- Lorusso, G., and C. Ruegg. 2008. The tumor microenvironment and its contribution to tumor evolution toward metastasis. *Histochem Cell Biol.* 130:1091-103.
- Maccalli, C., S. Scaramuzza, and G. Parmiani. 2009. TNK cells (NKG2D+ CD8+ or CD4+ T lymphocytes) in the control of human tumors. *Cancer Immunol Immunother.* 58:801-8.
- Maloy, K.J., and F. Powrie. 2005. Fueling regulation: IL-2 keeps CD4+ Treg cells fit. *Nat Immunol.* 6:1071-2.
- Mami-Chouaib, F., H. Echchakir, G. Dorothee, I. Vergnon, and S. Chouaib. 2002. Antitumor cytotoxic T-lymphocyte response in human lung carcinoma: identification of a tumor-associated antigen. *Immunol Rev.* 188:114-21.

- Martinhalet, D., P. Zhu, and J. Lieberman. 2005. Granzyme A induces caspase-independent mitochondrial damage, a required first step for apoptosis. *Immunity*. 22:355-70.
- Matsumoto, S., H. Yasui, J.B. Mitchell, and M.C. Krishna. 2010. Imaging cycling tumor hypoxia. *Cancer Res*. 70:10019-23.
- Mavoungou, E., M.K. Bouyou-Akotet, and P.G. Kremsner. 2005. Effects of prolactin and cortisol on natural killer (NK) cell surface expression and function of human natural cytotoxicity receptors (NKp46, NKp44 and NKp30). *Clin Exp Immunol*. 139:287-96.
- Medzhitov, R. 2007. Recognition of microorganisms and activation of the immune response. *Nature*. 449:819-26.
- Meresse, B., Z. Chen, C. Ciszewski, M. Tretiakova, G. Bhagat, T.N. Krausz, D.H. Raulet, L.L. Lanier, V. Groh, T. Spies, E.C. Ebert, P.H. Green, and B. Jabri. 2004. Coordinated induction by IL15 of a TCR-independent NKG2D signaling pathway converts CTL into lymphokine-activated killer cells in celiac disease. *Immunity*. 21:357-66.
- Miyara, M., and S. Sakaguchi. 2007. Natural regulatory T cells: mechanisms of suppression. *Trends Mol Med*. 13:108-16.
- Mizukami, Y., K. Kono, Y. Kawaguchi, H. Akaike, K. Kamimura, H. Sugai, and H. Fujii. 2008a. CCL17 and CCL22 chemokines within tumor microenvironment are related to accumulation of Foxp3(+) regulatory T cells in gastric cancer. *International Journal of Cancer*. 122:2286-2293.
- Mizukami, Y., K. Kono, Y. Kawaguchi, H. Akaike, K. Kamimura, H. Sugai, and H. Fujii. 2008b. CCL17 and CCL22 chemokines within tumor microenvironment are related to accumulation of Foxp3+ regulatory T cells in gastric cancer. *Int J Cancer*. 122:2286-93.
- Mlecnik, B., M. Tosolini, P. Charoentong, A. Kirilovsky, G. Bindea, A. Berger, M. Camus, M. Gillard, P. Bruneval, W.H. Fridman, F. Pages, Z. Trajanoski, and J. Galon. 2010a. Biomolecular network reconstruction identifies T-cell homing factors associated with survival in colorectal cancer. *Gastroenterology*. 138:1429-40.
- Mlecnik, B., M. Tosolini, A. Kirilovsky, A. Berger, G. Bindea, T. Meatchi, P. Bruneval, Z. Trajanoski, W.H. Fridman, F. Pages, and J. Galon. 2010b. Histopathologic-based prognostic factors of colorectal cancers are associated with the state of the local immune reaction. *J Clin Oncol*. 29:610-8.
- Moretta, L., C. Bottino, D. Pende, M. Vitale, M.C. Mingari, and A. Moretta. 2005. Human natural killer cells: Molecular mechanisms controlling NK cell activation and tumor cell lysis. *Immunol Lett*. 100:7-13.
- Morgan, M.E., J.H. van Bilsen, A.M. Bakker, B. Heemskerk, M.W. Schilham, F.C. Hartgers, B.G. Elferink, L. van der Zanden, R.R. de Vries, T.W. Huizinga, T.H. Ottenhoff, and R.E. Toes. 2005. Expression of FOXP3 mRNA is not confined to CD4+CD25+ T regulatory cells in humans. *Hum Immunol*. 66:13-20.

- Nagorsen, D., C. Scheibenbogen, A. Letsch, C.T. Germer, H.J. Buhr, S. Hegewisch-Becker, L. Rivoltini, E. Thiel, and U. Keilholz. 2005. T cell responses against tumor associated antigens and prognosis in colorectal cancer patients. *J Transl Med.* 3:3.
- Nakamura, K., A. Kitani, I. Fuss, A. Pedersen, N. Harada, H. Nawata, and W. Strober. 2004. TGF-beta 1 plays an important role in the mechanism of CD4+CD25+ regulatory T cell activity in both humans and mice. *J Immunol.* 172:834-42.
- Nakamura, K., A. Kitani, and W. Strober. 2001. Cell contact-dependent immunosuppression by CD4(+)CD25(+) regulatory T cells is mediated by cell surface-bound transforming growth factor beta. *J Exp Med.* 194:629-44.
- Niederman, T.M., J.V. Garcia, W.R. Hastings, S. Luria, and L. Ratner. 1992. Human immunodeficiency virus type 1 Nef protein inhibits NF-kappa B induction in human T cells. *J Virol.* 66:6213-9.
- Ohtani, H., and O. Yoshie. 2010. Morphometric analysis of the balance between CXCR3+ T cells and FOXP3+ regulatory T cells in lymphocyte-rich and conventional gastric cancers. *Virchows Arch.* 456:615-23.
- Pages, F., A. Berger, M. Camus, F. Sanchez-Cabo, A. Costes, R. Molidor, B. Mlecnik, A. Kirilovsky, M. Nilsson, D. Damotte, T. Meatchi, P. Bruneval, P.H. Cugnenc, Z. Trajanoski, W.H. Fridman, and J. Galon. 2005. Effector memory T cells, early metastasis, and survival in colorectal cancer. *N Engl J Med.* 353:2654-66.
- Pages, F., J. Galon, M.C. Dieu-Nosjean, E. Tartour, C. Sautes-Fridman, and W.H. Fridman. 2010. Immune infiltration in human tumors: a prognostic factor that should not be ignored. *Oncogene.* 29:1093-102.
- Pages, F., J. Galon, and W.H. Fridman. 2008. The essential role of the in situ immune reaction in human colorectal cancer. *J Leukoc Biol.* 84:981-7.
- Pages, F., A. Kirilovsky, B. Mlecnik, M. Asslaber, M. Tosolini, G. Bindea, C. Lagorce, P. Wind, F. Marliot, P. Bruneval, K. Zatloukal, Z. Trajanoski, A. Berger, W.H. Fridman, and J. Galon. 2009. In situ cytotoxic and memory T cells predict outcome in patients with early-stage colorectal cancer. *J Clin Oncol.* 27:5944-51.
- Peng, Y., Y. Laouar, M.O. Li, E.A. Green, and R.A. Flavell. 2004. TGF-beta regulates in vivo expansion of Foxp3-expressing CD4+CD25+ regulatory T cells responsible for protection against diabetes. *Proc Natl Acad Sci U S A.* 101:4572-7.
- Piccirillo, C.A., and E.M. Shevach. 2001. Cutting edge: control of CD8+ T cell activation by CD4+CD25+ immunoregulatory cells. *J Immunol.* 167:1137-40.
- Pietras, K., and A. Ostman. 2010. Hallmarks of cancer: interactions with the tumor stroma. *Exp Cell Res.* 316:1324-31.
- Qian, B.Z., and J.W. Pollard. 2010. Macrophage diversity enhances tumor progression and metastasis. *Cell.* 141:39-51.

- Qiu, H., W. Xiao-Jun, Z. Zhi-Wei, C. Gong, W. Guo-Qiang, Z. Li-Yi, L. Yuan-Fang, and K. Rajiv-Prasad. 2009. The prognostic significance of peripheral T-lymphocyte subsets and natural killer cells in patients with colorectal cancer. *Hepatogastroenterology*. 56:1310-5.
- Read, S., V. Malmstrom, and F. Powrie. 2000. Cytotoxic T lymphocyte-associated antigen 4 plays an essential role in the function of CD25(+)CD4(+) regulatory cells that control intestinal inflammation. *J Exp Med*. 192:295-302.
- Read, S., S. Mauze, C. Asseman, A. Bean, R. Coffman, and F. Powrie. 1998. CD38+ CD45RB(low) CD4+ T cells: a population of T cells with immune regulatory activities in vitro. *Eur J Immunol*. 28:3435-47.
- Reed, J.C. 2003. Apoptosis-targeted therapies for cancer. *Cancer Cell*. 3:17-22.
- Roncador, G., P.J. Brown, L. Maestre, S. Hue, J.L. Martinez-Torrecuadrada, K.L. Ling, S. Pratap, C. Toms, B.C. Fox, V. Cerundolo, F. Powrie, and A.H. Banham. 2005. Analysis of FOXP3 protein expression in human CD4+CD25+ regulatory T cells at the single-cell level. *Eur J Immunol*. 35:1681-91.
- Roncarolo, M.G., S. Gregori, M. Battaglia, R. Bacchetta, K. Fleischhauer, and M.K. Levings. 2006. Interleukin-10-secreting type 1 regulatory T cells in rodents and humans. *Immunol Rev*. 212:28-50.
- Rudge, G., P.A. Gleeson, and I.R. van Driel. 2006. Control of immune responses by immunoregulatory T cells. *Arch Immunol Ther Exp (Warsz)*. 54:381-91.
- Ruffell, B., D.G. DeNardo, N.I. Affara, and L.M. Coussens. 2010. Lymphocytes in cancer development: polarization towards pro-tumor immunity. *Cytokine Growth Factor Rev*. 21:3-10.
- Sakaguchi, S., and F. Powrie. 2007. Emerging challenges in regulatory T cell function and biology. *Science*. 317:627-9.
- Sakaguchi, S., N. Sakaguchi, M. Asano, M. Itoh, and M. Toda. 1995. Immunologic self-tolerance maintained by activated T cells expressing IL-2 receptor alpha-chains (CD25). Breakdown of a single mechanism of self-tolerance causes various autoimmune diseases. *J Immunol*. 155:1151-64.
- Salama, P., M. Phillips, F. Grieu, M. Morris, N. Zeps, D. Joseph, C. Platell, and B. Iacopetta. 2009. Tumor-infiltrating FOXP3+ T regulatory cells show strong prognostic significance in colorectal cancer. *J Clin Oncol*. 27:186-92.
- Sasada, T., M. Kimura, Y. Yoshida, M. Kanai, and A. Takabayashi. 2003. CD4+CD25+ regulatory T cells in patients with gastrointestinal malignancies: possible involvement of regulatory T cells in disease progression. *Cancer*. 98:1089-99.
- Schreiber, R.D., L.J. Old, and M.J. Smyth. 2011. Cancer immunoediting: integrating immunity's roles in cancer suppression and promotion. *Science*. 331:1565-70.

- Schroder, K., P.J. Hertzog, T. Ravasi, and D.A. Hume. 2004. Interferon-gamma: an overview of signals, mechanisms and functions. *J Leukoc Biol.* 75:163-89.
- Sebens, S., and H. Schafer. 2011. The Tumor Stroma as Mediator of Drug Resistance - A Potential Target to Improve Cancer Therapy? *Curr Pharm Biotechnol.*
- Semenza, G.L. 1999. Regulation of mammalian O₂ homeostasis by hypoxia-inducible factor 1. *Annu Rev Cell Dev Biol.* 15:551-78.
- Shevach, E.M. 2002. CD4⁺ CD25⁺ suppressor T cells: more questions than answers. *Nat Rev Immunol.* 2:389-400.
- Shevach, E.M. 2004. Fatal attraction: tumors beckon regulatory T cells. *Nat Med.* 10:900-1.
- Shimizu, J., S. Yamazaki, and S. Sakaguchi. 1999. Induction of tumor immunity by removing CD25⁺CD4⁺ T cells: a common basis between tumor immunity and autoimmunity. *J Immunol.* 163:5211-8.
- Smith, N.R., D. Baker, N.H. James, K. Ratcliffe, M. Jenkins, S.E. Ashton, G. Sproat, R. Swann, N. Gray, A. Ryan, J.M. Jurgensmeier, and C. Womack. 2010. Vascular endothelial growth factor receptors VEGFR-2 and VEGFR-3 are localized primarily to the vasculature in human primary solid cancers. *Clin Cancer Res.* 16:3548-61.
- Smyth, M.J., N.Y. Crowe, and D.I. Godfrey. 2001. NK cells and NKT cells collaborate in host protection from methylcholanthrene-induced fibrosarcoma. *Int Immunol.* 13:459-63.
- Smyth, M.J., M.W. Teng, J. Swann, K. Kyparissoudis, D.I. Godfrey, and Y. Hayakawa. 2006. CD4⁺CD25⁺ T regulatory cells suppress NK cell-mediated immunotherapy of cancer. *J Immunol.* 176:1582-7.
- Smyth, M.J., K.Y. Thia, S.E. Street, E. Cretney, J.A. Trapani, M. Taniguchi, T. Kawano, S.B. Pelikan, N.Y. Crowe, and D.I. Godfrey. 2000. Differential tumor surveillance by natural killer (NK) and NKT cells. *J Exp Med.* 191:661-8.
- Stephens, L.A., C. Mottet, D. Mason, and F. Powrie. 2001. Human CD4⁽⁺⁾CD25⁽⁺⁾ thymocytes and peripheral T cells have immune suppressive activity in vitro. *Eur J Immunol.* 31:1247-54.
- Stern-Ginossar, N., and O. Mandelboim. 2009. An integrated view of the regulation of NKG2D ligands. *Immunology.* 128:1-6.
- Sutmoller, R.P., L.M. van Duivenvoorde, A. van Elsas, T.N. Schumacher, M.E. Wildenberg, J.P. Allison, R.E. Toes, R. Offringa, and C.J. Melief. 2001. Synergism of cytotoxic T lymphocyte-associated antigen 4 blockade and depletion of CD25⁽⁺⁾ regulatory T cells in antitumor therapy reveals alternative pathways for suppression of autoreactive cytotoxic T lymphocyte responses. *J Exp Med.* 194:823-32.
- Suzuki, H., N. Chikazawa, T. Tasaka, J. Wada, A. Yamasaki, Y. Kitaura, M. Sozaki, M. Tanaka, H. Onishi, T. Morisaki, and M. Katano. 2010. Intratumoral CD8⁽⁺⁾ T/FOXP3⁽⁺⁾ cell ratio is a predictive marker for survival in patients with colorectal cancer. *Cancer Immunol Immunother.* 59:653-61.

- Takahashi, T., Y. Kuniyasu, M. Toda, N. Sakaguchi, M. Itoh, M. Iwata, J. Shimizu, and S. Sakaguchi. 1998. Immunologic self-tolerance maintained by CD25+CD4+ naturally anergic and suppressive T cells: induction of autoimmune disease by breaking their anergic/suppressive state. *Int Immunol.* 10:1969-80.
- Takahashi, T., T. Tagami, S. Yamazaki, T. Uede, J. Shimizu, N. Sakaguchi, T.W. Mak, and S. Sakaguchi. 2000. Immunologic self-tolerance maintained by CD25(+)CD4(+) regulatory T cells constitutively expressing cytotoxic T lymphocyte-associated antigen 4. *J Exp Med.* 192:303-10.
- Tam, Y.K., J.A. Martinson, K. Doligosa, and H.G. Klingemann. 2003. Ex vivo expansion of the highly cytotoxic human natural killer-92 cell-line under current good manufacturing practice conditions for clinical adoptive cellular immunotherapy. *Cytotherapy.* 5:259-72.
- Tanchot, C., F. Vasseur, C. Pontoux, C. Garcia, and A. Sarukhan. 2004. Immune regulation by self-reactive T cells is antigen specific. *J Immunol.* 172:4285-91.
- Tang, R., F. Beuvon, M. Ojeda, V. Mosseri, P. Pouillart, and S. Scholl. 1992. M-CSF (monocyte colony stimulating factor) and M-CSF receptor expression by breast tumour cells: M-CSF mediated recruitment of tumour infiltrating monocytes? *J Cell Biochem.* 50:350-6.
- Thijssen, V.L., R.J. Brandwijk, R.P. Dings, and A.W. Griffioen. 2004. Angiogenesis gene expression profiling in xenograft models to study cellular interactions. *Exp Cell Res.* 299:286-93.
- Thornton, A.M., and E.M. Shevach. 1998. CD4+CD25+ immunoregulatory T cells suppress polyclonal T cell activation in vitro by inhibiting interleukin 2 production. *J Exp Med.* 188:287-96.
- Thorstenson, K.M., and A. Khoruts. 2001. Generation of anergic and potentially immunoregulatory CD25+CD4 T cells in vivo after induction of peripheral tolerance with intravenous or oral antigen. *J Immunol.* 167:188-95.
- Topham, N.J., and E.W. Hewitt. 2009. Natural killer cell cytotoxicity: how do they pull the trigger? *Immunology.* 128:7-15.
- Tsujino, T., I. Seshimo, H. Yamamoto, C.Y. Ngan, K. Ezumi, I. Takemasa, M. Ikeda, M. Sekimoto, N. Matsuura, and M. Monden. 2007. Stromal myofibroblasts predict disease recurrence for colorectal cancer. *Clin Cancer Res.* 13:2082-90.
- Valencia, X., and P.E. Lipsky. 2007. CD4+CD25+FoxP3+ regulatory T cells in autoimmune diseases. *Nat Clin Pract Rheumatol.* 3:619-26.
- van Maren, W.W., J.F. Jacobs, I.J. de Vries, S. Nierkens, and G.J. Adema. 2008. Toll-like receptor signalling on Tregs: to suppress or not to suppress? *Immunology.* 124:445-52.

- Vaupel, P., and A. Mayer. 2007. Hypoxia in cancer: significance and impact on clinical outcome. *Cancer Metastasis Rev.* 26:225-39.
- Vergati, M., V. Cereda, R.A. Madan, J.L. Gulley, N.Y. Huen, C.J. Rogers, K.W. Hance, P.M. Arlen, J. Schlom, and K.Y. Tsang. 2011. Analysis of circulating regulatory T cells in patients with metastatic prostate cancer pre- versus post-vaccination. *Cancer Immunol Immunother.* 60:197-206.
- Vignali, D.A., L.W. Collison, and C.J. Workman. 2008. How regulatory T cells work. *Nat Rev Immunol.* 8:523-32.
- Vulcano, M., C. Albanesi, A. Stoppacciaro, R. Bagnati, G. D'Amico, S. Struyf, P. Transidico, R. Bonecchi, A. Del Prete, P. Allavena, L.P. Ruco, C. Chiabrando, G. Girolomoni, A. Mantovani, and S. Sozzani. 2001. Dendritic cells as a major source of macrophage-derived chemokine/CCL22 in vitro and in vivo. *Eur J Immunol.* 31:812-22.
- Wahl, S.M., J. Wen, and N.M. Moutsopoulos. 2006. The kiss of death: interrupted by NK-cell close encounters of another kind. *Trends Immunol.* 27:161-4.
- Walker, M.R., D.J. Kasprovicz, V.H. Gersuk, A. Benard, M. Van Landeghen, J.H. Buckner, and S.F. Ziegler. 2003. Induction of FoxP3 and acquisition of T regulatory activity by stimulated human CD4+CD25- T cells. *J Clin Invest.* 112:1437-43.
- Wang, J., A. Ioan-Facsinay, E.I. van der Voort, T.W. Huizinga, and R.E. Toes. 2007. Transient expression of FOXP3 in human activated nonregulatory CD4+ T cells. *Eur J Immunol.* 37:129-38.
- Wang, R.F. 2006. Functional control of regulatory T cells and cancer immunotherapy. *Semin Cancer Biol.* 16:106-14.
- Weitz, J., M. Koch, J. Debus, T. Hohler, P.R. Galle, and M.W. Buchler. 2005. Colorectal cancer. *Lancet.* 365:153-65.
- West, N.P., M. Dattani, P. McShane, G. Hutchins, J. Grabsch, W. Mueller, D. Treanor, P. Quirke, and H. Grabsch. 2010. The proportion of tumour cells is an independent predictor for survival in colorectal cancer patients. *Br J Cancer.* 102:1519-23.
- Whiteside, T.L., and R.B. Herberman. 1990. The biology of human natural killer cells. *Ann Ist Super Sanita.* 26:335-48.
- Whiteside, T.L., and R.B. Herberman. 1994. Role of human natural killer cells in health and disease. *Clin Diagn Lab Immunol.* 1:125-33.
- Wiemann, K., H.W. Mittrucker, U. Feger, S.A. Welte, W.M. Yokoyama, T. Spies, H.G. Rammensee, and A. Steinle. 2005. Systemic NKG2D down-regulation impairs NK and CD8 T cell responses in vivo. *J Immunol.* 175:720-9.
- Wolf, A.M., D. Wolf, M. Steurer, G. Gastl, E. Gunsilius, and B. Grubeck-Loebenstien. 2003. Increase of regulatory T cells in the peripheral blood of cancer patients. *Clin Cancer Res.* 9:606-12.

- Wolf, D., A.M. Wolf, H. Rumpold, H. Fiegl, A.G. Zeimet, E. Muller-Holzner, M. Deibl, G. Gastl, E. Gunsilius, and C. Marth. 2005. The expression of the regulatory T cell-specific forkhead box transcription factor FoxP3 is associated with poor prognosis in ovarian cancer. *Clin Cancer Res.* 11:8326-31.
- Wolke, C., J. Tadge, A. Bukowska, M. Tager, U. Bank, A. Ittenson, S. Ansorge, and U. Lendeckel. 2006. Assigning the phenotype of a natural regulatory T-cell to the human T-cell line, KARPAS-299. *Int J Mol Med.* 17:275-8.
- Woo, E.Y., C.S. Chu, T.J. Goletz, K. Schlienger, H. Yeh, G. Coukos, S.C. Rubin, L.R. Kaiser, and C.H. June. 2001. Regulatory CD4(+)CD25(+) T cells in tumors from patients with early-stage non-small cell lung cancer and late-stage ovarian cancer. *Cancer Res.* 61:4766-72.
- Yamaguchi, T., K. Hirota, K. Nagahama, K. Ohkawa, T. Takahashi, T. Nomura, and S. Sakaguchi. 2007. Control of immune responses by antigen-specific regulatory T cells expressing the folate receptor. *Immunity.* 27:145-59.
- Yancopoulos, G.D., S. Davis, N.W. Gale, J.S. Rudge, S.J. Wiegand, and J. Holash. 2000. Vascular-specific growth factors and blood vessel formation. *Nature.* 407:242-8.
- Yi, H., Y. Zhen, L. Jiang, J. Zheng, and Y. Zhao. 2006. The phenotypic characterization of naturally occurring regulatory CD4+CD25+ T cells. *Cell Mol Immunol.* 3:189-95.
- Yun, T.J., and M.J. Bevan. 2001. The Goldilocks conditions applied to T cell development. *Nature Immunology.* 2:13-14.
- Zelenay, S., T. Lopes-Carvalho, I. Caramalho, M.F. Moraes-Fontes, M. Rebelo, and J. Demengeot. 2005. Foxp3+ CD25- CD4 T cells constitute a reservoir of committed regulatory cells that regain CD25 expression upon homeostatic expansion. *Proc Natl Acad Sci U S A.* 102:4091-6.
- Zheng, S.G., J.H. Wang, J.D. Gray, H. Soucier, and D.A. Horwitz. 2004. Natural and induced CD4+CD25+ cells educate CD4+CD25- cells to develop suppressive activity: the role of IL-2, TGF-beta, and IL-10. *J Immunol.* 172:5213-21.
- Zhong, H., G.L. Semenza, J.W. Simons, and A.M. De Marzo. 2004. Up-regulation of hypoxia-inducible factor 1alpha is an early event in prostate carcinogenesis. *Cancer Detect Prev.* 28:88-93.
- Zimmer, J., E. Andres, and F. Hentges. 2008. NK cells and Treg cells: a fascinating dance cheek to cheek. *Eur J Immunol.* 38:2942-5.